GeoPlanet: Earth and Planetary Sciences

Robert Jankowski
Sayed Mahmoud

Earthquake-Induced Structural Pounding

Springer

GeoPlanet: Earth and Planetary Sciences

More information about this series at http://www.springer.com/series/8821

Robert Jankowski · Sayed Mahmoud

Earthquake-Induced Structural Pounding

Springer

Robert Jankowski
Faculty of Civil and Environmental Engineering
Gdansk University of Technology
Gdansk
Poland

Sayed Mahmoud
Department of Construction Engineering
College of Engineering
University of Dammam
Dammam
Kingdom of Saudi Arabia

The GeoPlanet: Earth and Planetary Sciences Book Series is in part a continuation of Monographic Volumes of Publications of the Institute of Geophysics, Polish Academy of Sciences, the journal published since 1962 (http://pub.igf.edu.pl/index.php).

ISSN 2190-5193 ISSN 2190-5207 (electronic)
GeoPlanet: Earth and Planetary Sciences
ISBN 978-3-319-16323-9 ISBN 978-3-319-16324-6 (eBook)
DOI 10.1007/978-3-319-16324-6

Library of Congress Control Number: 2015933363

Springer Cham Heidelberg New York Dordrecht London

Printed on acid-free paper

Springer International Publishing AG Switzerland is part of Springer Science+Business Media (www.springer.com)

Series Editors

Managing Editor

Anna Dziembowska
Institute of Geophysics, Polish Academy of Sciences

Advisory Board

Kon-Kee Liu
Institute of Hydrological
and Oceanic Sciences
National Central University Jhongli
Jhongli, Taiwan

Teresa Madeyska
Research Centre in Warsaw
Institute of Geological Sciences
Warszawa, Poland

Stanisław Massel
Institute of Oceanology
Polish Academy of Sciences
Sopot, Polska

Antonio Meloni
Instituto Nazionale di Geofisica
Rome, Italy

Evangelos Papathanassiou
Hellenic Centre for Marine Research
Anavissos, Greece

Kaja Pietsch
AGH University of Science
and Technology
Kraków, Poland

Dušan Plašienka
Prírodovedecká fakulta, UK
Univerzita Komenského
Bratislava, Slovakia

Barbara Popielawska
Space Research Centre
Polish Academy of Sciences
Warszawa, Poland

Tilman Spohn
Deutsches Zentrum für Luftund
Raumfahrt in der Helmholtz
Gemeinschaft
Institut für Planetenforschung
Berlin, Germany

Krzysztof Stasiewicz
Swedish Institute of Space Physics
Uppsala, Sweden

Roman Teisseyre
Earth's Interior Dynamics Lab
Institute of Geophysics
Polish Academy of Sciences
Warszawa, Poland

Jacek Tronczynski
Laboratory of Biogeochemistry
of Organic Contaminants
IFREMER DCN_BE
Nantes, France

Steve Wallis
School of the Built Environment
Heriot-Watt University
Riccarton, Edinburgh
Scotland, UK

Wacław M. Zuberek
Department of Applied Geology
University of Silesia
Sosnowiec, Poland

Acknowledgments

The authors would like to thank Profs. Yozo Fujino, Krzysztof Wilde, Henryk Walukiewicz, Xiaojun Chen and Per-Erik Austrell for their advice and valuable comments at different stages of the study.

Words of thanks are also directed to Dr. Ayman Abd-Elhamed and Mr. Marek Kotwicki for help in some numerical simulations, as well as to Mr. Eugeniusz Lilla and Mr. Jan Jagiełło for help in conducting experimental tests.

The second author is on leave from the Faculty of Engineering at Mataria, Helwan University, Cairo, Egypt.

Contents

1 Introduction 1
References. 6

2 Modelling of Structural Pounding 9
2.1 Classical Theory of Impact. 9
2.2 Models of Pounding Force During Collision Between Structures. 11
2.2.1 Linear Elastic Model 13
2.2.2 Linear Viscoelastic Model 13
2.2.3 Modified Linear Viscoelastic Model 14
2.2.4 Hertz Non-linear Elastic Model. 15
2.2.5 Hertzdamp Non-linear Model 16
2.2.6 Non-linear Viscoelastic Model 16
2.3 Experimental Verification of the Effectiveness of Pounding Force Models 17
2.3.1 Impact Between a Ball Falling Onto a Rigid Surface. 17
2.3.2 Pounding Between Models of Tower Structures 23
2.3.3 Conclusions 31
References. 31

3 Pounding Between Buildings 35
3.1 Pounding-Involved Response of Buildings Modelled as SDOF Systems 36
3.2 Pounding-Involved Response of Buildings Modelled as MDOF Systems 38
3.3 Pounding-Involved Response of Base-Isolated Buildings 44
3.3.1 Pounding Between Isolated and Non-isolated Building 46
3.3.2 Pounding Between Two Isolated Buildings 48
3.4 Pounding-Involved Response of Buildings Considering SSI . . . 51

3.5 Pounding-Involved Response Analysis Using FEM 62
3.5.1 Response in the Longitudinal Direction 64
3.5.2 Response in the Transverse Direction 64
3.5.3 Torsional Response 67
References 68

4 Pounding Between Bridge Segments 73
4.1 Pounding-Involved Response of the Bridge Modelled as MDOF System 73
4.1.1 Description of the Analyzed Structure 74
4.1.2 Response of the Bridge Using One-Dimensional Structural Model 74
4.1.3 Response of the Bridge Using Two-Dimensional Structural Model 81
4.2 Pounding-Involved Response Analysis Using FEM 87
4.2.1 Detailed Modelling of Structural Members of the Bridge 87
4.2.2 Modelling of Earthquake Records for Different Bridge Supports 90
4.2.3 Response of the Bridge Using One-Dimensional Structural Model 93
4.2.4 Response of the Bridge Using Three-Dimensional Structural Model 96
References 100

5 Mitigation of Pounding Effects 103
5.1 Large Gap Size to Prevent Pounding 105
5.2 Link Elements 108
5.2.1 Buildings Linked with Spring Elements 109
5.2.2 Buildings Linked with Dashpot Elements 113
5.2.3 Buildings Linked with Viscoelastic Elements 116
5.3 Bumpers 118
5.4 Other Methods 123
5.4.1 Increasing Stiffness of Structures 123
5.4.2 Supplemental Energy Dissipation Devices 126
References 128

6 Design of Structures Prone to Pounding 133
6.1 Procedures in the Building Codes Related to the Minimum Seismic Gap 133
6.2 Pounding Force Response Spectrum 135
6.2.1 Response Spectrum for One Existing and One New Structure 135
6.2.2 Response Spectrum for Two New Structures 136

6.3 Assessment of Structural Damage 144
6.3.1 Damage Indices in Non-isolated Buildings 145
6.3.2 Damage Indices in Base-Isolated Buildings 149
References. 154

Chapter 1
Introduction

It has been observed during earthquakes that adjacent building, or bridge segments, might come into contact if the separation distance between them is not sufficient so as to accommodate their relative movements. This phenomenon, known as the earthquake-induced structural pounding, may lead to local damage at the contact locations during moderate seismic excitations or may result in significant damage or even total collapse of colliding structures in the case of severe ground motions.

The report after the Kaliningrad earthquake (21.09.2004), for example, shows that interaction between adjacent parts of the apartment building led to spalling of plaster at the contact locations, as can be seen in Fig. 1.1 (Zembaty et al. 2005). Local damage at the interaction points was also observed in a number of buildings after the Darfield earthquake of September 2, 2010 (Cole et al. 2011). Vasiliadis and Elenas (2002) reported considerable damage at the locations of impacts due to pounding between two different parts of a school building during the Athens earthquake (7.09.1999). The SSK Hospital in Izmit suffered major damage during the Kocaeli earthquake (17.08.1999) due to interactions between different parts of the structure (Gillies et al. 2001). Extensive pounding damage was also observed in low-rise unreinforced masonry buildings after the Christchurch earthquake of 2011 (Cole et al. 2012). It was observed after the Mexico City earthquake (19.09.1985) that about 40 % of the damaged structures experienced some level of pounding and, in the case of 15 % of them, pounding was identified as one of the reasons of structural collapse (Rosenblueth and Meli 1986). During the San Fernando earthquake (09.02.1971), structural interactions between the main building of the Olive View Hospital and one of its independently standing stairway towers resulted in substantial damage and permanent tilting of the weaker stairway tower (Bertero and Collins 1973). Over 200 pounding occurrences, involving more than 500 buildings, were observed at locations within the distance of 90 km from the epicentre after the Loma Prieta earthquake (17.10.1989). Structural pounding during that earthquake was identified as the reason for collapses of some of buildings (see, for example, Fig. 1.2) (Kasai and Maison 1997).

R. Jankowski and S. Mahmoud, *Earthquake-Induced Structural Pounding*,
GeoPlanet: Earth and Planetary Sciences, DOI 10.1007/978-3-319-16324-6_1

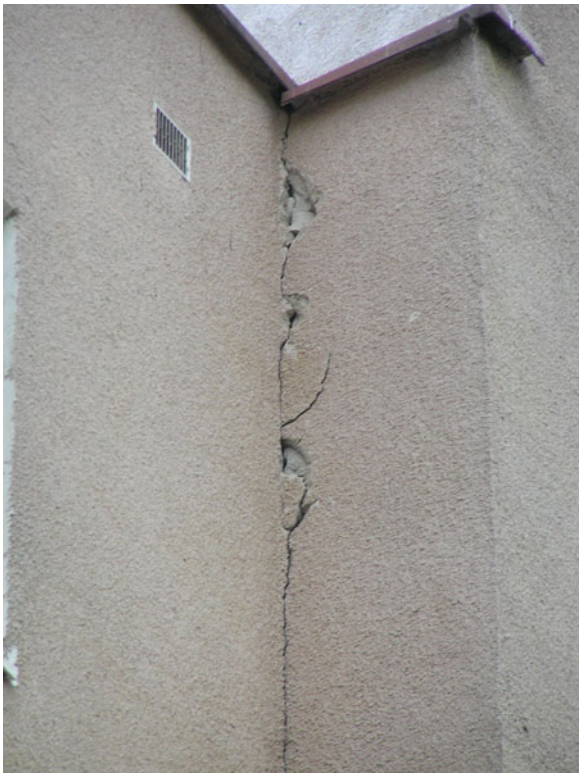

Fig. 1.1 Local damage at the contact locations (Kaliningrad earthquake, 2004)

The negative effects of earthquake-induced structural interactions were also observed in the case of bridge structures. Priestley et al. (1996) reported that impacts between the lower roadway and columns supporting the upper-level deck of the Southern viaduct section of the China Basin during the Loma Prieta earthquake of 1989 resulted in significant structural damage. After the Northridge earthquake of January 17, 1994, substantial pounding damage was observed at expansion hinges and abutments of standing portions of bridges at the Interstate 5 and State Road 14 interchange (EERI 1995). The report after the Kobe earthquake (17.01.1995) identifies pounding, due to fracture of bearing supports, as a reason leading to considerable local damage at the contact points (see Fig. 1.3) and a contribution to falling down of superstructure segments, as can be seen in Fig. 1.4 (Otsuka et al. 1996). Severe damage due to pounding between adjacent segments of the New Surajbadi Highway Bridge was also observed during the January 26, 2001 Gujarat (India) earthquake (Singh et al. 2002).

In the case of buildings, the major factor recognised as the reason of structural pounding is the difference in natural periods of vibrations (see Anagnostopoulos 1988; Anagnostopoulos and Spiliopoulos 1992; Maison and Kasai 1990, 1992; Tena-Colunga et al. 1996; Karayannis and Favvata 2005a, b; Jankowski 2005, 2007, 2008; Komodromos 2008; Mahmoud and Jankowski 2009, 2011; Polycarpou and

Fig. 1.2 Collapse of a building (Loma Prieta earthquake, 1989) (reprinted from Kasai and Maison 1997 with permission from Elsevier)

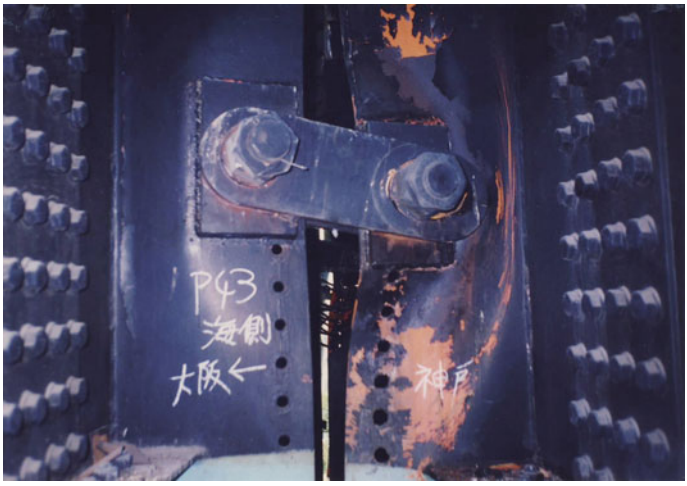

Fig. 1.3 Local damage at the ends of superstructure segments (Kobe earthquake 1995)

Fig. 1.4 Pounding as one of the reasons for falling down of superstructure segments (Kobe earthquake, 1995)

Komodromos 2010; Mahmoud et al. 2012, 2013; Falborski and Jankowski 2013; Sołtysik and Jankowski 2013; Polycarpou et al. 2014). The difference in mass or stiffness makes the adjacent buildings to vibrate out-of-phase during the earthquake and increases the probability of structural interactions (see Fig. 1.5). In contrast to buildings, pounding in bridges is usually caused by the spatial seismic effects related to the propagation of the seismic wave (see, for example, Jankowski et al. 1998, 2000; Kim et al. 2000; Zanardo et al. 2002; Chouw and Hao 2005). These effects, which may include time lag and lack of coherence of seismic wave as well as spatially varying local soil conditions (see Der Kiureghian 1996), lead to different earthquake excitations acting at different structural supports (see Fig. 1.6) resulting in the out-of-phase vibrations of adjacent superstructure segments (Jeng and Kasai 1996; Hao and Liu 1998). Spatial seismic effects may also be responsible for earthquake-induced pounding between buildings with spatially extended foundations (Jankowski 2009, 2012) or buildings in a row (Athanassiadou et al. 1994; Hao and Zhang 1999).

Earthquake-induced structural pounding is a complex phenomenon, often involving plastic deformations, local cracking or crushing at the points of contact, fracturing due to impact, friction, etc. Impact induces forces which are applied and removed during a very short time, what initiates stress waves travelling away from the impact location. The process of energy transfer during collision is much complicated making the analysis of this type of problem to be highly difficult.

In spite of its complexity, the phenomenon of structural pounding during earthquakes has recently been intensively studied applying various structural

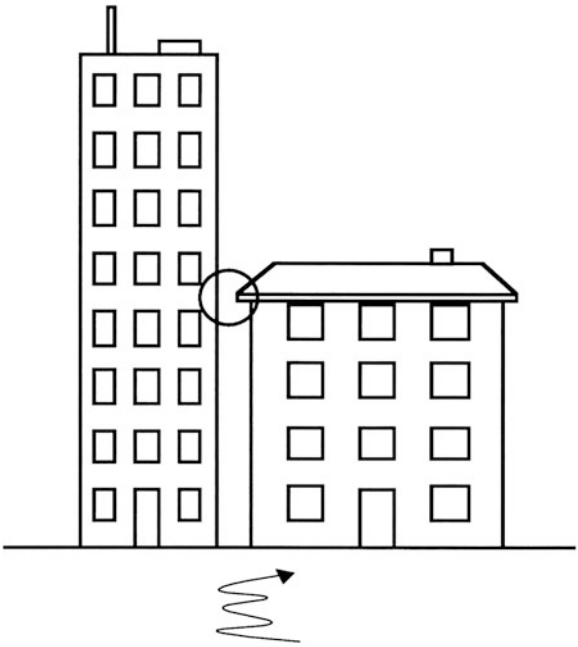

Fig. 1.5 Difference in mass or stiffness as the major reason of pounding between buildings

models and using different models of impacts. The aim of the present book is to analyse different approaches to modelling the earthquake-induced structural pounding as well as to show major results of the studies on collisions between buildings and between bridge segments during ground motions. The aspects related to mitigation of pounding effects as well as the design of structures prone to pounding are also discussed. The book consists of the following chapters:

This chapter introduces the subject of earthquake-induced structural pounding. The examples of damages due to collisions during previous ground motions are also described.

Different approaches to modelling the earthquake-induced structural pounding are described in Chap. 2. The classical theory of impact as well as the methods of modelling the pounding force directly are considered. The results of the experimental verification of the effectiveness of different pounding force models are also presented.

Chapter 3 deals with pounding between insufficiently separated buildings. The pounding-involved response of buildings under seismic excitation is analysed by using different structural models. The aspects of collisions between base-isolated buildings as well as the influence of incorporation the soil-structure interaction are also discussed.

The studies on pounding between adjacent superstructure segments of a bridge during earthquake are described in Chap. 4. The analyses are conducted using various structural models as well as incorporating the spatial seismic effects related to the propagation of seismic wave.

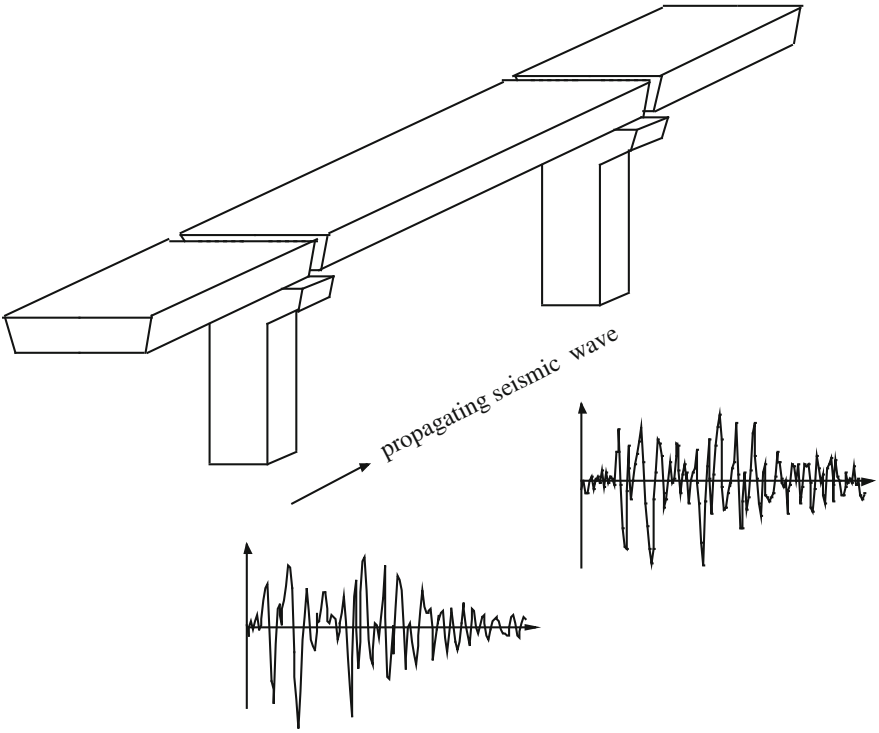

Fig. 1.6 Spatial seismic effects related to the propagation of the seismic wave as the major reason of pounding between superstructure segments in bridges

Chapter 5 deals with the methods of mitigation the negative pounding effects. First, the most natural solution of assuring the sufficiently large gap size to prevent collisions is analysed. Then, the efficiency of other methods, such as incorporation of link elements or bumpers, increasing stiffness of structures or using the supplemental energy dissipation devices, is investigated.

Finally, the aspects of design of structures prone to pounding during earthquakes are discussed in Chap. 6. Procedures specified in the building codes related to the minimum seismic gap are first described. Then, the idea of pounding force response spectrum is presented. The aspects of assessment of structural damage are also discussed.

References

Anagnostopoulos, S.A.: Pounding of buildings in series during earthquakes. Earthq. Eng. Struct. Dynam. **16**, 443–456 (1988)

Anagnostopoulos, S.A., Spiliopoulos, K.V.: An investigation of earthquake induced pounding between adjacent buildings. Earthq. Eng. Struct. Dynam. **21**, 289–302 (1992)

Athanassiadou, C.J., Penelis, G.G., Kappos, A.J.: Seismic response of adjacent buildings with similar or different dynamic characteristics. Earthq. Spectra **10**, 293–317 (1994)

Bertero, V.V., Collins, R.G.: Investigation of the failures of the Olive view Stairtowers during the San Fernando earthquake and their implications on seismic design. EERC Report No. 73–26. Earthquake Engineering Research Center, University of California, Berkeley (1973)

Chouw, N., Hao, H.: Study of SSI and non-uniform ground motion effect on pounding between bridge girders. Soil Dyn. Earthq. Eng. **25**, 717–728 (2005)

Cole, G.L., Dhakal, R.P., Carr, A.J., Bull, D.K.: Case studies of observed pounding damage during the 2010 Darfield earthquake. In: Proceedings of the Ninth Pacific Conference on Earthquake Engineering Building an Earthquake-Resilient Society, Auckland, New Zealand, 14–16 April 2011, Paper no. 173

Cole, G.L., Dhakal, R.P., Turner, F.M.: Building pounding damage observed in the 2011 Christchurch earthquake. Earthq. Eng. Struct. Dyn. **41**, 893–913 (2012)

Der Kiureghian, A.: A coherency model for spatially varying ground motions. Earthq. Eng. Struct. Dyn. **25**, 99–111 (1996)

EERI: Northridge Earthquake of January 17, 1994—Reconnaissance Report. EERI Report 95–03, vol. 1. Earthquake Engineering Research Institute, Oakland (1995)

Falborski, T., Jankowski, R.: Polymeric bearings—a new base isolation system to reduce structural damage during earthquakes. Key Eng. Mater. **569–570**, 143–150 (2013)

Gillies, A.G., Anderson, D.L., Mitchell, D., Tinawi, R., Saatcioglu, M., Gardner, N.J., Ghoborah, A.: The August 17, 1999, Kocaeli (Turkey) earthquake—lifelines and preparedness. Can. J. Civ. Eng. **28**, 881–890 (2001)

Hao, H., Liu, X.: Estimation of required separations between adjacent structures under spatial ground motions. J. Earthq. Eng. **2**, 197–215 (1998)

Hao, H., Zhang, S.-R.: Spatial ground motion effect on relative displacement of adjacent building structures. Earthq. Eng. Struct. Dyn. **28**, 333–349 (1999)

Jankowski, R.: Impact force spectrum for damage assessment of earthquake-induced structural pounding. Key Eng. Mater. **293–294**, 711–718 (2005)

Jankowski, R.: Assessment of damage due to earthquake-induced pounding between the main building and the stairway tower. Key Eng. Mater. **347**, 339–344 (2007)

Jankowski, R.: Earthquake-induced pounding between equal height buildings with substantially different dynamic properties. Eng. Struct. **30**(10), 2818–2829 (2008)

Jankowski, R.: Non-linear FEM analysis of earthquake-induced pounding between the main building and the stairway tower of the Olive View Hospital. Eng. Struct. **31**, 1851–1864 (2009)

Jankowski, R.: Non-linear FEM analysis of pounding-involved response of buildings under non-uniform earthquake excitation. Eng. Struct. **37**, 99–105 (2012)

Jankowski, R., Wilde, K., Fujino, Y.: Pounding of superstructure segments in isolated elevated bridge during earthquakes. Earthq. Eng. Struct. Dyn. **27**, 487–502 (1998)

Jankowski, R., Wilde, K., Fujino, Y.: Reduction of pounding effects in elevated bridges during earthquakes. Earthq. Eng. Struct. Dyn. **29**, 195–212 (2000)

Jeng, V., Kasai, K.: Spectral relative motion of two structures due to seismic travel waves. J. Struct. Eng. **122**, 1128–1135 (1996)

Karayannis, C.G., Favvata, M.J.: Earthquake-induced interaction between adjacent reinforced concrete structures with non-equal heights. Earthq. Eng. Struct. Dyn. **34**, 1–20 (2005a)

Karayannis, C.G., Favvata, M.J.: Inter-story pounding between multistory reinforced concrete structures. Struct. Eng. Mech. **20**, 505–526 (2005b)

Kasai, K., Maison, B.F.: Building pounding damage during the 1989 Loma Prieta earthquake. Eng. Struct. **19**, 195–207 (1997)

Kim, S.-H., Lee, S.-W., Mha, H.-S.: Dynamic behaviors of the bridge considering pounding and friction effects under seismic excitations. Struct. Eng. Mech. **10**, 621–633 (2000)

Komodromos, P.: Simulation of the earthquake-induced pounding of seismically isolated buildings. Comput. Struct. **86**, 618–626 (2008)

Mahmoud, S., Abd-Elhamed, A., Jankowski, R.: Earthquake-induced pounding between equal height multi-storey buildings considering soil-structure interaction. Bull. Earthq. Eng. **11**(4), 1021–1048 (2013)

Mahmoud, S., Austrell, P.-E., Jankowski, R.: Simulation of the response of base-isolated buildings under earthquake excitations considering soil flexibility. Earthq. Eng. Eng. Vibr. **11**, 359–374 (2012)

Mahmoud, S., Jankowski, R.: Elastic and inelastic multi-storey buildings under earthquake excitation with the effect of pounding. J. Appl. Sci. **9**(18), 3250–3262 (2009)

Mahmoud, S., Jankowski, R.: Modified linear viscoelastic model of earthquake-induced structural pounding. Iran. J. Sci. Technol. **35**(C1), 51–62 (2011)

Maison, B.F., Kasai, K.: Analysis for type of structural pounding. J. Struct. Eng. **116**, 957–977 (1990)

Maison, B.F., Kasai, K.: Dynamics of pounding when two buildings collide. Earthq. Eng. Struct. Dyn. **21**, 771–786 (1992)

Otsuka, H., Unjoh, S., Terayama, T., Hoshikuma, J., Kosa, K.: Damage to highway bridges by the 1995 Hyogoken Nanbu earthquake and the retrofit of highway bridges in Japan. Third U.S.–Japan Workshop on Seismic Retrofit of Bridges. Osaka, Japan, 10–11 Dec 1996

Priestley, M.J.N., Seible, F., Calvi, G.M.: Seismic Design and Retrofit of Bridges. Wiley, New York (1996)

Polycarpou, P.C., Komodromos, P.: Earthquake-induced poundings of a seismically isolated building with adjacent structures. Eng. Struct. **32**, 1937–1951 (2010)

Polycarpou, P.C., Papaloizou, L., Komodromos, P.: An efficient methodology for simulating earthquake-induced 3D pounding of buildings. Earthq. Eng. Struct. Dyn. **43**, 985–1003 (2014)

Rosenblueth, E., Meli, R.: The 1985 earthquake: causes and effects in Mexico City. Concr. Int. **8**, 23–34 (1986)

Singh, M.P., Khaleghi, B., Saraf, V.K., Jain, S.K., Norris, G., Goel, R., Murty, C.V.R.: Roads and bridges. Earthq. Spectra **18**(S1), 363–379 (2002)

Sołtysik, B., Jankowski, R.: Non-linear strain rate analysis of earthquake-induced pounding between steel buildings. Int. J. Earth Sci. Eng. **6**, 429–433 (2013)

Tena-Colunga, A., Del Valle, E., Pérez-Moreno, D.: Issues on the seismic retrofit of a building near resonant response and structural pounding. Earthq. Spectra **12**, 567–597 (1996)

Vasiliadis, L., Elenas, A.: Performance of school buildings during the Athens earthquake of 7 September 1999. In: 12th European Conference on Earthquake Engineering, London, UK, 9–13 Sept 2002, Paper Ref. 264

Zanardo, G., Hao, H., Modena, C.: Seismic response of multi-span simply supported bridges to a spatially varying earthquake ground motion. Earthq. Eng. Struct. Dyn. **31**, 1325–1345 (2002)

Zembaty, Z., Cholewicki, A., Jankowski, R., Szulc, J.: Trzęsienia ziemi 21 września 2004 r. w Polsce północno-wschodniej oraz ich wpływ na obiekty budowlane (Earthquakes of September 21, 2004 in north eastern Poland and their effects on structures). Inżynieria i Budownictwo. **61**, 3–9 (2005) (in Polish)

Chapter 2
Modelling of Structural Pounding

Modelling of earthquake-induced pounding between buildings, or bridge segments, requires the use of accurate structural models as well as appropriate models of the effects of collisions. Two different approaches can be found in the literature, which are usually used to simulate structural pounding during ground motions. The first approach considers the classical theory of impact, which is based on the laws of conservation of energy and momentum and does not consider stresses and deformations in the colliding structural elements during impact. Since this is not a force-based approach, the effect of collisions is accounted through updating the velocities of the considered bodies or structural elements. In the second approach, the earthquake-induced structural pounding is simulated using the direct model of impact force during collision.

2.1 Classical Theory of Impact

The classical theory of impact, called stereomechanics, is focuses on determination of velocities of colliding elements after collision without tracing structural response during impact (Goldsmith 1960). The analysis is based on the values of velocities of structural elements before collision with the use of the coefficient of restitution, which accounts for the energy dissipation during impact due to such effects as, for example, plastic deformations, local cracking and friction (see Leibovich et al. 1996; Ruangrassamee and Kawashima 2001; DesRoches and Muthukumar 2002). The formulae for the final (after impact) velocities $\dot{x}_1^f$, $\dot{x}_2^f$ of two colliding elements with masses m_1 and m_2 (see Fig. 2.1) can be expressed as (Goldsmith 1960):

$$\dot{x}_1^f = \dot{x}_1^0 - (1+e)\frac{m_2\dot{x}_1^0 - m_2\dot{x}_2^0}{m_1+m_2} \tag{2.1a}$$

$$\dot{x}_2^f = \dot{x}_2^0 + (1+e)\frac{m_1\dot{x}_1^0 - m_1\dot{x}_2^0}{m_1+m_2} \tag{2.1b}$$

R. Jankowski and S. Mahmoud, *Earthquake-Induced Structural Pounding*,
GeoPlanet: Earth and Planetary Sciences, DOI 10.1007/978-3-319-16324-6_2

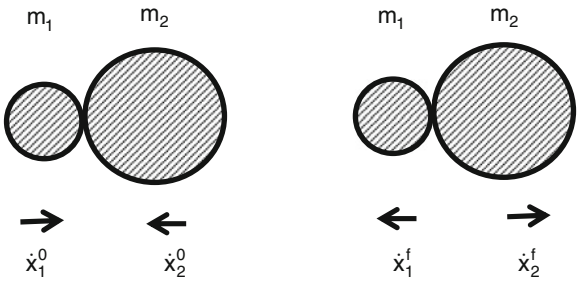

Fig. 2.1 Initial (before impact) and final (after impact) velocities of colliding bodies

where $\dot{x}_1^0$, $\dot{x}_2^0$ are the initial (before impact) velocities and e is a coefficient of restitution, which can be obtained from the equation:

$$e = \frac{\dot{x}_2^f - \dot{x}_1^f}{\dot{x}_1^0 - \dot{x}_2^0} \tag{2.2}$$

The value of $e = 1$ is related to the case of a fully elastic collision, while the value of $e = 0$ deals with a fully plastic impact. The basic value of the coefficient of restitution can be determined experimentally by dropping a sphere, made of the specific material, on a massive plane plate of the same material from a height h. Then, after recording the rebound height h^*, the following formula can be used (see Goldsmith 1960):

$$e^2 = \frac{h^*}{h} \tag{2.3}$$

It has been confirmed through experimental studies that the value of the coefficient of restitution usually ranges from 0.4 up to about 0.8 in the case of collisions between structural elements made of building materials (see Anagnostopoulos and Spiliopoulos 1992; Zhu et al. 2002; Jankowski 2010). Azevedo and Bento (1996) suggested that $e = 0.65$ should be used for typical concrete structures. In fact, this value has been used by a number of researchers in the analyses of pounding between different types of structures (see, for example, Anagnostopoulos 1988; Papadrakakis et al. 1991; Anagnostopoulos and Spiliopoulos 1992; Jankowski et al. 1998; Jankowski 2006b, 2008; Mahmoud et al. 2013). However, the results of the impact experiments indicate that the value of the coefficient of restitution might substantially depend on the prior-impact velocity as well as on the material of colliding elements (Jankowski 2010). The general trend for the typical building materials, such as: steel, concrete, timber and ceramic, shows a decrease in the coefficient of restitution as the prior impact velocity increases (see Fig. 2.2).

The value of the coefficient of restitution for colliding elements made of two different materials can be determined from the following formula (Goldsmith 1960):

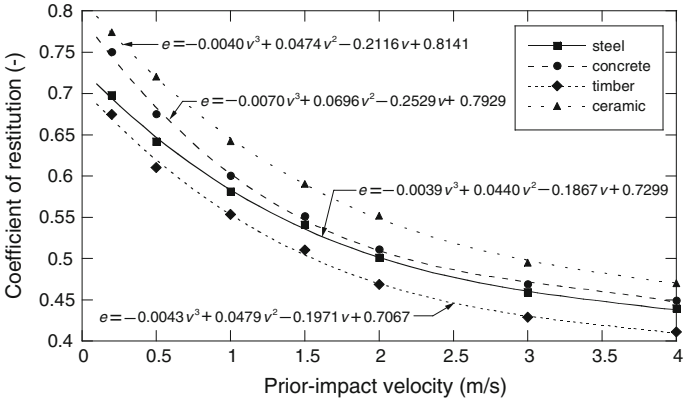

Fig. 2.2 Coefficient of restitution with respect to the prior-impact velocity (Jankowski 2010)

$$e = \frac{e_1 E_2 + e_2 E_1}{E_1 + E_2} \tag{2.4}$$

where e_i, E_i are the coefficient of restitution and modulus of elasticity for material i ($i = 1, 2$), respectively.

The use of the classical theory of impact is recommended for predicting the global effects on colliding bodies (Goldsmith 1960). However, its use in the analysis of earthquake-induced structural pounding is actually limited to the cases of collisions between only two structures which are modelled as lumped mass single-degree-of-freedom (SDOF) systems (see, for example, Ruangrassamee and Kawashima 2001). This limitation results from the fact that the approach does not consider stresses and deformations in the colliding structural elements during impact (it is assumed that contact lasts negligibly short time) and the behaviour of structures during impact is not obtained. Therefore, the approach is not recommended when structures are modelled as multi-degree-of freedom systems or when the study on pounding of buildings in series, or between several segments of a bridge, is conducted. In such cases, the structural response during the whole time of contact is important, since collision between other structural elements might take place at the same time. It is also possible that when two structural elements rebound after collision they might come into contact with other elements.

2.2 Models of Pounding Force During Collision Between Structures

The second approach, which has been applied to model structural pounding during earthquakes, is to use directly the model of impact force during contact (force-based models). The experimental results (see Goland 1955; Goldsmith 1960;

Van Mier et al. 1991; Jankowski 2010) show that the impact force history depends substantially on a number of factors, such as masses of colliding structures, contact surface geometry, material properties, relative prior-impact velocity, structural material properties and even history of previous impacts.

The pounding force time history during impact consists of two phases (periods). The approach period starts at the beginning of contact and lasts till the peak deformation. It is followed by a restitution period which is finished at the moment of separation. The results of experiments indicate (see Goldsmith 1960; Jankowski 2010) that, at the beginning of the approach period, colliding elements are within the elastic range but, later on, plastic deformations, local cracking or crushing usually take place. On the other hand, the accumulated elastic strain energy is released without major plastic effects in the second phase of impact, i.e. during the restitution period. It has been observed that majority of the energy dissipated during impact is lost during the approach period of collision, while relatively small amount of energy is dissipated during the restitution period (Goldsmith 1960). Moreover, the experimental results show that during the approach period, a rapid increase in the pounding force is usually observed, whereas, during the restitution period, the force decreases with a lower rate, which is often reduced even further just before the separation (see Fig. 2.3a). It has also been observed that the relation between pounding force and deformation is non-linear with larger increase in values of pounding force for larger deformations (see Fig. 2.3b).

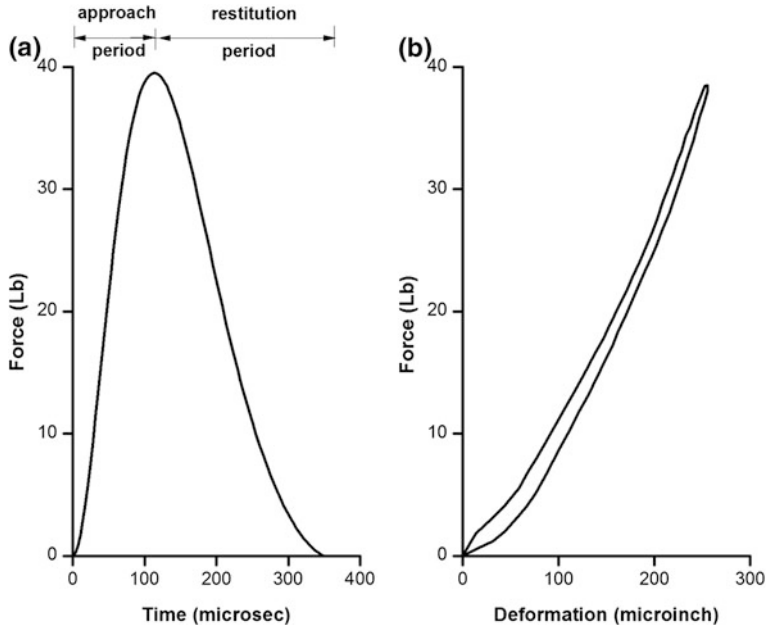

Fig. 2.3 Example of pounding force diagrams obtained from experiments: **a** pounding force time history; **b** relation between pounding force and deformation (after Crook 1952 and Goldsmith 1960)

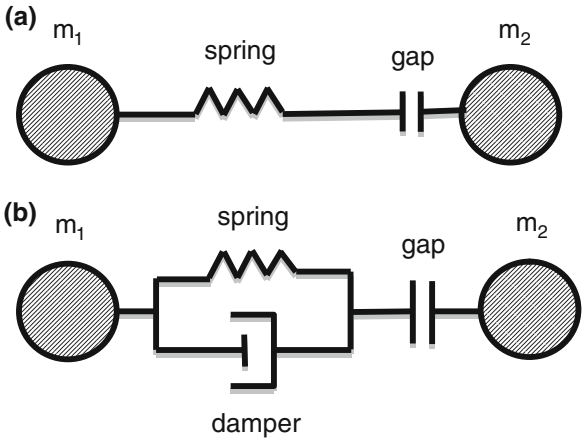

Fig. 2.4 Equivalent force-based models of pounding: **a** with only spring; **b** with spring and damper

The pounding force between structures is usually simulated by the use of elastic or viscoelastic impact elements, which become active when contact starts, i.e. when the gap between elements is reduced to zero (see Fig. 2.4). Several types of such elements have been employed by researchers to model the phenomenon.

2.2.1 Linear Elastic Model

The basic impact element consists of a simple linear elastic spring (see Maison and Kasai 1990, 1992; Filiatrault et al. 1995; Zanardo et al. 2002; Kim and Shinozuka 2003; Karayannis and Favvata 2005). The pounding force during impact, $F(t)$, for this model is expressed as:

$$F(t) = k\delta(t) \tag{2.5}$$

where $\delta(t)$ is the deformation of colliding structural elements and k denotes the impact element's stiffness which accounts for the local stiffness at the contact location. The major drawback of the linear elastic model is that it does not account for the energy dissipation during collision.

2.2.2 Linear Viscoelastic Model

The lack of energy dissipation properties is overcame in the linear viscoelastic model (Kelvin-Voigt model), in which the impact element consists of a linear spring with addition of linear damper (Wolf and Skrikerud 1980; Anagnostopoulos 1988, 1995, 1996; Anagnostopoulos and Spiliopoulos 1992; Jankowski et al. 1998; Zhu et al. 2002; Pekau and Zhu 2006; Komodromos et al. 2007; Polycarpou and

Komodromos 2010). The pounding force during impact, $F(t)$, for the linear viscoelastic model is expressed as:

$$F(t) = k\delta(t) + c\dot{\delta}(t) \tag{2.6}$$

where $\dot{\delta}(t)$ describes the relative velocity between colliding structural elements and c is the impact element's damping, which can be calculated based on the formula (Anagnostopoulos 1988, 2004):

$$c = 2\xi\sqrt{k\frac{m_1 m_2}{m_1 + m_2}} \tag{2.7}$$

in which ξ denotes the damping ratio related to the coefficient of restitution, e, by the following relation (Anagnostopoulos 2004):

$$\xi = \frac{-\ln e}{\sqrt{\pi^2 + (\ln e)^2}} \tag{2.8}$$

A shortcoming of the linear spring-damper element is a negative impact force observed just before separation which does not have a physical explanation (Goldsmith 1960; Hunt and Crossley 1975; Marhefka and Orin 1999). This effect is related to the fact that the viscous component is active during the whole time of the restitution period [see Eq. (2.6)]. Moreover, the activation of the viscous component with the same damping coefficient during the approach and restitution period results in a uniform dissipation of energy during the whole time of collision, which is also not fully consistent with the reality (Goldsmith 1960; Valles and Reinhorn 1996, 1997). As described before, most of the energy is lost during the approach period and in the second phase of impact, i.e. in the restitution period, the accumulated elastic strain energy is released with only minor energy dissipation. Nevertheless, due to its simplicity, the linear viscoelastic model has been widely and successfully used in a number of analyses of earthquake-induced structural pounding.

2.2.3 Modified Linear Viscoelastic Model

In order to eliminate the sticky tensile force that appears just before separation of colliding structures in the case of the linear viscoelastic model, a modified version of the model, in which the damping term is activated only during the approach period of collision, was proposed (Mahmoud and Jankowski 2011). The pounding force during impact, $F(t)$, for this model is defined as:

$$\begin{aligned} F(t) &= k\delta(t) + c\dot{\delta}(t) \quad \text{for } \dot{\delta}(t) > 0 \text{ (approach period)} \\ F(t) &= k\delta(t) \quad\quad\quad\quad\quad \text{for } \dot{\delta}(t) \leq 0 \text{ (restitution period)} \end{aligned} \tag{2.9}$$

where the impact element's damping, c, is defined by Eq. (2.7). However, the relation between the impact damping ratio and the coefficient of restitution from Eq. (2.8) is no longer valid and, in order to satisfy the relation between the post-impact and the prior-impact relative velocities [see Eq. (2.2)], the following relation has been determined (see Mahmoud and Jankowski 2011):

$$\xi = \frac{1 - e^2}{e(e(\pi - 2) + 2)} \tag{2.10}$$

2.2.4 Hertz Non-linear Elastic Model

In order to model the pounding force-deformation relation more realistically (see Fig. 2.3b), a non-linear elastic spring following the Hertz law of contact (Hertz 1882) has been used in a number of studies (Jing and Young 1991; Davis 1992; Pantelides and Ma 1998; Chau and Wei 2001). The pounding force during impact, $F(t)$, for the Hertz non-linear elastic model is expressed as:

$$F(t) = \beta \delta^{\frac{3}{2}}(t) \tag{2.11}$$

where β is the impact stiffness parameter which depends on material properties and geometry of colliding bodies. A wide range of impact stiffness parameters for collisions between concrete elements has been determined by Van Mier et al. (1991) based on the results of experiments. It has been verified that the impact stiffness parameters for steel-to-steel collisions take even higher values (Goldsmith 1960; Chau et al. 2003). Goldsmith (1960) described simplified formulae to calculate the impact stiffness parameters for certain shapes of colliding bodies. For example, the impact stiffness parameter for collisions between two spheres can be calculated as:

$$\beta = \frac{4}{3\pi(h_1 + h_2)} \sqrt{\frac{R_1 R_2}{R_1 + R_2}} \tag{2.12}$$

where R_i, $(i = 1, 2)$ is a radius of the colliding body with mass m_i, and h_i is defined as (Goldsmith 1960):

$$h_i = \frac{1 - \nu_i^2}{\pi E_i} \tag{2.13}$$

where ν_i stands for the Poisson's ratio and E_i denotes the Young's modulus of the material. When $R_2 \to \infty$, i.e. when the second body becomes a massive plane surface, the impact stiffness parameter, β, is defined as (Goldsmith 1960):

$$\beta = \frac{4}{3\pi(h_1 + h_2)}\sqrt{R_1} \tag{2.14}$$

The disadvantage of the Hertz contact law model is that it is fully elastic and does not account for the energy dissipation during contact due to plastic deformations, local cracking, friction, etc.

2.2.5 Hertzdamp Non-linear Model

Although the non-linear Hertz model effectively captures the relation between pounding force and deformation, its drawback, related to the fact that it does not account for the dissipated energy during collisions, causes serious problems. Therefore, the Hertzdamp model was considered to study the pounding phenomenon in the field of earthquake engineering (see Muthukumar and DesRoches 2006; Ye et al. 2009). The energy loss during impact is taken into account by adding non-linear damping to the Hertz model (see Lankarani and Nikravesh 1990, 1994). The pounding force during impact, $F(t)$, for the Hertzdamp non-linear model is expressed as (Lankarani and Nikravesh 1990, 1994; Muthukumar and DesRoches 2006):

$$F(t) = \beta\delta^{\frac{3}{2}}(t)\left[1 + \frac{3(1-e^2)}{4\left(\dot{x}_1^0 - \dot{x}_2^0\right)}\dot{\delta}(t)\right] \tag{2.15}$$

2.2.6 Non-linear Viscoelastic Model

Disadvantage of the non-linear Hertz model is also overcome in the non-linear viscoelastic model (see Jankowski 2005a, b, 2006b, 2007a, 2008; Mahmoud and Jankowski 2009, 2010; Mahmoud et al. 2012, 2013; Sołtysik and Jankowski 2013), in which the non-linear spring, following the Hertz law of contact, is applied together with the non-linear damper activated during the approach period of collision. This approach allows us to simulate more accurately the process of energy dissipation, which takes place mainly during that period (Goldsmith 1960). The pounding force during impact, $F(t)$, for the non-linear viscoelastic model is expressed as (Jankowski 2005b):

$$\begin{aligned} F(t) &= \bar{\beta}\delta^{\frac{3}{2}}(t) + \bar{c}(t)\dot{\delta}(t) \quad \text{for } \dot{\delta}(t) > 0 \text{ (approach period)} \\ F(t) &= \bar{\beta}\delta^{\frac{3}{2}}(t) \quad \text{for } \dot{\delta}(t) \leq 0 \text{ (restitution period)} \end{aligned} \tag{2.16}$$

where $\bar{\beta}$ is the impact stiffness parameter and $\bar{c}(t)$ is the impact element's damping, which can be obtained from the formula (Jankowski 2005b):

$$\bar{c}(t) = 2\bar{\xi}\sqrt{\bar{\beta}\sqrt{\delta(t)}\frac{m_1 m_2}{m_1 + m_2}} \tag{2.17}$$

where $\bar{\xi}$ denotes the damping ratio related to the coefficient of restitution, e (Jankowski 2006a):

$$\bar{\xi} = \frac{9\sqrt{5}}{2}\frac{1 - e^2}{e(e(9\pi - 16) + 16)} \tag{2.18}$$

2.3 Experimental Verification of the Effectiveness of Pounding Force Models

For the purposes of verification the accuracy of different models of structural pounding, the results of the numerical analyses have been compared with the results of the experimental studies conducted for various types of colliding elements (see also Jankowski 2005b; Mahmoud et al. 2008). The values of the impact stiffness parameters: k, β and $\bar{\beta}$, defining the models used in the numerical analysis, have been determined through iterative procedure so as to equalize the peak pounding force determined from the simulations with the peak pounding force obtained from the experiment. The difference between the experimental results and the results from the numerical analysis has been assessed by calculating the normalized root mean square (RMS) error (see Bendat and Piersol 1971):

$$RMSE = \frac{\sqrt{\sum_{i=1}^{NV}(H_i - \bar{H}_i)^2}}{\sqrt{\sum_{i=1}^{NV} H_i^2}} \cdot 100\,\% \tag{2.19}$$

where H_i, $\bar{H}_i$ are the values from the time history record obtained from the experiment and from the numerical analysis, respectively; and NV denotes a number of values in these history records. In the numerical analysis concerning examples presented in this chapter, the time-stepping Newmark method (Newmark 1959), with the standard parameters: $\gamma_N = 0.5$ and $\beta_N = 0.25$ assuring the stability and accuracy of the results (see Bathe 1982; Chopra 1995), has been applied to determine the structural response.

2.3.1 Impact Between a Ball Falling Onto a Rigid Surface

In this section, the results of the numerical analysis are compared with the results of impact experiment conducted by dropping steel, concrete and timber balls of different masses onto a rigid surface (compare also Jankowski 2010). Balls have been

Table 2.1 Properties of balls used in the impact experiment

Material	Ball diameter (mm)	Ball mass (kg)
Steel (type 18G2A)	21	0.053–0.054
	50	0.538–0.541
	83	2.013
Concrete (grade C30/37)	103	1.329–1.350
	114	1.763–1.835
	128	2.531–2.636
Timber (pinewood)	55	0.065–0.066
	71	0.109–0.112
	118	0.493–0.497

dropped from various height levels in order to obtain different impact velocities. The properties of balls used in the experiment are specified in Table 2.1. B&K type 4344 accelerometer attached to the ball was used to measure the force time histories during impacts. System PULSE was applied for measuring and data acquisition purposes. The experimental setup is shown in Fig. 2.5.

Fig. 2.5 Setup of the impact experiment

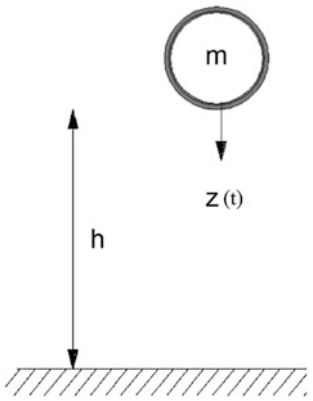

Fig. 2.6 Model of a ball falling onto a rigid surface

In the numerical analysis, the model of a ball falling onto a rigid surface, shown in Fig. 2.6, has been used. The dynamic equation of motion for such a model can be expressed as (Jankowski 2005b):

$$m\ddot{z}(t) + F(t) = mg \tag{2.20}$$

where m is mass of a ball, $\ddot{z}(t)$ its vertical acceleration, g stands for the acceleration of gravity and $F(t)$ is the pounding force, which is equal to zero when $z(t) \leq h$ (h is a drop height) and is defined by Eqs. (2.5), (2.6), (2.9), (2.11), (2.15) and (2.16) when $z(t) > h$, where deformation $\delta(t)$ is expressed as:

$$\delta(t) = z(t) - h \tag{2.21}$$

2.3.1.1 Impact Between Steel Elements

In the first example, the results of the numerical analysis are compared with the results of the experiment conducted for a steel ball of mass 2.013 kg impacting the steel surface with the velocity of 0.92 m/s. The following values of parameters defining different pounding force models have been used in the numerical analysis: $k = 3.45 \times 10^8$ N/m for the linear elastic model, $k = 4.82 \times 10^8$ N/m, $\xi = 0.17$ ($e = 0.58$) for the linear viscoelastic model, $k = 5.03 \times 10^8$ N/m, $\xi = 0.43$ ($e = 0.58$) for the modified linear viscoelastic model, $\beta = 2.94 \times 10^{10}$ N/m$^{3/2}$ for the Hertz non-linear elastic model, $\beta = 3.76 \times 10^{10}$ N/m$^{3/2}$, $e = 0.58$ for the Hertz-damp non-linear model and $\bar{\beta} = 6.60 \times 10^{10}$ N/m$^{3/2}$, $\bar{\xi} = 0.49$ ($e = 0.58$) for the non-linear viscoelastic model. The time-stepping Newmark method with constant time step $\Delta t = 1 \times 10^{-6}$ s has been used to solve the equation of motion (2.20) numerically. The pounding force time history measured during the experiment and the histories received from the numerical analysis, for the considered example of

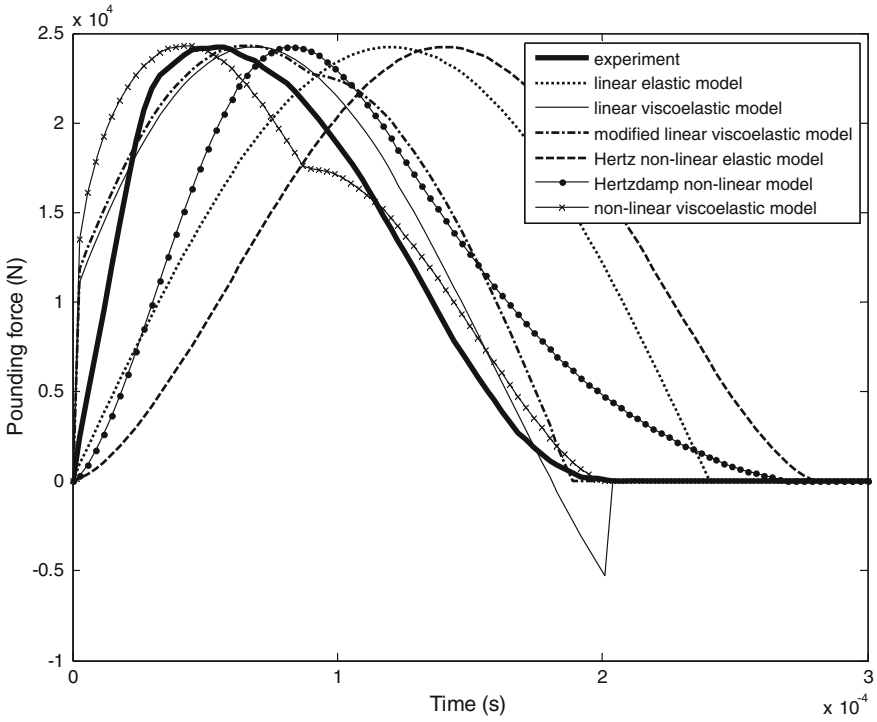

Fig. 2.7 Pounding force time histories for impact between steel elements

impact between steel elements, are presented in Fig. 2.7. Using Eq. (2.19), the RMS errors for pounding force histories have been calculated as equal to: 72.3 % for the linear elastic model, 18.6 % for the linear viscoelastic model, 26.5 % for the modified linear viscoelastic model, 93.1 % for the Hertz non-linear elastic model, 39.1 % for the Hertzdamp non-linear model and 21.9 % for the non-linear viscoelastic model.

2.3.1.2 Impact Between Concrete Elements

The second example concerns the comparison between the results of the numerical simulations and the experiment conducted for a concrete ball of mass 1.763 kg impacting the concrete surface with the velocity of 0.13 m/s. In the numerical analysis, the following values of parameters, defining different pounding force models, have been used: $k = 4.33 \times 10^7$ N/m for the linear elastic model, $k = 4.91 \times 10^7$ N/m, $\xi = 0.09$ $(e = 0.76)$ for the linear viscoelastic model, $k = 5.47 \times 10^7$ N/m, $\xi = 0.19$ $(e = 0.76)$ for the modified linear viscoelastic model, $\beta = 5.92 \times 10^9$ N/m$^{3/2}$ for the Hertz non-linear elastic model, $\beta = 6.39 \times 10^9$ N/m$^{3/2}$, $e = 0.76$ for the

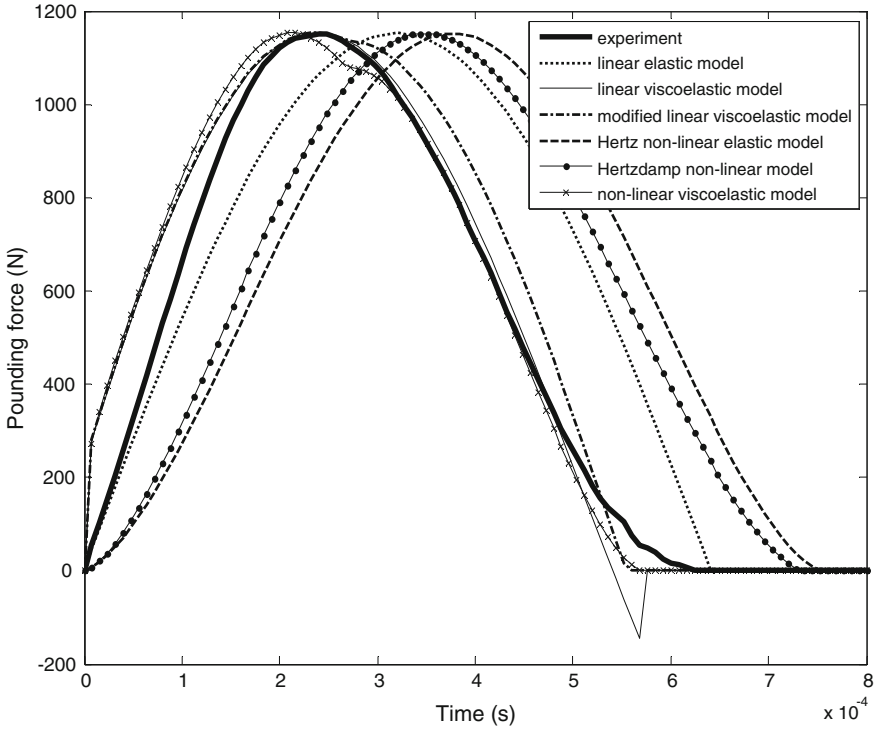

Fig. 2.8 Pounding force time histories for impact between concrete elements

Hertzdamp non-linear model and $\bar{\beta} = 1.02 \times 10^{10}$ N/m$^{3/2}$, $\bar{\xi} = 0.22$ ($e = 0.76$) for the non-linear viscoelastic model. The time-stepping Newmark method with constant time step $\Delta t = 1 \times 10^{-5}$ s has been used to solve the equation of motion (2.20) numerically. The pounding force time history measured during the experiment and the histories received from the numerical analysis, for the considered example of impact between concrete elements, are presented in Fig. 2.8. The RMS errors for these pounding force time histories have been calculated as equal to: 36.1 % for the linear elastic model, 12.7 % for the linear viscoelastic model, 15.7 % for the modified linear viscoelastic model, 59.3 % for the Hertz non-linear elastic model, 49.4 % for the Hertzdamp non-linear model and 11.9 % for the non-linear viscoelastic model.

2.3.1.3 Impact Between Timber Elements

In the third example, the results of the numerical analysis are compared with the results of the experiment conducted for a timber ball of mass 0.109 kg impacting the timber surface with the velocity of 0.39 m/s. The following values of parameters, defining different pounding force models, have been used in the numerical

analysis: $k = 1.83 \times 10^6$ N/m for the linear elastic model, $k = 2.28 \times 10^6$ N/m, $\xi = 0.16$ $(e = 0.61)$ for the linear viscoelastic model, $k = 2.62 \times 10^6$ N/m, $\xi = 0.38$ $(e = 0.61)$ for the modified linear viscoelastic model, $\beta = 1.33 \times 10^8$ N/m$^{3/2}$ for the Hertz non-linear elastic model, $\beta = 1.66 \times 10^8$ N/m$^{3/2}$, $e = 0.61$ for the Hertzdamp non-linear model and $\bar{\beta} = 3.11 \times 10^8$ N/m$^{3/2}$, $\bar{\xi} = 0.43$ $(e = 0.61)$ for the non-linear viscoelastic model. The time-stepping Newmark method with constant time step $\Delta t = 1 \times 10^{-5}$ s has been used to solve the equation of motion (2.20) numerically. The pounding force time history measured during the experiment and the histories received from the numerical analysis, for the considered example of impact between timber elements, are presented in Fig. 2.9. Using Eq. (2.19), the RMS errors for pounding force histories have been calculated as equal to: 64.3 % for the linear elastic model, 20.7 % for the linear viscoelastic model, 26.6 % for the modified linear viscoelastic model, 85.8 % for the Hertz non-linear elastic model, 53.6 % for the Hertzdamp non-linear model and 20.8 % for the non-linear viscoelastic model.

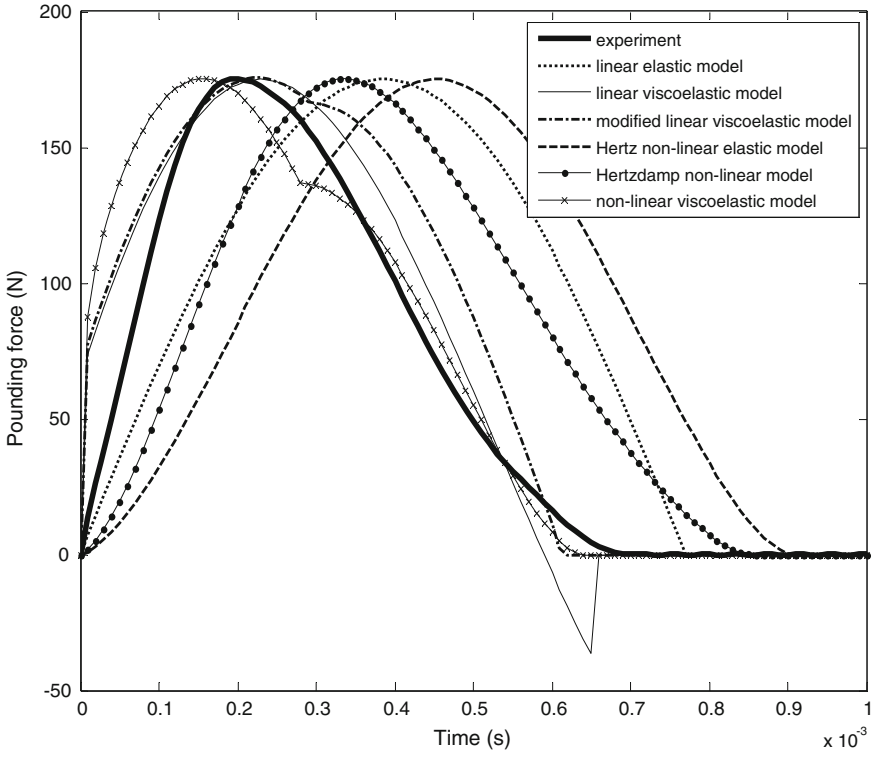

Fig. 2.9 Pounding force time histories for impact between timber elements

Fig. 2.10 Setup of the shaking table experiment

2.3.2 Pounding Between Models of Tower Structures

In this section, the results of the numerical analysis are compared with the results of the shaking table experiment focused on pounding between two tower models with different impacting materials (compare also Jankowski 2007b, 2010). Two 1 m high tower models (see Fig. 2.10) with different dynamic properties were built to be tested during the experiment. The columns were arranged in a rectangular pattern with a spacing of 0.22 m along the shaking direction (longitudinal one) and a spacing of 0.3 m along the orthogonal (transverse) direction (compare also Falborski and Jankowski 2013). All supporting elements used in the left tower model had a rectangular cross section with dimensions: 6 × 6 mm, whereas the model of the right tower was constructed of members with a section of 8 × 8 mm. The total mass of the supporting columns with horizontal connections and additional bracings was equal to $m_{c1} = 2.258$ kg for the left tower model and $m_{c2} = 3.864$ kg for the right one. Elements of external dimensions 0.25 × 0.25 × 0.05 m made of different building materials, i.e. steel, concrete and timber (see Figs. 2.11 and 2.12), were fixed at the top of each tower. With the help of additional masses in the form of plates and bolts (see Figs. 2.11 and 2.12), the top mass of the tower models was kept constant for all experimental tests, apart from the material used, and was equal to $m_{t1} = 9.485$ kg for the left tower model and $m_{t2} = 18.337$ kg for the right one. Based on the free

Fig. 2.11 Top view of the left tower with impacting elements (made of steel, concrete and timber) and additional masses

Fig. 2.12 Top view of the right tower with impacting elements (made of steel, concrete and timber) and additional masses

vibration tests, the following dynamic parameters have been determined for both tower models: $f_1 = 2.59$ Hz, $\xi_{S1} = 0.004$, $f_2 = 2.99$ Hz, $\xi_{S2} = 0.01$, where f_i, ξ_{Si} $(i = 1, 2)$ are the natural frequency and the structural damping ratio, respectively. The initial gap size of $d = 0.04$ m between the towers has been considered in the study. The tower models have been excited in the horizontal direction by the NS component of the El Centro earthquake (18.05.1940). Two ENDEVCO type 7752 accelerometers, which were attached to the tower models at their top (see Fig. 2.10), were used to measure the time histories during the ground motion.

In the numerical analysis, a model, in which both towers are simulated as SDOF systems, as shown in Fig. 2.13, has been used. The dynamic equation of motion for such a model can be written as (Jankowski 2005b):

$$\begin{bmatrix} m_1 & 0 \\ 0 & m_2 \end{bmatrix} \begin{bmatrix} \ddot{x}_1(t) \\ \ddot{x}_2(t) \end{bmatrix} + \begin{bmatrix} C_1 & 0 \\ 0 & C_2 \end{bmatrix} \begin{bmatrix} \dot{x}_1(t) \\ \dot{x}_2(t) \end{bmatrix} + \begin{bmatrix} K_1 & 0 \\ 0 & K_2 \end{bmatrix} \begin{bmatrix} x_1(t) \\ x_2(t) \end{bmatrix} + \begin{bmatrix} F(t) \\ -F(t) \end{bmatrix} = -\begin{bmatrix} m_1 & 0 \\ 0 & m_2 \end{bmatrix} \begin{bmatrix} \ddot{x}_g(t) \\ \ddot{x}_g(t) \end{bmatrix} \tag{2.22}$$

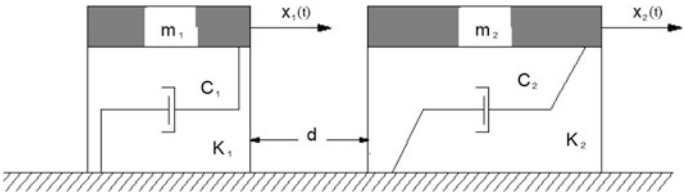

Fig. 2.13 Model of two colliding SDOF systems

where $x_i(t)$, $\dot{x}_i(t)$, $\ddot{x}_i(t)$ are the horizontal displacement, velocity and acceleration of tower i ($i = 1, 2$), respectively, $K_i = 4\pi^2 f_i^2 m_i$, $C_i = 2\xi_{Si}\sqrt{K_i m_i}$ denote stiffness and damping coefficients, $\ddot{x}_g(t)$ stands for the acceleration of input ground motion and $F(t)$ is the pounding force, which is equal to zero when $\delta(t) \leq 0$ and is defined by Eqs. (2.5), (2.6), (2.9), (2.11), (2.15) and (2.16) if $\delta(t) > 0$, where deformation $\delta(t)$ is defined as:

$$\delta(t) = x_1(t) - x_2(t) - d \tag{2.23}$$

The following mass values: $m_1 = 10.004$ kg, $m_2 = 19.226$ kg have been applied in the numerical analysis, as calculated from the formula (Harris and Piersol 2002):

$$m_i = m_{ti} + 0.23 m_{ci} \quad (i = 1, 2) \tag{2.24}$$

In order to solve the equation of motion (2.22) numerically, the time-stepping Newmark method with constant time step $\Delta t = 0.002$ s has been used.

2.3.2.1 Pounding Between Steel Elements

The first example shows a comparison between the results of the numerical analysis and the experiment conducted for pounding of tower models with impacting steel elements (steel type 18G2A). The following values of parameters of different pounding force models have been applied in the numerical analysis: $k = 5.67 \times 10^7$ N/m for the linear elastic model, $k = 7.93 \times 10^7$ N/m, $\xi = 0.12$ ($e = 0.68$) for the linear viscoelastic model, $k = 8.54 \times 10^7$ N/m, $e = 0.68$ for the modified linear viscoelastic model, $\beta = 3.94 \times 10^9$ N/m$^{3/2}$ for the Hertz non-linear elastic model, $\beta = 5.14 \times 10^9$ N/m$^{3/2}$, $e = 0.68$ for the Hertzdamp non-linear model and $\bar{\beta} = 8.32 \times 10^9$ N/m$^{3/2}$, $\bar{\xi} = 0.31$ ($e = 0.68$) for the non-linear viscoelastic model. The displacement time history of the left tower model (lighter and more flexible one) obtained from the experiment and the histories received from the numerical analysis are shown in Fig. 2.14. Using Eq. (2.19), the RMS errors for the time histories have been calculated as equal to: 28.7 % for the linear elastic model,

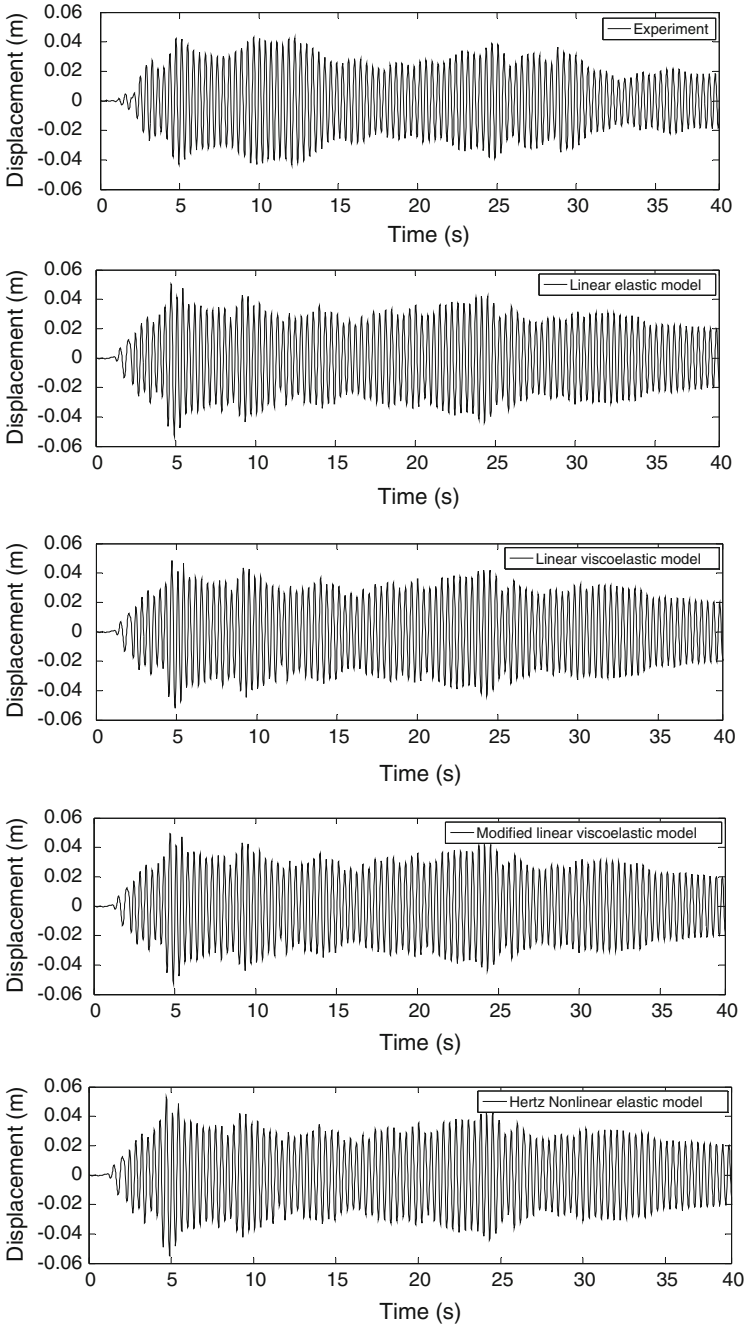

Fig. 2.14 Displacement time histories of the left tower model for pounding between steel elements under the El Centro earthquake

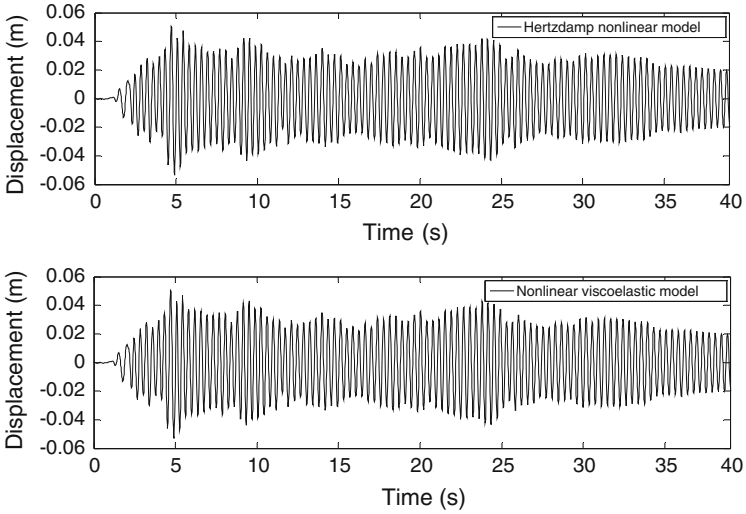

Fig. 2.14 (continued)

23.2 % for the linear viscoelastic model, 24.3 % for the modified linear viscoelastic model, 22.9 % for the Hertz non-linear elastic model, 22.5 % for the Hertzdamp non-linear model and 22.6 % for the non-linear viscoelastic model.

2.3.2.2 Pounding Between Concrete Elements

In this example, the results of the numerical analysis are compared with the results of the experiment conducted for pounding of tower models with impacting concrete elements (concrete grade C30/37). In the numerical analysis, the following values of parameters, defining different pounding force models, have been used: $k = 1.87 \times 10^7$ N/m for the linear elastic model, $k = 2.05 \times 10^7$ N/m, $\xi = 0.14$ $(e = 0.65)$ for the linear viscoelastic model, $k = 2.36 \times 10^7$ N/m, $e = 0.65$ for the modified linear viscoelastic model, $\beta = 9.75 \times 10^8$ N/m$^{3/2}$ for the Hertz non-linear elastic model, $\beta = 1.17 \times 10^9$ N/m$^{3/2}$, $e = 0.65$ for the Hertzdamp non-linear model and $\bar{\beta} = 2.53 \times 10^9$ N/m$^{3/2}$, $\bar{\xi} = 0.35$ $(e = 0.65)$ for the non-linear viscoelastic model. The displacement time history of the left tower model obtained from the experiment and the histories received from the numerical analysis are shown in Fig. 2.15. The RMS errors for these time histories have been calculated using Eq. (2.19) as equal to: 22.6 % for the linear elastic model, 15.3 % for the linear viscoelastic model, 18.7 % for the modified linear viscoelastic model, 22.4 % for the Hertz non-linear elastic model, 16.3 % for the Hertzdamp non-linear model and 14.8 % for the non-linear viscoelastic model.

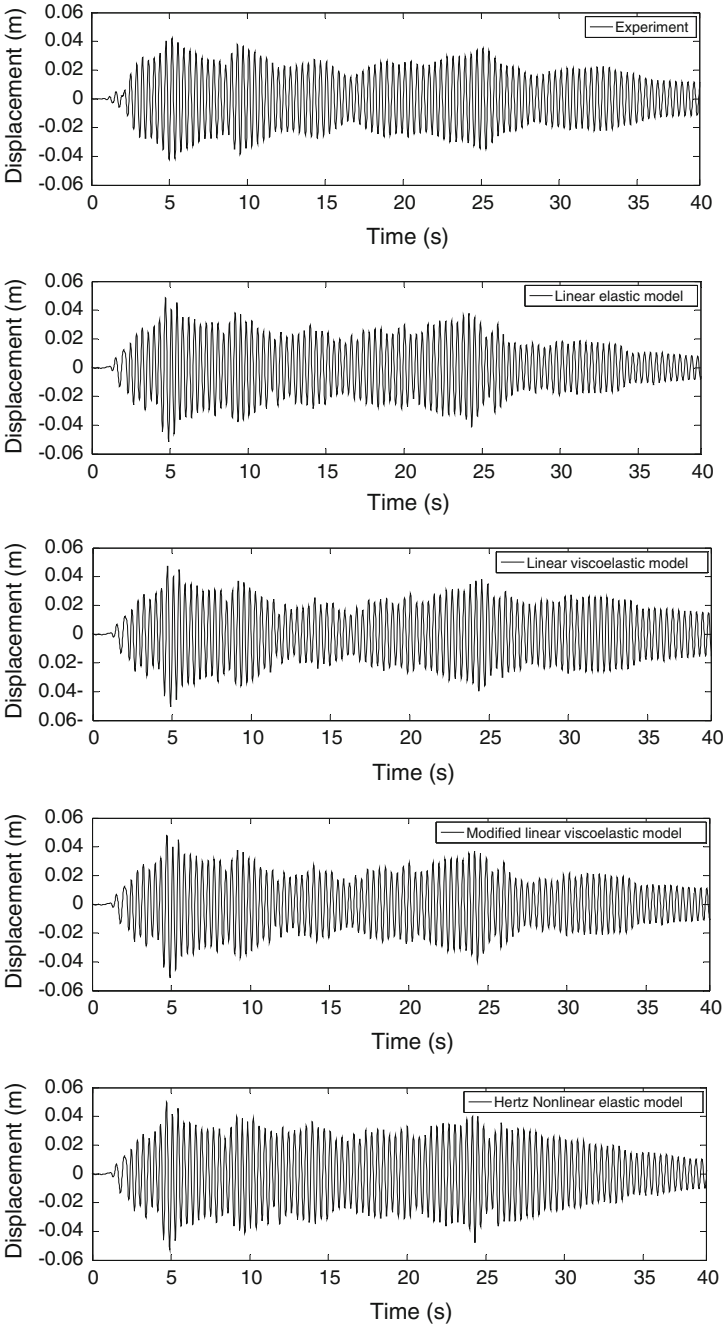

Fig. 2.15 Displacement time histories of the left tower model for pounding between concrete elements under the El Centro earthquake

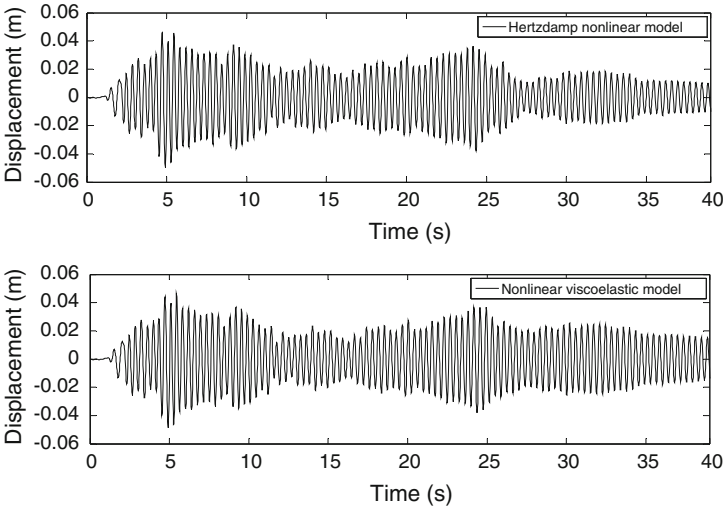

Fig. 2.15 (continued)

2.3.2.3 Pounding Between Timber Elements

The third example concerns a comparison between the results of the numerical analysis and the experiment conducted for pounding of tower models with impacting timber elements made of pinewood. The following values of parameters of different pounding force models have been applied in the numerical analysis: $k = 1.47 \times 10^6$ N/m for the linear elastic model, $k = 1.97 \times 10^6$ N/m, $\xi = 0.16$ $(e = 0.60)$ for the linear viscoelastic model, $k = 2.33 \times 10^6$ N/m, $e = 0.60$ for the modified linear viscoelastic model, $\beta = 1.50 \times 10^8$ N/m$^{3/2}$ for the Hertz non-linear elastic model, $\beta = 1.74 \times 10^8$ N/m$^{3/2}$, $e = 0.60$ for the Hertzdamp non-linear model and $\bar{\beta} = 2.85 \times 10^8$ N/m$^{3/2}$, $\bar{\xi} = 0.44$ $(e = 0.60)$ for the non-linear viscoelastic model. The displacement time history of the left tower model obtained from the experiment and the histories received from the numerical analysis are shown in Fig. 2.16. The RMS errors for these time histories have been calculated using Eq. (2.19) as equal to: 38.7 % for the linear elastic model, 25.2 % for the linear viscoelastic model, 27.6 % for the modified linear viscoelastic model, 43.8 % for the Hertz non-linear elastic model, 26.3 % for the Hertzdamp non-linear model and 24.8 % for the non-linear viscoelastic model.

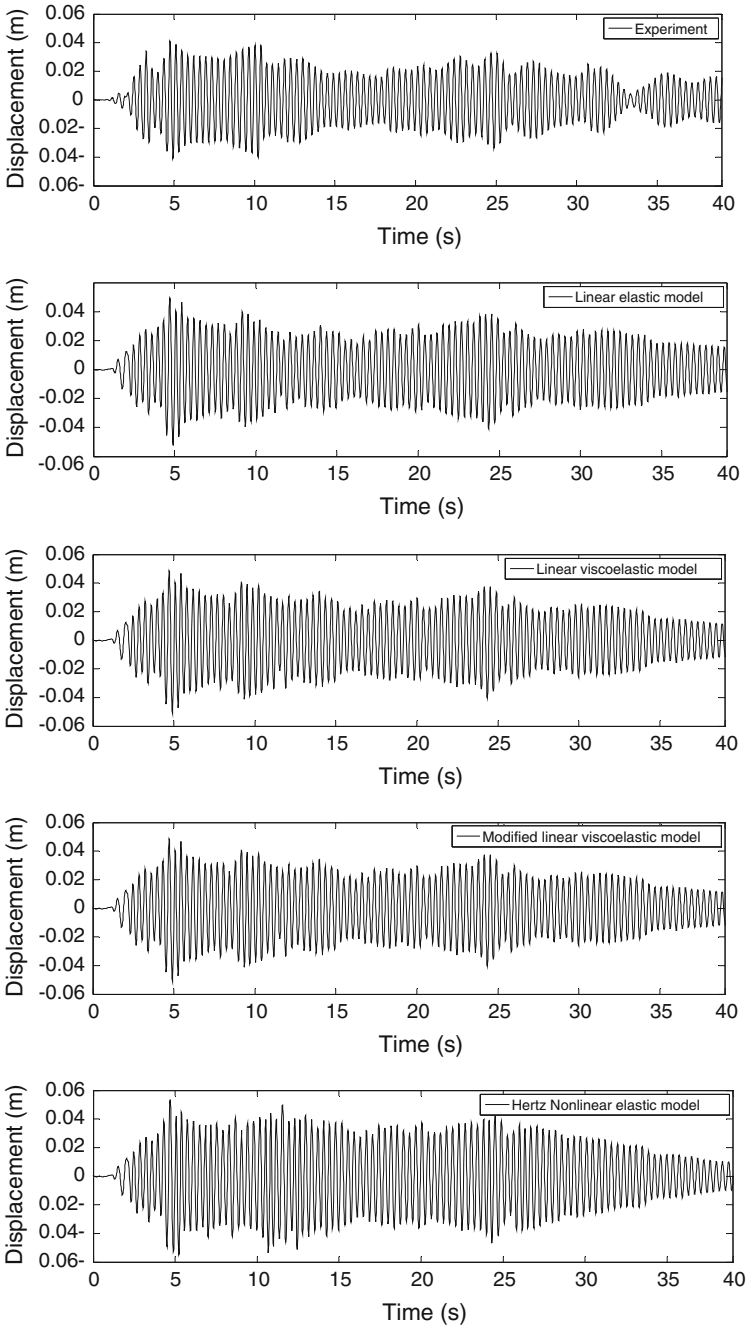

Fig. 2.16 Displacement time histories of the left tower model for pounding between timber elements under the El Centro earthquake

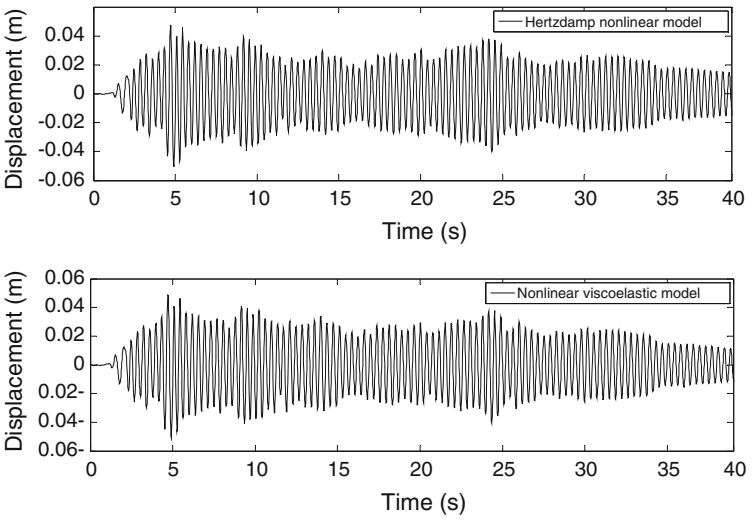

Fig. 2.16 (continued)

2.3.3 Conclusions

The results of the studies show that the linear viscoelastic and the non-linear viscoelastic models give the smallest errors in the pounding force time histories during single impact. In the case of the linear viscoelastic model, a negative impact force just before separation, which does not have a physical explanation, has been observed. However, the improvement introduced in the modified linear viscoelastic model, in order to overcome this drawback, does not really lead to the increase in the accuracy of the model.

Further analysis has shown that the application of the linear viscoelastic, the Hertzdamp and the non-linear viscoelastic models results in the smallest errors in the response time histories of the analysed examples of structural pounding under earthquake excitation. The impact force models have been found to have some advantages and disadvantages when used for modelling of structural pounding. The results of the study indicate that the efficiency of them depends on the type of analysis conducted.

References

Anagnostopoulos, S.A.: Pounding of buildings in series during earthquakes. Earthquake Eng. Struct. Dynam. **16**, 443–456 (1988)

Anagnostopoulos S.A.: Earthquake induced pounding: state of the art. In: Proceedings of 10th European Conference on Earthquake Engineering, Vienna, Austria, 28 Aug–2 Sept 1994. pp. 897–905, Balkema, Rotterdam (1995)

Anagnostopoulos, S.A.: Building pounding re-examined: how serious a problem is it? In: Eleventh World Conference on Earthquake Engineering, Acapulco, Mexico, Paper No. 2108, 23–28 June 1996

Anagnostopoulos, S.A.: Equivalent viscous damping for modeling inelastic impacts in earthquake pounding problems. Earthquake Eng. Struct. Dynam. **33**, 897–902 (2004)

Anagnostopoulos, S.A., Spiliopoulos, K.V.: An investigation of earthquake induced pounding between adjacent buildings. Earthquake Eng. Struct. Dynam. **21**, 289–302 (1992)

Azevedo, J., Bento, R.: Design criteria for buildings subjected to pounding. In: Eleventh World Conference on Earthquake Engineering, Acapulco, Mexico, Paper No. 1063, 23–28 June 1996

Bathe, K.J.: Finite Element Procedures in Engineering Analysis. Prentice-Hall, Englewood Cliffs (1982)

Bendat, J.S., Piersol, A.G.: Random Data: Analysis and Measurement Procedures. Wiley, New York (1971)

Chau, K.T., Wei, X.X.: Pounding of structures modelled as non-linear impacts of two oscillators. Earthquake Eng. Struct. Dynam. **30**, 633–651 (2001)

Chau, K.T., Wei, X.X., Guo, X., Shen, C.Y.: Experimental and theoretical simulations of seismic poundings between two adjacent structures. Earthquake Eng. Struct. Dynam. **32**, 537–554 (2003)

Chopra, A.K.: Dynamics of Structures: Theory and Applications to Earthquake Engineering. Prentice-Hall, Englewood Cliffs (1995)

Crook, A.W.: A study on some impacts between metal bodies by a piezoelectric method. Proc. Roy. Soc. A **212**, 377–390 (1952)

Davis, R.O.: Pounding of buildings modelled by an impact oscillator. Earthquake Eng. Struct. Dynam. **21**, 253–274 (1992)

DesRoches, R., Muthukumar, S.: Effect of pounding and restrainers on seismic response of multiple-frame bridges. J. Struct. Eng. **128**, 860–869 (2002)

Falborski, T., Jankowski, R.: Polymeric bearings—a new base isolation system to reduce structural damage during earthquakes. Key Eng. Mater. **569–570**, 143–150 (2013)

Filiatrault, A., Wagner, P., Cherry, S.: Analytical prediction of experimental building pounding. Earthquake Eng. Struct. Dynam. **24**, 1131–1154 (1995)

Goland, M., Wickersham, P.D., Dengler, M.A.: Propagation of elastic impact in beams in bending. J. Appl. Mech. **22**, 1–7 (1955)

Goldsmith, W.: Impact: The Theory and Physical Behaviour of Colliding Solids. Edward Arnold, London (1960)

Harris, C.M., Piersol, A.G.: Harris' Shock and Vibration Handbook. McGraw-Hill, New York (2002)

Hertz, H.: Über die Berührung fester elastischer Körper (On the contact of elastic solids). J. für die Reine und Angewandte Mathematik **29**, 156–171 (1882). (in German)

Hunt, K.H., Crossley, F.R.E.: Coefficient of restitution interpreted as damping in vibroimpact. J. Appl. Mech. ASME **42**, 440–445 (1975)

Jankowski, R.: Impact force spectrum for damage assessment of earthquake-induced structural pounding. Key Eng. Mater. **293–294**, 711–718 (2005a)

Jankowski, R.: Non-linear viscoelastic modelling of earthquake-induced structural pounding. Earthquake Eng. Struct. Dynam. **34**, 595–611 (2005b)

Jankowski, R.: Analytical expression between the impact damping ratio and the coefficient of restitution in the non-linear viscoelastic model of structural pounding. Earthquake Eng. Struct. Dynam. **35**, 517–524 (2006a)

Jankowski, R.: Pounding force response spectrum under earthquake excitation. Eng. Struct. **28**, 1149–1161 (2006b)

Jankowski, R.: Assessment of damage due to earthquake-induced pounding between the main building and the stairway tower. Key Eng. Mater. **347**, 339–344 (2007a)

Jankowski, R.: Non-linear analysis of pounding-involved response of equal height buildings under earthquake excitation. DSc dissertation, Wydawnictwo Politechniki Gdańskiej, Gdańsk, Poland (2007b)

Jankowski, R.: Earthquake-induced pounding between equal height buildings with substantially different dynamic properties. Eng. Struct. **30**(10), 2818–2829 (2008)

Jankowski, R.: Experimental study on earthquake-induced pounding between structural elements made of different building materials. Earthquake Eng. Struct. Dynam. **39**, 343–354 (2010)

Jankowski, R., Wilde, K., Fujino, Y.: Pounding of superstructure segments in isolated elevated bridge during earthquakes. Earthquake Eng. Struct. Dynam. **27**, 487–502 (1998)

Jing, H.-S., Young, M.: Impact interactions between two vibration systems under random excitation. Earthquake Eng. Struct. Dynam. **20**, 667–681 (1991)

Karayannis, C.G., Favvata, M.J.: Earthquake-induced interaction between adjacent reinforced concrete structures with non-equal heights. Earthquake Eng. Struct. Dynam. **34**, 1–20 (2005)

Kim, S.-H., Shinozuka, M.: Effects of seismically induced pounding at expansion joints of concrete bridges. J. Eng. Mech. **129**, 1225–1234 (2003)

Komodromos, P., Polycarpou, P.C., Papaloizou, L., Phocas, M.C.: Response of seismically isolated buildings considering poundings. Earthquake Eng. Struct. Dynam. **36**, 1605–1622 (2007)

Lankarani, H.M., Nikravesh, P.E.: A contact force model with hysteresis damping for impact analysis of multibody systems. J. Mech. Design ASME **112**, 369–376 (1990)

Lankarani, H.M., Nikravesh, P.E.: Continuous contact force models for impact analysis in multibody systems. Nonlinear Dyn. **5**, 193–207 (1994)

Leibovich, E., Rutenberg, A., Yankelevsky, D.Z.: On eccentric seismic pounding of symmetric buildings. Earthquake Eng. Struct. Dynam. **25**, 219–233 (1996)

Mahmoud, S., Abd-Elhamed, A., Jankowski, R.: Earthquake-induced pounding between equal height multi-storey buildings considering soil-structure interaction. Bull. Earthq. Eng. **11**(4), 1021–1048 (2013)

Mahmoud, S., Austrell, P.-E., Jankowski, R.: Simulation of the response of base-isolated buildings under earthquake excitations considering soil flexibility. Earthq. Eng. Eng. Vibr. **11**, 359–374 (2012)

Mahmoud, S., Chen, X., Jankowski, R.: Structural pounding models with Hertz spring and nonlinear damper. J. Appl. Sci. **8**, 1850–1858 (2008)

Mahmoud, S., Jankowski, R.: Elastic and inelastic multi-storey buildings under earthquake excitation with the effect of pounding. J. Appl. Sci. **9**(18), 3250–3262 (2009)

Mahmoud, S., Jankowski, R.: Pounding-involved response of isolated and non-isolated buildings under earthquake excitation. Earthq. Struct. **1**(3), 231–252 (2010)

Mahmoud, S., Jankowski, R.: Modified linear viscoelastic model of earthquake-induced structural pounding. Iran. J. Sci. Technol. **35**(C1), 51–62 (2011)

Maison, B.F., Kasai, K.: Analysis for type of structural pounding. J. Struct. Eng. **116**, 957–977 (1990)

Maison, B.F., Kasai, K.: Dynamics of pounding when two buildings collide. Earthquake Eng. Struct. Dynam. **21**, 771–786 (1992)

Marhefka, D.W., Orin, D.E.: A compliant contact model with nonlinear damping for simulation of robotic systems. IEEE Trans. Syst. Man Cyber. Part A Syst. Hum. **29**, 566–572 (1999)

Muthukumar, S., DesRoches, R.: A Hertz contact model with nonlinear damping for pounding simulation. Earthquake Eng. Struct. Dynam. **35**, 811–828 (2006)

Newmark, N.: A method of computation for structural dynamics. J. Eng. Mech. Div. ASCE **85**, 67–94 (1959)

Pantelides, C.P., Ma, X.: Linear and nonlinear pounding of structural systems. Comput. Struct. **66**, 79–92 (1998)

Papadrakakis, M., Mouzakis, H., Plevris, N., Bitzarakis, S.A.: Lagrange multiplier solution method for pounding of buildings during earthquakes. Earthquake Eng. Struct. Dynam. **20**, 981–998 (1991)

Pekau, O.A., Zhu, X.: Seismic behaviour of cracked concrete gravity dams. Earthquake Eng. Struct. Dynam. **35**, 477–495 (2006)

Polycarpou, P.C., Komodromos, P.: On poundings of a seismically isolated building with adjacent structures during strong earthquakes. Earthquake Eng. Struct. Dynam. **39**, 933–940 (2010)

Ruangrassamee, A., Kawashima, K.: Relative displacement response spectra with pounding effect. Earthquake Eng. Struct. Dynam. **30**, 1511–1538 (2001)

Sołtysik, B., Jankowski, R.: Non-linear strain rate analysis of earthquake-induced pounding between steel buildings. Int. J. Earth Sci. Eng. **6**, 429–433 (2013)

Van Mier, J.G.M., Pruijssers, A.F., Reinhardt, H.W., Monnier, T.: Load-time response of colliding concrete bodies. J. Struct. Eng. **117**, 354–374 (1991)

Valles, R.E., Reinhorn, A.M.: Evaluation, prevention and mitigation of pounding effects in building structures. In Eleventh World Conference on Earthquake Engineering, Acapulco, Mexico, Paper No. 26. 23–28 June 1996

Valles, R.E., Reinhorn, A.M.: Evaluation, prevention and mitigation of pounding effects in building structures. Technical Report NCEER-97-0001. National Center for Earthquake Engineering Research, State University of New York, Buffalo, USA (1997)

Wolf, J.P., Skrikerud, P.E.: Mutual pounding of adjacent structures during earthquakes. Nucl. Eng. Des. **57**, 253–275 (1980)

Ye, K., Li, L., Zhu, H.: A note on the Hertz contact model with nonlinear damping for pounding simulation. Earthquake Eng. Struct. Dynam. **38**, 1135–1142 (2009)

Zanardo, G., Hao, H., Modena, C.: Seismic response of multi-span simply supported bridges to a spatially varying earthquake ground motion. Earthquake Eng. Struct. Dynam. **31**, 1325–1345 (2002)

Zhu, P., Abe, M., Fujino, Y.: Modelling three-dimensional non-linear seismic performance of elevated bridges with emphasis on pounding of girders. Earthquake Eng. Struct. Dynam. **31**, 1891–1913 (2002)

Chapter 3
Pounding Between Buildings

Different structural models can be used to simulate the behaviour of colliding buildings under earthquake excitations. The basic analysis is often conducted using lumped mass single-degree-of-freedom (SDOF) systems as models of structures. Anagnostopoulos (1988) used such models to carry out fundamental study on pounding between adjacent buildings in series. Davis (1992) incorporated a SDOF system to analyze pounding of a building against an infinitely rigid neighbouring structure. Pounding between two adjacent structures with different dynamic properties, using SDOF models, was also studied by other researchers (see, for example, Jing and Young 1991; Chau and Wei 2001; Jankowski 2006; Mahmoud et al. 2008; Mahmoud and Jankowski 2011).

More detailed analysis can be carried out on multi-degree-of-freedom (MDOF) models of interacting buildings, in which mass of each storey is lumped on the floor level. Maison and Kasai (1990, 1992) employed such models to study the response of a light high-rise building colliding against a massive low structure. Anagnostopoulos and Spiliopoulos (1992) used lumped mass models of 5-storey and 10-storey buildings with bilinear force-deformation characteristics to conduct the parametric study on pounding-involved structural behaviour. Similar structural models were used in the analysis of collisions between buildings with equal heights (see Papadrakakis et al. 1991). Non-linear analyses of pounding between two neighbouring 3-storey and 4-storey buildings with substantially different dynamic properties were also conducted (Jankowski 2008; Mahmoud and Jankowski 2009). Karayannis and Favvata (2005a, b) carried out the investigation on MDOF models of colliding structures of unequal storey heights to study the effect of inter-storey pounding. MDOF structural models were also considered by other researchers to investigate earthquake-induced pounding between buildings (see, for example, Cole et al. 2011; Efraimiadou et al. 2013).

The most precise results are usually obtained with the use of finite element method (FEM) which allows us to create models of buildings with detailed representation of their geometry. Papadrakakis et al. (1991) used the method in the

R. Jankowski and S. Mahmoud, *Earthquake-Induced Structural Pounding*,
GeoPlanet: Earth and Planetary Sciences, DOI 10.1007/978-3-319-16324-6_3

analysis of pounding between buildings, in which floors of structures were modelled by single four-node plane stress elements and walls by four linear beam-column elements. The non-linear analyses of interactions between two neighbouring buildings using FEM were also conducted in other studies (see Jankowski 2007a, b, 2009, 2012; Sołtysik and Jankowski 2013).

3.1 Pounding-Involved Response of Buildings Modelled as SDOF Systems

Let us first consider two buildings as elastic SDOF systems so as to conduct a basic analysis on pounding-involved response of structures under earthquake excitation. The model of two colliding SDOF systems is shown in Fig. 2.13 and the dynamic equation of motion for such a model is defined by Eq. (2.22). The following basic values describing the structural properties have been used in the numerical simulations: $m_1 = 75 \times 10^3$ kg, $K_1 = 2.056 \times 10^6$ N/m$(T_1 = 1.2$ s$)$, $C_1 = 39270$ kg/s $(\xi_{S1} = 0.05)$, $m_2 = 3000 \times 10^3$ kg, $K_2 = 1.316 \times 10^9$ N/m$(T_2 = 0.3$ s$)$, $C_2 = 6.283 \times 10^6$ kg/s$(\xi_{S2} = 0.05)$, where K_i, C_i, T_i, ξ_{Si} $(i = 1, 2)$ are the stiffness coefficient, damping coefficient, natural period and damping ratio of the structure with mass m_i, respectively. Pounding force has been simulated with the help of the non-linear viscoelastic model (Jankowski 2005, 2006, 2008) according to Eq. (2.16) with the following parameters: $\bar{\beta} = 2.75 \times 10^9$ N/m$^{3/2}$, $\bar{\xi} = 0.35$, $(e = 0.65)$. In order to solve the equation of motion (2.22) numerically, the time-stepping Newmark method (Newmark 1959), with the standard parameters: $\gamma_N = 0.5$, $\beta_N = 0.25$ and constant time step $\Delta t = 0.005$ s, has been used. The example of the displacement time histories under the NS component of the El Centro earthquake (18 May 1940), for the case when the initial separation gap between buildings, d, is equal to 0.03 m, is shown in Fig. 3.1a. The corresponding pounding force history is presented in Fig. 3.1b. The examples of the results of the parametric study are shown in Figs. 3.2, 3.3 and 3.4. The numerical analysis has been conducted for different values of gap size, natural structural period and mass of the left building. When the effect of one parameter has been investigated, the values of others have been kept unchanged.

The results of the basic response analysis, with the use of elastic SDOF systems as structural models, clearly show that structural pounding during earthquakes has a significant influence on the behaviour of the left building, which is lighter and more flexible structure. It can be seen from Figs. 3.1a and 3.2a that pounding may substantially amplify the response of this structure and the largest increase in the peak displacement (for $d = 0.03$ m) is as large as 47.1 %. On the other hand, the results indicate (see Figs. 3.1a and 3.2b) that the behaviour of a stiffer and heavier right building is nearly unaffected by collisions. In the case of this structure, the difference between the peak displacement responses for different gap sizes is equal to 2.8 %. The results of the parametric investigation (see Figs. 3.2, 3.3 and 3.4)

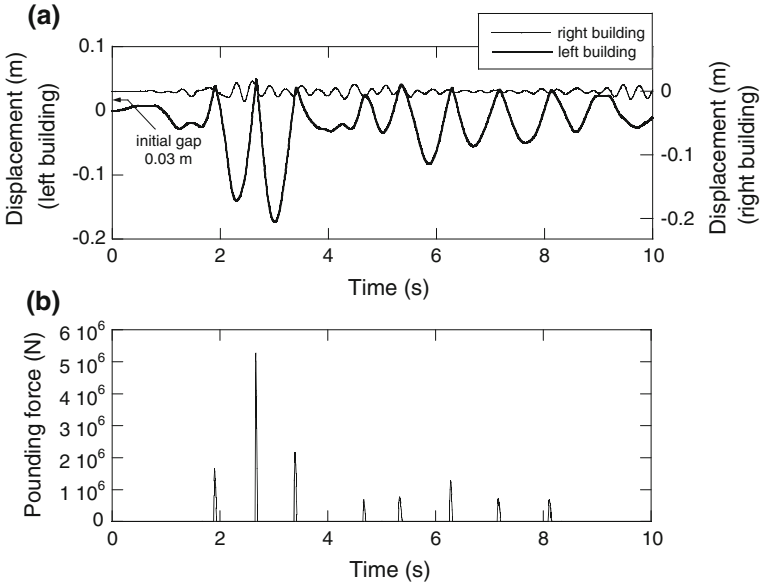

Fig. 3.1 Response time histories for buildings. **a** Displacement histories. **b** Pounding force history

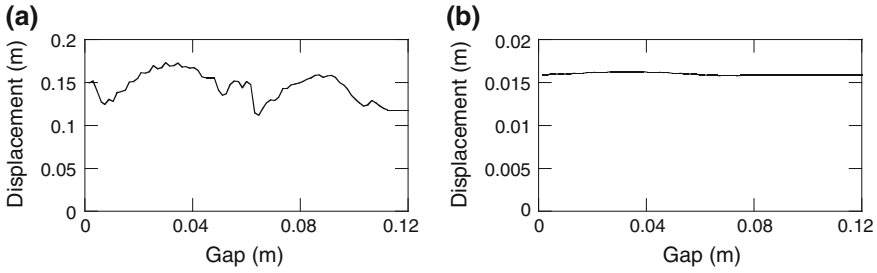

Fig. 3.2 Peak displacement with respect to the gap size between buildings. **a** Left building. **b** Right building

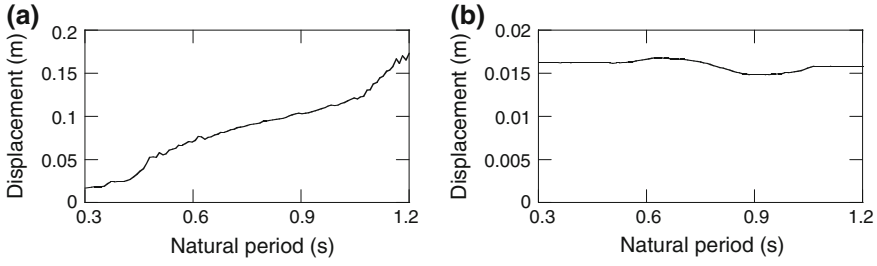

Fig. 3.3 Peak displacement with respect to the natural period of the left building. **a** Left building. **b** Right building

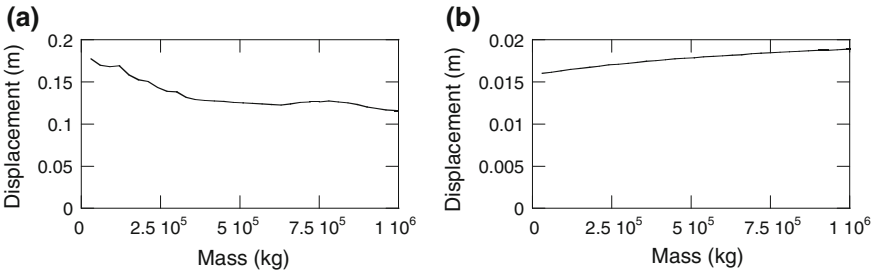

Fig. 3.4 Peak displacement with respect to the mass of the left building. **a** Left building. **b** Right building

prove that the peak displacement of the lighter left building is very sensitive to a change of different structural parameters, such as gap size between structures as well as the period and mass of that structure. On the other hand, the response of the heavier right building has been found to be influenced only slightly.

3.2 Pounding-Involved Response of Buildings Modelled as MDOF Systems

More detailed analysis on earthquake-induced pounding between buildings can be carried out on lumped mass MDOF models, assuming their elastic or inelastic behaviour. As an example, let us consider two three-storey buildings with different dynamic properties (see Fig. 3.5). The dynamic equation of motion for such a structural model, including pounding between buildings at each floor level and

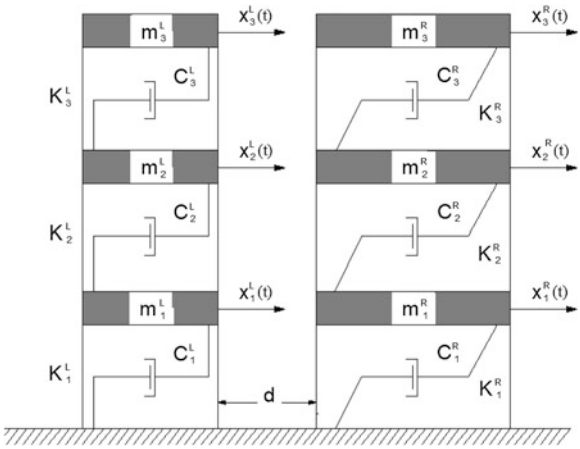

Fig. 3.5 Model of colliding three-storey buildings

elastic-perfectly plastic approximation of storey shear force-drift relation, can be written as:

$$\mathbf{M}\,\ddot{\mathbf{x}}(t) + \mathbf{C}\,\dot{\mathbf{x}}(t) + \mathbf{F}_S(t) + \mathbf{F}(t) = -\mathbf{M}\mathbf{1}\,\ddot{x}_g(t) \tag{3.1a}$$

$$\mathbf{M} = \begin{bmatrix} m_1^L & 0 & 0 & 0 & 0 & 0 \\ 0 & m_2^L & 0 & 0 & 0 & 0 \\ 0 & 0 & m_3^L & 0 & 0 & 0 \\ 0 & 0 & 0 & m_1^R & 0 & 0 \\ 0 & 0 & 0 & 0 & m_2^R & 0 \\ 0 & 0 & 0 & 0 & 0 & m_3^R \end{bmatrix}; \quad \ddot{\mathbf{x}}(t) = \begin{bmatrix} \ddot{x}_1^L(t) \\ \ddot{x}_2^L(t) \\ \ddot{x}_3^L(t) \\ \ddot{x}_1^R(t) \\ \ddot{x}_2^R(t) \\ \ddot{x}_3^R(t) \end{bmatrix}; \quad \dot{\mathbf{x}}(t) = \begin{bmatrix} \dot{x}_1^L(t) \\ \dot{x}_2^L(t) \\ \dot{x}_3^L(t) \\ \dot{x}_1^R(t) \\ \dot{x}_2^R(t) \\ \dot{x}_3^R(t) \end{bmatrix} \tag{3.1b}$$

$$\mathbf{C} = \begin{bmatrix} C_1^L + C_2^L & -C_2^L & 0 & 0 & 0 & 0 \\ -C_2^L & C_2^L + C_3^L & -C_3^L & 0 & 0 & 0 \\ 0 & -C_3^L & C_3^L & 0 & 0 & 0 \\ 0 & 0 & 0 & C_1^R + C_2^R & -C_2^R & 0 \\ 0 & 0 & 0 & -C_2^R & C_2^R + C_3^R & -C_3^R \\ 0 & 0 & 0 & 0 & -C_3^R & C_3^R \end{bmatrix} \tag{3.1c}$$

$$\mathbf{F}_S(t) = \begin{bmatrix} F_{S1}^L(t) - F_{S2}^L(t) \\ F_{S2}^L(t) - F_{S3}^L(t) \\ F_{S3}^L(t) \\ F_{S1}^R(t) - F_{S2}^R(t) \\ F_{S2}^R(t) - F_{S3}^R(t) \\ F_{S3}^R(t) \end{bmatrix}; \quad \mathbf{F}(t) = \begin{bmatrix} F_1(t) \\ F_2(t) \\ F_3(t) \\ -F_1(t) \\ -F_2(t) \\ -F_3(t) \end{bmatrix}; \quad \mathbf{1} = \begin{bmatrix} 1 \\ 1 \\ 1 \\ 1 \\ 1 \\ 1 \end{bmatrix} \tag{3.1d}$$

where $\ddot{x}_i^L(t)$, $\ddot{x}_i^R(t)$, $\dot{x}_i^L(t)$, $\dot{x}_i^R(t)$, $x_i^L(t)$, $x_i^R(t)$, $(i = 1, \ldots, 3)$ are the acceleration, velocity and displacement of a single storey of the left (upper index L) and the right (upper index R) building, respectively; $F_{Si}^L(t)$, $F_{Si}^R(t)$ are inelastic storey shear forces equal to: $F_{Si}^L(t) = K_i^L\big(x_i^L(t) - x_{i-1}^L(t)\big)$, $F_{Si}^R(t) = K_i^R\big(x_i^R(t) - x_{i-1}^R(t)\big)$ for the elastic range till the storey yield strength F_{Yi}^L, F_{Yi}^R is reached and $F_{Si}^L(t) = \pm F_{Yi}^L$, $F_{Si}^R(t) = \pm F_{Yi}^R$ for the plastic range; K_i^L, C_i^L, K_i^R, C_i^R are elastic structural stiffness and damping coefficients; $\ddot{x}_g(t)$ is the acceleration of input ground motion and $F_i(t)$ denotes pounding force between storeys with masses m_i^L, m_i^R.

The following basic values describing the structural properties have been used in the analysis described in this section (compare Jankowski 2008):

- left building:

$$
\begin{aligned}
&m_1^L = m_2^L = m_3^L = 25 \times 10^3 \text{ kg},\\
&K_1^L = K_2^L = K_3^L = 3.460 \times 10^6 \text{ N/m } (T^L = 1.2 \text{ s}),\\
&C_1^L = C_2^L = C_3^L = 6.609 \times 10^4 \text{ kg/s } (\xi^L = 0.05),\\
&F_{Y1}^L = F_{Y2}^L = F_{Y3}^L = 1.369 \times 10^5 \text{ N},
\end{aligned}
$$

- right building:

$$
\begin{aligned}
&m_1^R = m_2^R = m_3^R = 1000 \times 10^3 \text{ kg},\\
&K_1^R = K_2^R = K_3^R = 2.215 \times 10^9 \text{ N/m } (T^R = 0.3 \text{ s}),\\
&C_1^R = C_2^R = C_3^R = 1.058 \times 10^7 \text{ kg/s } (\xi^R = 0.05),\\
&F_{Y1}^R = F_{Y2}^R = F_{Y3}^R = 1.442 \times 10^7 \text{ N}.
\end{aligned}
$$

Pounding force, $F_i(t)$, between storeys with masses m_i^L, m_i^R $(i = 1, \ldots, 3)$ has been simulated with the help of the non-linear viscoelastic model according to the formula [compare Eq. (2.16)]:

$$
\begin{aligned}
&F_i(t) = 0 && \text{for } \delta_i(t) \le 0 \text{ (no contact)}\\
&F_i(t) = \bar{\beta}\delta_i^{\frac{3}{2}}(t) + \bar{c}_i(t)\dot{\delta}_i(t) && \text{for } \delta_i(t) > 0 \text{ and } \dot{\delta}_i(t) > 0 \text{ (contact}-\text{approach period)}\\
&F_i(t) = \bar{\beta}\delta_i^{\frac{3}{2}}(t) && \text{for } \delta_i(t) > 0 \text{ and } \dot{\delta}_i(t) \le 0 \text{ (contact}-\text{restitution period)}
\end{aligned}
\tag{3.2}
$$

where:

$$
\delta_i(t) = x_i^L(t) - x_i^R(t) - d; \quad \bar{c}_i(t) = 2\bar{\xi}\sqrt{\bar{\beta}\sqrt{\delta_i(t)}\frac{m_i^L m_i^R}{m_i^L + m_i^R}} \tag{3.3}
$$

The initial separation gap between buildings has been set to $d = 0.02$ m. The following values of the non-linear viscoelastic pounding force model's parameters have been applied in the analysis: $\bar{\beta} = 2.75 \times 10^9$ N/m$^{3/2}$, $\bar{\xi} = 0.35$ $(e = 0.65)$. The time-stepping Newmark method with constant time step $\Delta t = 0.002$ s has been used in order to solve the equation of motion (3.1a–3.1d) numerically. Different earthquake records have been incorporated in the analysis. The examples of the results of the study for the NS component of the El Centro earthquake are presented below (see also Jankowski 2008).

The results of the analysis in the form of displacement, pounding force and storey shear force time histories are presented in Figs. 3.6, 3.7 and 3.8 for the first, the second and the third storeys of the buildings, respectively. A comparison between the case of pounding-involved displacement responses and the case of

responses with independent vibrations (large separation gap preventing contacts), for the third storeys of buildings, is also shown in Fig. 3.9.

It can be seen from Figs. 3.6b, 3.7b and 3.8b that both structures came into contact three times during the earthquake, although the second and the third

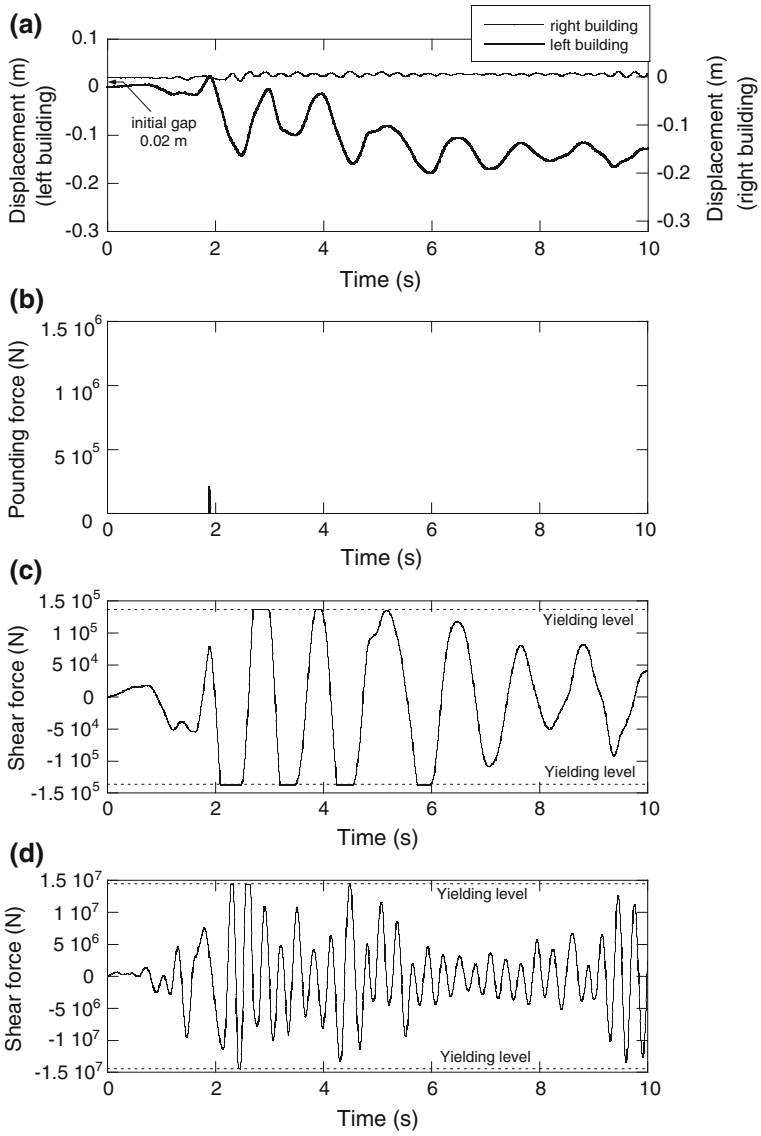

Fig. 3.6 Response time histories for the first storeys of buildings (Jankowski 2008). **a** Displacement histories. **b** Pounding force history. **c** Storey shear force history for the left building. **d** Storey shear force history for the right building

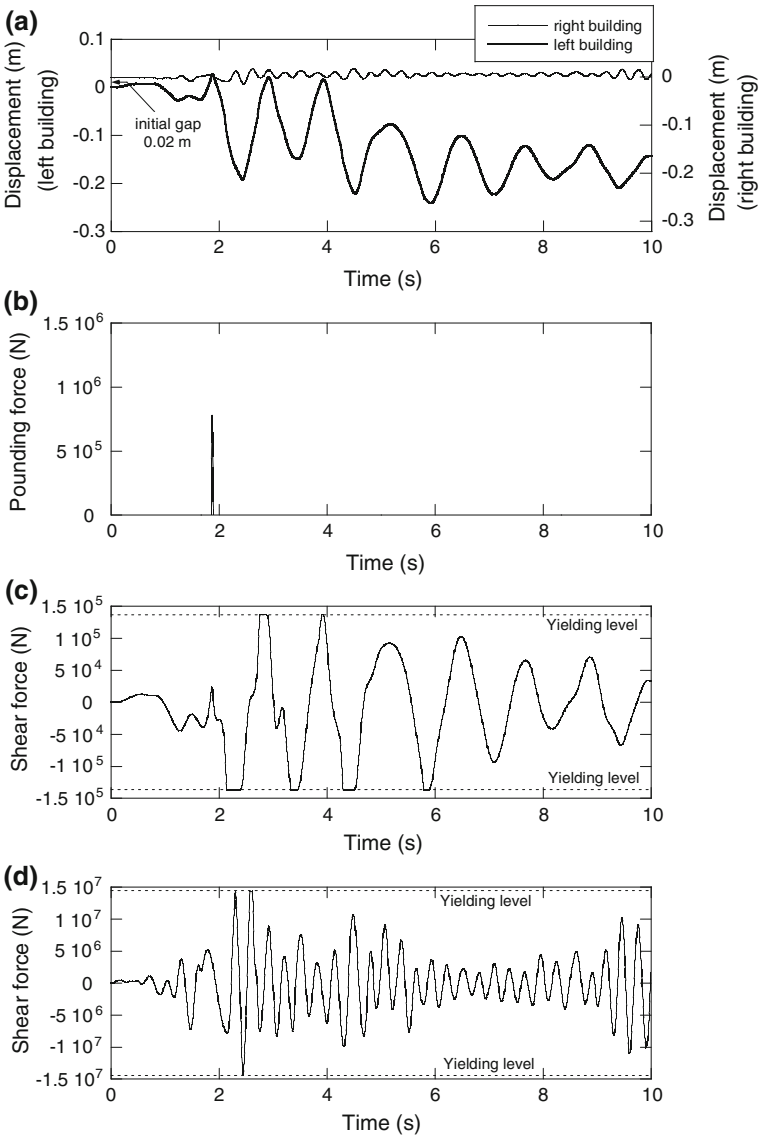

Fig. 3.7 Response time histories for the second storeys of buildings (Jankowski 2008). **a** Displacement histories. **b** Pounding force history. **c** Storey shear force history for the left building. **d** Storey shear force history for the right building

collision took place only at the level of the third storeys. Figures 3.6a, 3.7a and 3.8a indicate that already after the first impact, the left building (lighter and more flexible one) rebounded so substantially that it entered into the yielding range at the level of all three storeys (see Figs. 3.6c, 3.7c and 3.8c). This finally resulted in a significant

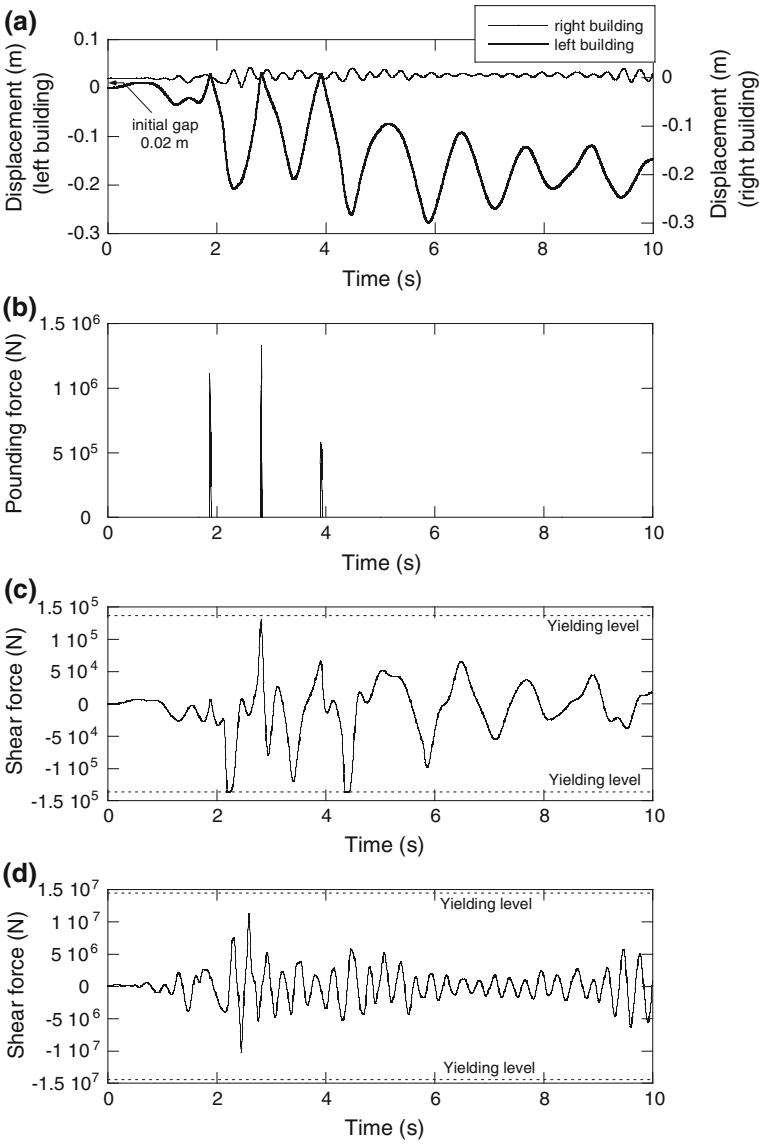

Fig. 3.8 Response time histories for the third storeys of buildings (Jankowski 2008). **a** Displacement histories. **b** Pounding force history. **c** Storey shear force history for the left building. **d** Storey shear force history for the right building

permanent deformation of the left structure, as it can be observed in Fig. 3.9a. On the other hand, the results of the analysis indicate that the response of the right building (heavier and stiffer one) was not considerably influenced by the earthquake-induced pounding between structures (see Fig. 3.9b). Also entering into inelastic range, which

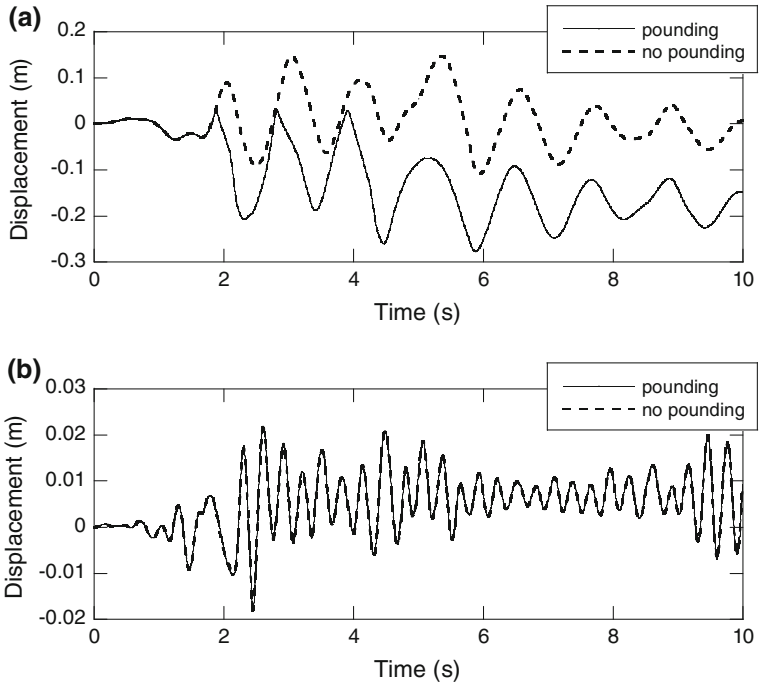

Fig. 3.9 Pounding-involved and independent vibration displacement time histories of the third storeys of buildings (Jankowski 2008). **a** Left building. **b** Right building

can be seen in Figs. 3.6d, 3.7d and 3.8d, was mainly due to intensive ground motion excitation rather than due to pounding with the left building.

The incorporation of the inelastic behaviour of colliding buildings in the numerical model is very important for modelling of pounding-involved structural response. In the study described in this section, elastic-perfectly plastic approximation of storey shear force-drift relation has been assumed. Employing a more precise model of the inelastic structural behaviour due to earthquake excitation can further increase the accuracy of the analysis.

The analysis on lumped mass models can also be extended into the transverse as well as vertical directions (see Jankowski 2008 for details) so as to study the three-dimensional response of colliding structures during earthquakes.

3.3 Pounding-Involved Response of Base-Isolated Buildings

The use of seismic isolation, which is considered as one of the most promising alternatives to enhance the structural safety against earthquakes (see, for example, Mostaghel and Khodaverdian 1987; Buckle and Mayes 1990; Kelly 1993; Jangid

and Datta 1995; Jankowski and Walukiewicz 1997; Komodromos 2000; Falborski and Jankowski 2013), results in larger structural displacements increasing the probability of collisions. Structural pounding in isolated buildings may occur either at the foundation (base) or at the storey level if structures are insufficiently separated (Tsai 1997; Malhotra 1997; Dimova 2000; Nagarajaiah and Sun 2001; Matsagar and Jangid 2003; Komodromos et al. 2007; Komodromos 2008; Ye et al. 2009; Polycarpou and Komodromos 2010a, b). In this section, let us consider earthquake-induced pounding between two three-storey buildings analyzed in Sect. 3.2, which have been additionally equipped with the base isolation system and arranged in two configurations (see also Mahmoud and Jankowski 2010):

- the left structure is seismically isolated, while the right building has fixed base (see Fig. 3.10);
- both structures have base isolation systems (see Fig. 3.11).

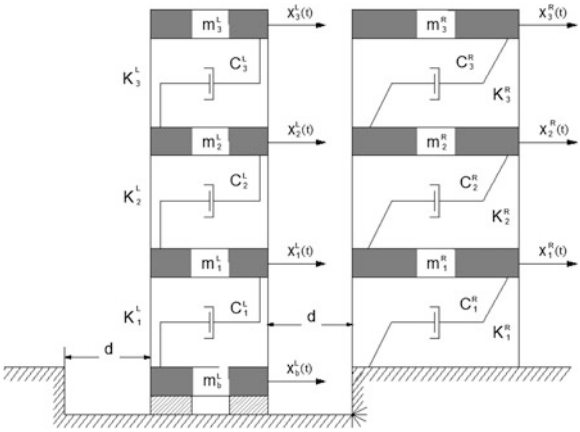

Fig. 3.10 Model of colliding three-storey buildings with isolated and non-isolated bases

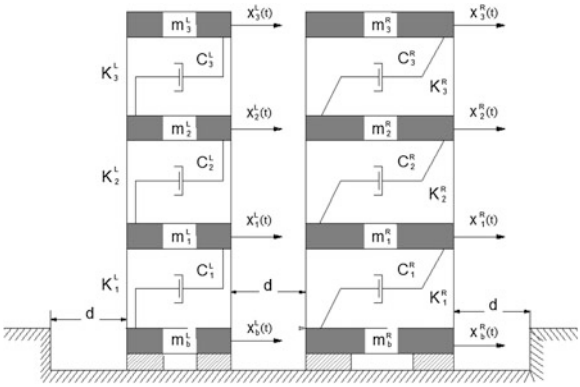

Fig. 3.11 Model of colliding three-storey buildings with isolated bases

Among the developed various types of isolation systems, the use of high damping rubber bearings (HDRBs) is one of the most attractive solutions. These bearings have also been used in the present study as the isolation devices. In order to simulate the behaviour of isolation system in the form of HDRBs, a non-linear strain-rate dependent model (see Jankowski 2003) has been applied in the analysis. The model describes the behaviour of the bearing by a non-linear elastic spring-dashpot element with the stiffness and damping coefficients, $K_b(t)$, $C_b(t)$, obtained for the actual values of displacement, $x_b(t)$, and velocity, $\dot{x}_b(t)$, of the structural base using the following formulae (Jankowski 2003):

$$K_b(t) = a_1 + a_2(x_b(t))^2 + a_3(x_b(t))^4 + \frac{a_4}{\cosh^2(a_5\dot{x}_b(t))} + \frac{a_6}{\cosh(a_7\dot{x}_b(t))\cosh(a_8x_b(t))} \tag{3.4a}$$

$$C_b(t) = \frac{a_9 + a_{10}(x_b(t))^2}{\sqrt{a_{11}^2 + (\dot{x}_b(t))^2}} \tag{3.4b}$$

where a_1–a_{11} are parameters of the model which are obtained by fitting the experimental data using the method of the least squares.

3.3.1 Pounding Between Isolated and Non-isolated Building

In the case when the left building is seismically isolated and the right one has fixed base (Fig. 3.10), the inelastic dynamic equation of motion can be written as [compare Eqs. (3.1a–3.1d)]:

$$\mathbf{M}\,\ddot{\mathbf{x}}(t) + \mathbf{C}(t)\dot{\mathbf{x}}(t) + \mathbf{F}_S(t) + \mathbf{F}(t) = -\mathbf{M1}\,\ddot{x}_g(t) \tag{3.5a}$$

$$\mathbf{M} = \begin{bmatrix} m_b^L & 0 & 0 & 0 & 0 & 0 & 0 \\ 0 & m_1^L & 0 & 0 & 0 & 0 & 0 \\ 0 & 0 & m_2^L & 0 & 0 & 0 & 0 \\ 0 & 0 & 0 & m_3^L & 0 & 0 & 0 \\ 0 & 0 & 0 & 0 & m_1^R & 0 & 0 \\ 0 & 0 & 0 & 0 & 0 & m_2^R & 0 \\ 0 & 0 & 0 & 0 & 0 & 0 & m_3^R \end{bmatrix}; \quad \ddot{\mathbf{x}}(t) = \begin{bmatrix} \ddot{x}_b^L(t) \\ \ddot{x}_1^L(t) \\ \ddot{x}_2^L(t) \\ \ddot{x}_3^L(t) \\ \ddot{x}_1^R(t) \\ \ddot{x}_2^R(t) \\ \ddot{x}_3^R(t) \end{bmatrix}; \quad \dot{\mathbf{x}}(t) = \begin{bmatrix} \dot{x}_b^L(t) \\ \dot{x}_1^L(t) \\ \dot{x}_2^L(t) \\ \dot{x}_3^L(t) \\ \dot{x}_1^R(t) \\ \dot{x}_2^R(t) \\ \dot{x}_3^R(t) \end{bmatrix} \tag{3.5b}$$

$$\mathbf{C}(t) = \begin{bmatrix} C_b^L(t) + C_1^L & -C_1^L & 0 & 0 & 0 & 0 & 0 \\ -C_1^L & C_1^L + C_2^L & -C_2^L & 0 & 0 & 0 & 0 \\ 0 & -C_2^L & C_2^L + C_3^L & -C_3^L & 0 & 0 & 0 \\ 0 & 0 & -C_3^L & C_3^L & 0 & 0 & 0 \\ 0 & 0 & 0 & 0 & C_1^R + C_2^R & -C_2^R & 0 \\ 0 & 0 & 0 & 0 & -C_2^R & C_2^R + C_3^R & -C_3^R \\ 0 & 0 & 0 & 0 & 0 & -C_3^R & C_3^R \end{bmatrix} \tag{3.5c}$$

$$\mathbf{F}_S(t) = \begin{bmatrix} K_b^L(t)x_b^L(t) - F_{S1}^L(t) \\ F_{S1}^L(t) - F_{S2}^L(t) \\ F_{S2}^L(t) - F_{S3}^L(t) \\ F_{S3}^L(t) \\ F_{S1}^R(t) - F_{S2}^R(t) \\ F_{S2}^R(t) - F_{S3}^R(t) \\ F_{S3}^R(t) \end{bmatrix}; \quad \mathbf{F}(t) = \begin{bmatrix} F_b(t) \\ F_1(t) \\ F_2(t) \\ F_3(t) \\ -F_1(t) \\ -F_2(t) \\ -F_3(t) \end{bmatrix}; \quad \mathbf{1} = \begin{bmatrix} 1 \\ 1 \\ 1 \\ 1 \\ 1 \\ 1 \\ 1 \end{bmatrix} \tag{3.5d}$$

where, m_b^L, $\ddot{x}_b^L(t)$, $\dot{x}_b^L(t)$ are the mass, acceleration and velocity of the base of the left building, respectively; and $F_b(t)$ is the pounding force at the base level [see Eq. (3.2)]. It has been assumed in the analysis that the left building has been equipped with 4 circular HDRBs with the following parameters of the bearing's model (see Example 3 in Jankowski 2003): $a_1 = 4.1051 \times 10^5$ N/m, $a_2 = -1.7238 \times 10^3$ N/m^3, $a_3 = -98.611$ N/m^5, $a_4 = 1.2261 \times 10^5$ N/m, $a_5 = 5.0777$ s/m, $a_6 = 3.5740 \times 10^5$ N/m, $a_7 = 6.9069$ s/m, $a_8 = 48.371$ 1/m, $a_9 = 1.0169 \times 10^4$ N, $a_{10} = 8.0471 \times 10^4$ N/m^2, $a_{11} = 0.15621$ m/s.

The examples of the peak responses of buildings with respect to the in-between gap size under the NS component of the El Centro earthquake are shown in Fig. 3.12. Additionally, the peak base displacements, accelerations and pounding forces are presented in Fig. 3.13 (see also Mahmoud and Jankowski 2010). It can be seen from Fig. 3.12b, d that the non-isolated left building (heavier and stiffer one) shows almost constant peak displacements and accelerations for all the gap distances considered in the study. On the other hand, the peak displacements and accelerations for the storeys of the isolated left building with lighter and more flexible superstructure show larger differences (see Fig. 3.12a, c). The results show the increase in the peak response values up to a certain gap size distance and with further increase in the gap value, a decrease trend can be observed. It can also be seen from Fig. 3.12e that pounding forces have a decrease tendency with the increase in the gap distance showing significant differences between higher and lower storey levels. Moreover, it has been noticed (see Fig. 3.13) that the peak pounding forces at the base level of isolated building increase up to a certain value

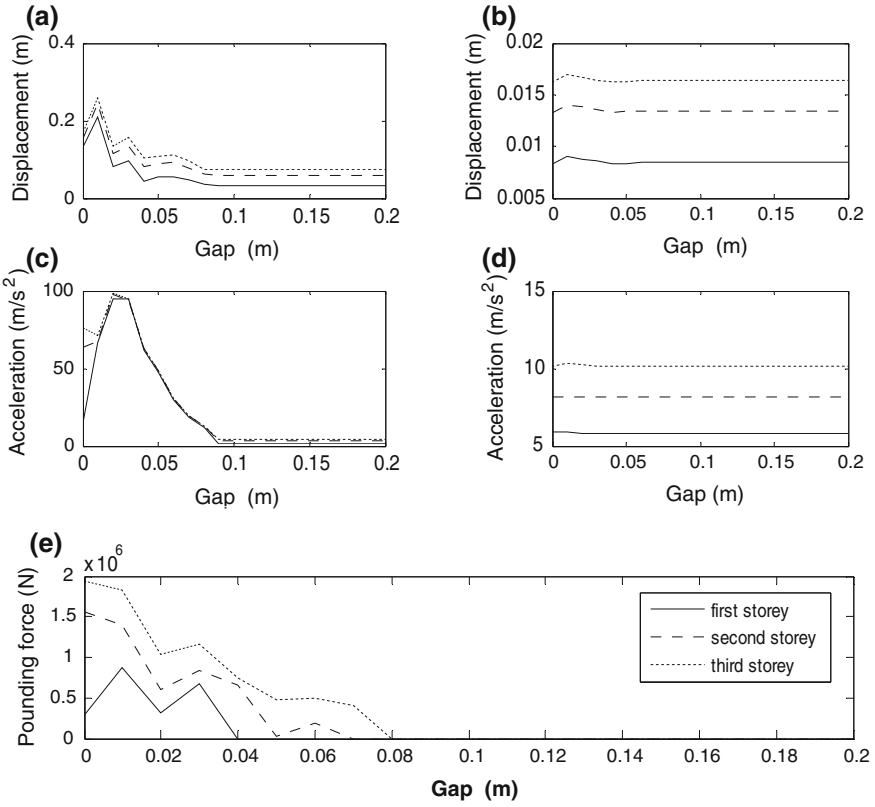

Fig. 3.12 Peak responses of isolated and non-isolated buildings with respect to the gap size (Mahmoud and Jankowski 2010). **a** Storeys of the left building. **b** Storeys of the right building. **c** Storeys of the left building. **d** Storeys of the right building. **e** Storeys of both buildings

of the gap distance and with further increase in the gap, a decrease trend can be observed. Similar trend can also be seen for the peak base accelerations obtained at different separation distances. On the other hand, the peak base displacements increase with the increase in the gap distance between buildings.

3.3.2 Pounding Between Two Isolated Buildings

In the second configuration, the pounding-involved seismic response of two buildings with isolated bases (see Fig. 3.11) has been considered. In this case, the dynamic equation of motion takes the form [compare Eqs. (3.1a–3.1d) and (3.5a–3.5d)]:

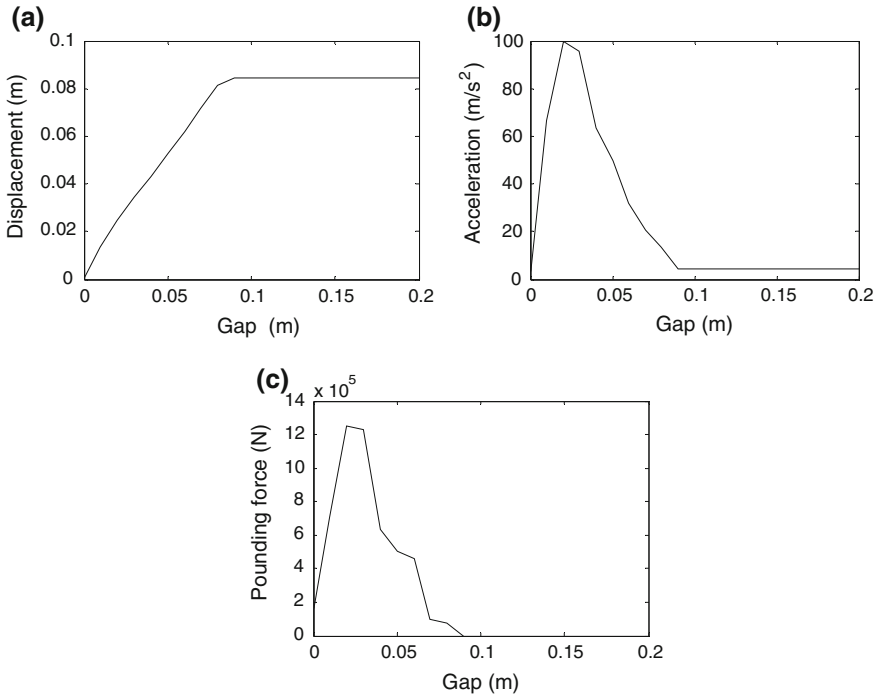

Fig. 3.13 Peak responses of isolated base of the left building with respect to the gap size (Mahmoud and Jankowski 2010). **a** Peak base displacement. **b** Peak base acceleration. **c** Peak pounding force at base

$$\mathbf{M}\,\ddot{\mathbf{x}}(t) + \mathbf{C}(t)\dot{\mathbf{x}}(t) + \mathbf{F}_S(t) + \mathbf{F}(t) = -\mathbf{M}\mathbf{1}\,\ddot{x}_g(t) \tag{3.6a}$$

$$\mathbf{M} = \begin{bmatrix} m_b^L & 0 & 0 & 0 & 0 & 0 & 0 & 0 \\ 0 & m_1^L & 0 & 0 & 0 & 0 & 0 & 0 \\ 0 & 0 & m_2^L & 0 & 0 & 0 & 0 & 0 \\ 0 & 0 & 0 & m_3^L & 0 & 0 & 0 & 0 \\ 0 & 0 & 0 & 0 & m_b^R & 0 & 0 & 0 \\ 0 & 0 & 0 & 0 & 0 & m_1^R & 0 & 0 \\ 0 & 0 & 0 & 0 & 0 & 0 & m_2^R & 0 \\ 0 & 0 & 0 & 0 & 0 & 0 & 0 & m_3^R \end{bmatrix}; \quad \ddot{\mathbf{x}}(t) = \begin{bmatrix} \ddot{x}_b^L(t) \\ \ddot{x}_1^L(t) \\ \ddot{x}_2^L(t) \\ \ddot{x}_3^L(t) \\ \ddot{x}_b^R(t) \\ \ddot{x}_1^R(t) \\ \ddot{x}_2^R(t) \\ \ddot{x}_3^R(t) \end{bmatrix}; \quad \dot{\mathbf{x}}(t) = \begin{bmatrix} \dot{x}_b^L(t) \\ \dot{x}_1^L(t) \\ \dot{x}_2^L(t) \\ \dot{x}_3^L(t) \\ \dot{x}_b^R(t) \\ \dot{x}_1^R(t) \\ \dot{x}_2^R(t) \\ \dot{x}_3^R(t) \end{bmatrix} \tag{3.6b}$$

$$\mathbf{C}(t) = \begin{bmatrix} C_b^L(t) + C_1^L & -C_1^L & 0 & 0 & 0 & 0 & 0 & 0 \\ -C_1^L & C_1^L + C_2^L & -C_2^L & 0 & 0 & 0 & 0 & 0 \\ 0 & -C_2^L & C_2^L + C_3^L & -C_3^L & 0 & 0 & 0 & 0 \\ 0 & 0 & -C_3^L & C_3^L & 0 & 0 & 0 & 0 \\ 0 & 0 & 0 & 0 & C_b^R(t) + C_1^R & -C_1^R & 0 & 0 \\ 0 & 0 & 0 & 0 & -C_1^R & C_1^R + C_2^R & -C_2^R & 0 \\ 0 & 0 & 0 & 0 & 0 & -C_2^R & C_2^R + C_3^R & -C_3^R \\ 0 & 0 & 0 & 0 & 0 & 0 & -C_3^R & C_3^R \end{bmatrix} \tag{3.6c}$$

$$\mathbf{F}_S(t) = \begin{bmatrix} K_b^L(t)x_b^L(t) - F_{S1}^L(t) \\ F_{S1}^L(t) - F_{S2}^L(t) \\ F_{S2}^L(t) - F_{S3}^L(t) \\ F_{S3}^L(t) \\ K_b^R(t)x_b^R(t) - F_{S1}^R(t) \\ F_{S1}^R(t) - F_{S2}^R(t) \\ F_{S2}^R(t) - F_{S3}^R(t) \\ F_{S3}^R(t) \end{bmatrix}; \quad \mathbf{F}(t) = \begin{bmatrix} F_b(t) \\ F_1(t) \\ F_2(t) \\ F_3(t) \\ -F_b(t) \\ -F_1(t) \\ -F_2(t) \\ -F_3(t) \end{bmatrix}; \quad \mathbf{1} = \begin{bmatrix} 1 \\ 1 \\ 1 \\ 1 \\ 1 \\ 1 \\ 1 \\ 1 \end{bmatrix} \tag{3.6d}$$

where m_b^R, $\ddot{x}_b^R(t)$, $\dot{x}_b^R(t)$ are the mass, acceleration and velocity of the base of the right building, respectively. In addition to the isolation of the left building (see Sect. 3.3.1 for details) it has been assumed in the analysis that the right building has been equipped with 4 square HDRBs with the following parameters of the bearing's model (see example 1 in Jankowski 2003): $a_1 = 7.5509 \times 10^6$ N/m, $a_2 = 3.8939 \times 10^6$ N/m^3, $a_3 = 1.3423 \times 10^8$ N/m^5, $a_4 = 3.1749 \times 10^6$ N/m, $a_5 = 1.4906$ s/m, $a_6 = 2.8303 \times 10^7$ N/m, $a_7 = 7.1213$ s/m, $a_8 = 45.693$ 1/m, $a_9 = 4.9075 \times 10^5$ N, $a_{10} = 2.2888 \times 10^6$ N/m^2, $a_{11} = 0.58681$ m/s.

The examples of the results of the study conducted under the NS component of the El Centro earthquake are shown in Figs. 3.14 and 3.15 (see also Mahmoud and Jankowski 2010). It can be seen from Fig. 3.14 that both isolated buildings are considerably influenced by earthquake-induced structural pounding. For both buildings, the peak displacements and accelerations for the storeys increase up to a certain value of the gap distance and with further increase in the gap, a decrease trend has been recorded. The impact forces first increase with the increase in the gap distance and then they show a decrease trend after passing a certain gap size value. All the storeys show quite similar relations between the peak responses (displacements and accelerations) and the gap distance. On the other hand, the peak pounding forces show significant differences between higher and lower storey levels. It can also be seen from Fig. 3.15 that the peak base displacements increase with the increase in the gap distance, whereas the curves of the peak base accelerations and the peak pounding forces at the bases show the initial increase with further decrease trend as the gap size increases.

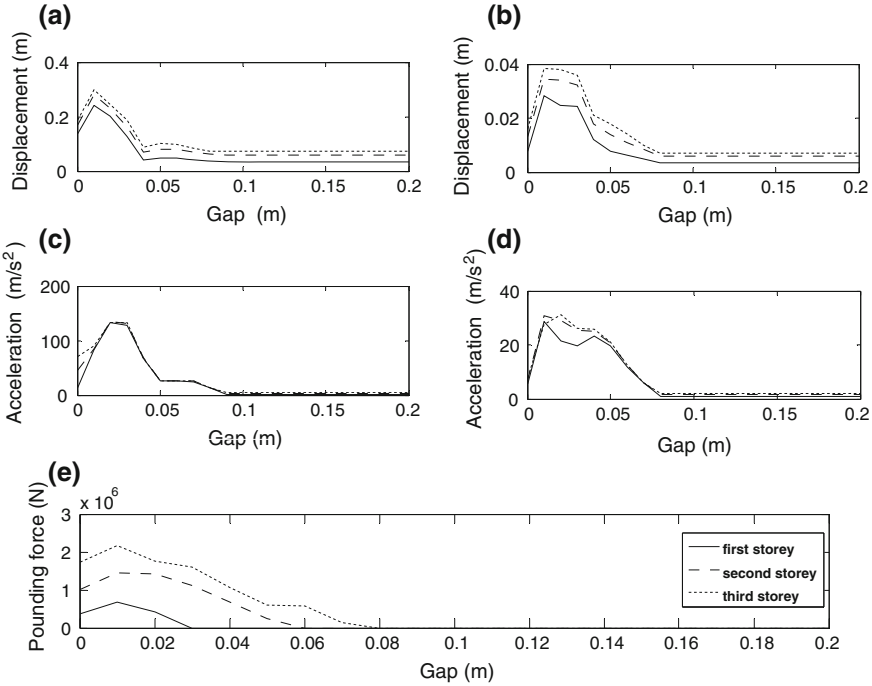

Fig. 3.14 Peak responses of two isolated buildings with respect to the gap size (Mahmoud and Jankowski 2010). **a** Storeys of the left building. **b** Storeys of the right building. **c** Storeys of the left building. **d** Storeys of the right building. **e** Storeys of both buildings

3.4 Pounding-Involved Response of Buildings Considering SSI

It has been considered in the analyses described in Sects. 3.1 and 3.2 that buildings have fixed structural supports. Also, the non-isolated right building analyzed in Sect. 3.3.1 has been considered to be fixed at its base. However, the assumption of fixed-base supports has been proved to be valid only for structures founded on rock or soil of high stiffness. In the reality, flexibility of supporting soil leads to movements of the foundation resulting in the decrease in global stiffness of structures (Wakabayashi 1985; Wolf 1987; Przewłócki and Knabe 1995; Stewart et al. 1999a). Soil-structure interaction (SSI) has captured the interest of a number of researchers who studied applications of SSI to buildings (see, for example, Stewart et al. 1999a, b; Bhattacharya et al. 2004; Dutta and Rana 2010; Halabian and Erfani 2010; Fariborz and Ali 2013; Mahmoud et al. 2012). In this section, let us study earthquake-induced pounding between two three-storey buildings considered in Sect. 3.2, taking into account the effect of the supporting soil flexibility (see also Mahmoud et al. 2013). In order to account for the horizontal and rotational movements of the supporting soil, swaying as well as rocking springs and dashpots

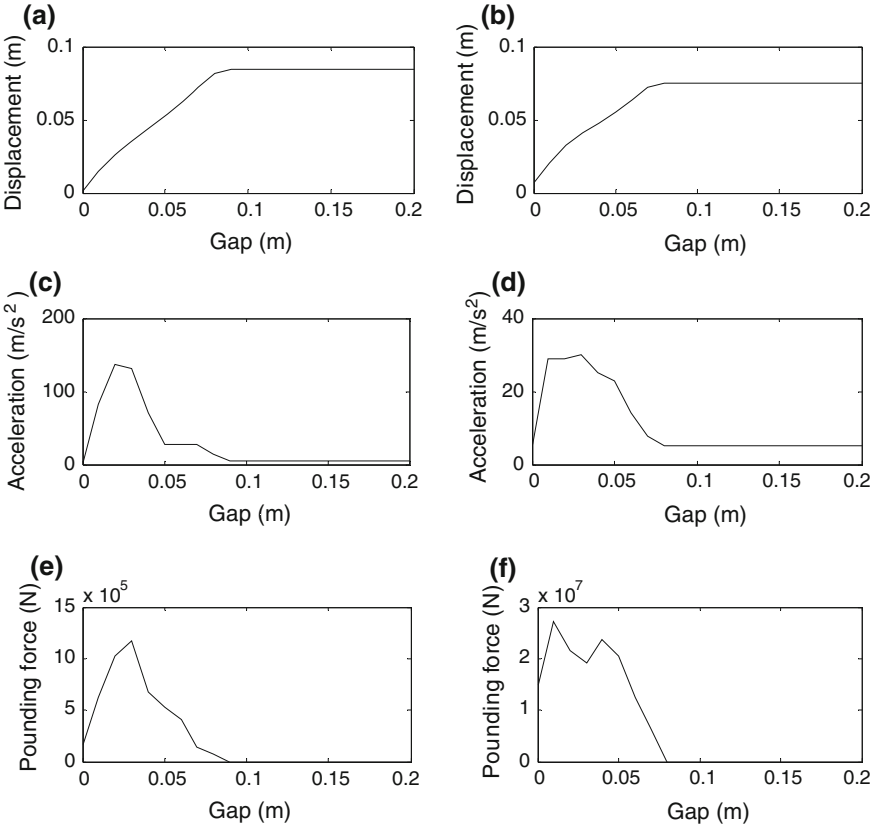

Fig. 3.15 Peak responses of isolated bases of building with respect to the gap size (Mahmoud and Jankowski 2010). **a** Peak left base displacement. **b** Peak right base displacement. **c** Peak left base acceleration. **d** Peak right base acceleration. **e** Peak pounding force at the left base. **f** Peak pounding force at the right base

(see Richart and Whitman 1967; Spyrakos et al. 2009) have been included in the numerical model (see Fig. 3.16). Additionally, let us also investigate in this section, the change in the energy imparted to buildings, as the result of incorporation of SSI in the numerical analysis.

The inelastic dynamic equation of motion for two colliding buildings with incorporation of SSI, as shown in Fig. 3.16, can be written as [see Spyrakos 2009; Mahmoud et al. 2013 and compare Eqs. (3.1a–3.1d)]:

$$\begin{bmatrix} \mathbf{M}^L & \mathbf{O} \\ \mathbf{O} & \mathbf{M}^R \end{bmatrix} \ddot{\mathbf{x}}(t) + \begin{bmatrix} \mathbf{C}^L & \mathbf{O} \\ \mathbf{O} & \mathbf{C}^R \end{bmatrix} \dot{\mathbf{x}}(t) + \mathbf{F}_S(t) + \mathbf{F}(t) = -\begin{bmatrix} \mathbf{M}^{*L} & \mathbf{O} \\ \mathbf{O} & \mathbf{M}^{*R} \end{bmatrix} \mathbf{1}\, \ddot{x}_g(t) \tag{3.7a}$$

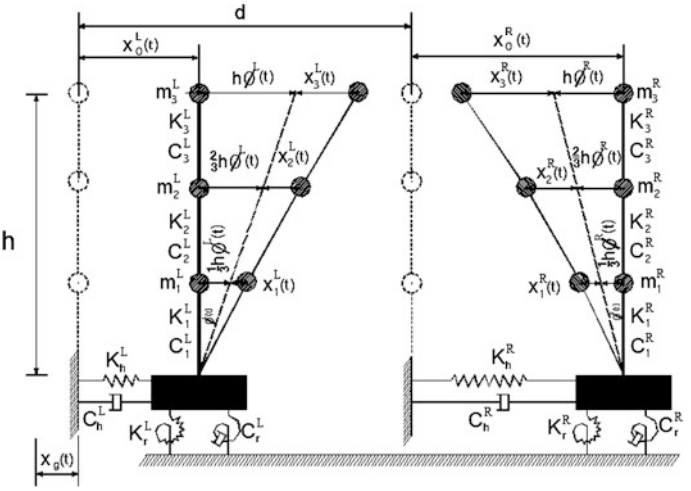

Fig. 3.16 Model of colliding three-storey buildings with incorporation of SSI

$$\mathbf{M}^L = \begin{bmatrix} m_1^L & 0 & 0 & m_1^L & \frac{m_1^L h}{3} \\ 0 & m_2^L & 0 & m_2^L & \frac{2m_2^L h}{3} \\ 0 & 0 & m_3^L & m_3^L & m_3^L h \\ m_1^L & m_2^L & m_3^L & m_1^L + m_2^L + m_3^L & h\left(\frac{m_1^L}{3} + \frac{2m_2^L}{3} + m_3^L\right) \\ \frac{m_1^L h}{3} & \frac{2m_2^L h}{3} & m_3^L h & h\left(\frac{m_1^L}{3} + \frac{2m_2^L}{3} + m_3^L\right) & h^2\left(\frac{m_1^L}{9} + \frac{4}{9}m_2^L + m_3^L\right) \end{bmatrix} \tag{3.7b}$$

$$\mathbf{M}^R = \begin{bmatrix} m_1^R & 0 & 0 & m_1^R & \frac{m_1^R h}{3} \\ 0 & m_2^R & 0 & m_2^R & \frac{2m_2^R h}{3} \\ 0 & 0 & m_3^R & m_3^R & m_3^R h \\ m_1^R & m_2^R & m_3^R & m_1^R + m_2^R + m_3^R & h\left(\frac{m_1^R}{3} + \frac{2m_2^R}{3} + m_3^R\right) \\ \frac{m_1^R h}{3} & \frac{2m_2^R h}{3} & m_3^R h & h\left(\frac{m_1^R}{3} + \frac{2m_2^R}{3} + m_3^R\right) & h^2\left(\frac{m_1^R}{9} + \frac{4}{9}m_2^R + m_3^R\right) \end{bmatrix} \tag{3.7c}$$

$$\mathbf{C}^L = \begin{bmatrix} C_1^L + C_2^L & -C_2^L & 0 & 0 & 0 \\ -C_2^L & C_2^L + C_3^L & -C_3^L & 0 & 0 \\ 0 & -C_3^L & C_3^L & 0 & 0 \\ 0 & 0 & 0 & C_h^L & 0 \\ 0 & 0 & 0 & 0 & C_r^L \end{bmatrix}; \quad \mathbf{1} = \begin{bmatrix} 1 \\ 1 \\ 1 \\ 1 \\ 1 \\ 1 \end{bmatrix} \tag{3.7d}$$

$$\mathbf{C}^R = \begin{bmatrix} C_1^R + C_2^R & -C_2^R & 0 & 0 & 0 \\ -C_2^R & C_2^R + C_3^R & -C_3^R & 0 & 0 \\ 0 & -C_3^R & C_3^R & 0 & 0 \\ 0 & 0 & 0 & C_h^R & 0 \\ 0 & 0 & 0 & 0 & C_r^R \end{bmatrix} \tag{3.7e}$$

$$\mathbf{F}_S(t) = \begin{bmatrix} F_{S1}^L(t) - F_{S2}^L(t) \\ F_{S2}^L(t) - F_{S3}^L(t) \\ F_{S3}^L(t) \\ K_h^L x_0^L(t) \\ K_r^L \phi^L(t) \\ F_{S1}^R(t) - F_{S2}^R(t) \\ F_{S2}^R(t) - F_{S3}^R(t) \\ F_{S3}^R(t) \\ K_h^R x_0^R(t) \\ K_r^R \phi^R(t) \end{bmatrix}; \mathbf{F}(t) = \begin{bmatrix} F_1(t) \\ F_2(t) \\ F_3(t) \\ 0 \\ 0 \\ -F_1(t) \\ -F_2(t) \\ -F_3(t) \\ 0 \\ 0 \end{bmatrix}; \ddot{\mathbf{x}}(t) = \begin{bmatrix} \ddot{x}_1^L(t) \\ \ddot{x}_2^L(t) \\ \ddot{x}_3^L(t) \\ \ddot{x}_0^L(t) \\ \ddot{\phi}^L(t) \\ \ddot{x}_1^R(t) \\ \ddot{x}_2^R(t) \\ \ddot{x}_3^R(t) \\ \ddot{x}_0^R(t) \\ \ddot{\phi}^R(t) \end{bmatrix}; \dot{\mathbf{x}}(t) = \begin{bmatrix} \dot{x}_1^L(t) \\ \dot{x}_2^L(t) \\ \dot{x}_3^L(t) \\ \dot{x}_0^L(t) \\ \dot{\phi}^L(t) \\ \dot{x}_1^R(t) \\ \dot{x}_2^R(t) \\ \dot{x}_3^R(t) \\ \dot{x}_0^R(t) \\ \dot{\phi}^R(t) \end{bmatrix} \tag{3.7f}$$

$$\mathbf{M}^{*L} = \begin{bmatrix} m_1^L & 0 & 0 & 0 & 0 \\ 0 & m_2^L & 0 & 0 & 0 \\ 0 & 0 & m_3^L & 0 & 0 \\ 0 & 0 & 0 & m_1^L + m_2^L + m_3^L & 0 \\ 0 & 0 & 0 & 0 & h\left(\frac{m_1^L}{3} + \frac{2m_2^L}{3} + m_3^L\right) \end{bmatrix} \tag{3.7g}$$

$$\mathbf{M}^{*R} = \begin{bmatrix} m_1^R & 0 & 0 & 0 & 0 \\ 0 & m_2^R & 0 & 0 & 0 \\ 0 & 0 & m_3^R & 0 & 0 \\ 0 & 0 & 0 & m_1^R + m_2^R + m_3^R & 0 \\ 0 & 0 & 0 & 0 & h\left(\frac{m_1^R}{3} + \frac{2m_2^R}{3} + m_3^R\right) \end{bmatrix} \tag{3.7h}$$

where h is the height of buildings, $x_0^L(t)$, $x_0^R(t)$, $\phi^L(t)$, $\phi^R(t)$ are the displacement and the rotation angle of the base of the left (upper index L) and the right (upper index R) building, respectively (see Fig. 3.16) and K_h^L, K_r^L, K_h^R, K_r^R, C_h^L, C_r^L, C_h^R, C_r^R denote the horizontal (lower index h) and rotational (lower index r) stiffness and damping coefficients of additional springs and dampers used to simulate the movements of supporting soil for the left and the right building, respectively; which can be evaluated using the following formulas (Richart and Whitman 1967):

$$K_h = 2(1-v)G\beta_x\sqrt{BL}; \quad C_h = 0.576K_h r_h\sqrt{\frac{\rho}{G}} \tag{3.8a}$$

$$K_r = \frac{G}{1-v}\beta_\phi BL^2; \quad C_r = \frac{0.3}{1+\beta_\phi}K_r r_r\sqrt{\frac{\rho}{G}} \tag{3.8b}$$

where v is the Poisson's ratio of the soil, G is the shear modulus, B and L denote the width and the length of foundation, β_x and β_ϕ are the corrected constants of swaying and rocking springs, respectively; r_h and r_r denote the equivalent radii of foundation for swaying and rocking springs and ρ is the density of soil. The maximum shear modulus at low strain, $G_{\max}$, is related to the shear wave velocity, V_s, according to the following expression (Richart and Whitman 1967):

$$G_{\max} = \rho(V_s)^2 \tag{3.9}$$

The shear modulus used in the analysis has been reduced in order to maintain closer behaviour of the soil. The modulus reduction curves are often used to solve dynamic problems when shear strains drive the soil beyond its elastic range. As the soil enters into the inelastic range, the shear modulus of the soil is reduced substantially what is related to the decrease in the shear wave velocity. In the case of the study described in this section, the reduced shear modulus G has been assumed to be 50 % of $G_{\max}$ calculated according to Eq. (3.9) (see Richart and Whitman 1967).

The seismic input energy imparted to building under earthquake loading can be divided into two parts. One part is related to the temporarily stored energy in the form of kinetic and strain energy. The other part is the energy dissipated through damping and inelastic deformation in the components of the structure. For the three-storey buildings, the input energy, $IE_i^L(t)$, $IE_i^R(t)$, at ith $(i = 1, \ldots, 3)$ storey level for the left and the right structure can be defined at each time, t, as (compare Zahrah and Hall 1984):

$$IE_i^L(t) = \int_0^t m_i^L \ddot{x}_g(t)\dot{x}_i^L(t)dt; \quad IE_i^R(t) = \int_0^t m_i^R \ddot{x}_g(t)\dot{x}_i^R(t)dt \tag{3.10}$$

Similarly, the damping energy, $DE_i^L(t)$, $DE_i^R(t)$, the yielding energy, $YE_i^L(t)$, $YE_i^R(t)$ and the absorbed kinetic energy, $KE_i^L(t)$, $KE_i^R(t)$ at each storey level take the form (compare Zahrah and Hall 1984):

$$DE_i^L(t) = \int_0^t C_i^L\left(\dot{x}_i^L(t)\right)^2 dt; \quad DE_i^R(t) = \int_0^t C_i^R\left(\dot{x}_i^R(t)\right)^2 dt \tag{3.11}$$

$$YE_i^L(t) = \int_0^t F_{Si}^L(t)\dot{x}_i^L(t)dt; \quad YE_i^R(t) = \int_0^t F_{Si}^R(t)\dot{x}_i^R(t)dt \tag{3.12}$$

$$KE_i^L(t) = \int_0^t m_i^L\ddot{x}_i^L(t)\dot{x}_i^L(t)dt; \quad KE_i^R(t) = \int_0^t m_i^R\ddot{x}_i^R(t)\dot{x}_i^R(t)dt \tag{3.13}$$

In the analysis described in this section, pounding force has been simulated with the help of the non-linear viscoelastic model according to Eq. (3.2) with the following parameters: $\bar{\beta} = 2.75 \times 10^9$ N/m$^{3/2}$, $\bar{\xi} = 0.35$ ($e = 0.65$). The initial separation gap between buildings has been set to $d = 0.05$ m. The soil density, Poisson's ratio and shear wave velocity have been taken to be equal to: $\rho = 1.89 \times 10^3$ kg/m^3, $v = 0.3$ and $V_s = 150$ m/s, respectively. The corrected constants of swaying and rocking springs have been taken as: $\beta_x = 0.96$, $\beta_\phi = 0.5$ and the equivalent radii of foundation for swaying and rocking springs have been estimated as equal to: $r_h = r_r = 4$ m (Takewaki 2005). The following basic values describing the structural properties have been used in the analysis (see Mahmoud et al. 2013):

- left building:

$$\begin{aligned} m_1^L &= m_2^L = m_3^L = 25 \times 10^3 \text{ kg}, \\ K_1^L &= K_2^L = K_3^L = 3.460 \times 10^6 \text{ N/m}, \\ C_1^L &= C_2^L = C_3^L = 6.609 \times 10^4 \text{ kg/s}, \\ F_{Y1}^L &= F_{Y2}^L = F_{Y3}^L = 1.369 \times 10^5 \text{ N}, \end{aligned}$$

- right building:

$$\begin{aligned} m_1^R &= m_2^R = m_3^R = 100 \times 10^3 \text{ kg}, \\ K_1^R &= K_2^R = K_3^R = 1.736 \times 10^8 \text{ N/m}, \\ C_1^R &= C_2^R = C_3^R = 8.749 \times 10^5 \text{ kg/s}, \\ F_{Y1}^R &= F_{Y2}^R = F_{Y3}^R = 1.442 \times 10^7 \text{ N}. \end{aligned}$$

For the above values, the natural period of the left building has been determined to be equal to $T^L = 1.2$ s ($T^L = 1.3$ s with SSI), while the natural period of the right structure has been calculated as equal to $T^R = 0.7$ s ($T^R = 0.75$ s with SSI). In order to solve the equation of motion (3.7a–3.7h) numerically, the time-stepping Newmark method (Newmark 1959), with constant time step $\Delta t = 0.001$ s, has been used.

The examples of the results of the study for the NS component of the Imperial Valley earthquake (15.10.1979, Meloland Overpass Station) are presented below

(see also Mahmoud et al. 2013). The displacement time histories with SSI [see Eqs. (3.7a–3.7h)] and without SSI [see Eq. (3.1a–3.1d)] are presented in Fig. 3.17. The results clearly show that taking into account the rotational and horizontal movements of the supporting soil leads to the reduction in displacements of the storeys of both buildings colliding under earthquake excitation. Moreover, the differences between the peak displacements for responses considering SSI and peak displacements obtained when SSI is ignored are much more pronounced for the left (lighter and more flexible) building. The peak displacements obtained for the first, the second and the third storey of the left building considering SSI are lower by 76.8, 67.0 and 61.8 %, respectively, comparing to the case when SSI is not incorporated in the numerical analysis.

Figure 3.18 shows the time histories of energy dissipated by damping [see Eq. (3.11)] for the case of buildings without considering SSI, as compared to the case when SSI is taken into account. It can be seen from the figure that incorporating the effects of soil flexibility results in the decrease in the amount of energy dissipated during the time of the ground motion. Moreover, the curves for each floor level show sudden jumps which are caused by collisions between buildings.

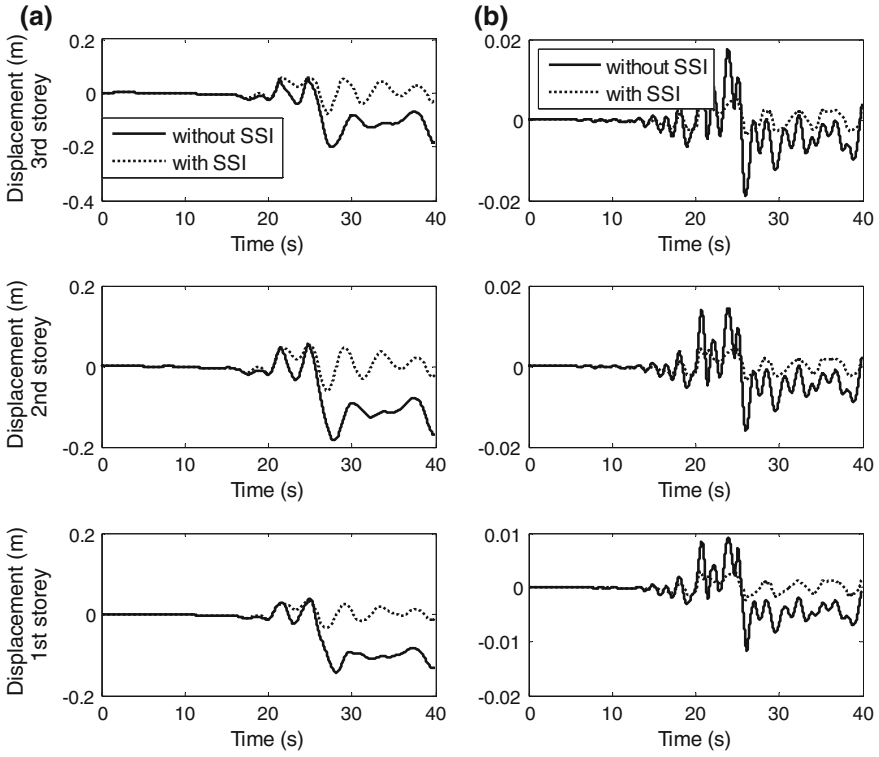

Fig. 3.17 Displacement time histories for different storeys of buildings with and without SSI considering pounding between structures (Mahmoud et al. 2013). **a** Left building. **b** Right building

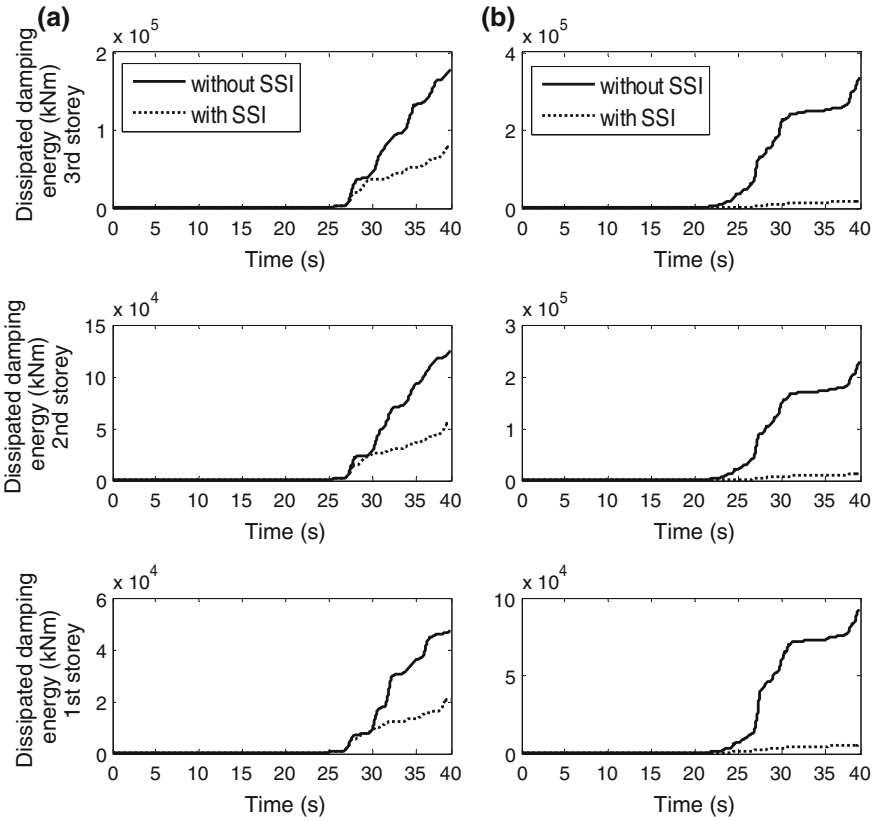

Fig. 3.18 Dissipated damping energy time histories with and without SSI. **a** Left building. **b** Right building

Ignoring SSI visibly amplifies those jumps leading to the increase in the amount of dissipated energy for all the considered storey levels of colliding buildings. Figure 3.18 clearly demonstrates that the influence of SSI on the obtained dissipated damping energy time histories of adjacent buildings is significant.

The time histories of energy dissipated by yielding [see Eq. (3.12)] with and without SSI are presented in Fig. 3.19. It is apparent that the obtained energy responses are highly affected by the simultaneous effect of collisions between buildings and the supporting base flexibility. The results of the analysis indicate that the induced pounding forces cause sudden increase in the dissipated yielding energy responses for the storeys of the left and the right building. However, generally speaking, the incorporation of the base flexibility decreases the amount of the energy dissipated by yielding (see Fig. 3.19). Moreover, the storeys of colliding buildings keep nearly constant values of dissipated yielding energy after the end of the range in which collisions between buildings take place.

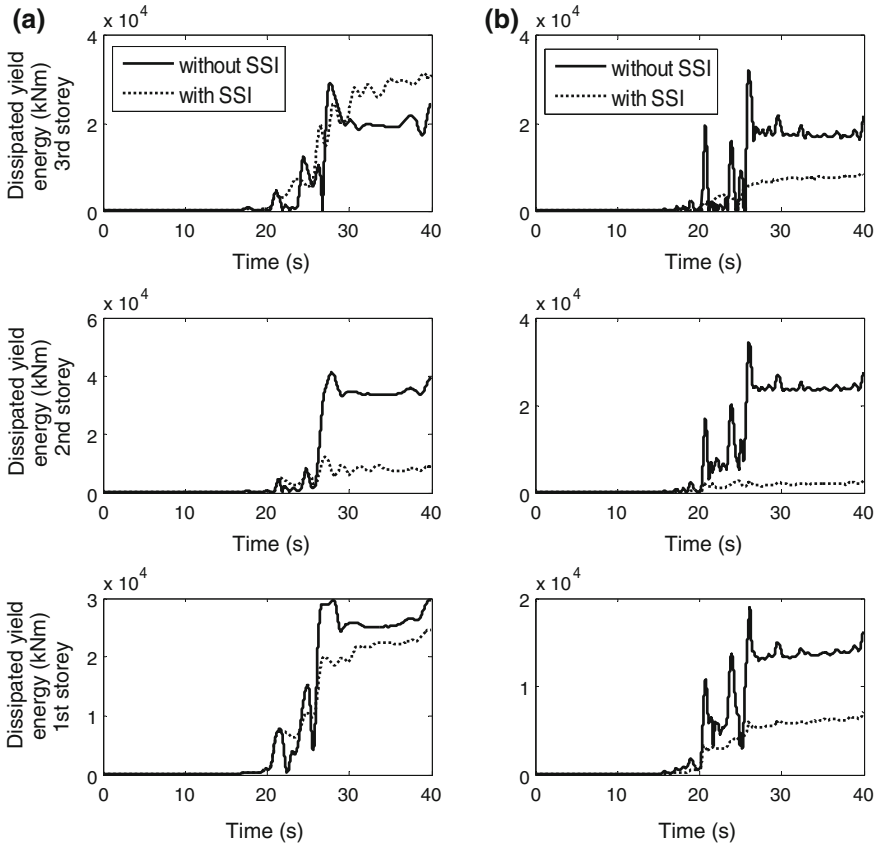

Fig. 3.19 Dissipated yielding energy time histories with and without SSI (Mahmoud et al. 2013). **a** Left building. **b** Right building

Figure 3.20 presents the absorbed kinetic energy time histories at each storey of colliding buildings [see Eq. (3.13)] with fixed bases as well as for the case when SSI is incorporated in the analysis. It can be seen from the figure that, for all the storeys of both buildings, high kinetic energy has been induced during the specific moments of the time histories, which are related to the moments of collisions. However, the incorporation of SSI in the analysis considerably decreases the amount of the absorbed kinetic energy. Moreover, it has been noticed that the kinetic energy absorbed at levels of lower storeys show smaller values comparing to the values obtained at higher storey levels. Also, the storeys of the lighter and more flexible left building absorb higher values of kinetic energy comparing to the energy which has been absorbed by the storeys of the heavier and stiffer right structure. As it could be expected, the absorbed kinetic energy represents relatively small amount of energy comparing to the amount of energy dissipated by damping and yielding.

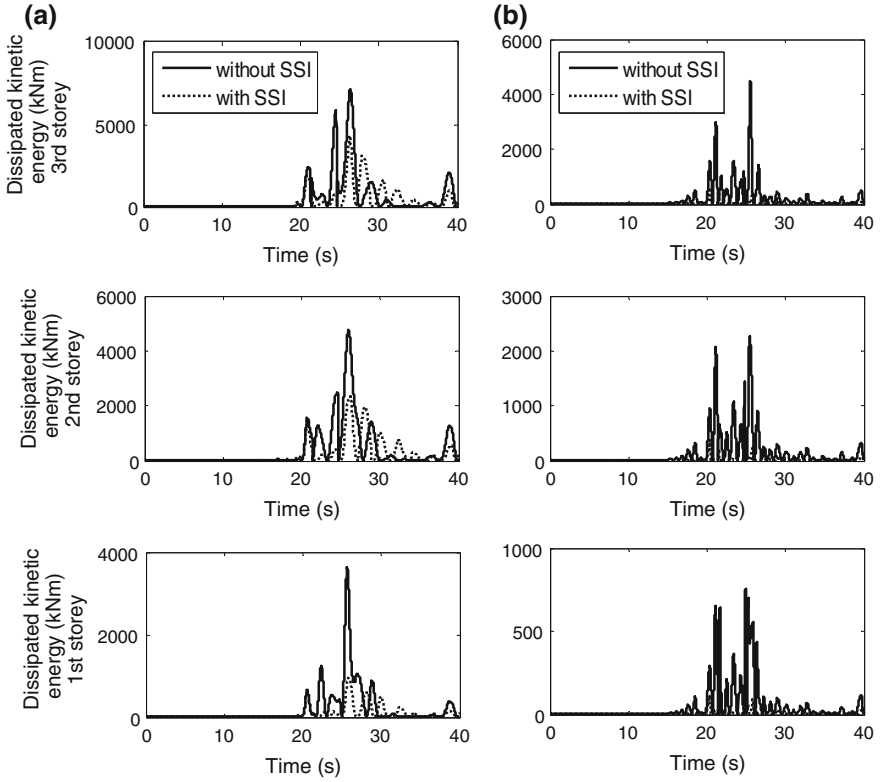

Fig. 3.20 Absorbed kinetic energy time histories with and without SSI (Mahmoud et al. 2013). **a** Left building. **b** Right building

Figure 3.21 shows the variation in the peak absorbed kinetic energy for colliding buildings considering and ignoring SSI for different values of the in-between gap size. It can be seen from the figure that the incorporation of the soil flexibility in the analysis results in substantial decrease in the peak absorbed kinetic energy values, especially for the storeys of the right building. The results indicate that neglecting SSI significantly influences the obtained peak values of both buildings and the influence is larger when the separation gap is small. It can be seen form Fig. 3.21 that, with the increase in separation gap, an increase trend can be observed up to a certain maximum value, which is followed by a decrease trend and with further increase in the gap size, the peak absorbed kinetic energy values remain nearly unchanged. Moreover, minor differences between the peak kinetic energy responses of the lower storeys of the left building with and without SSI have been obtained at larger gaps. On the other hand, a significant variation between the obtained peak energy responses for considering and ignoring the effects of SSI is visible for the storeys of the right building for all the considered separation gap size values.

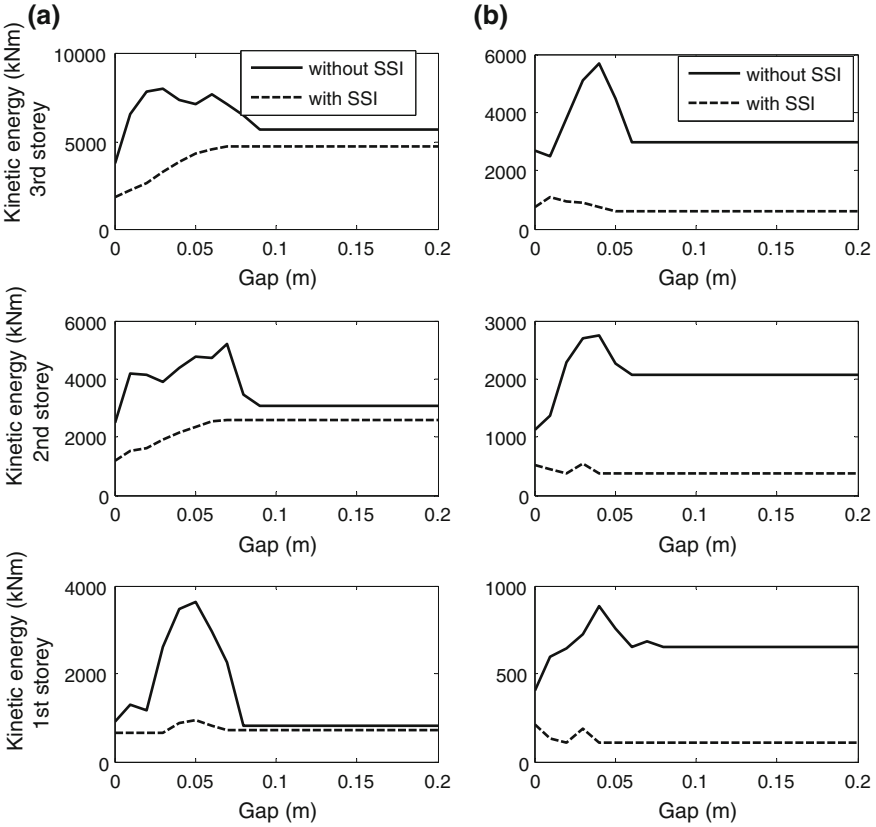

Fig. 3.21 Peak absorbed kinetic energy with and without SSI with respect to the gap size between buildings (Mahmoud et al. 2013). **a** Left building. **b** Right building

The results from the non-linear analysis of the insufficiently separated three-storey buildings shown in Figs. 3.17, 3.18, 3.19, 3.20 and 3.21 indicate that the incorporation of the soil flexibility decreases the dissipated and absorbed energy demand and consequently leads generally to the reduction in structural responses. It is worth noting that the measure of structural damage is highly related to the ductility and hysteretic energy demands, i.e. the hysteretic (yielding) energy demand is an important factor for the damage index (see Symans et al. 2008). Generally speaking, the smaller the hysteretic (yielding) energy demand the smaller the damage index measure. Therefore, the results of the study indicate that ignoring the effects of SSI overestimates the damage measure of colliding structures under earthquake excitations.

3.5 Pounding-Involved Response Analysis Using FEM

The most precise results are usually obtained with the help of FEM which allows us to create models of buildings with detailed representation of their geometry. It can be especially important in the case of the analysis on eccentric pounding, which is induced due to torsional vibrations of structures (Polycarpou et al. 2014). In this section, as an example of such analysis, let us consider a case of pounding between the Olive View Hospital main building and one of its independently standing stairway towers during the San Fernando earthquake of 1971 (see also Jankowski 2009, 2012).

The FE model of interacting buildings (two reinforced concrete structures) consisting of 11,610 elements is shown in Fig. 3.22. All structural members, i.e. columns, walls and slabs have been modelled by multi-layer (rebar elements embedded into concrete) four-node quadrilateral shell elements with multiple integration points through the thickness. The details of geometric properties have been specified according to the descriptions given by Bertero and Collins (1973) and Mahin et al. (1976). Structural bases of the main building have been rigidly fixed to the ground and the soil-structure interaction has not been considered. In the case of the stairway tower, however, rocking of its foundation has been taken into account by introducing rotational springs with the rotational stiffness of 10^9 Nm/rad for both horizontal directions. The natural periods for the main building have been determined as equal to: $T_1 = 0.64$ s, $T_2 = 0.61$ s, $T_3 = 0.52$ s for the transverse (Y direction), longitudinal (X direction) and torsional vibrations, respectively. On the other hand, the stairway tower has been characterized by the natural periods equal to: $T_1 = 0.40$ s, $T_2 = 0.21$ s, $T_3 = 0.15$ s for the longitudinal (X direction), transverse (Y direction) and torsional vibrations, respectively. Viscous damping of the Rayleigh type has been employed in the models to simulate the dissipation of energy during vibration of structures (see Clough and Penzien 1993; Hall 2006). The damping matrix has been assumed to be linearly proportional to the stiffness matrix. Structural damping has been taken to be equal to 5 % of critical in the elastic mode of vibration in the longitudinal direction for each structure (see Bertero and Collins 1973; Mahin et al. 1976). The non-linear material behaviour, including stiffness degradation of concrete under cyclic loading as well as elasto-plastic model of steel, has been incorporated in the models of analyzed structures (see Jankowski 2009 for details). Pounding between the stairway tower and the main building has been controlled by gap-friction elements, placed between the structures (see Fig. 3.22b), allowing to close the gap in the longitudinal direction and impose friction forces in the transverse and vertical directions when contact has been detected. The separation gap of 0.1016 m (4 inches) has been left between the structures (see Bertero and Collins 1973). In the analysis, the friction coefficient of 0.5 has been applied.

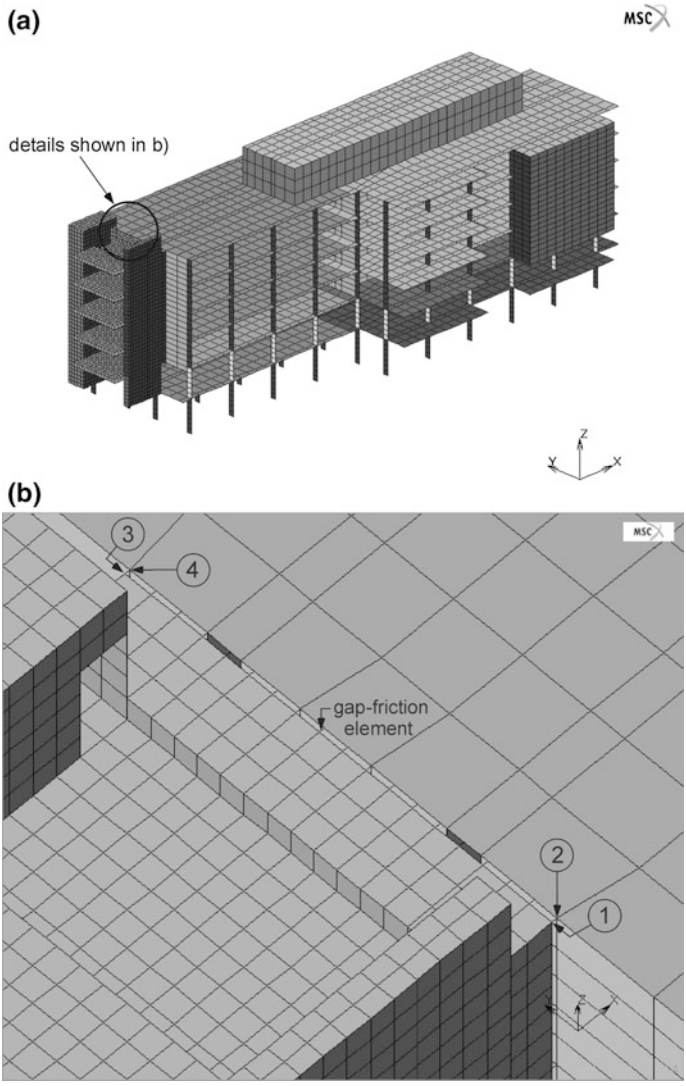

Fig. 3.22 FE model of interacting stairway tower and main building (Jankowski 2009). **a** General view. **b** Details of separation gap

The detailed, three-dimensional pounding-involved analysis has been conducted with the time step of $\Delta t = 0.001$ s. The scaled N16°W, N74°E and UD components of the San Fernando earthquake of 1971, recorded at the Pacoima Dam station (see Mahin et al. 1976 for details), have been applied along the longitudinal, transverse and vertical direction, respectively. The structural response has been determined using the time-stepping Newmark method with the standard parameters: $\gamma = 0.5$ and $\beta = 0.25$. The examples of the results are presented below.

3.5.1 Response in the Longitudinal Direction

Figure 3.23 shows the displacement time histories for the stairway tower (node 1) and the main building (node 2), whereas Figs. 3.24 and 3.25 present a comparison between the pounding-involved and independent vibration (large separation gap) responses of both structures. It can be clearly seen from Figs. 3.23 and 3.24 that the behaviour of the stairway tower (lighter structure) in the longitudinal direction is substantially influenced by earthquake-induced pounding. The results indicate that the peak response of this structure is increased due to collisions by as much as 46.8 %. On the other hand, Figs. 3.23 and 3.25 show that the longitudinal response of the Olive View Hospital main building (heavier building) is nearly unaffected by structural pounding. In the case of this structure, a change in the peak displacement during the analyzed earthquake is as low as 0.4 %.

3.5.2 Response in the Transverse Direction

The pounding-involved and independent vibration displacement time histories of the stairway tower (node 1) and the main building (node 2) in the transverse direction are shown in Figs. 3.26 and 3.27, respectively. It can be seen from the first figure that, similarly as in the case of the longitudinal direction, the transverse response of the stairway tower is changed substantially due to impacts. In the case of the transverse direction, however, the value of the peak displacement of the

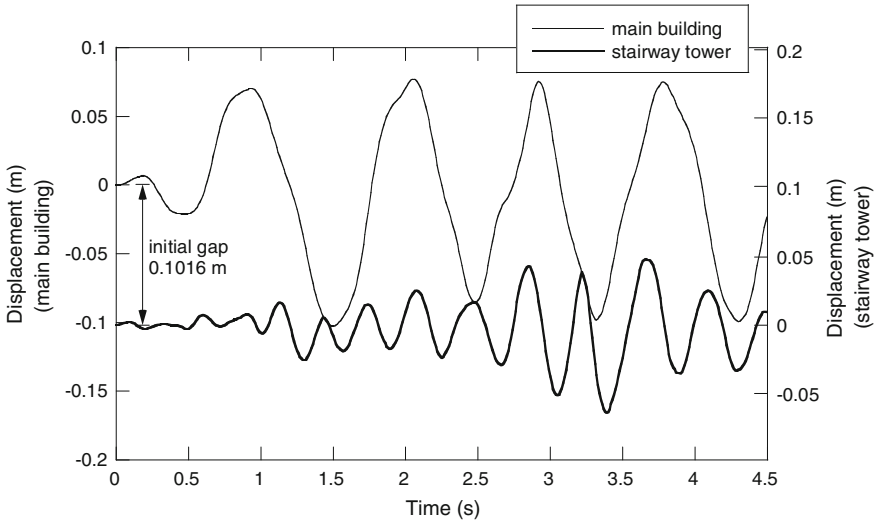

Fig. 3.23 Displacement time histories for the stairway tower (node 1) and the main building (node 2) in the longitudinal direction (Jankowski 2009)

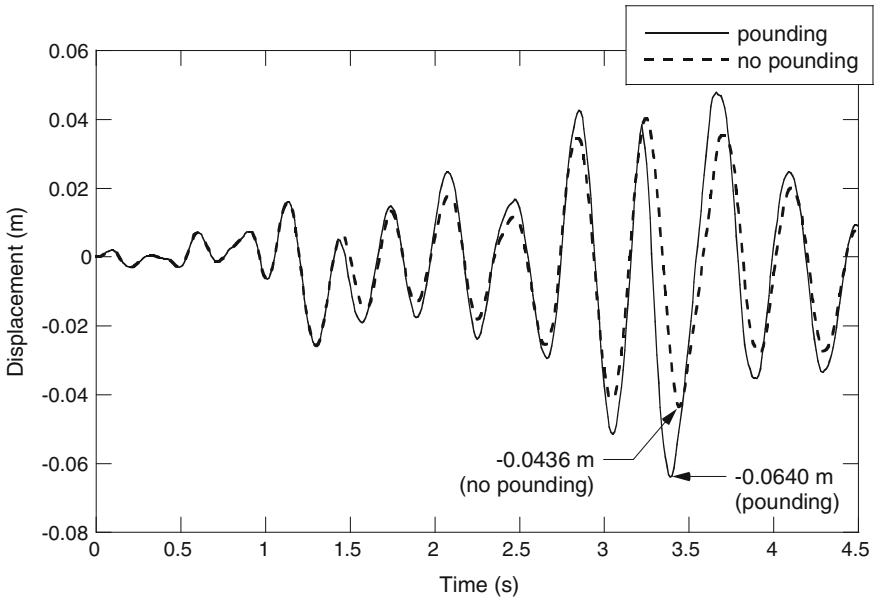

Fig. 3.24 Comparison between pounding-involved and independent vibration responses of the stairway tower (node 1) in the longitudinal direction (Jankowski 2009)

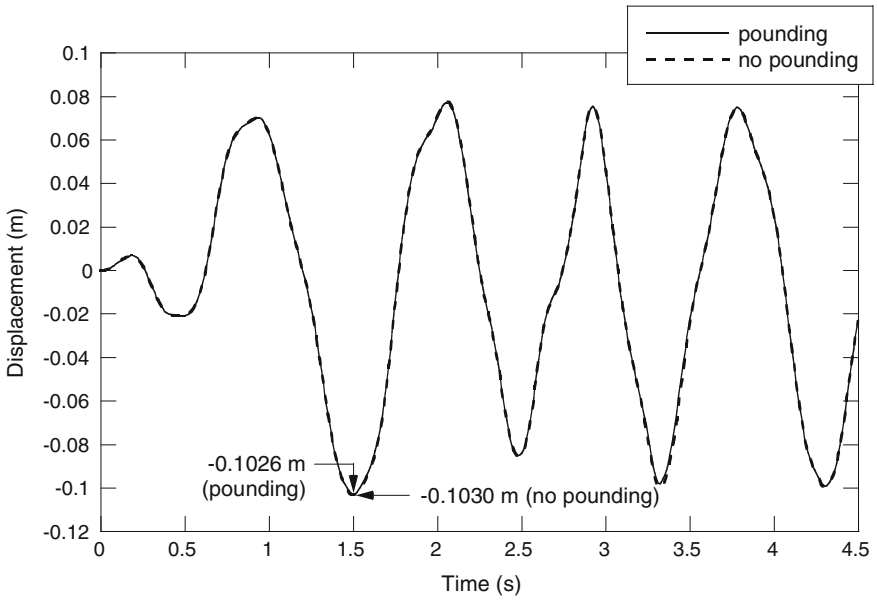

Fig. 3.25 Comparison between pounding-involved and independent vibration responses of the main building (node 2) in the longitudinal direction (Jankowski 2009)

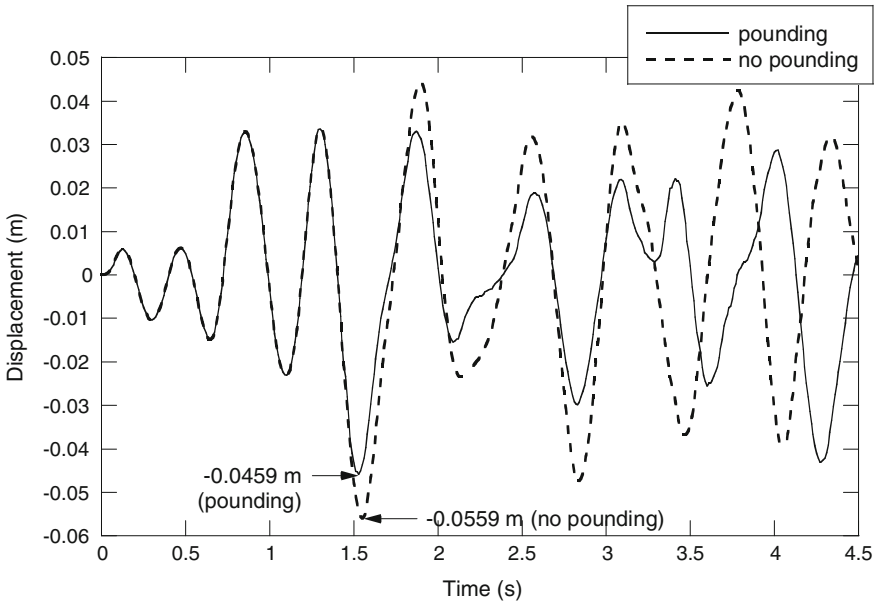

Fig. 3.26 Comparison between pounding-involved and independent vibration responses of the stairway tower (node 1) in the transverse direction (Jankowski 2009)

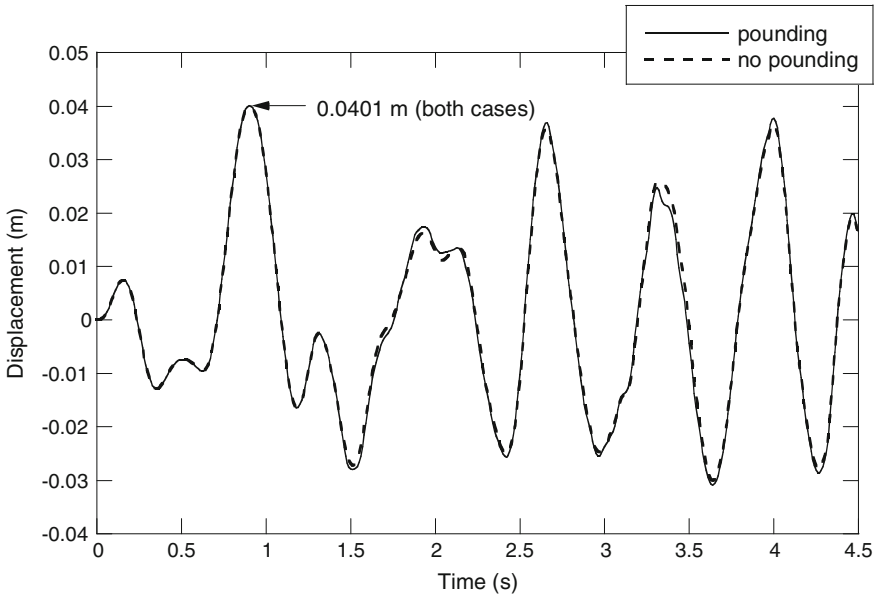

Fig. 3.27 Comparison between pounding-involved and independent vibration responses of the main building (node 2) in the transverse direction (Jankowski 2009)

pounding-involved response decreases, and this reduction is equal to 17.9 %. On the contrary to the stairway tower, the behaviour of the main building in the transverse direction is only slightly influenced by structural interactions, as it can be seen in Fig. 3.27. In this case, the peak displacement obtained during the earthquake is the same for the pounding-involved and independent vibration response cases, since this value has been reached before the first contact.

3.5.3 Torsional Response

Figures 3.28 and 3.29 show the comparison between the pounding-involved and independent vibration time histories of the rotation angle at the top floor of the stairway tower and the main building, respectively. The results presented in the figures indicate that torsional vibrations of both structures are important components of the overall structural responses, even without pounding. They are induced during the earthquake due to structural eccentricity caused by asymmetric plan of the structures. However, it can be clearly observed from Fig. 3.28, that torsional vibrations of the stairway tower are substantially increased as the result of collisions. In the case of this structure, the increase in the peak value of the rotation angle at the top floor is as high as 122.1 %. On the other hand, Fig. 3.29 shows that the torsional response of the Olive View Hospital main building is only slightly

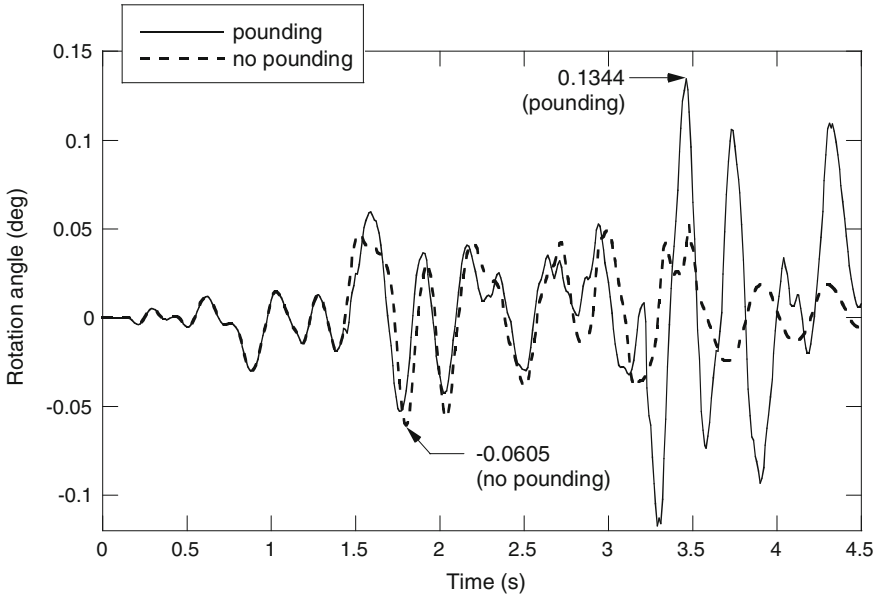

Fig. 3.28 Comparison between pounding-involved and independent vibration time history of the rotation angle at the top floor of the stairway tower (Jankowski 2009)

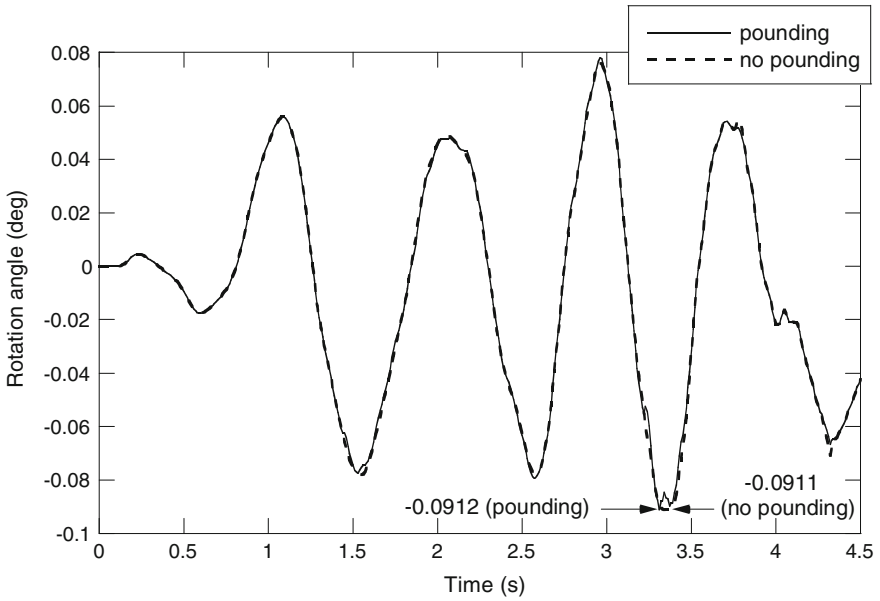

Fig. 3.29 Comparison between pounding-involved and independent vibration time history of the rotation angle at the top floor of the main building (Jankowski 2009)

influenced by structural interactions. A change in the peak value of the rotation angle at the top floor of this structure during the whole time of the seismic excitation is only 0.1 %.

References

Anagnostopoulos, S.A.: Pounding of buildings in series during earthquakes. Earthquake Eng. Struct. Dynam. **16**, 443–456 (1988)

Anagnostopoulos, S.A., Spiliopoulos, K.V.: An investigation of earthquake induced pounding between adjacent buildings. Earthquake Eng. Struct. Dynam. **21**, 289–302 (1992)

Bertero, V.V., Collins, R.G.: Investigation of the failures of the Olive View stairtowers during the San Fernando earthquake and their implications on seismic design. EERC report No. 73–26. Earthquake Engineering Research Center, University of California, Berkeley, USA (1973)

Bhattacharya, K.: Dutta. S. Dasgupta, C.S.: Effect of soil-flexibility on dynamic behaviour of building frames on raft foundation. Sound Vibr. **274**, 111–135 (2004)

Buckle, I.G., Mayes, R.L.: Seismic isolation: history, application and performance-A world overview. Earthq. Spectra **6**, 161–202 (1990)

Chau, K.T., Wei, X.X.: Pounding of structures modelled as non-linear impacts of two oscillators. Earthquake Eng. Struct. Dynam. **30**, 633–651 (2001)

Clough, R.W., Penzien, J.: Dynamics of Structures. McGraw-Hill, New York (1993). (International Edition)

Cole, G., Dhakal, R., Carr, A., Bull, D.: An investigation of the effects of mass distribution on pounding structures. Earthquake Eng. Struct. Dynam. **40**, 641–659 (2011)

Davis, R.O.: Pounding of buildings modelled by an impact oscillator. Earthquake Eng. Struct. Dynam. **21**, 253–274 (1992)
Dimova S.L.: Numerical problems in modelling of collision in sliding systems subjected to seismic excitations. Adv. Eng. Softw. **31**, 467–471 (2000)
Dutta, S.C., Rana, R.: Inelastic seismic demand of low-rise buildings with soil-flexibility. Int. J. Non-Linear Mech. **45**, 419–432 (2010)
Efraimiadou, S., Hatzigeorgiou, G.D., Beskos, D.E.: Structural pounding between adjacent buildings subjected to strong ground motions. Part I: the effect of different structures arrangement. Earthquake Eng. Struct. Dynam. **42**, 1509–1528 (2013)
Falborski, T., Jankowski, R.: Polymeric bearings—a new base isolation system to reduce structural damage during earthquakes. Key Eng. Mater. **569–570**, 143–150 (2013)
Fariborz, A.N., Ali, T.R.: Nonlinear dynamic response of tall buildings considering structure-soil-structure effects. Struct. Des. Tall Spec. Build. **22**, 1075–1082 (2013)
Halabian, A.M., Erfani, M.: The effect of foundation flexibility and structural strength on response reduction factor of RC frame structures. Struct. Des. Tall Spec. Build. **22**, 1–28 (2010)
Hall, J.F.: Problems encountered from the use (or misuse) of Rayleigh damping. Earthquake Eng. Struct. Dynam. **35**, 525–545 (2006)
Jangid, R.S., Datta, T.K.: Seismic behavior of base-isolated buildings: a state-of-the-art review. J. Struct. Build. **110**, 186–203 (1995)
Jankowski, R.: Nonlinear rate dependent model of high damping rubber bearing. Bull. Earthq. Eng. **1**, 397–403 (2003)
Jankowski, R.: Impact force spectrum for damage assessment of earthquake-induced structural pounding. Key Eng. Mater. **293–294**, 711–718 (2005)
Jankowski, R.: Pounding force response spectrum under earthquake excitation. Eng. Struct. **28**, 1149–1161 (2006)
Jankowski, R.: Assessment of damage due to earthquake-induced pounding between the main building and the stairway tower. Key Eng. Mater. **347**, 339–344 (2007a)
Jankowski, R.: Non-linear analysis of pounding-involved response of equal height buildings under earthquake excitation. DSc dissertation, Wydawnictwo Politechniki Gdańskiej, Gdańsk, Poland (2007b)
Jankowski, R.: Earthquake-induced pounding between equal height buildings with substantially different dynamic properties. Eng. Struct. **30**(10), 2818–2829 (2008)
Jankowski, R.: Non-linear FEM analysis of earthquake-induced pounding between the main building and the stairway tower of the Olive View Hospital. Eng. Struct. **31**, 1851–1864 (2009)
Jankowski, R.: Non-linear FEM analysis of pounding-involved response of buildings under non-uniform earthquake excitation. Eng. Struct. **37**, 99–105 (2012)
Jankowski, R., Walukiewicz, H.: Modeling of two-dimensional random fields. Probab. Eng. Mech. **12**, 115–121 (1997)
Jing, H.-S., Young, M.: Impact interactions between two vibration systems under random excitation. Earthquake Eng. Struct. Dynam. **20**, 667–681 (1991)
Karayannis, C.G., Favvata, M.J.: Earthquake-induced interaction between adjacent reinforced concrete structures with non-equal heights. Earthquake Eng. Struct. Dynam. **34**, 1–20 (2005a)
Karayannis, C.G., Favvata, M.J.: Inter-story pounding between multistory reinforced concrete structures. Struct. Eng. Mech. **20**, 505–526 (2005b)
Kelly, J.M.: Earthquake-Resistant Design with Rubber. Springer, London (1993)
Komodromos P.: Seismic Isolation of Earthquake-Resistant Structures. WIT Press, Southampton (2000)
Komodromos, P.: Simulation of the earthquake-induced pounding of seismically isolated buildings. Comput. Struct. **86**, 618–626 (2008)
Komodromos, P., Polycarpou, P.C., Papaloizou, L., Phocas, M.C.: Response of seismically isolated buildings considering poundings. Earthquake Eng. Struct. Dynam. **36**, 1605–1622 (2007)

Mahin, S.A., Bertero, V.V., Chopra, A.K., Collins, R.G.: Response of the Olive View Hospital main building during the San Fernando earthquake. EERC report no. 76–22. Earthquake Engineering Research Center, University of California, Berkeley, USA (1976)

Mahmoud, S., Abd-Elhamed, A., Jankowski, R.: Earthquake-induced pounding between equal height multi-storey buildings considering soil-structure interaction. Bull. Earthq. Eng. **11**(4), 1021–1048 (2013)

Mahmoud, S., Austrell, P.-E., Jankowski, R.: Simulation of the response of base-isolated buildings under earthquake excitations considering soil flexibility. Earthquake Eng. Vibr. **11**, 359–374 (2012)

Mahmoud, S., Chen, X., Jankowski, R.: Structural pounding models with Hertz spring and nonlinear damper. J. Appl. Sci. **8**, 1850–1858 (2008)

Mahmoud, S., Jankowski, R.: Elastic and inelastic multi-storey buildings under earthquake excitation with the effect of pounding. J. Appl. Sci. **9**(18), 3250–3262 (2009)

Mahmoud, S., Jankowski, R.: Pounding-involved response of isolated and non-isolated buildings under earthquake excitation. Earthq. Struct. **1**(3), 231–252 (2010)

Mahmoud, S., Jankowski, R.: Modified linear viscoelastic model of earthquake-induced structural pounding. Iran. J. Sci. Technol. **35**(C1), 51–62 (2011)

Maison, B.F., Kasai, K.: Analysis for type of structural pounding. J. Struct. Eng. **116**, 957–977 (1990)

Maison, B.F., Kasai, K.: Dynamics of pounding when two buildings collide. Earthquake Eng. Struct. Dynam. **21**, 771–786 (1992)

Malhotra, P.K.: Dynamics of seismic impacts in base-isolated buildings. Earthquake Eng. Struct. Dynam. **26**, 797–813 (1997)

Matsagar, V.A., Jangid, R.S.: Seismic response of base-isolated structures during impact with adjacent structures. Eng. Struct. **25**, 1311–1323 (2003)

Mostaghel, N., Khodaverdian, M.: Dynamics of resilient-friction base isolator (R-FBI). Earthquake Eng. Struct. Dynam. **15**, 379–390 (1987)

Nagarajaiah, S., Sun, X.: Base-isolated FCC building: impact response in Northridge earthquake. J. Struct. Eng. **127**, 1063–1075 (2001)

Newmark, N.: A method of computation for structural dynamics. J. Eng. Mech. Div. ASCE **85**, 67–94 (1959)

Papadrakakis, M., Mouzakis, H., Plevris, N., Bitzarakis, S.A.: Lagrange multiplier solution method for pounding of buildings during earthquakes. Earthquake Eng. Struct. Dynam. **20**, 981–998 (1991)

Polycarpou, P.C., Komodromos, P.: Earthquake-induced poundings of a seismically isolated building with adjacent structures. Eng. Struct. **32**, 1937–1951 (2010a)

Polycarpou, P.C., Komodromos, P.: On poundings of a seismically isolated building with adjacent structures during strong earthquakes. Earthquake Eng. Struct. Dynam. **39**, 933–940 (2010b)

Polycarpou, P.C., Papaloizou, L., Komodromos, P.: An efficient methodology for simulating earthquake-induced 3D pounding of buildings. Earthquake Eng. Struct. Dynam. **43**, 985–1003 (2014)

Przewłócki, J., Knabe, W.: Settlement of a soil stratum subjected to an earthquake. Int. J. Numer. Anal. Meth. Geomech. **19**, 813–821 (1995)

Richart, F.E., Whitman, R.V.: Comparison of footing vibration tests with theory. Soil Mech. Found. Div. **93**(SM6), 143–168 (1967)

Sołtysik, B., Jankowski, R.: Non-linear strain rate analysis of earthquake-induced pounding between steel buildings. Int. J. Earth Sci. Eng. **6**, 429–433 (2013)

Spyrakos, C.C., Koutromanos, I.A., Maniatakis, C.A.: Seismic response of base-isolated buildings including soil-structure interaction. Soil Dyn. Earthq. Eng. **29**, 658–668 (2009)

Symans, M.D., Charney, F.A., Whittaker, A.S., Constantinou, M.C., Kircher, C.A., Johnson, M.W., McNamara, R.J.: Energy dissipation systems for seismic applications: current practice and recent developments. J. Struct. Eng. **134**, 3–21 (2008)

Stewart, J.P., Fenves, G.L., Seed, R.B.: Seismic soil-structure interaction in buildings, I: analytical methods. Geotech. Geoenviron. Eng. **125**, 26–37 (1999a)

Stewart, J.P., Seed, R.B., Fenves, G.L.: Seismic soil-structure interaction in buildings, II: empirical findings. Geotechn. Geoenviron. Eng. **125**, 38–48 (1999b)

Takewaki, I.: Bound of earthquake input energy to soil-structure interaction systems. Soil Dyn. Earthq. Eng. **25**, 741–752 (2005)

Tsai, H.C.: Dynamics analysis of base-isolated shear beams bumping against stops. Earthquake Eng. Struct. Dynam. **26**, 515–528 (1997)

Wakabayashi, M.: Design of Earthquake-Resistant Buildings. Mc Graw-Hill, Texas (1985)

Wolf, J.P.: Dynamic Soil-Structure Interaction. Prentice Hall, Englewood Cliffs (1987)

Ye, K., Li, L., Zhu, H.P.: A modified Kelvin impact model for pounding simulation of base-isolated building with adjacent structures. Earthquake Eng. Vibr. **8**, 433–446 (2009)

Zahrah, T.F., Hall, W.J.: Earthquake energy absorption in SDOF structures. J. Struct. Eng. ASCE **110**, 1757–1772 (1984)

Chapter 4
Pounding Between Bridge Segments

On the contrary to buildings (see, for example, Anagnostopoulos 1988; Maison and Kasai 1992; Jankowski 2005, 2007; Karayannis and Favvata 2005; Mahmoud and Jankowski 2009, 2011; Mahmoud et al. 2013; Sołtysik and Jankowski 2013; Polycarpou et al. 2014), earthquake-induced structural pounding in bridges has not been studied so intensively. Fundamental analysis on interactions between superstructure segments in elevated bridges was conducted using a multi-degree-of-freedom (MDOF) lumped mass model of the structure (Jankowski et al. 1998). The relative displacement spectra of two colliding single-degree-of-freedom (SDOF) bridge systems were studied by Ruangrassamee and Kawashima (2001). DesRoches and Muthukumar (2002) applied the simplified lumped mass model of the structure to investigate the effects of pounding on seismic response of multi-frame bridges. The influence of ground motion spatial variation and the soil-structure interaction (SSI) on the relative response of two bridge frames was also studied by Chouw and Hao (2005, 2008).

More detailed analyses focused on earthquake-induced interactions in bridge structures were conducted with the use of finite element method (FEM). A number of pounding reduction methods were investigated by considering a model of the bridge with superstructure segments and piers modelled as elastic beam-column elements (Jankowski et al. 2000). Chouw et al. (2006) modelled girders and piers as beam-column elements to study the influence of multi-sided collisions on the bridge response due to spatially varying ground excitations. The detailed three-dimensional FEM analysis of pounding-involved response of the bridge to spatially varying ground motions was also conducted by Bi et al. (2013).

4.1 Pounding-Involved Response of the Bridge Modelled as MDOF System

Let us first consider a bridge structure as a MDOF system so as to conduct a basic analysis on the influence of pounding between superstructure segments on the structural response under earthquake excitation. The fundamental analysis can be

R. Jankowski and S. Mahmoud, *Earthquake-Induced Structural Pounding*,
GeoPlanet: Earth and Planetary Sciences, DOI 10.1007/978-3-319-16324-6_4

conducted using a simplified lumped mass bridge model with every superstructure segment discretized as a SDOF system. In the model, pounding between segments is induced by the seismic wave passage effect (see Der Kiureghian 1996). The ground motion excitation is described by identical acceleration records shifted in time for different structural supports along the bridge.

4.1.1 Description of the Analyzed Structure

A model of an isolated elevated highway bridge, specified according to the *Manual for Menshin Design of Highway Bridges*, has been used to study the influence of pounding on the structural response (Kawashima et al. 1993). The deck of the bridge consists of three-span-continuous prestressed concrete segments with a mass of 2×10^4 kg/m. The span length and the width of one superstructure segment are 40 and 14 m, respectively. A substructure consists of reinforced concrete piers of equal height of 11.5 m. Two high damping rubber bearings (HDRBs) support the superstructure at every pier. The cross section area and the thickness of rubber layers in a single bearing are 0.7921 m^2 and 0.082 m, respectively. The view of the bridge is presented in Fig. 4.1. Its longitudinal and transverse cross section as well as the cross section of pier are shown in Figs. 4.2 and 4.3, respectively. The properties of structural members of the bridge are summarized in Tables 4.1 and 4.2.

4.1.2 Response of the Bridge Using One-Dimensional Structural Model

In order to obtain a better performance of an isolated bridge, the natural period of superstructure is usually extended, whereas piers are constructed possibly rigid. In the case of the analyzed structure, the ratio between the natural frequencies of the pier-dominant mode and the deck-dominant mode is equal to 11. Thus, in the fundamental analysis of pounding, the contribution of the dynamics of piers to the response of the bridge can be neglected. Under this simplification, every superstructure segment can be treated as SDOF system with lumped mass m_i. It is assumed to be mounted on non-linear spring-dashpot element, which combines stiffness and damping coefficients, $K_i(t)$, $C_i(t)$, of all HDRBs supporting the segment as shown in Fig. 4.4.

Let us focus the analysis on a single superstructure segment of an infinitely long bridge. It has been noticed that, because of pounding, its response substantially depends on the displacement histories of a few adjacent bridge segments from both sides (Jankowski et al. 1998). It can be expected that the influence of vibrations of the segments located far from the section of interest decreases with distance. Since the theoretical derivation of the necessary bridge model and edge conditions practically is impossible, the selection of the model has been determined through

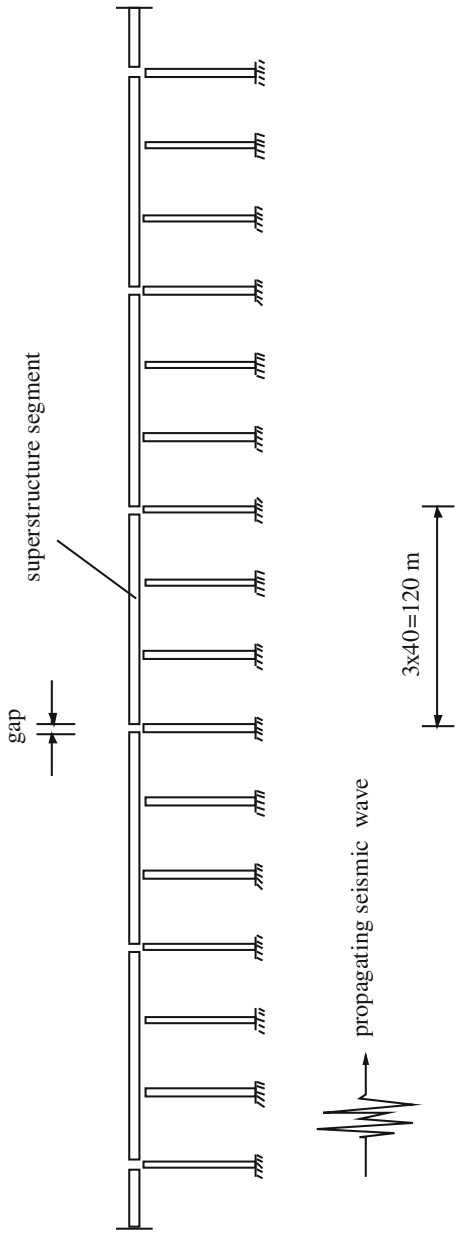

Fig. 4.1 View of analyzed elevated highway bridge

numerical simulations (see Jankowski et al. 1998 for details). By decreasing the number of superstructure segments taken into account, it has been found that for models consisting of seven or more segments, the response of the middle segment is very similar. In order to reduce the size of the bridge model even further, and thus

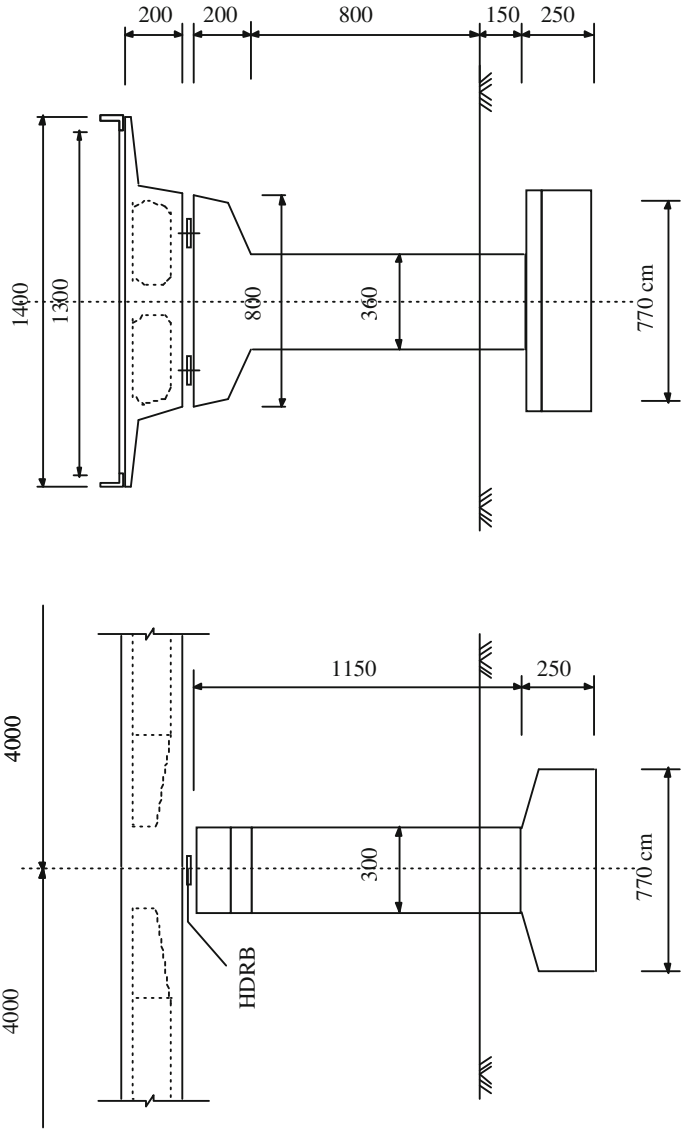

Fig. 4.2 Longitudinal and transverse cross section of the bridge (Jankowski et al. 2000)

speed up the numerical calculations, a five-segment model with simulation of neglected segments by spring-dashpots (with the same properties as impact elements) has been considered. Such a simplified 5 degree-of-freedom model of the bridge is shown in Fig. 4.5. For this configuration, the influence of edge conditions is reduced and the peak response of the middle superstructure segment for different gap sizes is similar to the case of model with seven segments (see Jankowski et al. 1998).

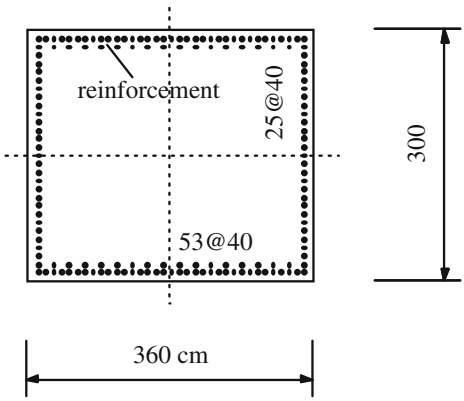

Fig. 4.3 Cross section of the pier

Table 4.1 Bridge material properties

Material	Young's modulus (GPa)	Strength (MPa)
Concrete	24.54	11.772
Reinforcement steel	200	425

Table 4.2 Properties of bridge structural members

Structural element	Mass density (kg/m^3)	Mean cross section area (m^2)	Modal damping ratio
Superstructure	1177	17	0.03
HDRB	–	0.7921	0.14
Top of pier	3788	15.408	0.05
Pier	3788	10.8	0.05
Footing	2520	59.29	0.1

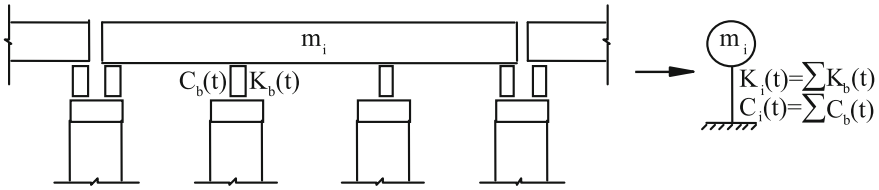

Fig. 4.4 Lumped mass model of a single superstructure segment

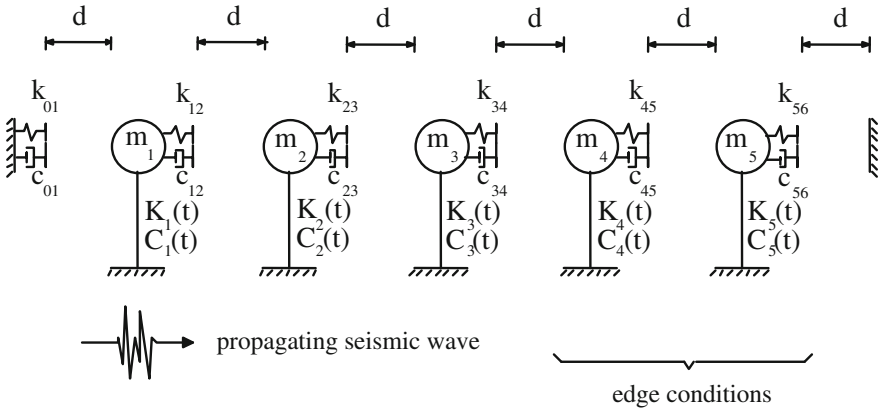

Fig. 4.5 Simplified model of the bridge

The dynamic equation of motion for the non-linear 5 degree-of-freedom model of the bridge under earthquake excitation (see Fig. 4.5) can be written in the matrix form as:

$$\mathbf{M}\ddot{\mathbf{x}}(t) + \mathbf{C}(t)\dot{\mathbf{x}}(t) + \mathbf{K}(t)\mathbf{x}(t) + \mathbf{F}(t) = -\mathbf{M}\ddot{\mathbf{x}}_g(t) \tag{4.1a}$$

$$\mathbf{M} = \begin{bmatrix} m_1 & 0 & 0 & 0 & 0 \\ 0 & m_2 & 0 & 0 & 0 \\ 0 & 0 & m_3 & 0 & 0 \\ 0 & 0 & 0 & m_4 & 0 \\ 0 & 0 & 0 & 0 & m_5 \end{bmatrix}; \quad \ddot{\mathbf{x}}(t) = \begin{bmatrix} \ddot{x}_1(t) \\ \ddot{x}_2(t) \\ \ddot{x}_3(t) \\ \ddot{x}_4(t) \\ \ddot{x}_5(t) \end{bmatrix}; \quad \dot{\mathbf{x}}(t) = \begin{bmatrix} \dot{x}_1(t) \\ \dot{x}_2(t) \\ \dot{x}_3(t) \\ \dot{x}_4(t) \\ \dot{x}_5(t) \end{bmatrix}; \quad \mathbf{x}(t) = \begin{bmatrix} x_1(t) \\ x_2(t) \\ x_3(t) \\ x_4(t) \\ x_5(t) \end{bmatrix} \tag{4.1b}$$

$$\mathbf{C}(t) = \begin{bmatrix} C_1(t) & 0 & 0 & 0 & 0 \\ 0 & C_2(t) & 0 & 0 & 0 \\ 0 & 0 & C_3(t) & 0 & 0 \\ 0 & 0 & 0 & C_4(t) & 0 \\ 0 & 0 & 0 & 0 & C_5(t) \end{bmatrix}; \quad \mathbf{F}(t) = \begin{bmatrix} F_{12}(t) - F_{01}(t) \\ F_{23}(t) - F_{12}(t) \\ F_{34}(t) - F_{23}(t) \\ F_{45}(t) - F_{34}(t) \\ F_{56}(t) - F_{45}(t) \end{bmatrix} \tag{4.1c}$$

$$\mathbf{K}(t) = \begin{bmatrix} K_1(t) & 0 & 0 & 0 & 0 \\ 0 & K_2(t) & 0 & 0 & 0 \\ 0 & 0 & K_3(t) & 0 & 0 \\ 0 & 0 & 0 & K_4(t) & 0 \\ 0 & 0 & 0 & 0 & K_5(t) \end{bmatrix}; \quad \ddot{\mathbf{x}}_g(t) = \begin{bmatrix} \ddot{x}_{g1}(t) \\ \ddot{x}_{g2}(t) \\ \ddot{x}_{g3}(t) \\ \ddot{x}_{g4}(t) \\ \ddot{x}_{g5}(t) \end{bmatrix} \tag{4.1d}$$

where $\ddot{x}_i(t)$, $\dot{x}_i(t)$, $x_i(t)$ $(i = 1, \ldots, 5)$ are the acceleration, velocity and displacement (in the longitudinal direction) of a superstructure segment with mass m_i, $\ddot{x}_{gi}(t)$ is the acceleration of input ground motion acting on ith superstructure segment and $F_{i,i+1}(t)$ denotes pounding force between superstructure segments with masses m_i, m_{i+1}.

In the analysis, pounding force, $F_{i,i+1}(t)$, has been simulated with the help of the linear viscoelastic model according to the formula [compare Eq. (2.6)]:

$$\begin{aligned} &F_{i,i+1}(t) = 0 && \text{for } \delta_{i,i+1}(t) \le 0 \quad \text{(no contact)} \\ &F_{i,i+1}(t) = k_{i,i+1}\delta_{i,i+1}(t) + c_{i,i+1}(t)\dot{\delta}_{i,i+1}(t) && \text{for } \delta_{i,i+1}(t) > 0 \quad \text{(contact)} \end{aligned} \tag{4.2}$$

where:

$$\delta_{i,i+1}(t) = x_i(t) - x_{i+1}(t) - d; \quad c_{i,i+1}(t) = 2\xi\sqrt{k_{i,i+1}\frac{m_i m_{i+1}}{m_i + m_{i+1}}} \tag{4.3}$$

and d is a gap size between superstructure segments of the bridge structure. Based on the bridge properties, the stiffness and damping coefficients of impact elements have been determined as equal to: $k_{i,i+1} = 3.4751 \times 10^9$ N/m and $c_{i,i+1} = 1.8081 \times 10^7$ kg/s ($\xi = 0.14, e = 0.65$), respectively (Jankowski et al. 1998). The mass of each superstructure segment has been calculated as: $m_i = 2.4 \times 10^6$ kg. The non-linear strain-rate dependent model, defined by Eq. (3.4), has been implemented to simulate the behaviour of HDRBs (see also Jankowski 2003; Mahmoud et al. 2012; Falborski and Jankowski 2013). The following parameters of the model have been used in the analysis for a single bearing (Jankowski et al. 1998): $a_1 = 1.6074 \times 10^7$ N/m, $a_2 = -3.7000 \times 10^7$ N/m^3, $a_3 = 8.8153 \times 10^8$ N/m^5, $a_4 = 5.9956 \times 10^6$ N/m, $a_5 = 1.5753$ s/m, $a_6 = 6.0450 \times 10^7$ N/m, $a_7 = 7.7280$ s/m, $a_8 = 48.013$ 1/m, $a_9 = 9.7679 \times 10^5$ N, $a_{10} = 5.1964 \times 10^6$ N/m^2, $a_{11} = 0.59601$ m/s. Due to the seismic wave passage effect, the input acceleration excitation, $\ddot{x}_{gi}(t)$, acting on every superstructure segment has been shifted in time by a time-delay parameter. This parameter depends on the length of segments and the mean apparent seismic wave velocity, which has been considered to be equal 1000 m/s in the analysis. In order to solve the equation of motion (4.1a–d) numerically, the time-stepping Newmark method (Newmark 1959), with parameters: $\gamma_N = 0.5, \beta_N = 0.25$ assuring the stability and accuracy of the results (see Bathe 1982; Chopra 1995) and constant time step $\Delta t = 0.005$ s, has been used.

Using the simplified 5 degree-of-freedom lumped mass model from Fig. 4.5, the response of the bridge in the longitudinal direction has been first studied. The analysis has been conducted for the NS component of the El Centro earthquake (18 May 1940) scaled to have the value of 8 m/s^2 as a peak ground acceleration (PGA). For such a scaled ground motion, the response of the single superstructure segment gives the maximum displacement equal to the design one of 0.185 m (Kawashima et al. 1993) and the maximum shear strain of HBRB approaches 300 % (see Jankowski et al. 1998). The examples of the results of the study in the form of the displacement time histories of the middle segment, m_3, for gaps $d = 0.01$ m and $d = 0.11$ m together with the response when no pounding occurs (large gap sizes) are presented in Fig. 4.6. For these values of the gap size, the relative displacements, velocities and pounding forces between segments m_3 and m_4 are also shown in Figs. 4.7, 4.8 and 4.9.

The results shown in Figs. 4.6, 4.7, 4.8 and 4.9 clearly indicate that pounding may significantly modify the behaviour of the analyzed bridge. It may either increase the response of the structure or play a positive role, depending on the pattern of collisions between adjacent bridge segments. It can be seen from Fig. 4.9a that the number of impacts for a gap size of 0.01 m is large, however, the peak pounding force hardly exceeds value of 5×10^7 N and the displacement of the analyzed segment is kept smaller than 0.06 m (see Fig. 4.6). On the other hand, the pounding force time history for gap values of 0.11 m (see Fig. 4.9b) shows only a few collisions. The first one results in the pounding force of a magnitude twice larger than for the bridge with small gaps. The force of this impact has been combined with the earthquake excitation and stored elastic energy resulting in very large deformation of the deck, as can be observed at Fig. 4.6. It should also be underlined, that the response of the bridge without pounding is larger than the

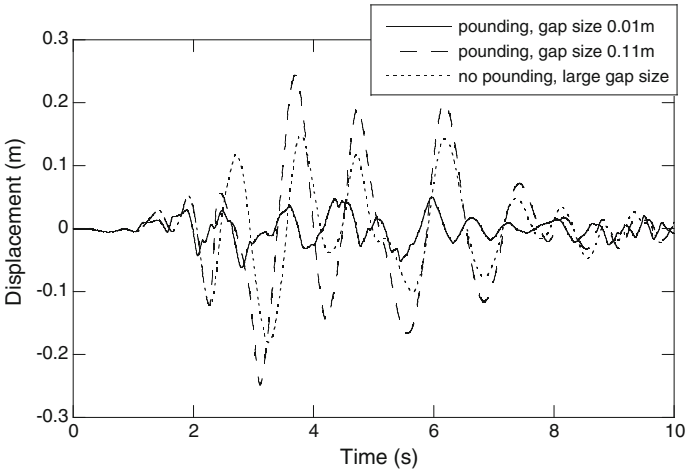

Fig. 4.6 Displacement time histories of the middle superstructure segment for different gap sizes between segments (Jankowski et al. 1998)

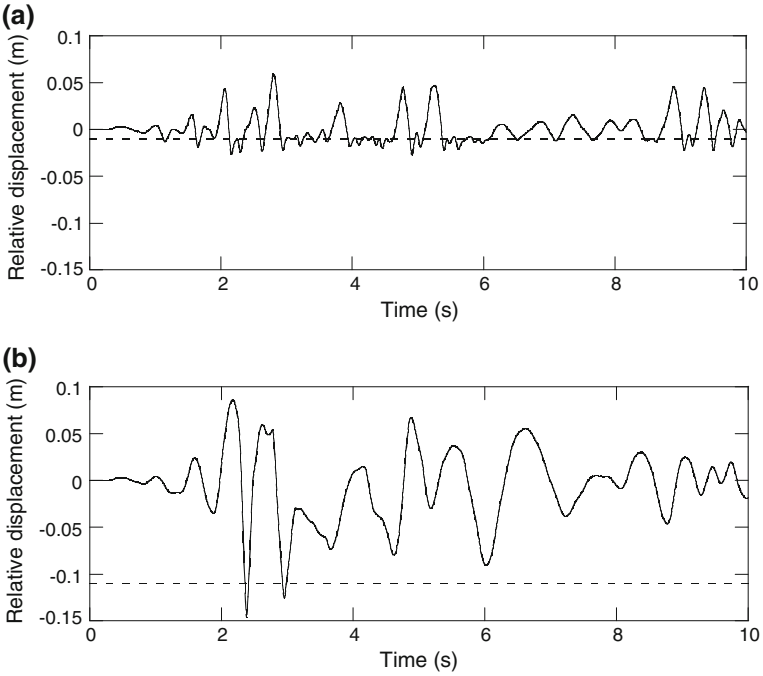

Fig. 4.7 Relative displacement time history of the middle superstructure segment for different gap sizes between segments **a** gap size 0.01 m; **b** gap size 0.11 m

response with very small gaps and many collisions, while it is smaller than the response with larger gaps for which pounding is still observed (see Fig. 4.6).

4.1.3 Response of the Bridge Using Two-Dimensional Structural Model

The real collision between superstructure segments of a bridge is a complicated multi-dimensional process. Besides modification of the bridge behaviour in the longitudinal direction, pounding may also change the structural response in the transverse direction (Malhotra et al. 1995). During impact, as schematically shown in Fig. 4.10, the large axial forces in the superstructures, $F_{i,i+1}(t)$, as well as some transverse friction forces, $\bar{F}_{i,i+1}(t)$, due to transverse relative motion of the decks, are induced. However, since the longitudinal forces, $F_{i,i+1}(t)$, are much higher than $\bar{F}_{i,i+1}(t)$, sliding in the transverse direction is usually not observed.

In order to simulate collisions between superstructure segments in a more precise way, the simplified model of the bridge (Fig. 4.5) has been extended to account for two-dimensional horizontal pounding in the way presented in Fig. 4.10. In the

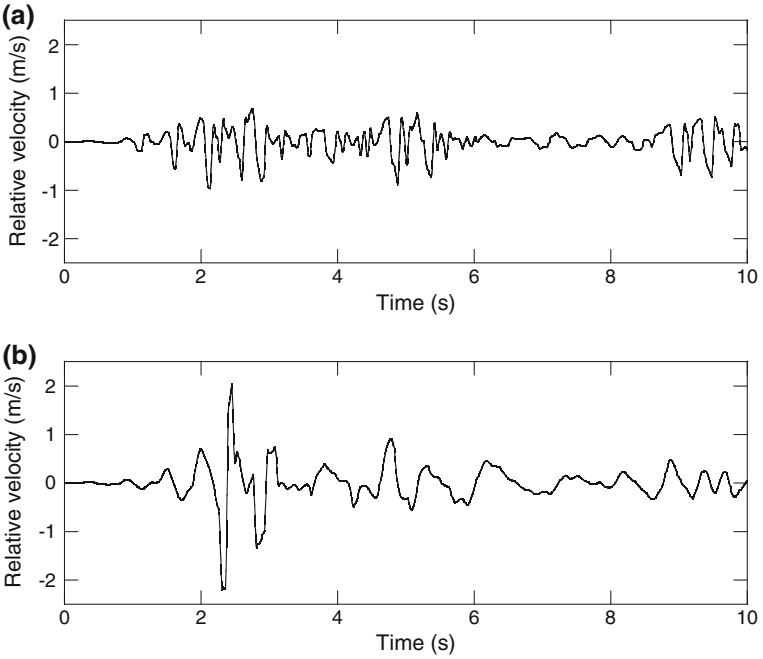

Fig. 4.8 Relative velocity time history of the middle superstructure segment for different gap sizes between segments **a** gap size 0.01 m; **b** gap size 0.11 m

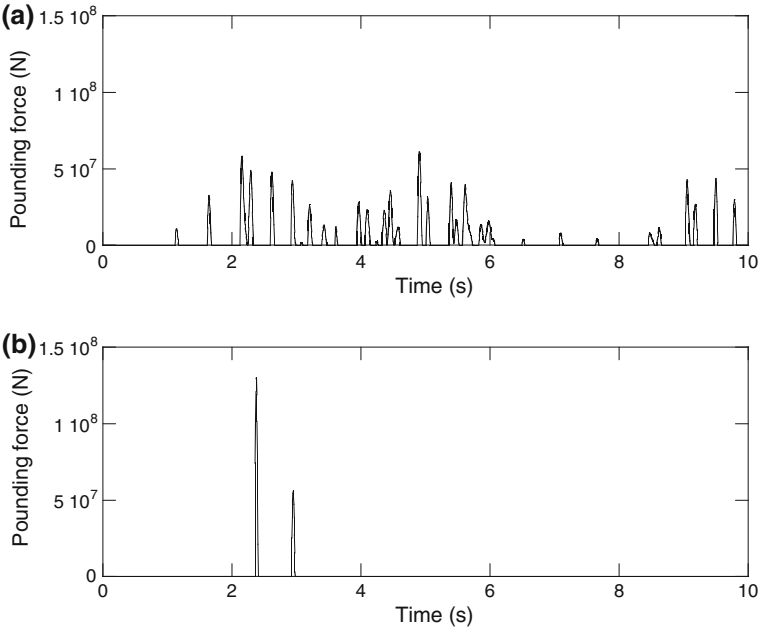

Fig. 4.9 Pounding force time history for different gap sizes between superstructure segments **a** gap size 0.01 m; **b** gap size 0.11 m

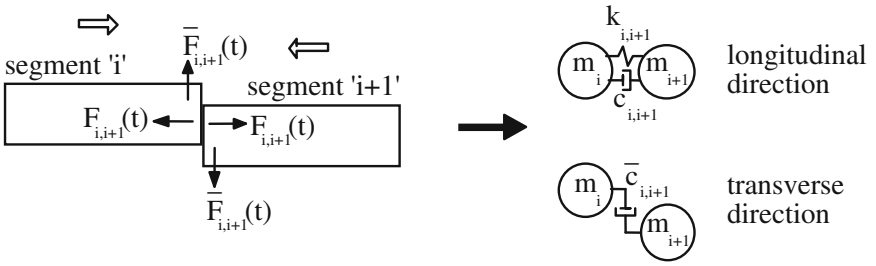

Fig. 4.10 Modelling of two-dimensional impact between superstructure segments of the bridge (*top view*)

modified model, the interaction between the segments in the transverse direction during collision is simulated by a linear dashpot element, $\bar{c}_{i,i+1}$, with high damping value describing the stick condition between the deck elements. Therefore, a formula for the transverse force, $\bar{F}_{i,i+1}(t)$, between superstructure segments with masses m_i and m_{i+1} can be written as:

$$\begin{aligned} \bar{F}_{i,i+1}(t) &= 0 && \text{for } \delta_{i,i+1}(t) \le 0 \quad \text{(no contact)} \\ \bar{F}_{i,i+1}(t) &= \bar{c}_{i,i+1}(t)(\dot{y}_i(t) - \dot{y}_{i+1}(t)) && \text{for } \delta_{i,i+1}(t) > 0 \quad \text{(contact)} \end{aligned} \tag{4.4}$$

where $\dot{y}_i(t)$ is a velocity of the ith bridge segment in the transverse direction.

The dynamic equation of motion for the extended non-linear model of the bridge (5 degrees-of-freedom in each horizontal direction) considering two-dimensional pounding can be written as:

$$\begin{bmatrix} \mathbf{M} & \mathbf{0} \\ \mathbf{0} & \mathbf{M} \end{bmatrix} \begin{bmatrix} \ddot{\mathbf{x}}(t) \\ \ddot{\mathbf{y}}(t) \end{bmatrix} + \begin{bmatrix} \mathbf{C}(t) & \mathbf{0} \\ \mathbf{0} & \bar{\mathbf{C}}(t) \end{bmatrix} \begin{bmatrix} \dot{\mathbf{x}}(t) \\ \dot{\mathbf{y}}(t) \end{bmatrix} + \begin{bmatrix} \mathbf{K}(t) & \mathbf{0} \\ \mathbf{0} & \bar{\mathbf{K}}(t) \end{bmatrix} \begin{bmatrix} \mathbf{x}(t) \\ \mathbf{y}(t) \end{bmatrix} + \begin{bmatrix} \mathbf{F}(t) \\ \bar{\mathbf{F}}(t) \end{bmatrix} = -\begin{bmatrix} \mathbf{M} & \mathbf{0} \\ \mathbf{0} & \mathbf{M} \end{bmatrix} \begin{bmatrix} \ddot{\mathbf{x}}_g(t) \\ \ddot{\mathbf{y}}_g(t) \end{bmatrix} \tag{4.5}$$

where $\ddot{\mathbf{x}}(t)$, $\dot{\mathbf{x}}(t)$, $\mathbf{x}(t)$, $\ddot{\mathbf{x}}_g(t)$, $\mathbf{M}$, $\mathbf{C}(t)$, $\mathbf{K}(t)$, $\mathbf{F}(t)$ are given in Eqs. (4.1a–d) and:

$$\ddot{\mathbf{y}}(t) = \begin{bmatrix} \ddot{y}_1(t) \\ \ddot{y}_2(t) \\ \ddot{y}_3(t) \\ \ddot{y}_4(t) \\ \ddot{y}_5(t) \end{bmatrix}; \quad \dot{\mathbf{y}}(t) = \begin{bmatrix} \dot{y}_1(t) \\ \dot{y}_2(t) \\ \dot{y}_3(t) \\ \dot{y}_4(t) \\ \dot{y}_5(t) \end{bmatrix}; \quad \mathbf{y}(t) = \begin{bmatrix} y_1(t) \\ y_2(t) \\ y_3(t) \\ y_4(t) \\ y_5(t) \end{bmatrix} \tag{4.6a}$$

$$\bar{\mathbf{C}}(t) = \begin{bmatrix} \bar{C}_1(t) & 0 & 0 & 0 & 0 \\ 0 & \bar{C}_2(t) & 0 & 0 & 0 \\ 0 & 0 & \bar{C}_3(t) & 0 & 0 \\ 0 & 0 & 0 & \bar{C}_4(t) & 0 \\ 0 & 0 & 0 & 0 & \bar{C}_5(t) \end{bmatrix}; \quad \bar{\mathbf{F}}(t) = \begin{bmatrix} \bar{F}_{12}(t) - \bar{F}_{01}(t) \\ \bar{F}_{23}(t) - \bar{F}_{12}(t) \\ \bar{F}_{34}(t) - \bar{F}_{23}(t) \\ \bar{F}_{45}(t) - \bar{F}_{34}(t) \\ \bar{F}_{56}(t) - \bar{F}_{45}(t) \end{bmatrix} \tag{4.6b}$$

$$\bar{\mathbf{K}}(t) = \begin{bmatrix} \bar{K}_1(t) & 0 & 0 & 0 & 0 \\ 0 & \bar{K}_2(t) & 0 & 0 & 0 \\ 0 & 0 & \bar{K}_3(t) & 0 & 0 \\ 0 & 0 & 0 & \bar{K}_4(t) & 0 \\ 0 & 0 & 0 & 0 & \bar{K}_5(t) \end{bmatrix}; \quad \ddot{\mathbf{y}}_g(t) = \begin{bmatrix} \ddot{y}_{g1}(t) \\ \ddot{y}_{g2}(t) \\ \ddot{y}_{g3}(t) \\ \ddot{y}_{g4}(t) \\ \ddot{y}_{g5}(t) \end{bmatrix} \tag{4.6c}$$

where $\ddot{y}_i(t)$, $\dot{y}_i(t)$, $y_i(t)$ $(i = 1, \ldots, 5)$ are the acceleration, velocity and displacement of a superstructure segment with mass m_i in the transverse direction and $\ddot{y}_{gi}(t)$ is the acceleration of input ground motion in the transverse direction acting on ith superstructure segment (shifted in time for every segment due to seismic wave passage effect).

In order to solve the equation of motion (4.5) numerically, the time-stepping Newmark method with constant time step $\Delta t = 0.005$ s, has been used. The analysis has been carried out for two different ground motions. Together with the previously used El Centro excitation, acceleration records of the Kobe earthquake (17 January 1995) have also been applied. NS components of the ground motions have been used to act in the longitudinal direction of the bridge axis and EW components in the transverse one. The records of the excitations have been scaled to give the response with the maximum shear strain of HDRB at the level of 300 % (see Jankowski et al. 1998 for details). Original and scaled PGA values of the earthquake excitations are shown in Table 4.3.

The parametric study has been conducted for different values of the gap size between superstructure segments and the apparent seismic wave velocity under specified in Table 4.3 earthquake excitations. The peak shear forces for the middle segment, m_3, with respect to these parameters for the longitudinal and transverse directions are presented in Figs. 4.11 and 4.12. It can be seen from the figures that the structural response under two-dimensional pounding follows a similar pattern for two different earthquake excitations. The results confirm the significant influence of the gap size between superstructure segments on the bridge behaviour in the longitudinal

Table 4.3 Earthquake excitations used in the two-dimensional analysis

Earthquake	Component	Original PGA (m/s^2)	PGA after scaling (m/s^2)
El Centro	NS	3.402	8.000
	EW	1.772	4.167
Kobe (JMA station)	NS	8.178	5.500
	EW	6.171	4.150

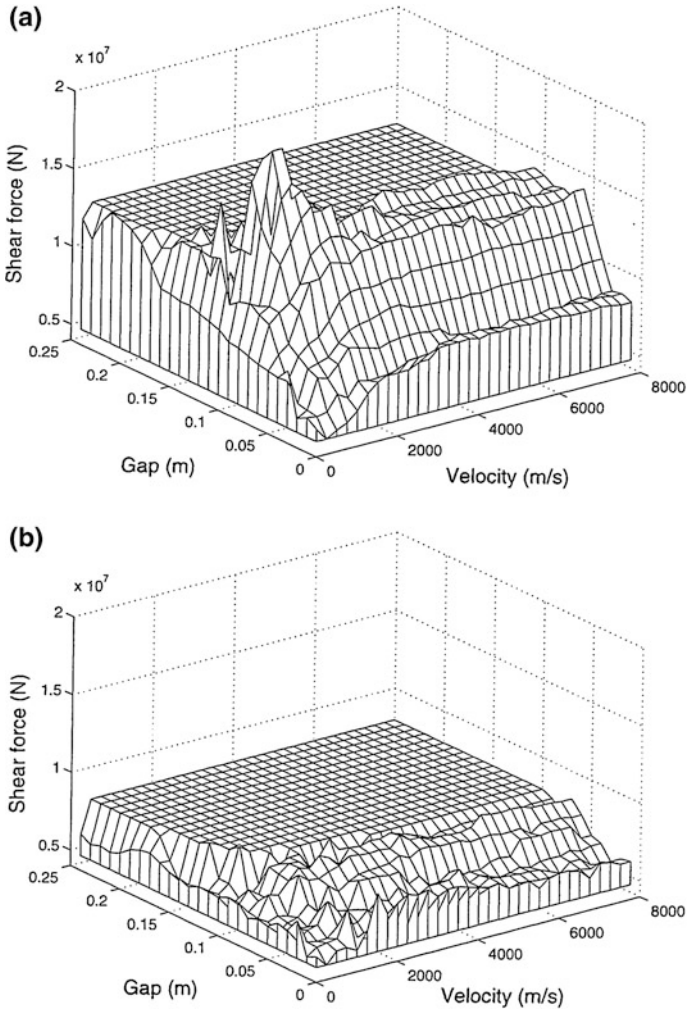

Fig. 4.11 Peak shear forces with respect to the gap size between superstructure segments and the seismic wave velocity under the El Centro earthquake (Jankowski et al. 1998) **a** longitudinal direction; **b** transverse direction

direction, as described previously in Sect. 4.1.2. They indicate that the largest shear forces can be expected for bigger gaps for which collisions are still observed. Figures 4.11 and 4.12 also show the dependence of the apparent seismic wave velocity on the response of the bridge structure. It can be seen that for smaller velocity values, peak shear forces are usually lower but bigger gaps are needed to prevent pounding. On the other hand, for higher velocities, shear forces are generally larger, although, smaller gaps can be applied to avoid collisions. A similar trend in relation to the gap size and the apparent seismic wave velocity is observed for both bridge

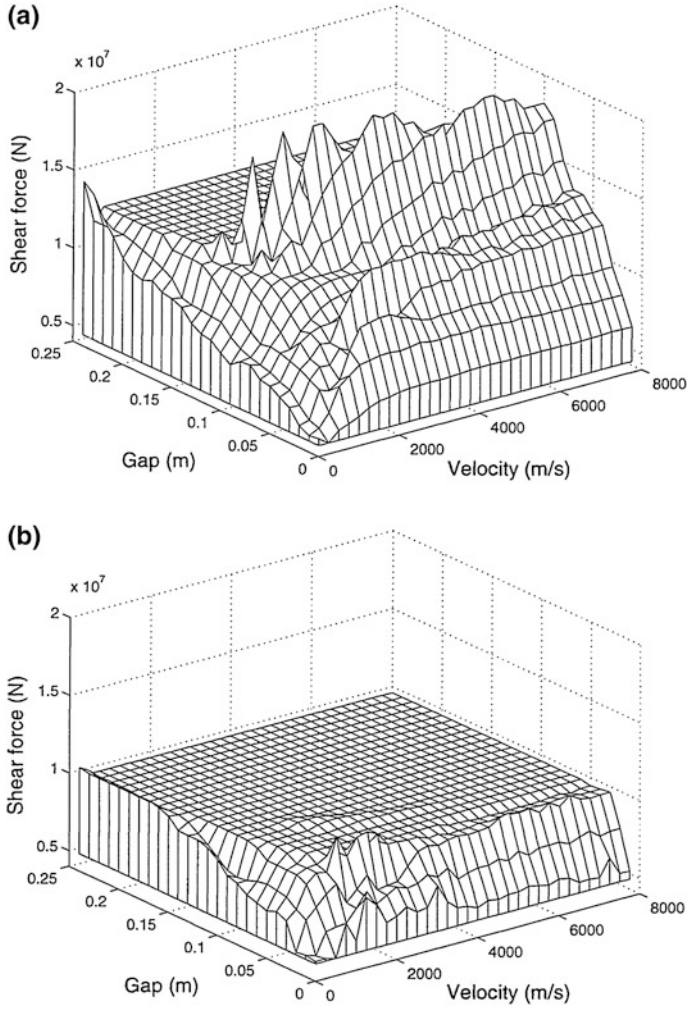

Fig. 4.12 Peak shear forces with respect to the gap size between superstructure segments and the seismic wave velocity under the Kobe earthquake (Jankowski et al. 1998) **a** longitudinal direction; **b** transverse direction

directions. In the case of the transverse direction, however, different values of these parameters do not modify the behaviour of the structure so significantly.

The peak pounding forces acting on the middle superstructure segment with respect to the gap size between segments for the apparent seismic wave velocity of 1000 m/s are shown in Fig. 4.13 (compare Jankowski et al. 1998). It can be seen from the figure that, for both the El Centro and Kobe earthquakes, with the increase

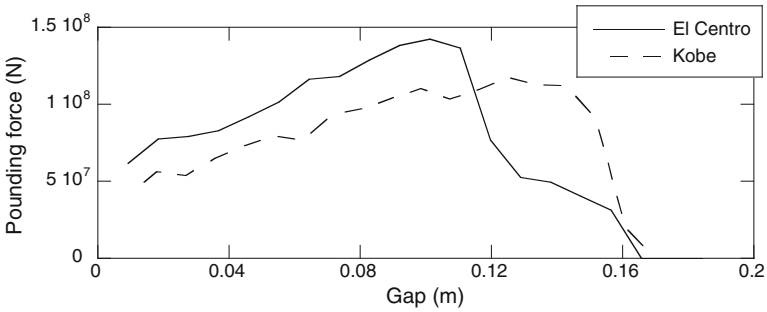

Fig. 4.13 Peak pounding forces with respect to the gap size between superstructure segments

in the gap size up to about 0.11–0.13 m, forces due to collisions become bigger. Then, their magnitudes fall sharply to zero when gaps are large enough to prevent collisions.

4.2 Pounding-Involved Response Analysis Using FEM

The fundamental analysis of pounding between superstructure segments of the bridge presented in Sect. 4.1 has provided the qualitative information about the influence of collisions on the overall structural response. That study, however, has been conducted on a simple lumped mass model in which the whole superstructure segments have been discretized as SDOF systems and the contribution of the dynamics of piers to the total response has not been taken into account. The influence of rotation of deck segments, due to corner collisions, as well as the spatial seismic effects, related to the propagation of seismic wave, have also been neglected. In this section, let us study the pounding-involved response of the bridge under earthquake excitation with the help of the FEM by considering a more detailed model of the structure.

4.2.1 Detailed Modelling of Structural Members of the Bridge

In order to carry out a more accurate study, the superstructure segments and piers of elevated highway bridge, presented in Figs. 4.1, 4.2 and 4.3 and described in Sect. 4.1.1, have been discretized as elastic beam-column elements with distributed mass and rubber bearings have been modelled by spring-dashpots. The three-dimensional single pier section model of the structure is shown in Fig. 4.14.

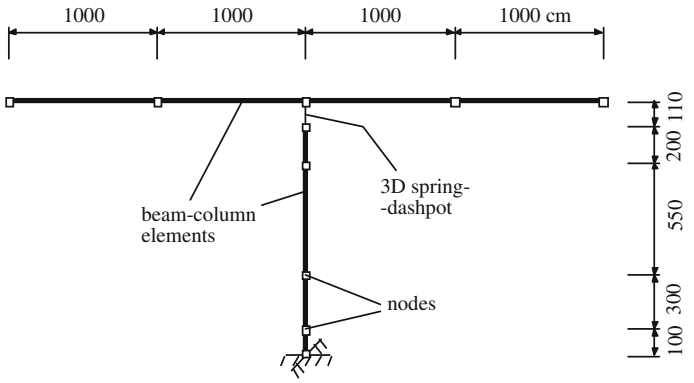

Fig. 4.14 Detailed three-dimensional model of a single pier section of the bridge

The non-linear strain-rate dependent model, with parameters described in Sect. 4.1, has been implemented in the numerical model to simulate the behaviour of HDRBs in the longitudinal and transverse directions. On the other hand, the effective vertical stiffness of rubber bearing can be calculated from the formula (Kelly 1993):

$$K_b^v = \frac{E_c A_b}{t_r} \tag{4.7}$$

where A_b is an area of bearing, t_r is a total thickness of rubber in bearing and E_c is the instantaneous compression modulus of the rubber-steel composite under the specified level of vertical load, which can be described as (Kelly 1993):

$$E_c = K_r \left[1 - \frac{\sinh \beta_s}{\beta_s \cosh \beta_s} - \frac{8}{\pi^2} \sum_{k=1,3,5\ldots}^{\infty} \frac{\beta_s^2}{k^2 \left(\beta_s^2 + \frac{k^2 \pi^2}{4} \right)} \cdot \frac{\sinh \beta_k}{\beta_k \cosh \beta_k} \right] \tag{4.8}$$

where:

$$\beta_s = \left(96 \frac{G_r}{K_r} \right)^{\frac{1}{2}} S_p \tag{4.9}$$

$$\beta_k = \left(\beta_s^2 + \frac{k^2 \pi^2}{4} \right)^{\frac{1}{2}} \tag{4.10}$$

In the above equations, K_r and G_r stand for the bulk and shear modulus of rubber, respectively; and S_p is a shape factor of a single rubber layer which, for a square pad of side, a_p, and thickness, t_p, can be computed from equation:

$$S_p = \frac{a_p}{4t_p} \tag{4.11}$$

The equivalent damping coefficient of a HDRB in the vertical direction, C_b^v, can be obtained using formula (Chopra 1995):

$$C_b^v = 2\xi_b^v \sqrt{mK_b^v} \tag{4.12}$$

where ξ_b^v is a damping ratio in the vertical direction and m is the mass of the superstructure being supported by bearing. Applying Eqs. (4.7)–(4.12), the effective vertical stiffness and damping (for $\xi_b^v = 0.14$) coefficients of analyzed pair of HDRBs have been calculated as: $K_b^v = 1.86657 \times 10^{10}$ N/m and $C_b^v = 3.4216 \times 10^7$ kg/s, respectively.

The linearized parameters of the pier, based on its cross section properties, have been applied to model its behaviour under dynamic load due to earthquake excitation. The cross section itself (shown in Fig. 4.3) has been designed to accommodate the internal forces occurring at the base of the pier under the Kobe earthquake (17 January 1995) applied in all three directions. For the design purposes, the three-dimensional single pier section model of the bridge (see Fig. 4.14) has been used. The iterative procedure has been conducted for different cross section dimensions and reinforcement ratios. The structural dynamic response for every analyzed case has been obtained using the time-stepping Newmark method (Newmark 1959) with the standard parameters: $\gamma_N = 0.5$, $\beta_N = 0.25$. Similarly as for the lumped mass 5 degree-of-freedom model, the constant time step of $\Delta t = 0.005$ s has been applied in the analysis. The bending moment time histories in the longitudinal and transverse directions as well as the time history of the vertical axial force at the pier base are presented in Figs. 4.15 and 4.16. The design of the pier has been conducted for the peak values of bending moments: $M_x = 6.2864 \times 10^7$ Nm, $M_y = 4.9886 \times 10^7$ Nm and the minimum axial force $P_v = 8.4931 \times 10^6$ N as yielding of the tensile reinforcement is expected to cause the failure in the analyzed structural member. The strength of the pier has been studied with the help of interaction diagram for biaxial loading of reinforced concrete column (see Fig. 4.17) representing a plot of moments and axial load for which failure occurs (White et al. 1974). The moments of inertia for the specified in this way and fully cracked pier cross section have been calculated using the transformed area concept (White et al. 1974) as: $I_x = 5.805$ m^4, $I_y = 7.253$ m^4 in the longitudinal and transverse direction, respectively.

Viscous damping of the Rayleigh type has been employed in the structural model to simulate the dissipation of energy during pier vibrations (see Clough and Penzien 1993; Hall 2006). The damping matrix has been assumed to be linearly proportional to the stiffness matrix with structural damping equal to 0.05.

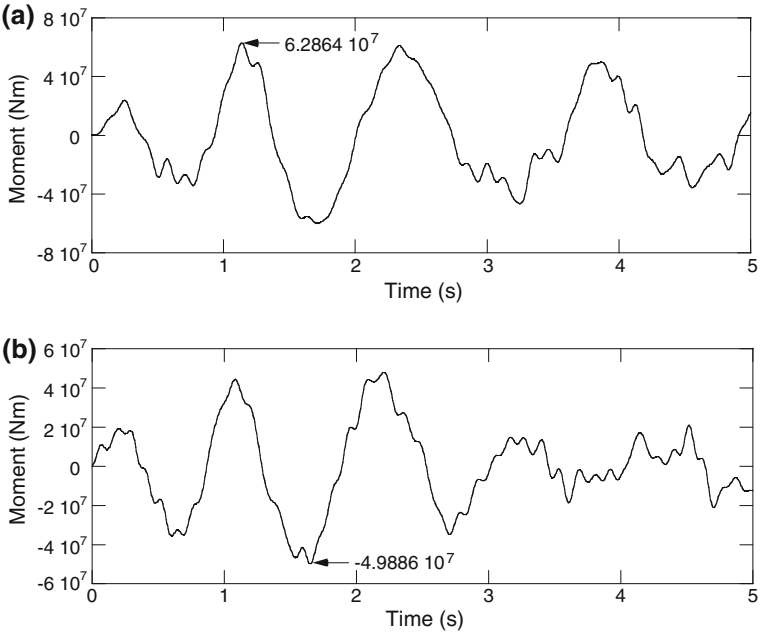

Fig. 4.15 Bending moment time histories at the base of the pier under the Kobe earthquake **a** longitudinal direction; **b** transverse direction

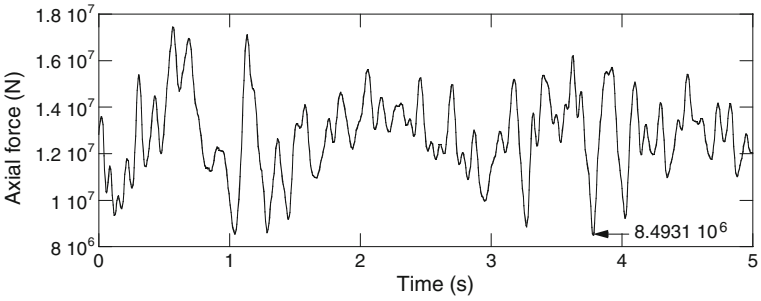

Fig. 4.16 Axial force time history at the base of the pier under the Kobe earthquake

4.2.2 Modelling of Earthquake Records for Different Bridge Supports

The difference in the arrival times of seismic wave at various support locations of the bridge piers has been assumed in the analysis described in Sect. 4.1. In the reality, however, the ground motion differs from place to place not only due to the wave passage effect but also due to other spatial seismic effects related to the

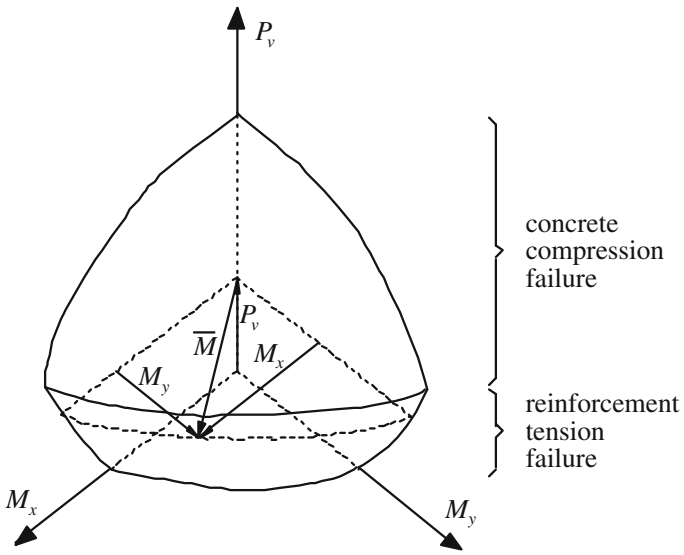

Fig. 4.17 Interaction diagram for biaxial loading of reinforced concrete column

propagation of seismic wave (see Pei and Papageorgiou 1996; Semblat et al. 2000; Dimitriu et al. 2001; Zendagui and Berrah 2002; Dulińska 2012). These effects include (Der Kiureghian 1996) the loss of coherency of seismic wave due to scattering in the heterogeneous medium of the ground and due to differential superimposition of waves arriving from an extended source (incoherence effect) as well as the spatially varying local soil conditions (site response effect). Previous studies have indicated that the variation of ground motion in space and time may significantly influence the dynamic response of long structures, especially long bridges (see, for example, Nazmy and Abdel-Ghaffar 1992; Harichandran et al. 1996; Zembaty 1997; Dulińska 2011).

The deterministic approach to the propagation of seismic wave is very complex and requires a detailed knowledge of the fault size, rupture mechanisms, propagation paths (reflections, refractions), distance from the epicentre and local geological and topographical conditions (O'Connor and Ellingwood 1992; Yuan and Men 1992; Reinoso et al. 1997; Semblat et al. 2005). Since these data are usually not fully available, the stochastic approach has been proved to be useful and successfully applied in problems of earthquake engineering (see Vanmarcke 1983; Sobczyk 1984; Harichandran and Vanmarcke 1986; Harada and Shinozuka 1988; Deodatis et al. 1990; Zerva and Shinozuka 1991).

In order to generate earthquake records for different structural supports based on the specified time history, the conditional stochastic modelling methods are often used (see, for example, Kameda and Morikawa 1992, 1994; Vanmarcke and Fenton 1991; Jankowski and Walukiewicz 1997). Such a method has also been applied in this work for the determination of ground motion records for different support

locations of the analyzed bridge structure shown in Fig. 4.1. The ground motion time histories for the support locations no. 2–16 have been generated based on the known record, which has been assumed to be specified for the bridge pier no. 1 (the first one from the left side of the structure). In order to generate the input ground motions along the bridge, the successive simulation procedure has been applied (Jankowski and Wilde 2000). It has been assumed during the generation procedure that the random field consisting of pier bases is highly correlated (scale parameter is equal to 100) and the seismic wave travels along the bridge with a constant apparent velocity of 1000 m/s (see Jankowski and Wilde 2000). The examples of the results of simulations for supports no. 8 and 16, together with the specified record for the first pier, are presented in Figs. 4.18, 4.19 and 4.20 for the NS, EW and UD component of the Kobe earthquake, respectively (Jankowski and Wilde 2000).

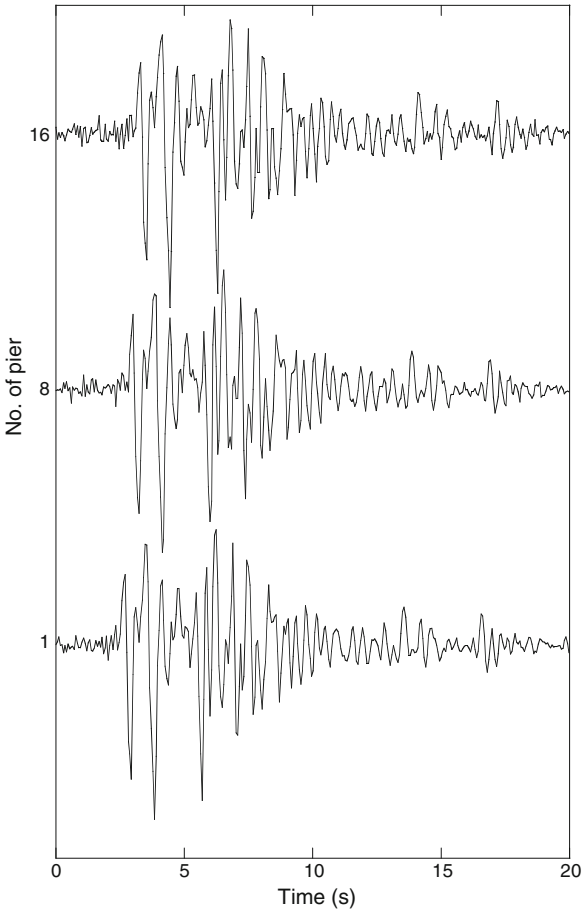

Fig. 4.18 Specified (pier no. 1) and simulated (piers no. 8 and 16) ground motions for the NS component of the Kobe earthquake (Jankowski and Wilde 2000)

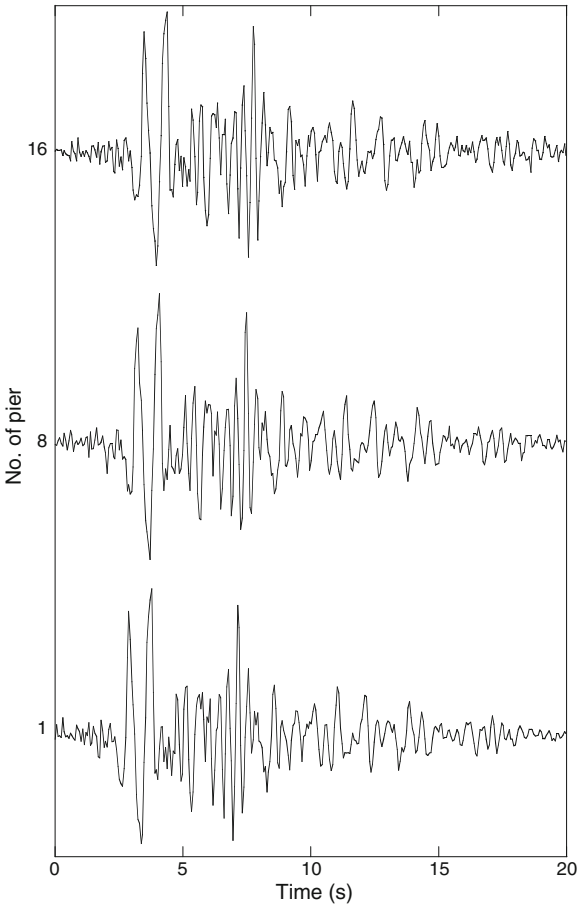

Fig. 4.19 Specified (pier no. 1) and simulated (piers no. 8 and 16) ground motions for the EW component of the Kobe earthquake

These time histories have been used in the dynamic analyses focused on pounding between bridge segments under non-uniform earthquake excitation described in the successive sections of the book.

4.2.3 Response of the Bridge Using One-Dimensional Structural Model

Similarly to the fundamental analysis of pounding between bridge segments (Sect. 4.1), a one-dimensional numerical model, shown in Fig. 4.21, has been first developed to study the influence of collisions on the response of the bridge in the longitudinal direction. In the detailed model, pounding between adjacent superstructure segments has been controlled by special gap-friction elements, allowing to

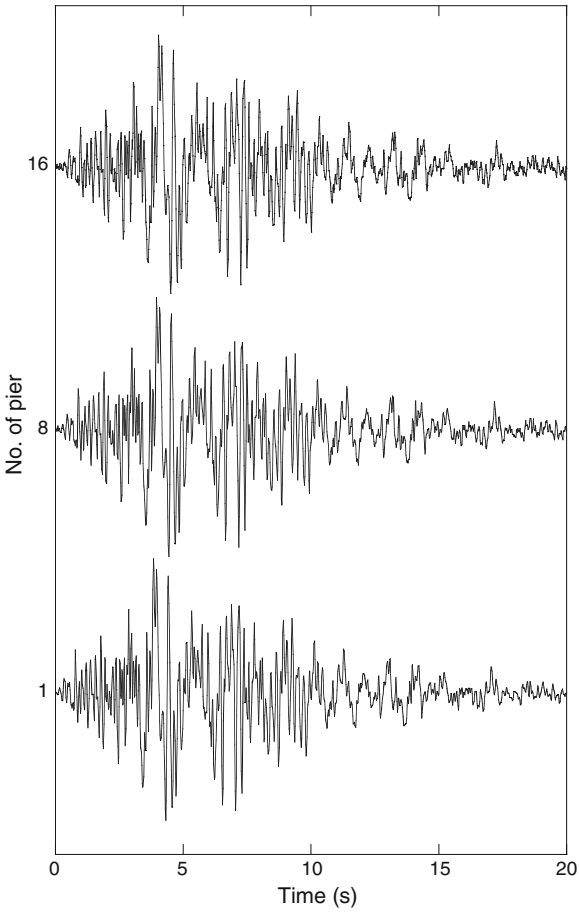

Fig. 4.20 Specified (pier no. 1) and simulated (piers no. 8 and 16) ground motions for the UD component of the Kobe earthquake

connect the ends of segments when they come into contact and thus leading to the longitudinal deformation of the decks due to collision. The stochastically generated acceleration records of the NS component of the Kobe earthquake (Fig. 4.18) has been applied on every pier along the bridge. It has been confirmed that, similarly as for the lumped mass model, at least five segments should be analyzed with neglected parts of the bridge simulated as viscoelastic elements, as shown in Fig. 4.21, in order to receive more accurate response of the middle segment.

The results of the analysis in the form of the peak shear forces and bending moments at the base of piers of the middle superstructure segment with respect to the gap size between segments are presented in Fig. 4.22. It can be seen from the figure that the reaction forces for all piers of analyzed segment show similar tendencies for different gap size values. For very small gap sizes up to about 0.02 m and big enough to prevent pounding (bigger than 0.22 m), the lowest response has been recorded. Additionally, smaller values of reaction forces have also been

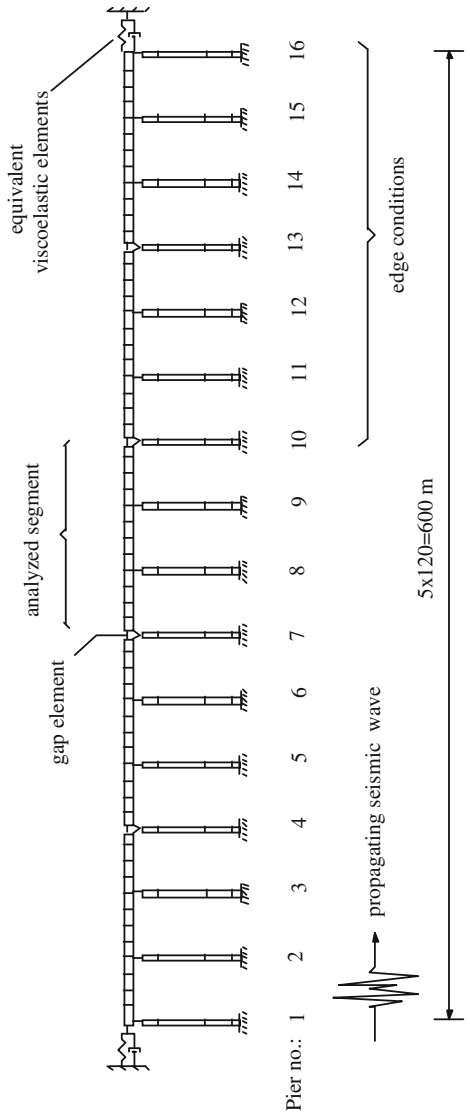

Fig. 4.21 Detailed one-dimensional model of the bridge

obtained for the middle gap interval of about 0.09–0.13 m. It has been noticed that, in this specific gap range, pounding itself has good effect leading to the reduction in the response, although, collision forces are still relatively high.

It can also be seen from Fig. 4.22 that in the range of the big gap size, where pounding is avoided, the peak reaction forces are different for all analyzed piers. Moreover, their values can be even larger (for example for pier no. 9) than the results from the analysis conducted for the single pier section model (see Fig. 4.15).

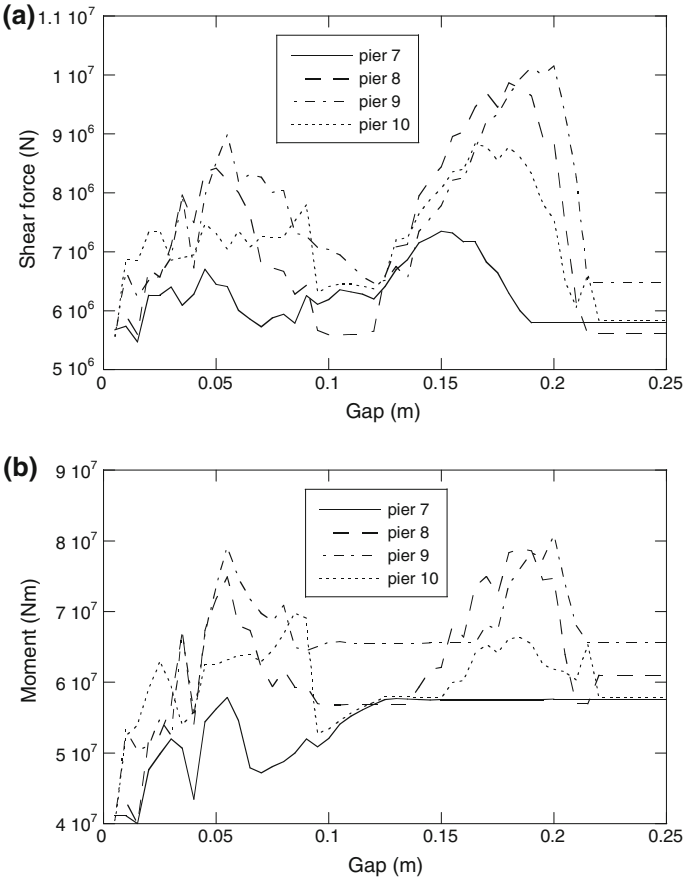

Fig. 4.22 Peak reaction forces of the middle segment piers with respect to the gap size between bridge segments **a** shear forces; **b** bending moments

This difference in the response of various piers is caused by the spatial seismic effects related to the propagation of seismic wave.

4.2.4 Response of the Bridge Using Three-Dimensional Structural Model

It has been assumed in the one-dimensional structural model, considered in Sect. 4.2.3, that pounding between superstructure segments occurs along the bridge

axis. In the reality, however, collisions usually take place at corners of the deck elements. Such contacts may lead to some rotation of segments in the horizontal plane (rotation in the vertical plane is prevented due to high vertical stiffness of bearings). The horizontal rotation of segments can have some influence on the overall response of the bridge and therefore this effect has been incorporated in the analysis.

For the purpose of a more accurate modelling of collisions, the detailed model of the bridge shown in Fig. 4.21 has been extended to allow for three-dimensional pounding occurring between corners of superstructure segments. The introduced modification of modelling of deck ends is presented in Fig. 4.23. In the model, stiff beam-column elements (denoted as arms) have been added at the end of every segment. Two additional gap-friction elements have also been placed between the potential points of collisions. When contact occurs, they fix the points in the longitudinal direction and impose friction forces in the transverse and vertical directions. The introduced modifications make the impact forces, due to collision occurring at the corners, to be transmitted through the stiff arms to the deck. That leads to the longitudinal deformation and horizontal rotation of colliding superstructure segments.

The analysis for the extended model has been conducted under the three-dimensional Kobe earthquake excitation. The stochastically generated acceleration records of the NS, EW and UD components of the earthquake (see Figs. 4.18, 4.19 and 4.20) have been applied in the longitudinal, transverse and vertical direction, respectively. The peak shear forces and bending moments at the bases of the middle segment piers for the extended three-dimensional model are shown in Figs. 4.24

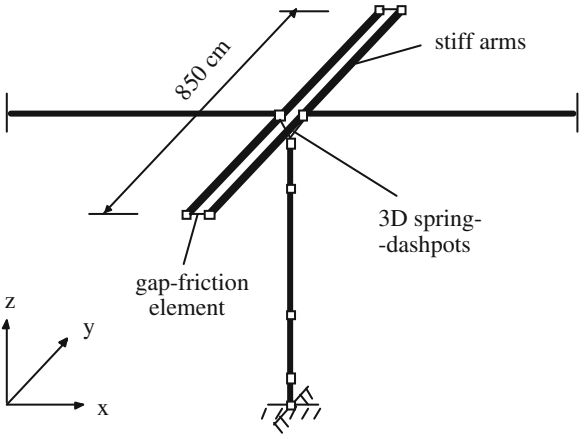

Fig. 4.23 Three-dimensional modification of modelling of the deck ends

and 4.25 for the longitudinal and transverse direction, respectively. The minimum vertical axial forces at the pier bases are also presented in Fig. 4.26. It can be seen comparing Fig. 4.24 with Fig. 4.22 that the difference between the structural response in the longitudinal direction using one-dimensional and extended three-dimensional models is not significant. Some minor changes in the peak reaction force values can be observed mainly in the smaller gap size range where collisions

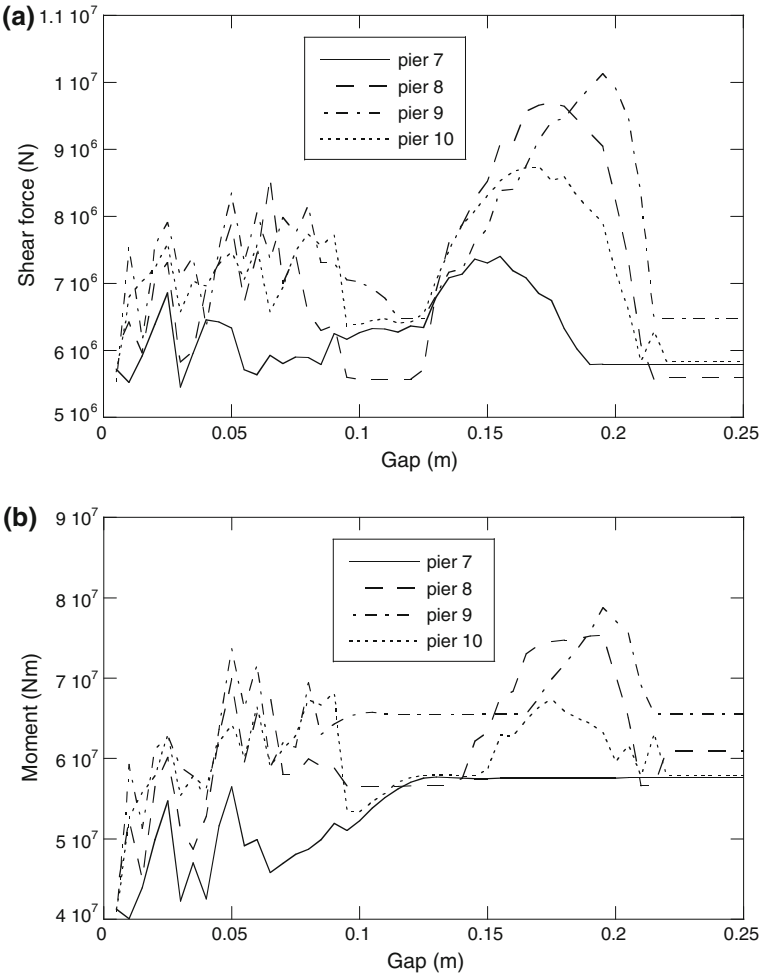

Fig. 4.24 Peak reaction forces in the longitudinal direction of the middle segment piers with respect to the gap size between bridge segments **a** shear forces; **b** bending moments

occur more often. This fact indicates that the horizontal rotation of the superstructure segments due to pounding does not modify much the bridge behaviour. Moreover, it can be seen from Fig. 4.25 that, similarly as for the lumped mass model (Sect. 4.1), the structural response in the transverse direction is not

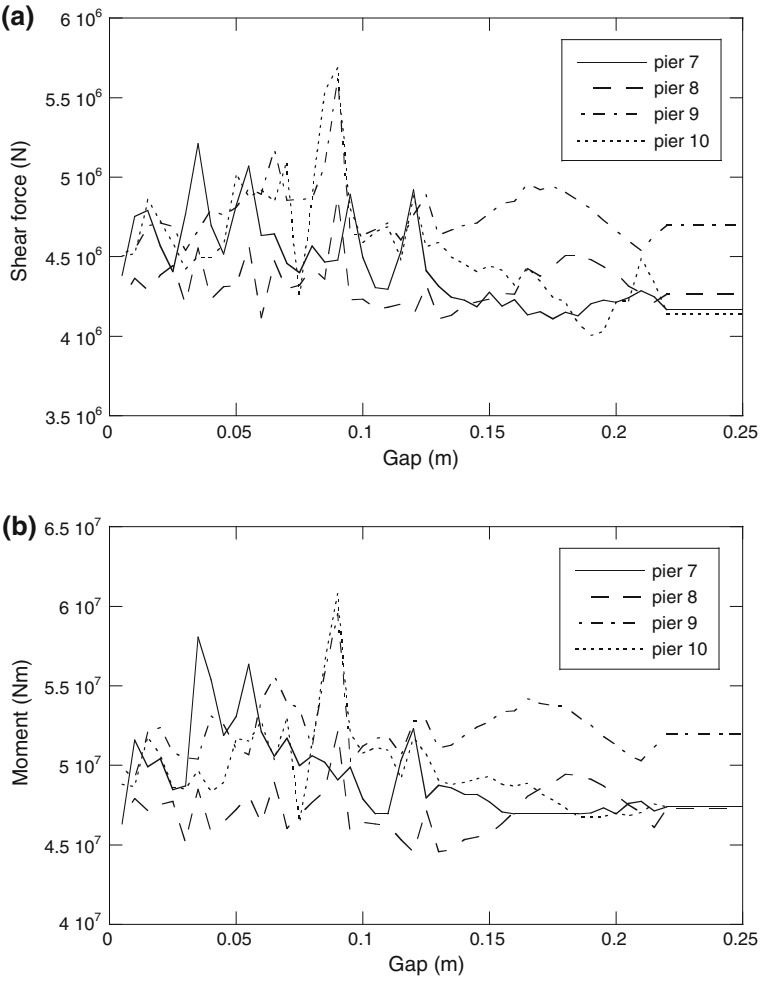

Fig. 4.25 Peak reaction forces in the transverse direction of the middle segment piers with respect to the gap size between bridge segments **a** shear forces; **b** bending moments

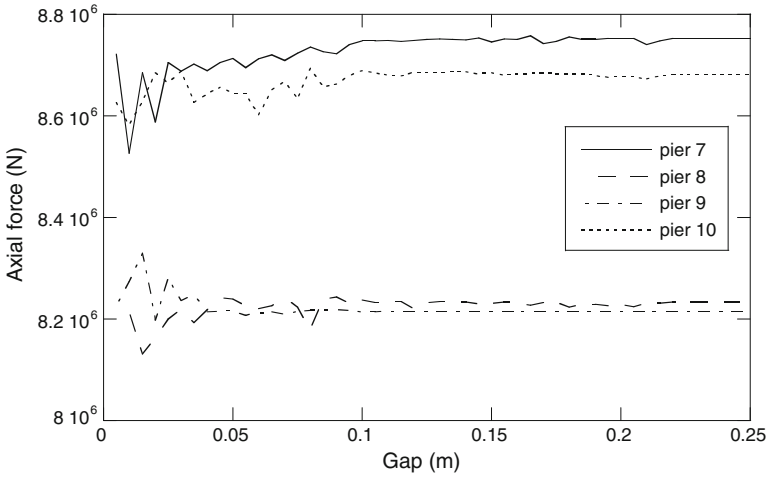

Fig. 4.26 Minimum axial reaction forces of the middle segment piers with respect to the gap size between bridge segments

significantly influenced by collisions. The same conclusion may also concern the bridge behaviour in the vertical direction since minimum axial forces shown in Fig. 4.26 are very similar for different gap size values.

References

Anagnostopoulos, S.A.: Pounding of buildings in series during earthquakes. Earthquake Eng. Struct. Dynam. **16**, 443–456 (1988)

Bathe, K.J.: Finite Element Procedures in Engineering Analysis. Prentice-Hall, Englewood Cliffs, USA (1982)

Bi, K., Hao, H., Chouw, N.: 3D FEM analysis of pounding response of bridge structures at a canyon site to spatially varying ground motions. Adv. Struct. Eng. **16**, 619–640 (2013)

Chopra, A.K.: Dynamics of Structures: Theory and Applications to Earthquake Engineering. Prentice-Hall, Englewood Cliffs (1995)

Chouw, N., Hao, H.: Study of SSI and non-uniform ground motion effects on pounding between bridge girders. Soil Dyn. Earthq. Eng. **23**, 717–728 (2005)

Chouw, N., Hao, H.: Significance of SSI and non-uniform near-fault ground motions in bridge response I: Effect on response with conventional expansion joint. Eng. Struct. **30**, 141–153 (2008)

Chouw, N., Hao, H., Su, H.: Multi-sided pounding response of bridge structures with non-linear bearings to spatially varying ground excitation. Adv. Struct. Eng. **9**, 55–66 (2006)

Clough R. W., Penzien J.: Dynamics of Structures. International Edition, McGraw-Hill (1993)

Der Kiureghian, A.: A coherency model for spatially varying ground motions. Earthq. Eng. Struct. Dyn. **25**, 99–111 (1996)

Deodatis, G., Shinozuka, M., Papageorgiou, A.: Stochastic wave representation of seismic ground motion. II: Simulation. J. Eng. Mech. **116**, 2381–2399 (1990)

DesRoches, R., Muthukumar, S.: Effect of pounding and restrainers on seismic response of multi-frame bridges. J. Struct. Eng. (ASCE) **128**, 860–869 (2002)
Dimitriu, P., Theodulidis, N., Hatzidimitriou, P., Anastasiadis, A.: Sediment non-linearity and attenuation of seismic waves: a study of accelerograms from Lefkas, Western Greece. Soil Dyn. Earthq. Eng. **21**, 63–73 (2001)
Dulińska, J.M.: Influence of wave velocity in the ground on dynamic response of large dimensional structures. Int. J. Earth Sci. Eng. **4**, 538–541 (2011)
Dulińska, J.M.: Importance of ground motion spatial variability effects on earth dam. Int. J. Earth Sci. Eng. **5**, 1–9 (2012)
Falborski, T., Jankowski, R.: Polymeric bearings – a new base isolation system to reduce structural damage during earthquakes. Key Eng. Mater. **569–570**, 143–150 (2013)
Hall, J.F.: Problems encountered from the use (or misuse) of Rayleigh damping. Earthq. Eng. Struct. Dyn. **35**, 525–545 (2006)
Harada T., Shinozuka M.: Stochastic analysis of seismic ground motions in space and time. In: Proceedings of Ninth World Conference on Earthquake Engineering. Vol. II, pp. 825–830 Tokyo–Kyoto, Japan, 2–9 Aug (1988)
Harichandran, R.S., Hawwari, A., Sweidan, B.N.: Response of long-span bridges to spatially varying ground motion. J. Struct. Eng. **122**, 476–484 (1996)
Harichandran, R.S., Vanmarcke, E.H.: Stochastic variation of earthquake ground motion in space and time. J. Eng. Mech. **112**, 154–174 (1986)
Jankowski, R.: Nonlinear rate dependent model of high damping rubber bearing. Bull. Earthq. Eng. **1**, 397–403 (2003)
Jankowski, R.: Impact force spectrum for damage assessment of earthquake-induced structural pounding. Key Eng. Mater. **293–294**, 711–718 (2005)
Jankowski, R.: Assessment of damage due to earthquake-induced pounding between the main building and the stairway tower. Key Eng. Mater. **347**, 339–344 (2007)
Jankowski, R., Walukiewicz, H.: Modeling of two-dimensional random fields. Probab. Eng. Mech. **12**, 115–121 (1997)
Jankowski, R., Wilde, K.: A simple method of conditional random field simulation of ground motions for long structures. Eng. Struct. **22**, 552–561 (2000)
Jankowski, R., Wilde, K., Fujino, Y.: Pounding of superstructure segments in isolated elevated bridge during earthquakes. Earthq. Eng. Struct. Dyn. **27**, 487–502 (1998)
Jankowski, R., Wilde, K., Fujino, Y.: Reduction of pounding effects in elevated bridges during earthquakes. Earthq. Eng. Struct. Dyn. **29**, 195–212 (2000)
Kameda, H., Morikawa, H.: An interpolating stochastic process for simulation of conditional random fields. Probab. Eng. Mech. **7**, 243–254 (1992)
Kameda, H., Morikawa, H.: Conditioned stochastic processes for conditional random fields. J. Eng. Mech. **120**, 855–875 (1994)
Karayannis, C.G., Favvata, M.J.: Inter-story pounding between multistory reinforced concrete structures. Struct. Eng. Mech. **20**, 505–526 (2005)
Kawashima, K., Okado, M. and Horikawa, M.: Design example of a highway bridge based on the manual for menshin design of highway bridges. Recent Selected Publications at Earthquake Engineering Division, Public Works Research Institute, vol. 2, pp. 191–208, May, (1993)
Kelly, J.M.: Earthquake-Resistant Design with Rubber. Springer, London (1993)
Mahmoud, S., Abd-Elhamed, A., Jankowski, R.: Earthquake-induced pounding between equal height multi-storey buildings considering soil-structure interaction. Bull. Earthq. Eng. **11**(4), 1021–1048 (2013)
Mahmoud, S., Austrell, P.-E., Jankowski, R.: Simulation of the response of base-isolated buildings under earthquake excitations considering soil flexibility. Earthq. Eng. Eng. Vibr. **11**, 359–374 (2012)
Mahmoud, S., Jankowski, R.: Elastic and inelastic multi-storey buildings under earthquake excitation with the effect of pounding. J. Appl. Sci. **9**(18), 3250–3262 (2009)
Mahmoud, S., Jankowski, R.: Modified linear viscoelastic model of earthquake-induced structural pounding. Iranian J. Sci. Technol. **35**(C1), 51–62 (2011)

Maison, B.F., Kasai, K.: Dynamics of pounding when two buildings collide. Earthq. Eng. Struct. Dyn. **21**, 771–786 (1992)
Malhotra, P.K., Huang, M.J., Shakal, A.F.: Seismic interaction at separation joints of an instrumented concrete bridge. Earthq. Eng. Struct. Dyn. **24**, 1055–1067 (1995)
Nazmy, A.S., Abdel-Ghaffar, A.M.: Effects of ground motion spatial variability on the response of cable-stayed bridges. Earthq. Eng. Struct. Dyn. **21**, 1–20 (1992)
Newmark, N.: A method of computation for structural dynamics. J. Eng. Mech. Div. ASCE **85**, 67–94 (1959)
O'Connor, J.M., Ellingwood, B.R.: Site-dependent models of earthquake ground motion. Earthquake Eng. Struct. Dynam. **21**, 573–589 (1992)
Pei, D., Papageorgiou, A.S.: Locally generated surface waves in Santa Clara Valley: analysis of observations and numerical simulation. Earthq. Eng. Struct. Dyn. **25**, 47–63 (1996)
Polycarpou, P.C., Papaloizou, L., Komodromos, P.: An efficient methodology for simulating earthquake-induced 3D pounding of buildings. Earthq. Eng. Struct. Dyn. **43**, 985–1003 (2014)
Reinoso, E., Wrobel, L.C., Power, H.: Three-dimensional scattering of seismic waves from topographical structures. Soil Dyn. Earthq. Eng. **16**, 41–61 (1997)
Ruangrassamee, A., Kawashima, K.: Relative displacement response spectra with pounding effect. Earthq. Eng. Struct. Dyn. **30**, 1511–1538 (2001)
Semblat, J.F., Duval, A.M., Dangla, P.: Numerical analysis of seismic wave amplification in Nice (France) and comparisons with experiments. Soil Dynamics and Earthquake Engineering **19**, 347–362 (2000)
Semblat, J.F., Kham, M., Parara, E., Bard, P.Y., Pitilakis, K., Makra, K., Raptakis, D.: Seismic wave amplification: Basin geometry vs soil layering. Soil Dyn. Earthq. Eng. **25**, 529–538 (2005)
Sobczyk, K.: Stochastic Wave Propagation. Elsevier Science Publishers, Amsterdam (1984)
Sołtysik, B., Jankowski, R.: Non-linear strain rate analysis of earthquake-induced pounding between steel buildings. Int. J. Earth Sci. Eng. **6**, 429–433 (2013)
Vanmarcke, E.H.: Random Fields: Analysis and Synthesis. MIT Press, Cambridge (1983)
Vanmarcke, E.H., Fenton, G.A.: Conditioned simulation of local fields of earthquake ground motion. Struct. Saf. **10**, 247–264 (1991)
White, R.N., Gergely, P., Sexsmith, R.G: Structural Engineering: Behavior of Members and Systems. Vol. 3, Wiley, New York (1974)
Yuan, X., Men, F.L.: Scattering of plane SH waves by a semi-cylindrical hill. Earthq. Eng. Struct. Dyn. **21**, 1091–1098 (1992)
Zembaty, Z.: Vibrations of bridge structure under kinematic wave excitations. J. Struct. Eng. **123**, 479–488 (1997)
Zendagui, D., Berrah, M.K.: Spatial variation of seismic motion induced by propagation of body waves. Soil Dyn. Earthq. Eng. **22**, 805–811 (2002)
Zerva, A., Shinozuka, M.: Stochastic differential ground motion. Struct. Saf. **10**, 129–143 (1991)

Chapter 5
Mitigation of Pounding Effects

An intensive study has been carried out on mitigation of pounding hazards. One of the objectives is to develop procedures for evaluating an adequate separation distance between buildings or bridge segments in order to prevent contacts during earthquakes. The minimum seismic gap is specified in the recent earthquake-resistant design codes for newly constructed structures (ECS 1998; IS 2002; NBC 2003; IBC 2009). However, due to land shortage and high prices of the land in many seismic regions, enlarging the separation gap between buildings is not an easy solution to be accepted by the land owners. The use of isolation devices (see, for example, Kelly 1993; Salomón et al. 1999; Komodromos 2000, 2008; Jankowski 2003; Mahmoud et al. 2012; Falborski and Jankowski 2013), which is considered to be a very effective earthquake-resistant technique (Naeim and Kelly 1999), makes this problem even worse since it leads to considerable increase in the structural displacements (Maison and Ventura 1992; Malhotra 1997; Mahmoud and Jankowski 2010; Polycarpou and Komodromos 2010a, b; Mahmoud and Gutub 2013). Moreover, there are many examples of old buildings, which have been constructed in contact with each other (see Jeng and Tzeng 2000; Wasti and Ozcebe 2003), as it was not prohibited by the old earthquake-resistant design codes. The problem with enlarging the separation gap between adjacent superstructure segments concerns also bridges. Expansion joints applied in bridge structures are designed to accommodate length changes of the superstructure due to thermal and rheological (creep, shrinkage) effects. They should also provide appropriate space for placement of deck elements. On the other hand, enlarging the separation gap between superstructure segments is undesirable solution having in mind the fact that heavy traffic loads moving on the deck have to be carried over the expansion joints.

Another approach to mitigate pounding effects during earthquakes is to consider some pounding reduction techniques so as to enhance the seismic performance of structures without sufficient in-between space. One of the methods is linking the bridge segments or buildings at certain locations which allow the forces to be transmitted between structural elements and thus eliminate collisions—see Fig. 5.1 (Westermo 1989; Jankowski et al. 2000; Abdullah et al. 2001; Kawashima et al. 2002; Ruangrassamee and Kawashima 2003). The connections between adjacent structures can also have some energy dissipating properties when links with

R. Jankowski and S. Mahmoud, *Earthquake-Induced Structural Pounding*,
GeoPlanet: Earth and Planetary Sciences, DOI 10.1007/978-3-319-16324-6_5

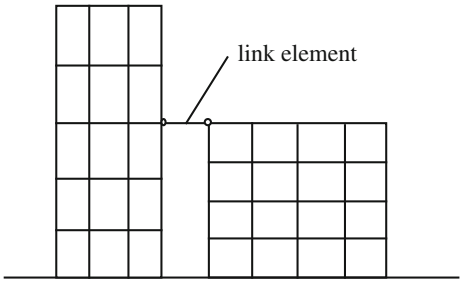

Fig. 5.1 Buildings connected by stiff link elements

additional dampers are used—see Fig. 5.2 (Kobori et al. 1988; Kasai et al. 1992; Xu et al. 1999; Zhang and Xu 1999; Ni et al. 2001). Another technique concerns installation of bumpers, shock absorbers, crushable devices or collision shear walls at the expected locations of impacts which can help in preventing sudden shocks due to collisions—see Figs. 5.3, 5.4 and 5.5 (Anagnostopoulos and Spiliopoulos 1992; Anagnostopoulos 1996; Jankowski et al. 2000; Anagnostopoulos and Karamaneas 2008; Abdel Raheem 2009; Polycarpou and Komodromos 2011).

It is also possible to decrease the displacement response of structures, and thus reduce the probability of impacts, by increasing their stiffness properties (Divyashree et al. 2014). The use of active, passive and semi-active control systems, as supplemental energy dissipation devices, can also be considered as a

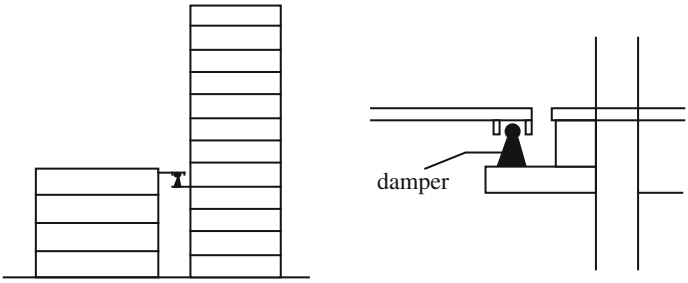

Fig. 5.2 Buildings connected by link elements with dampers (after Kobori et al. 1988)

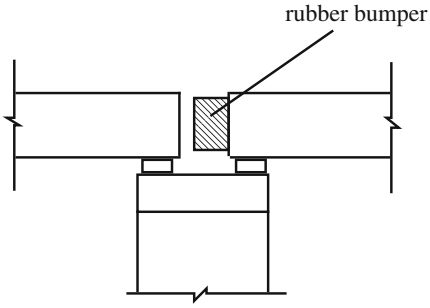

Fig. 5.3 Bridge segments equipped with bumpers

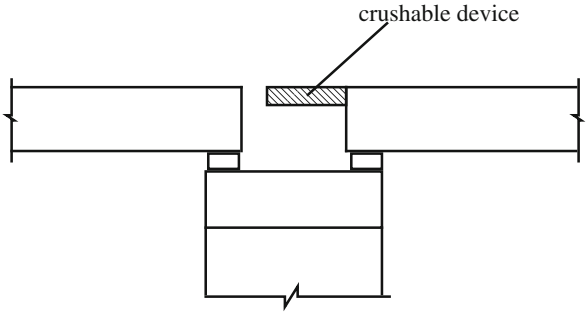

Fig. 5.4 Bridge segments equipped with crushable devices

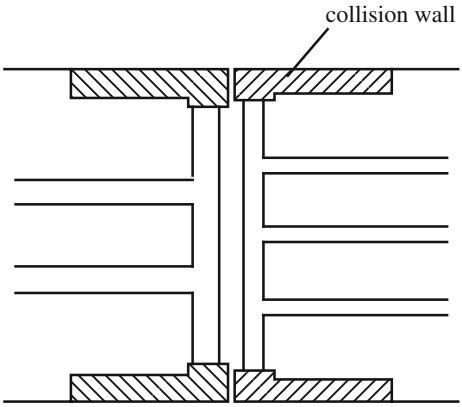

Fig. 5.5 Buildings equipped with collision walls (*horizontal cross section*)

pounding mitigation technique (Hrovat et al. 1983; Kobori et al. 1988; Soong and Constantinou 1994; Spiliopoulos and Anagnostopoulos 1996; Soong and Dargush 1997; Luco and De Barros 1998; Yang et al. 2003).

5.1 Large Gap Size to Prevent Pounding

The most natural way to prevent earthquake-induced structural pounding is to assure the sufficiently large gap size between structural elements (Jeng et al. 1992; Kasai et al. 1996; Lin 1997; Penzien 1997; Valles and Reinhorn 1997; Hao and Shen 2001; Lin and Weng 2001a, b; Lopez-Garcia 2004; Jankowski 2005, 2007, 2012; Mahmoud and Jankowski 2009, 2011; Rajaram and Kumar 2012; Mahmoud et al. 2013; Sołtysik and Jankowski 2013; Abdel Raheem 2014). Several research works were conducted for the purpose of estimation the required seismic gap through performing dynamic response analysis of adjacent buildings. In those analyses, the adjacent buildings were modelled as either single-degree-of-freedom (SDOF) or multi-degree-of-freedom (MDOF) systems. In addition, linear elastic as well as non-linear responses were

analyzed (see Anagnostopoulos 1988; Maison and Kasai 1990; Jeng et al. 1992; Filiatrault et al. 1994). A similar approach was applied to determine the optimal seismic gap required to prevent pounding between superstructure segments in elevated bridges (see, for example, Jankowski et al. 1998).

Let us denote the earthquake-induced displacement time histories of the left and the right structure at the potential pounding location as $x^L(t)$ and $x^R(t)$ (see Fig. 5.6). The minimum separation distance, $d_{\min}$, to be provided between the structures in order to avoid pounding can be easily calculated either as the absolute sum (ABS) (IBC 2009):

$$d_{\min} = x^L_{\max} + x^R_{\max} \tag{5.1}$$

or as the square root of sum of squares (SRSS) (Lopez-Garcia 2004):

$$d_{\min} = \sqrt{\left(x^L_{\max}\right)^2 + \left(x^R_{\max}\right)^2} \tag{5.2}$$

where $x^L_{\max} = \max|x^L(t)|$, $x^R_{\max} = \max|x^R(t)|$ are the peak displacements during the whole time of the earthquake for the left and the right structure, respectively.

In order to account for the phase of vibration and damping of adjacent two structures, which are not included in the aforementioned two formulas, the double difference formula for computing the minimum separation distance following the spectral difference method (SPD) was also derived (Jeng et al. 1992; Penzien 1997; Lopez-Garcia 2004):

$$d_{\min} = \sqrt{\left(x^L_{\max}\right)^2 + \left(x^R_{\max}\right)^2 - 2\rho x^L_{\max} x^R_{\max}} \tag{5.3}$$

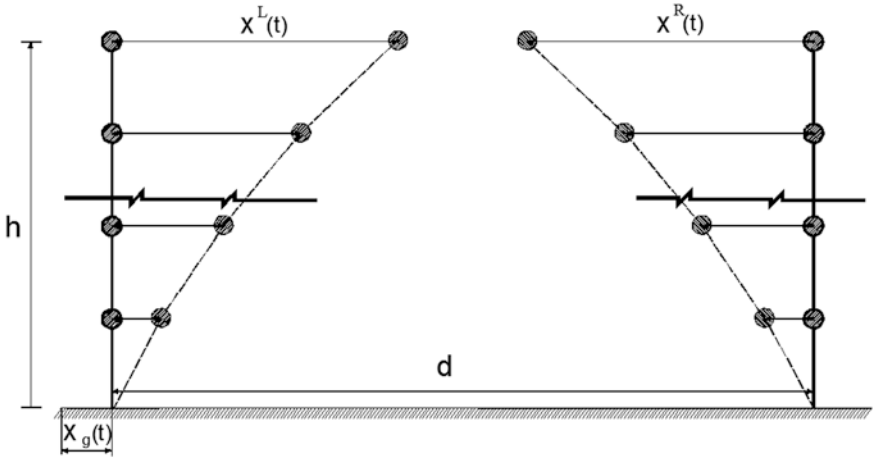

Fig. 5.6 Schematic representation of the induced structural displacements under earthquake excitation

where ρ is the cross-correlation coefficient which is a function of the natural periods T^L, T^R as well as the damping ratios ξ^L, ξ^R of the left and the right structure, respectively. The relation is described as (Jeng et al. 1992; Penzien 1997; Lopez-Garcia 2004):

$$\rho = \frac{8\sqrt{\xi^L \xi^R}\left(\xi^L + \frac{T^L}{T^R}\xi^R\right)\left(\frac{T_L}{T^R}\right)^{1.5}}{\left[1-\left(\frac{T^L}{T^R}\right)^2\right]^2 + 4\xi^L\xi^R\left(\frac{T^L}{T^R}\right)\left[1+\left(\frac{T^L}{T^R}\right)^2\right] + 4\left((\xi^L)^2 + (\xi^R)^2\right)\left(\frac{T^L}{T^R}\right)^2} \tag{5.4}$$

It can be noticed that substituting $\rho = -1$ and $\rho = 0$ into Eq. (5.3) leads to Eqs. (5.1) and (5.2), respectively.

For the purpose of numerical simulations, focused on computing the minimum separation gap required to prevent pounding using different expressions (Eqs. 5.1–5.3), the model of colliding three-storey buildings shown in Fig. 3.5 has been used. The details concerning the properties of structures have been described in Sect. 3.2. A suit of ground motion records from different locations, characterized with different peak ground accelerations (PGA), have been considered in the analysis. The set of records has included the following strong ground motions: 1940 El Centro, 1999 Kocaeli, 1989 Loma Prieta, 1999 Duzce, 1995 Kobe, 1978 Tabas, 1985 Nahanni, 1971 San Fernando and 1994 Northridge earthquake. The results of the analysis are summarized in Table 5.1.

As it could be expected, the use of ABS formula has resulted in the highest seismic gap values for all ground motions since it is based on the most conservative assumption. More reasonable values have been obtained for SSRS and SPD formulae in which the assumption is made that the peak responses of two structures do not take place at the same time. The results presented in Table 5.1 indicate that the differences between the seismic gap values obtained for SSRS and SPD formulae are insignificant in the case of the structures analyzed, which are characterized by

Table 5.1 Seismic gaps required to prevent pounding calculated by using different methods for various earthquakes

Earthquake	Station	Component	PGA (m/s^2)	Seismic gap (m)		
				ABS	SSRS	SPD
El Centro	El Centro	NS	3.402	0.1616	0.1441	0.1440
Kocaeli (Izmit)	Sakarya	EW	3.693	0.1725	0.1514	0.1513
Loma Prieta	Corralitos	NS	6.315	0.1685	0.1247	0.1245
Duzce	Bolu	EW	7.907	0.3518	0.3252	0.3251
Kobe	JMA	NS	8.178	0.4437	0.3972	0.3970
Tabas	Tabas	TAB-LN	8.201	0.1489	0.1271	0.1270
Nahanni	Site1	S1280	10.75	0.1599	0.1283	0.1281
San Fernando	Pacoima Dam	N16°W	12.03	0.5506	0.5028	0.5026
Northridge	Terzana, Cedar Hill	EW	17.46	0.3697	0.2903	0.2900

substantially different dynamics properties. This is due to very small value of the cross-correlation coefficient, ρ, which depends on the ratio between natural periods of adjacent two buildings (see Eq. 5.4). It is also worth mentioning looking at Table 5.1 that substantially different separation gaps are required for different ground motion excitations. The largest values have been obtained for the San Fernando earthquake, while the smallest separation gaps have been calculated for the Tabas (ABS formula) as well as the Loma Prieta (SSRS and SPD formulae) earthquakes.

5.2 Link Elements

Connecting adjacent structures is another approach to avoid structural interactions under earthquake excitations. Stiff connectors as well as some viscoelastic elements can be used for such purposes. Westermo (1989) suggested, for example, linking buildings by additional beams, which can fully transmit the forces between the structures. The connections between adjacent structures can also have some energy dissipating properties and impacts can be partly absorbed (Kobori et al. 1988). In order to control and eliminate the earthquake-induced interactions between two neighbouring structures, a coupling element was used by Zhu and Iemura (2000). Kasai et al. (1992) applied viscoelastic dampers for the purpose of linking insufficiently separated adjacent buildings and mitigate pounding effects. Similar studies concerning adjacent buildings interconnected by damping devices were also conducted by other researchers (see, for example, Xu et al. 1999; Zhang and Xu 1999; Ni et al. 2001). The optimal values for the distribution of viscous dampers in linking adjacent structures of different heights were determined by Luco and De Barros (1998). Investigations on the dynamic characteristics and seismic response of adjacent structures connected by fluid dampers were conducted by Zhang and Xu (2000) as well as Zhu and Xu (2005). The effectiveness of dampers and restrainers to reduce the negative pounding effects was also investigated in a number of other studies (DesRoches and Muthukumar 2002; Ruangrassamee and Kawashima 2003; Yang et al. 2003).

In this part of the chapter, the effects of connecting adjacent three-storey buildings by link elements, as a strategy for mitigating pounding between insufficiently separated structures, is investigated. Using the discrete three-degree-of-freedom numerical models of buildings, three cases have been studied. In the first one, spring elements have been applied as links at all the storey levels (see Fig. 5.7), linking elements in the form of dashpots have been considered in the second one (see Fig. 5.8), whereas the third case deals with the application of viscoelastic elements combining both springs and dashpots. The effectiveness of the link elements has been tested for different values of spring stiffness and dashpot damping and the optimum values required to obtain the largest reduction in the structural response have been analyzed.

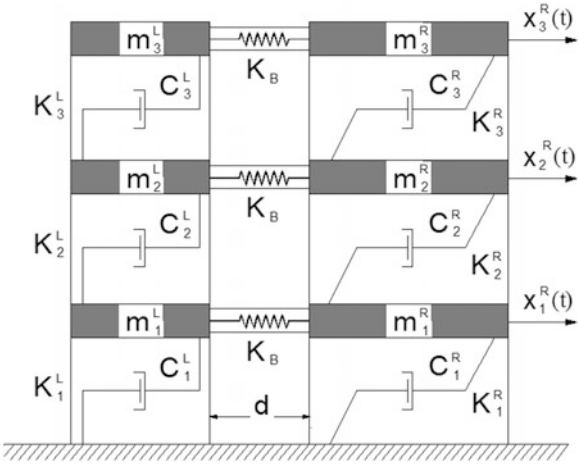

Fig. 5.7 Model of three-storey buildings linked with spring elements

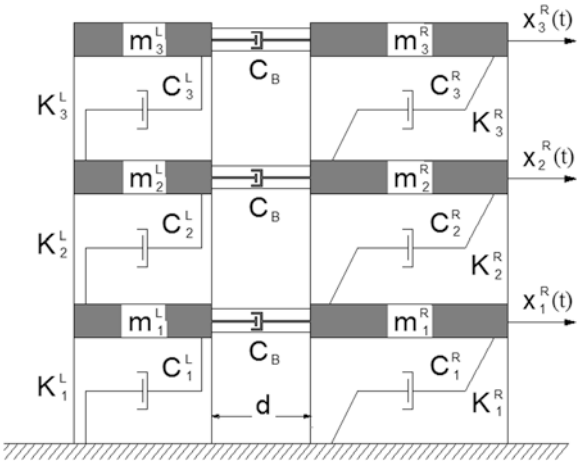

Fig. 5.8 Model of three-storey buildings linked with dashpot elements

5.2.1 Buildings Linked with Spring Elements

The elastic dynamic equation of motion under earthquake excitation for the model of two three-storey buildings linked with spring elements, shown in Fig. 5.7, can be written as [see Cimellaro and Lopez-Garcia 2011 and compare Eq. (3.1)]:

$$\mathbf{M}\ddot{\mathbf{x}}(t) + \mathbf{C}\dot{\mathbf{x}}(t) + (\mathbf{K} + \mathbf{K}_B)\mathbf{x}(t) = -\mathbf{M}\mathbf{1}\ddot{x}_g(t) \tag{5.5a}$$

$$\mathbf{M}=\begin{bmatrix} m_1^L & 0 & 0 & 0 & 0 & 0\\ 0 & m_2^L & 0 & 0 & 0 & 0\\ 0 & 0 & m_3^L & 0 & 0 & 0\\ 0 & 0 & 0 & m_1^R & 0 & 0\\ 0 & 0 & 0 & 0 & m_2^R & 0\\ 0 & 0 & 0 & 0 & 0 & m_3^R \end{bmatrix};\quad \ddot{\mathbf{x}}(t)=\begin{bmatrix} \ddot{x}_1^L(t)\\ \ddot{x}_2^L(t)\\ \ddot{x}_3^L(t)\\ \ddot{x}_1^R(t)\\ \ddot{x}_2^R(t)\\ \ddot{x}_3^R(t) \end{bmatrix};\quad \dot{\mathbf{x}}(t)=\begin{bmatrix} \dot{x}_1^L(t)\\ \dot{x}_2^L(t)\\ \dot{x}_3^L(t)\\ \dot{x}_1^R(t)\\ \dot{x}_2^R(t)\\ \dot{x}_3^R(t) \end{bmatrix} \tag{5.5b}$$

$$\mathbf{C}=\begin{bmatrix} C_1^L+C_2^L & -C_2^L & 0 & 0 & 0 & 0\\ -C_2^L & C_2^L+C_3^L & -C_3^L & 0 & 0 & 0\\ 0 & -C_3^L & C_3^L & 0 & 0 & 0\\ 0 & 0 & 0 & C_1^R+C_2^R & -C_2^R & 0\\ 0 & 0 & 0 & -C_2^R & C_2^R+C_3^R & -C_3^R\\ 0 & 0 & 0 & 0 & -C_3^R & C_3^R \end{bmatrix} \tag{5.5c}$$

$$\mathbf{K}=\begin{bmatrix} K_1^L+K_2^L & -K_2^L & 0 & 0 & 0 & 0\\ -K_2^L & K_2^L+K_3^L & -K_3^L & 0 & 0 & 0\\ 0 & -K_3^L & K_3^L & 0 & 0 & 0\\ 0 & 0 & 0 & K_1^R+K_2^R & -K_2^R & 0\\ 0 & 0 & 0 & -K_2^R & K_2^R+K_3^R & -K_3^R\\ 0 & 0 & 0 & 0 & -K_3^R & K_3^R \end{bmatrix} \tag{5.5d}$$

$$\mathbf{K}_B=\begin{bmatrix} K_B & 0 & 0 & -K_B & 0 & 0\\ 0 & K_B & 0 & 0 & -K_B & 0\\ 0 & 0 & K_B & 0 & 0 & -K_B\\ -K_B & 0 & 0 & K_B & 0 & 0\\ 0 & -K_B & 0 & 0 & K_B & 0\\ 0 & 0 & -K_B & 0 & 0 & K_B \end{bmatrix};\quad \mathbf{x}(t)=\begin{bmatrix} x_1^L(t)\\ x_2^L(t)\\ x_3^L(t)\\ x_1^R(t)\\ x_2^R(t)\\ x_3^R(t) \end{bmatrix};\quad \mathbf{1}=\begin{bmatrix} 1\\ 1\\ 1\\ 1\\ 1\\ 1 \end{bmatrix} \tag{5.5e}$$

where $\ddot{x}_i^L(t)$, $\ddot{x}_i^R(t)$, $\dot{x}_i^L(t)$, $\dot{x}_i^R(t)$, $x_i^L(t)$, $x_i^R(t)$ $(i=1,\ldots,3)$ are the acceleration, velocity and displacement of a single storey of the left (upper index L) and the right (upper index R) building, respectively; m_i^L, m_i^R stand for the storey masses; K_i^L, C_i^L, K_i^R, C_i^R are elastic structural stiffness and damping coefficients; K_B denotes stiffness coefficient of spring elements and $\ddot{x}_g(t)$ is the acceleration of input ground motion. It should be underlined that the above equation of motion is valid for such values of stiffness coefficient of spring elements which are large enough to prevent pounding for the considered gap size between buildings.

As the example, two three-storey buildings, with the structural properties described in Sect. 3.2, have been considered in the analysis. The stiffness coefficient of spring elements, K_B, has been allowed to vary from 0 to 8×10^7 N/m. The time-stepping Newmark method (Newmark 1959) with constant time step $\Delta t=0.002$ s has been used in order to solve the equation of motion (5.5a–e) numerically. Different earthquake records have been incorporated in the analysis. The examples

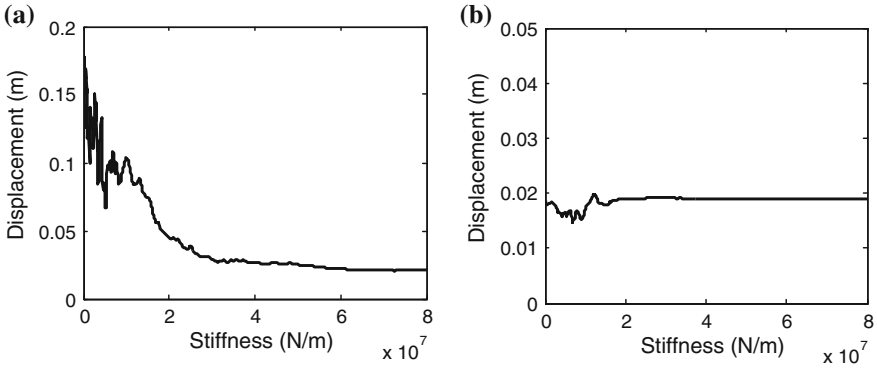

Fig. 5.9 Peak displacement of the third storeys of buildings with respect to stiffness of linking spring elements under the El Centro earthquake. **a** Left building, **b** right building

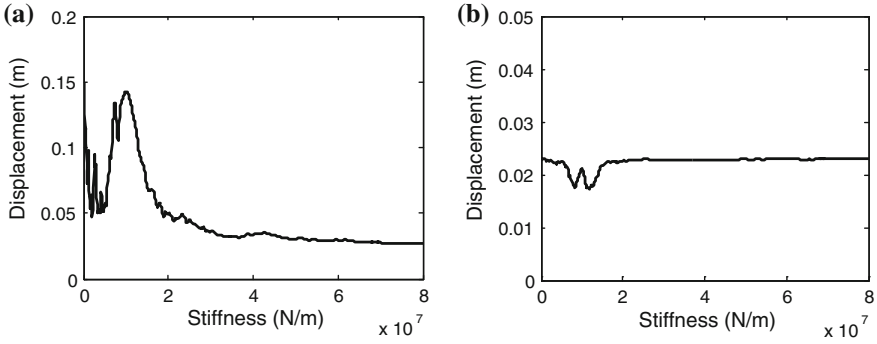

Fig. 5.10 Peak displacement of the third storeys of buildings with respect to stiffness of linking spring elements under the Kocaeli earthquake. **a** Left building, **b** right building

of the results of the study for the El Centro, Kocaeli, Kobe and Duzce earthquakes are presented in Figs. 5.9, 5.10, 5.11 and 5.12. They show the peak displacements of the third storeys of both buildings with respect to the stiffness of spring elements.

The results obtained for the left building (lighter and more flexible one) indicate that the increase in the stiffness value of spring elements is very beneficial for the response of this structure. In the case when stiffness is equal to zero (buildings are not connected and move out-of-phase), the obtained peak displacements of the left building under the El Centro, Kocaeli, Kobe and Duzce earthquakes are equal to: 0.1429, 0.1496, 0.3941 and 0.3240 m, respectively. For stiff linking with high stiffness value (buildings are fully connected and move in-phase), the obtained peak displacements of the structure are as small as: 0.0213, 0.0263, 0.0560 and 0.0342 m for the El Centro, Kocaeli, Kobe and Duzce earthquakes, respectively. The

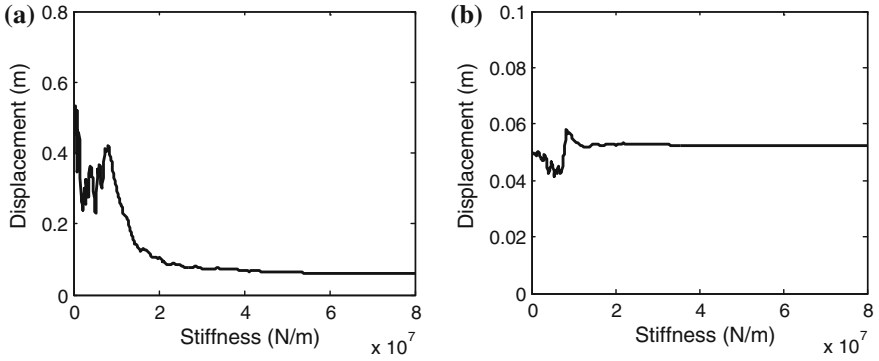

Fig. 5.11 Peak displacement of the third storeys of buildings with respect to stiffness of linking spring elements under the Kobe earthquake. **a** Left building, **b** right building

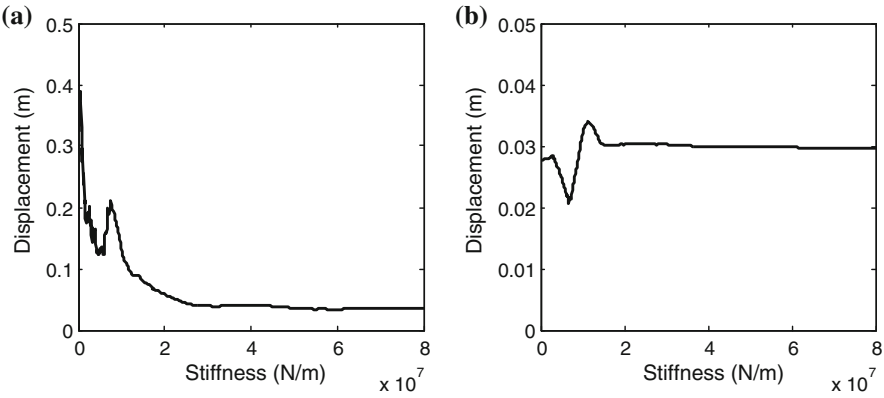

Fig. 5.12 Peak displacement of the third storeys of buildings with respect to stiffness of linking spring elements under the Duzce earthquake. **a** Left building, **b** right building

aforementioned obtained values for the left building in the case of independent vibrations and stiff linking under the considered earthquake records show the significant reductions in the peak displacements, which is equal to 85, 82, 86 and 89 %, respectively. On the other hand, it can be seen from Figs. 5.9b, 5.10b, 5.11b and 5.12b that applying the additional springs does not really change the response of the right building (heavier and stiffer one). The differences between the case of independent vibrations (spring stiffness is equal to zero) and stiff linking (high value of spring stiffness) is relatively small and is equal to: 2.7, 0.4, 5.6 and 7.2 % under the El Centro, Kocaeli, Kobe and Duzce ground motion records, respectively.

5.2.2 Buildings Linked with Dashpot Elements

The elastic dynamic equation of motion under earthquake excitation for the model of two three-storey buildings linked with dashpot elements, shown in Fig. 5.8, can be written as [see Cimellaro and Lopez-Garcia (2011) as well as compare Eqs. (3.1) and (5.5a–e)]:

$$\mathbf{M}\ddot{\mathbf{x}}(t) + (\mathbf{C} + \mathbf{C}_B)\dot{\mathbf{x}}(t) + \mathbf{K}\mathbf{x}(t) = -\mathbf{M}\mathbf{1}\ddot{x}_g(t) \tag{5.6a}$$

$$\mathbf{M} = \begin{bmatrix} m_1^L & 0 & 0 & 0 & 0 & 0 \\ 0 & m_2^L & 0 & 0 & 0 & 0 \\ 0 & 0 & m_3^L & 0 & 0 & 0 \\ 0 & 0 & 0 & m_1^R & 0 & 0 \\ 0 & 0 & 0 & 0 & m_2^R & 0 \\ 0 & 0 & 0 & 0 & 0 & m_3^R \end{bmatrix}; \quad \ddot{\mathbf{x}}(t) = \begin{bmatrix} \ddot{x}_1^L(t) \\ \ddot{x}_2^L(t) \\ \ddot{x}_3^L(t) \\ \ddot{x}_1^R(t) \\ \ddot{x}_2^R(t) \\ \ddot{x}_3^R(t) \end{bmatrix}; \quad \dot{\mathbf{x}}(t) = \begin{bmatrix} \dot{x}_1^L(t) \\ \dot{x}_2^L(t) \\ \dot{x}_3^L(t) \\ \dot{x}_1^R(t) \\ \dot{x}_2^R(t) \\ \dot{x}_3^R(t) \end{bmatrix} \tag{5.6b}$$

$$\mathbf{C} = \begin{bmatrix} C_1^L + C_2^L & -C_2^L & 0 & 0 & 0 & 0 \\ -C_2^L & C_2^L + C_3^L & -C_3^L & 0 & 0 & 0 \\ 0 & -C_3^L & C_3^L & 0 & 0 & 0 \\ 0 & 0 & 0 & C_1^R + C_2^R & -C_2^R & 0 \\ 0 & 0 & 0 & -C_2^R & C_2^R + C_3^R & -C_3^R \\ 0 & 0 & 0 & 0 & -C_3^R & C_3^R \end{bmatrix} \tag{5.6c}$$

$$\mathbf{K} = \begin{bmatrix} K_1^L + K_2^L & -K_2^L & 0 & 0 & 0 & 0 \\ -K_2^L & K_2^L + K_3^L & -K_3^L & 0 & 0 & 0 \\ 0 & -K_3^L & K_3^L & 0 & 0 & 0 \\ 0 & 0 & 0 & K_1^R + K_2^R & -K_2^R & 0 \\ 0 & 0 & 0 & -K_2^R & K_2^R + K_3^R & -K_3^R \\ 0 & 0 & 0 & 0 & -K_3^R & K_3^R \end{bmatrix} \tag{5.6d}$$

$$\mathbf{C}_B = \begin{bmatrix} C_B & 0 & 0 & -C_B & 0 & 0 \\ 0 & C_B & 0 & 0 & -C_B & 0 \\ 0 & 0 & C_B & 0 & 0 & -C_B \\ -C_B & 0 & 0 & C_B & 0 & 0 \\ 0 & -C_B & 0 & 0 & C_B & 0 \\ 0 & 0 & -C_B & 0 & 0 & C_B \end{bmatrix}; \quad \dot{\mathbf{x}}(t) = \begin{bmatrix} \dot{x}_1^L(t) \\ \dot{x}_2^L(t) \\ \dot{x}_3^L(t) \\ \dot{x}_1^R(t) \\ \dot{x}_2^R(t) \\ \dot{x}_3^R(t) \end{bmatrix}; \quad \mathbf{1} = \begin{bmatrix} 1 \\ 1 \\ 1 \\ 1 \\ 1 \\ 1 \end{bmatrix} \tag{5.6e}$$

where $\ddot{x}_i^L(t)$, $\ddot{x}_i^R(t)$, $\dot{x}_i^L(t)$, $\dot{x}_i^R(t)$, $x_i^L(t)$, $x_i^R(t)$ $(i = 1, \ldots, 3)$ are the acceleration, velocity and displacement of a single storey of the left (upper index L) and the right (upper index R) building, respectively; m_i^L, m_i^R stand for the storey masses; K_i^L, C_i^L, K_i^R, C_i^R are elastic structural stiffness and damping coefficients; C_B denotes damping

coefficient of dashpot elements and $\ddot{x}_g(t)$ is the acceleration of input ground motion. It should be underlined that the above equation of motion is valid for such values of damping coefficient of dashpot elements which are large enough to prevent pounding for the considered gap size between buildings.

Similarly as in Sect. 5.2.1, the earthquake-induced response of two three-storey buildings with different (substantially different) dynamic properties has been analyzed. The damping coefficient of dashpot elements, C_B, has been considered to vary from 0 to 1×10^7 kg/s. The time-stepping Newmark method with constant time step $\Delta t = 0.002$ s has been used in order to solve the equation of motion (5.6a–e) numerically. The examples of the results for the El Centro, Kocaeli, Kobe and Duzce earthquakes are presented in Figs. 5.13, 5.14, 5.15 and 5.16. They show the peak displacements of the third storeys of both buildings with respect to the damping of dashpot elements.

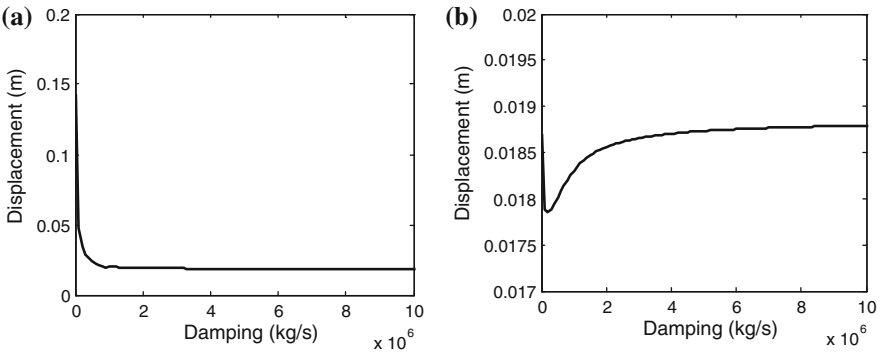

Fig. 5.13 Peak displacement of the third storeys of buildings with respect to damping of linking dashpot elements under the El Centro earthquake. **a** Left building, **b** right building

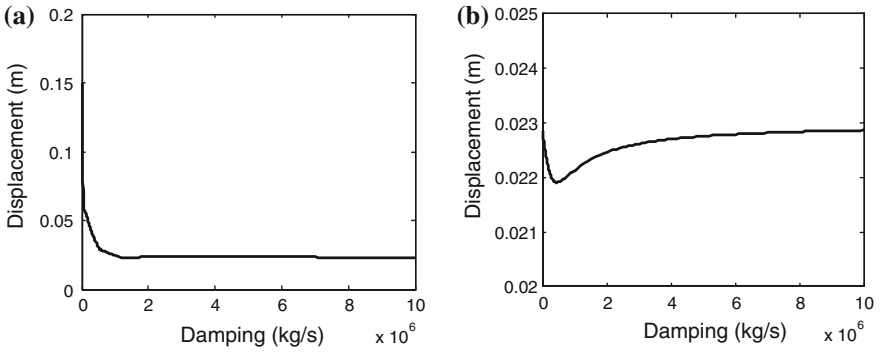

Fig. 5.14 Peak displacement of the third storeys of buildings with respect to damping of linking dashpot elements under the Kocaeli earthquake. **a** Left building, **b** right building

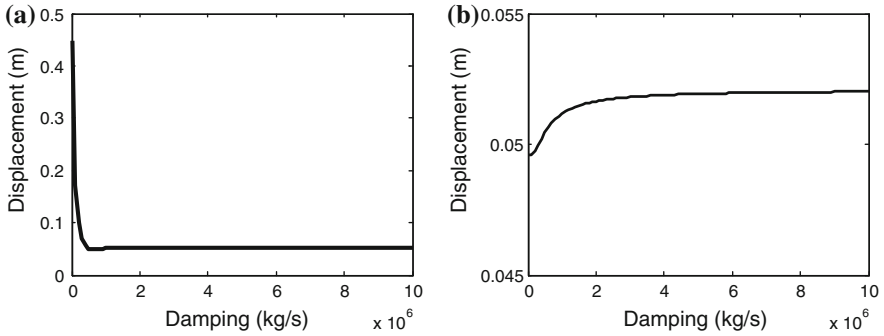

Fig. 5.15 Peak displacement of the third storeys of buildings with respect to damping of linking dashpot elements under the Kobe earthquake. **a** Left building, **b** right building

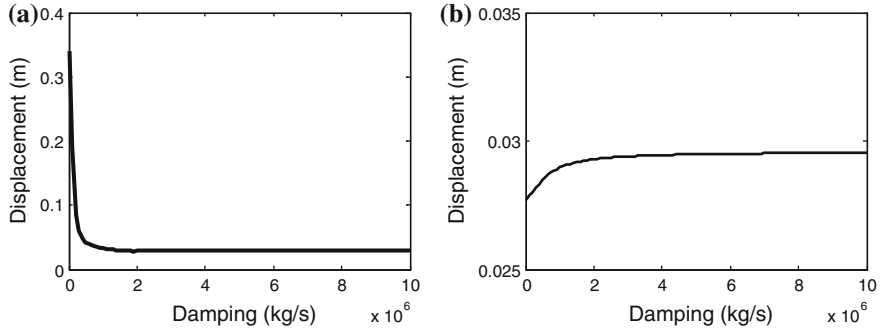

Fig. 5.16 Peak displacement of the third storeys of buildings with respect to damping of linking dashpot elements under the Duzce earthquake. **a** Left building, **b** right building

The results of the study indicate that, with the initial increase in the damping coefficient value, a significant reduction in the peak displacements of the left building (lighter and more flexible one) has been obtained for all analyzed seismic excitations. However, it can be seen from Figs. 5.13a, 5.14a, 5.15a and 5.16a that, after passing some threshold value, with further increase in damping coefficient, the response of the structure is nearly unchanged. In the case when damping of link elements is equal to zero (buildings are not connected and move out-of-phase), the obtained peak displacements of the left structure under the El Centro, Kocaeli, Kobe and Duzce earthquakes are equal to: 0.1429, 0.1496, 0.3941 and 0.324 m, respectively. For high damping values of dashpot elements (buildings are fully connected and move in-phase), the obtained peak displacements of the structure are as small as: 0.0192, 0.0228, 0.054 and 0.0296 m for the El Centro, Kocaeli, Kobe and Duzce earthquakes, respectively. The above values for the left building show significant reductions in the peak displacements, which is equal to 87, 85, 86 and 91 %, respectively, in the case when two cases are compared. On the other hand, it

can be seen from Figs. 5.13b, 5.14b, 5.15b and 5.16b that applying the additional dashpot elements between structures does not change the response of the right building (heavier and stiffer one) substantially, although the change in the response is more visible than in the case of the results obtained for different values of stiffness coefficient shown in Figs. 5.9b, 5.10b, 5.11b and 5.12b. Anyway, the differences between the case of independent vibrations (dashpot damping is equal to zero) and stiff linking (high value of dashpot damping) is also relatively small and is equal to: 2.7, 0.4, 5.0 and 6.5 % under the El Centro, Kocaeli, Kobe and Duzce ground motion records, respectively.

5.2.3 Buildings Linked with Viscoelastic Elements

A reasonable solution might also be to combine spring as well as dashpot link elements together. The elastic dynamic equation of motion under earthquake excitation for the model of two three-storey buildings linked with such viscoelastic elements can be written as [compare Eqs. (5.5a–e) and (5.6a–e)]:

$$\mathbf{M}\ddot{\mathbf{x}}(t) + (\mathbf{C} + \mathbf{C}_B)\dot{\mathbf{x}}(t) + (\mathbf{K} + \mathbf{K}_B)\mathbf{x}(t) = -\mathbf{M}\mathbf{1}\ddot{x}_g(t) \tag{5.7}$$

where all vectors and matrices of the above equation are defined in Eqs. (5.5a–e) and (5.6a–e). The parametric analysis has been conducted so as to verify the effectiveness of viscoelastic link elements in mitigation of pounding effects and reduction of structural vibrations. The investigation has been conducted for different values of spring stiffness and dashpot damping coefficients. When one parameter has been altered, the value of the second one has been kept constant. The following arbitrary chosen basic values have been considered in the analysis: $K_B = 1 \times 10^5$ N/m, $C_B = 5 \times 10^4$ kg/s. The examples of the results of the study

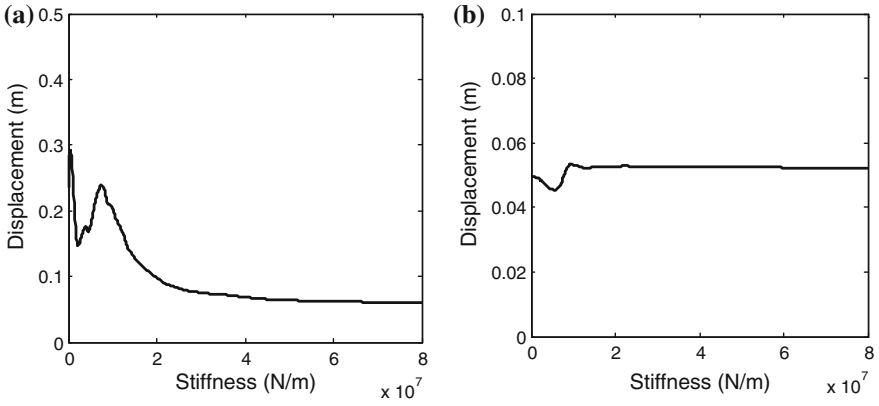

Fig. 5.17 Peak displacement of the third storeys of buildings with respect to stiffness of linking viscoelastic elements under the Kobe earthquake. **a** Left building, **b** right building

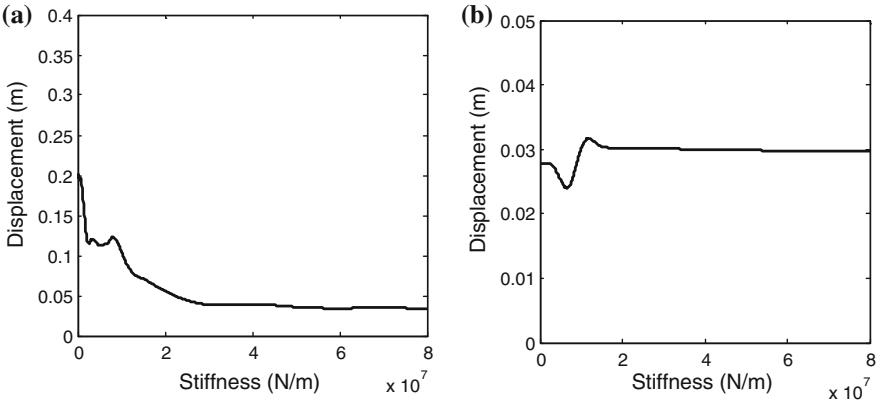

Fig. 5.18 Peak displacement of the third storeys of buildings with respect to stiffness of linking viscoelastic elements under the Duzce earthquake. **a** Left building, **b** right building

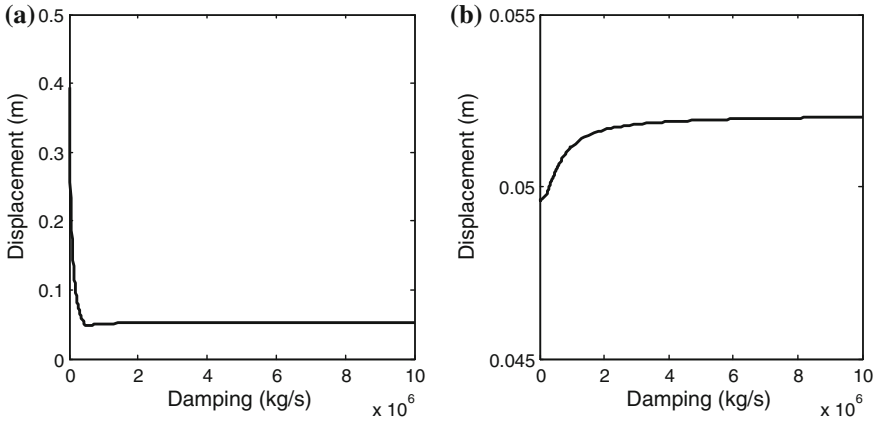

Fig. 5.19 Peak displacement of the third storeys of buildings with respect to damping of linking viscoelastic elements under the Kobe earthquake. **a** Left building, **b** right building

for the Kobe and Duzce earthquakes are presented in Figs. 5.17, 5.18, 5.19 and 5.20. They show the peak displacements of the third storeys of both buildings with respect to the stiffness of spring elements (Figs. 5.17 and 5.18) as well as with respect to the damping of dashpot elements (Figs. 5.19 and 5.20).

The results shown in Figs. 5.17a, 5.18a, 5.19a and 5.20a indicate that with the initial increase in stiffness (damping) values, a decrease trend in the obtained top storey displacements of the left building has been observed, and with further increase in the analyzed parameter, the peak storey displacements remain nearly unchanged showing significant reduction. Such results could be expected based on previous findings described in Sects. 5.2.1 and 5.2.2. It is worth noting, however, that the use of viscoelastic elements reduces the peak displacement of the lighter

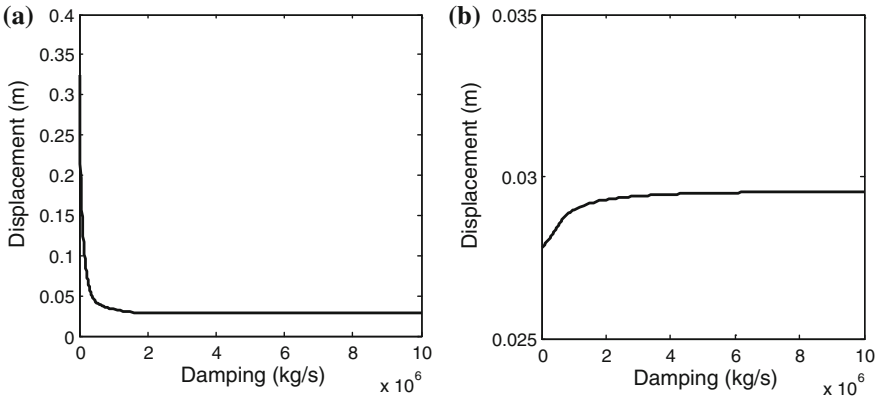

Fig. 5.20 Peak displacement of the third storeys of buildings with respect to damping of linking viscoelastic elements under the Duzce earthquake. **a** Left building, **b** right building

and more flexible structure at lower stiffness and damping values comparing to the case of spring and dashpot elements applied alone (compare especially Figs. 5.11a and 5.12a with Figs. 5.17a and 5.18a). On the other hand, the results from Figs. 5.17b, 5.18b, 5.19b and 5.20b show insignificant changes in the behaviour of heavier and stiffer building. Moreover, the peak displacements for this building show very similar results as those obtained for spring and dashpot elements used alone (compare Figs. 5.11b and 5.12b with Figs. 5.17b and 5.18b as well as Figs. 5.15b and 5.16b with Figs. 5.19b and 5.20b).

5.3 Bumpers

The use of some kind of bumpers is another technique in mitigating the detrimental effects of earthquake-induced pounding between insufficiently separated structures. Anagnostopoulos (1996) as well as Anagnostopoulos and Karamaneas (2008) considered the idea of filling the separation gap by some energy absorbing material or providing strong collision walls to protect part of the structure. The use of rubber bumpers, as well as crushable devices, to suppress the blows of impacts in elevated bridges was studied by Jankowski et al. (2000). Abdel Raheem (2009) examined the effect of incorporating rubber pads placed between girder ends in order to mitigate the effect of collisions in isolated bridge structures. The effectiveness of using rubber bumpers as pounding mitigation technique was also considered by Polycarpou et al. (2013).

In this section, let us study the influence of rubber bumpers on the behaviour of colliding three-storey buildings during ground motion. The model of the structures equipped with the devices is shown in Fig. 5.21. The elastic dynamic equation of

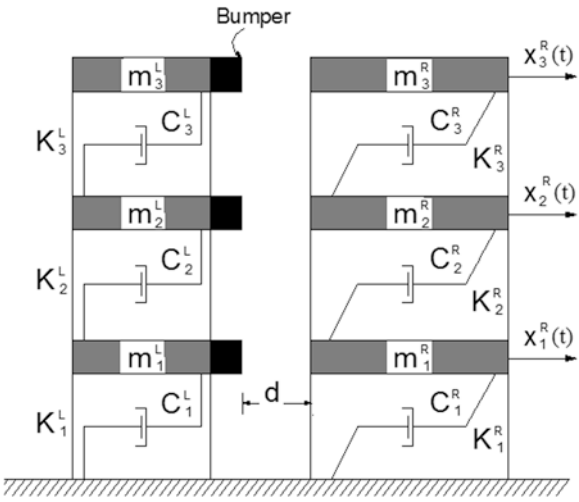

Fig. 5.21 Model of three-storey buildings equipped with bumpers

motion under earthquake excitation for such a model can be written as [compare Eq. (5.5a–e) and Eq. (3.1)]:

$$\mathbf{M}\ddot{\mathbf{x}}(t) + \mathbf{C}\dot{\mathbf{x}}(t) + \mathbf{K}\mathbf{x}(t) + \mathbf{F}(t) = -\mathbf{M}\mathbf{1}\ddot{x}_g(t) \tag{5.8a}$$

$$\mathbf{M} = \begin{bmatrix} m_1^L & 0 & 0 & 0 & 0 & 0 \\ 0 & m_2^L & 0 & 0 & 0 & 0 \\ 0 & 0 & m_3^L & 0 & 0 & 0 \\ 0 & 0 & 0 & m_1^R & 0 & 0 \\ 0 & 0 & 0 & 0 & m_2^R & 0 \\ 0 & 0 & 0 & 0 & 0 & m_3^R \end{bmatrix}; \quad \ddot{\mathbf{x}}(t) = \begin{bmatrix} \ddot{x}_1^L(t) \\ \ddot{x}_2^L(t) \\ \ddot{x}_3^L(t) \\ \ddot{x}_1^R(t) \\ \ddot{x}_2^R(t) \\ \ddot{x}_3^R(t) \end{bmatrix}; \quad \dot{\mathbf{x}}(t) = \begin{bmatrix} \dot{x}_1^L(t) \\ \dot{x}_2^L(t) \\ \dot{x}_3^L(t) \\ \dot{x}_1^R(t) \\ \dot{x}_2^R(t) \\ \dot{x}_3^R(t) \end{bmatrix} \tag{5.8b}$$

$$\mathbf{C} = \begin{bmatrix} C_1^L + C_2^L & -C_2^L & 0 & 0 & 0 & 0 \\ -C_2^L & C_2^L + C_3^L & -C_3^L & 0 & 0 & 0 \\ 0 & -C_3^L & C_3^L & 0 & 0 & 0 \\ 0 & 0 & 0 & C_1^R + C_2^R & -C_2^R & 0 \\ 0 & 0 & 0 & -C_2^R & C_2^R + C_3^R & -C_3^R \\ 0 & 0 & 0 & 0 & -C_3^R & C_3^R \end{bmatrix} \tag{5.8c}$$

$$\mathbf{K} = \begin{bmatrix} K_1^L + K_2^L & -K_2^L & 0 & 0 & 0 & 0 \\ -K_2^L & K_2^L + K_3^L & -K_3^L & 0 & 0 & 0 \\ 0 & -K_3^L & K_3^L & 0 & 0 & 0 \\ 0 & 0 & 0 & K_1^R + K_2^R & -K_2^R & 0 \\ 0 & 0 & 0 & -K_2^R & K_2^R + K_3^R & -K_3^R \\ 0 & 0 & 0 & 0 & -K_3^R & K_3^R \end{bmatrix} \tag{5.8d}$$

$$\mathbf{F}(t) = \begin{bmatrix} F_1(t) \\ F_2(t) \\ F_3(t) \\ -F_1(t) \\ -F_2(t) \\ -F_3(t) \end{bmatrix}; \quad \mathbf{x}(t) = \begin{bmatrix} x_1^L(t) \\ x_2^L(t) \\ x_3^L(t) \\ x_1^R(t) \\ x_2^R(t) \\ x_3^R(t) \end{bmatrix}; \quad \mathbf{1} = \begin{bmatrix} 1 \\ 1 \\ 1 \\ 1 \\ 1 \\ 1 \end{bmatrix} \tag{5.8e}$$

where $\ddot{x}_i^L(t)$, $\ddot{x}_i^R(t)$, $\dot{x}_i^L(t)$, $\dot{x}_i^R(t)$, $x_i^L(t)$, $x_i^R(t)$ $(i = 1, \ldots, 3)$ are the acceleration, velocity and displacement of a single storey of the left (upper index L) and the right (upper index R) building, respectively; K_i^L, C_i^L, K_i^R, C_i^R are elastic structural stiffness and damping coefficients; $F_i(t)$ denotes impact force due to activation of the bumper placed between storeys with masses m_i^L, m_i^R and $\ddot{x}_g(t)$ is the acceleration of input ground motion. It should be underlined that the above equation of motion is valid for such properties of bumpers that pounding between structural elements is prevented for the considered in-between gap size.

Rubber is supposed to be the most appropriate material to be used for bumpers, which act as shock absorbers. However, the simulation of the behaviour of rubber bumpers is not an easy task since they behave in a non-linear way under static and dynamic compressive loading (see, for example, Kajita et al. 2001; Kawashima et al. 2002; Shim et al. 2004). The experimentally obtained stress-strain curves for the devices show the exponential trend (Kajita et al. 2006). Therefore, the use of linear models for simulating the rubber behaviour does not seem to be appropriate solution. Polycarpou et al. (2013) employed a non-linear spring in conjunction with a dashpot element for performing the numerical simulations focused on the use of rubber bumpers in mitigating structural pounding during earthquakes. The impact force, $F_i(t)$ (see Eq. 5.8a–e) for the proposed non-linear impact model of the devices, also used in the present study, can be expressed as (Polycarpou et al. 2013):

- during the approach period of collision, i.e. for $\dot{\delta}_i(t) > 0$:

$$\begin{aligned} F_i(t) &= k_{imp}\delta_i^n(t) && \text{for } \delta_i(t) < \delta_u \\ F_i(t) &= k_{imp}\delta_i^n(t) + k_{imp-PY}(\delta_i(t) - \delta_u) && \text{for } \delta_i(t) \geq \delta_u \end{aligned} \tag{5.9}$$

- during the restitution period of collision, i.e. for $\dot{\delta}_i(t) \leq 0$:

$$F_i(t) = k_{imp}\delta_i^n(t)(1 + c_{imp}\dot{\delta}_i(t)) \tag{5.10}$$

where: $\delta_i(t)$ is the actual indentation of the rubber bumper: $\delta_i(t) = x_i^L(t) - x_i^R(t) - d$, δ_u is the indentation which corresponds to the ultimate compressive capacity of the device, d is the initial separation gap (see Fig. 5.21), n denotes the impact exponent $(n > 1)$, k_{imp} is the impact stiffness coefficient, k_{imp-PY} defines the linear post-yield stiffness and c_{imp} is the impact damping coefficient which can be calculated as (Polycarpou et al. 2013):

$$c_{imp} = 1.55 \frac{1 - e^2}{e^{0.7076} \left(\frac{m_i^L m_i^R}{m_i^L + m_i^R} \right)^{0.0025} \left(\dot{x}_i^{L0} - \dot{x}_i^{R0} \right)^{0.9755}} \tag{5.11}$$

where e is the coefficient of restitution and $\dot{x}_i^{L0}$, $\dot{x}_i^{R0}$ are the prior-impact velocities.

In order to examine the effect of rubber bumpers in mitigating the detrimental effects due to earthquake-induced collisions, two three-storey buildings, with the structural properties described in Sect. 3.2, have been considered in the analysis. The initial separation gap between buildings has been set to $d = 0.04$ m. The impact stiffness coefficient, k_{imp}, has been allowed to vary from 0 to 8×10^7 N/m. The following other basic values of the parameters for the impact model of rubber bumpers have been applied in the analysis (see Polycarpou et al. 2013): $\delta_u = 0.032\,\text{m}$, $k_{imp-PY} = 2.50 \times 10^9$ N/m, $n = 2.65$, $e = 0.5$. The time-stepping Newmark method with constant time step $\Delta t = 0.002$ s has been used in order to solve the equation of motion (5.8a–e) numerically. Different earthquake records have been applied in the analysis. The examples of the results of the study for the El Centro, Kocaeli, Kobe and Duzce earthquakes are presented in Figs. 5.22, 5.23, 5.24 and 5.25. They show the peak displacements of the third storeys of both buildings with respect to the impact stiffness coefficient of rubber bumpers.

The results shown in Figs. 5.22, 5.23, 5.24 and 5.25 indicate that the application of rubber bumpers between analyzed buildings is less effective than connecting the structures by additional links (see Sect. 5.2). This is due to the fact that links allow the buildings to vibrate together, while bumpers may lead to substantial rebound of one the structures after collision. That is why the results obtained for the left building (lighter and more flexible one) indicate that the increase in the impact stiffness coefficient of rubber bumpers might have considerable positive as well as negative effect on the peak response of the structure. It can be seen from Figs. 5.22 and 5.24. that, for the El Centro and Kobe earthquake records, an increase trend in

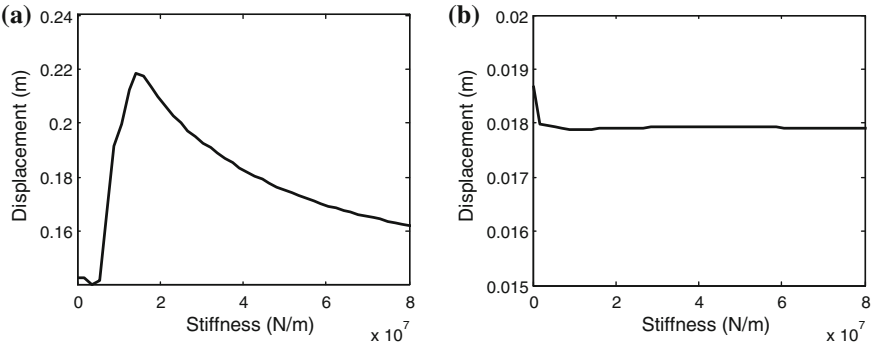

Fig. 5.22 Peak displacement of the third storeys of buildings with respect to impact stiffness coefficient of rubber bumpers under the El Centro earthquake. **a** Left building, **b** right building

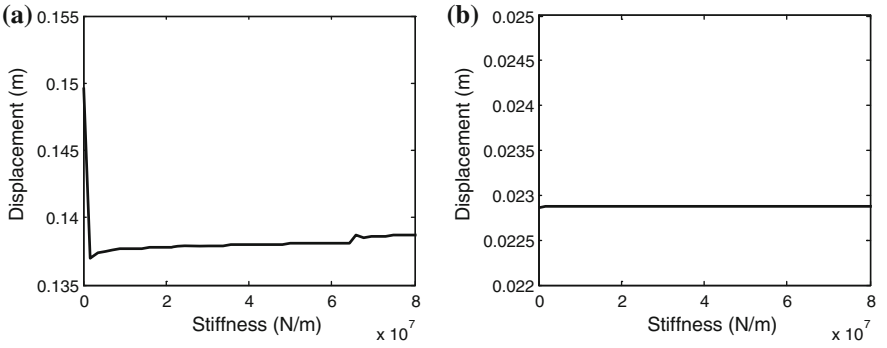

Fig. 5.23 Peak displacement of the third storeys of buildings with respect to impact stiffness coefficient of rubber bumpers under the Kocaeli earthquake. **a** Left building, **b** right building

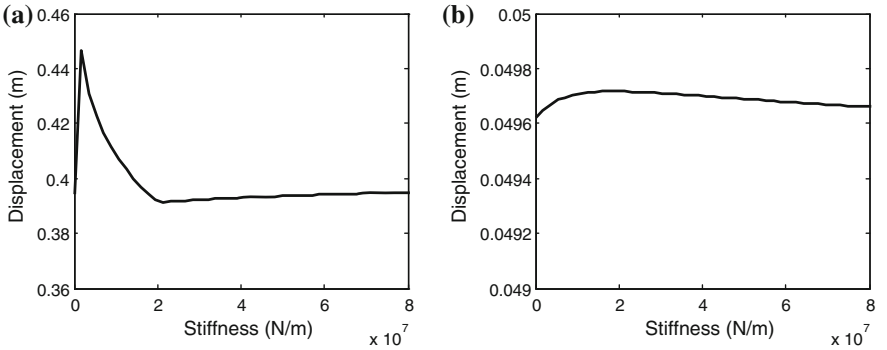

Fig. 5.24 Peak displacement of the third storeys of buildings with respect to impact stiffness coefficient of rubber bumpers under the Kobe earthquake. **a** Left building, **b** right building

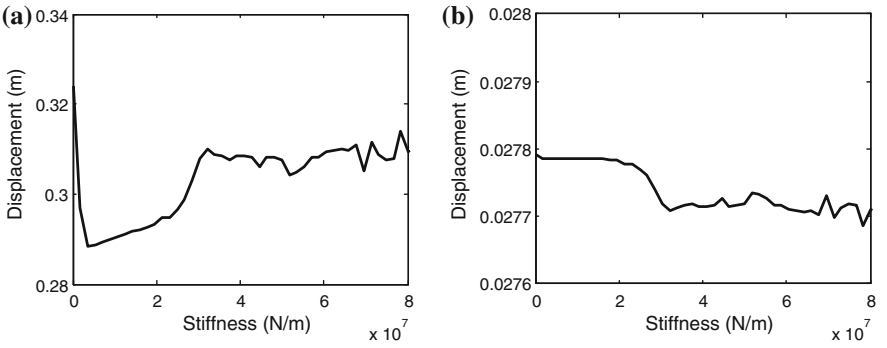

Fig. 5.25 Peak displacement of the third storeys of buildings with respect to impact stiffness coefficient of rubber bumpers under the Duzce earthquake. **a** Left building, **b** right building

the obtained third storey peak displacement curves take place at very low impact stiffness values, and the beneficial effect appears with further increase in the stiffness values. However, different response of the left structure has been obtained for the Kocaeli and Duzce ground motion records (see Figs. 5.23 and 5.25). In this case, the application of bumpers with very low impact stiffness values leads to a decrease trend in the peak displacements. However, the relation is reversed with further increase in impact stiffness of rubber bumpers. On the contrary to the left building, the results obtained for the right structure (heavier and stiffer one) indicate that the increase in the impact stiffness value of bumpers have nearly insignificant effect on the structural response for all considered ground motion records.

5.4 Other Methods

5.4.1 Increasing Stiffness of Structures

Another approach to mitigate structural pounding is to increase stiffness of structures prone to collisions so as to reduce excessive structural displacements. Such a solution might also lead to the reduction in the acceleration response values since the increased stiffness results in the increased natural frequency of the structure which, in this way, can be shifted away from the range of the dominant frequencies of excitations. The method itself is generally considered as an effective one in seismic strengthening (Loring and Wyllie 1996). In the case of buildings, one of the possible and attractive ways to increase structural stiffness is to add shear walls which act as a part of the earthquake resistant system (Divyashree et al. 2014). Another possible solution for enhancing the building's stiffness is to add a bracing system (Malhotra et al. 2004). Bracing systems are mainly used to resist lateral loads, however, they also improve the overall stiffness of the building and can be used as an effective mitigation technique against pounding (Hameed et al. 2012). Similar approach can be applied in the case of bridge structures, where additional active stiffeners can be placed between the top of piers and superstructure segments (Shigeki 2012; Mitoulis et al. 2013).

Let us verify the effect of increasing structural stiffness by analyzing the response of an exemplary three-storey building under earthquake excitations. The discrete three-degree-of-freedom numerical model of the flexible structure (see the left building in Figs. 5.7 and 5.8) has been used in the study. The elastic dynamic equation of motion for the model of the structure assuming its unrestrained vibrations (no interactions with adjacent structure) during ground motion can be written as:

$$\mathbf{M}\ddot{\mathbf{x}}(t) + \mathbf{C}\dot{\mathbf{x}}(t) + \mathbf{K}\mathbf{x}(t) = -\mathbf{M}\mathbf{1}\ddot{x}_g(t) \tag{5.12a}$$

$$\mathbf{M} = \begin{bmatrix} m_1^L & 0 & 0 \\ 0 & m_2^L & 0 \\ 0 & 0 & m_3^L \end{bmatrix}; \quad \ddot{\mathbf{x}}(t) = \begin{bmatrix} \ddot{x}_1^L(t) \\ \ddot{x}_2^L(t) \\ \ddot{x}_3^L(t) \end{bmatrix}; \quad \mathbf{1} = \begin{bmatrix} 1 \\ 1 \\ 1 \end{bmatrix} \tag{5.12b}$$

$$\mathbf{C} = \begin{bmatrix} C_1^L + C_2^L & -C_2^L & 0 \\ -C_2^L & C_2^L + C_3^L & -C_3^L \\ 0 & -C_3^L & C_3^L \end{bmatrix}; \quad \dot{\mathbf{x}}(t) = \begin{bmatrix} \dot{x}_1^L(t) \\ \dot{x}_2^L(t) \\ \dot{x}_3^L(t) \end{bmatrix} \tag{5.12c}$$

$$\mathbf{K} = \begin{bmatrix} K_1^L + K_2^L & -K_2^L & 0 \\ -K_2^L & K_2^L + K_3^L & -K_3^L \\ 0 & -K_3^L & K_3^L \end{bmatrix}; \quad \mathbf{x}(t) = \begin{bmatrix} x_1^L(t) \\ x_2^L(t) \\ x_3^L(t) \end{bmatrix} \tag{5.12d}$$

where $\ddot{x}_i^L(t)$, $\dot{x}_i^L(t)$, $x_i^L(t)$ $(i = 1, \ldots, 3)$ are the acceleration, velocity and displacement of a single storey of the building, respectively; m_i^L stands for the storey mass; K_i^L, C_i^L are elastic structural stiffness and damping coefficients and $\ddot{x}_g(t)$ is the acceleration of input ground motion.

As the example, a flexible three-storey building, with the structural properties described in Sect. 3.2, has been considered in the parametric analysis. The structural storey stiffness coefficient, K_i^L $(i = 1, \ldots, 3)$, has been allowed to vary from nearly 0 to 1×10^8 N/m. The time-stepping Newmark method with constant time step $\Delta t = 0.002$ s has been used in order to solve the equation of motion (5.12a–d) numerically. Different earthquake records have been incorporated in the study. The examples of the results, in the form of the peak displacements of the third storey of building with respect to the storey stiffness, for the El Centro, Kocaeli, Kobe and Duzce earthquakes are presented Figs. 5.26, 5.27, 5.28 and 5.29.

It can be seen from Figs. 5.26, 5.27, 5.28 and 5.29 that, with the initial increase in storey stiffness values, a significant decrease trend in the obtained top storey displacement is observed. However, with further increase in the storey stiffness, the

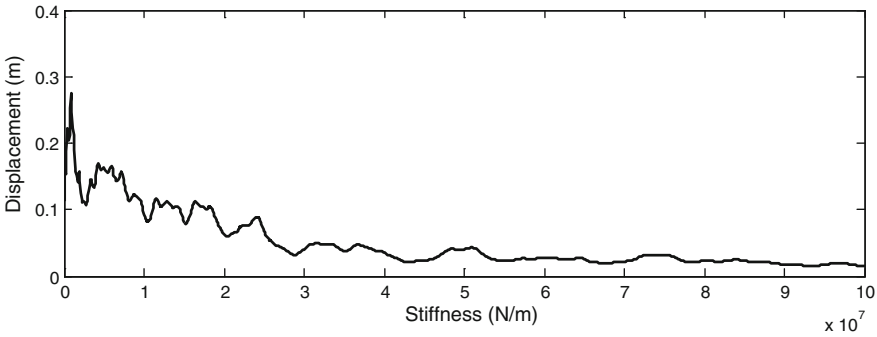

Fig. 5.26 Peak displacement of the third storey of building with respect to storey stiffness under the El Centro earthquake

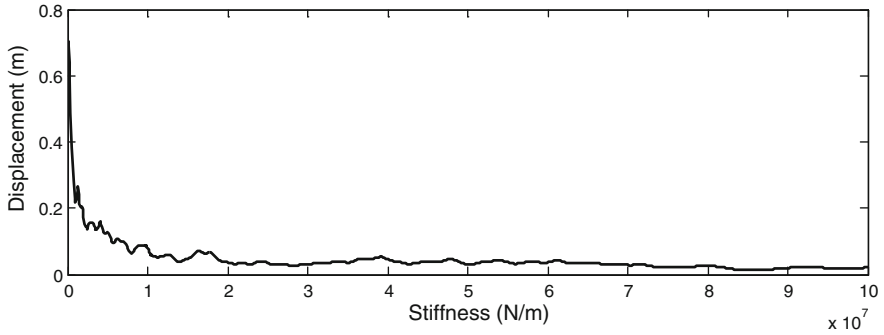

Fig. 5.27 Peak displacement of the third storey of building with respect to storey stiffness under the Kocaeli earthquake

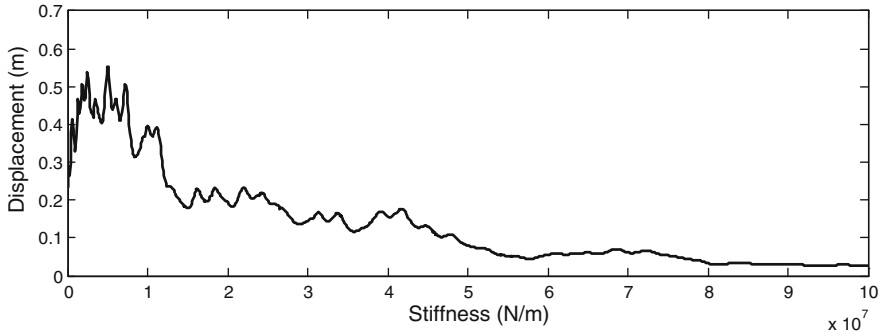

Fig. 5.28 Peak displacement of the third storey of building with respect to storey stiffness under the Kobe earthquake

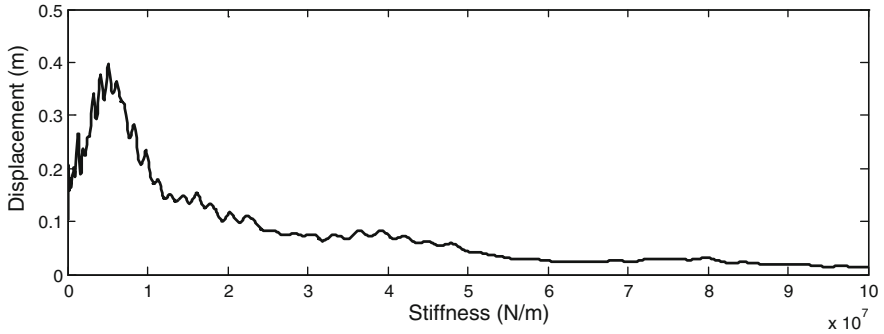

Fig. 5.29 Peak displacement of the third storey of building with respect to storey stiffness under the Duzce earthquake

top storey displacement is reduced with much lower rate. In the range of relatively low storey stiffness (very flexible building), the obtained peak displacements of the building under the El Centro, Kocaeli, Kobe and Duzce earthquakes are equal to: 0.2717, 0.7034, 0.5520 and 0.3976 m, respectively. A reduction in displacements by 94, 98, 95 and 96 % has been observed after comparing the above values with the peak displacements for the storey stiffness of $K_i^L = 1 \times 10^8$ N/m. This confirms that enhancing stiffness of the flexible building can be used efficiently to reduce the storey deformations and consequently to prevent from structural pounding. It should be underlined, however, that increasing stiffness to high levels can be in practice very expensive and difficult from the technological point of view.

5.4.2 Supplemental Energy Dissipation Devices

Another technique to prevent adjacent structures from interactions during earthquakes is to increase their damping properties through providing supplemental energy dissipation devices. Installation of such devices reduces structural displacements and improves the overall behaviour of the structures under seismic excitations (Kasai and Jagiasi 1993). Even if the reduction in the structural displacements, after installing supplemental energy dissipation devices, is not sufficient to prevent collisions, the impact force can be substantially reduced (Pantelides and Ma 1998). In the case of buildings, such devices can be installed as diagonal elements connecting adjacent floor slabs (Patel and Jangid 2010). On the other hand, additional dampers can also be placed between the top of piers and superstructure segments in bridge structures (Kawashima and Unjoh 1994).

Similarly as in Sect. 5.4.1, the response of a three-storey flexible building (left building in Figs. 5.7 and 5.8) has been analyzed as the example of investigation focus on effectiveness of supplemental energy dissipation devices in reduction of structural displacements. In the parametric analysis, the structural storey damping coefficient, C_i^L $(i = 1, \ldots, 3)$, has been allowed to vary from 0 to 1×10^7 kg/s. The time-stepping Newmark method with constant time step $\Delta t = 0.002$ s has been used in order to solve the equation of motion (5.12a–d) numerically. The examples of the results for the El Centro, Kocaeli, Kobe and Duzce earthquakes are presented in Figs. 5.30, 5.31, 5.32 and 5.33. They show the peak displacements of the third storey of building with respect to the storey damping.

The results of the study shown in Figs. 5.30, 5.31, 5.32 and 5.33 indicate that with the initial increase in storey damping values, a substantial decrease trend in the obtained top storey displacement is visible. Then, with further increase in the storey damping, the top storey displacement reaches minimum values and remains nearly unchanged, as indicated by the obtained horizontal lines. In the case when storey damping is equal to zero, the obtained peak displacements of the building under the El Centro, Kocaeli, Kobe and Duzce earthquakes are equal to: 0.2464, 0.2404, 0.6068 and 0.5035 m, respectively. A significant reduction in peak displacements

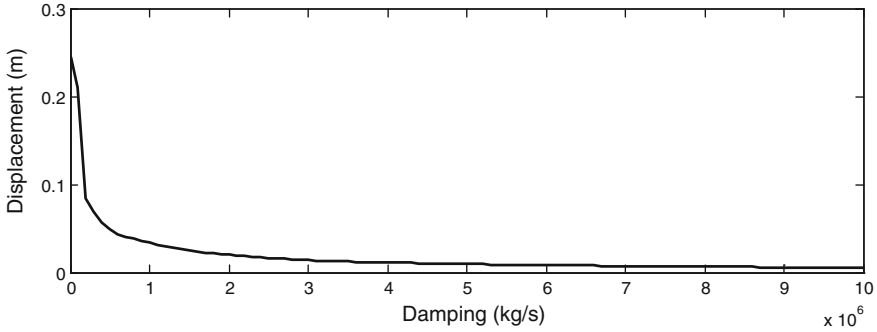

Fig. 5.30 Peak displacement of the third storey of building with respect to storey damping under the El Centro earthquake

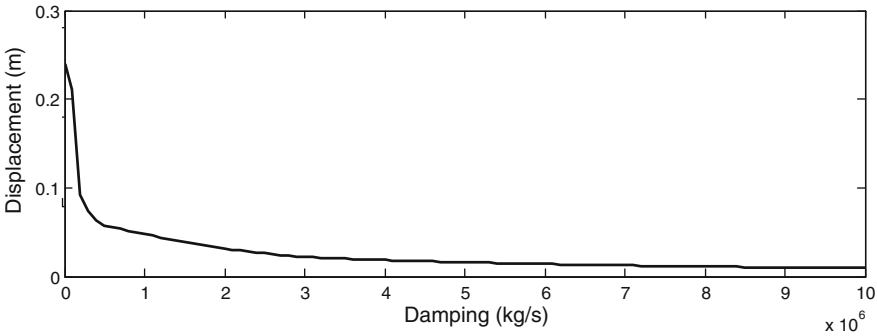

Fig. 5.31 Peak displacement of the third storey of building with respect to storey damping under the Kocaeli earthquake

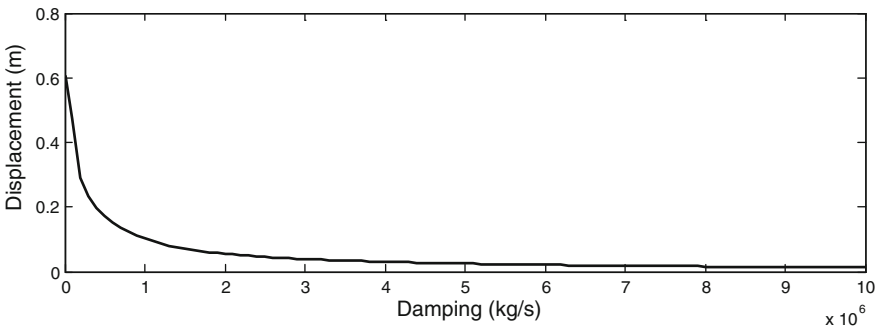

Fig. 5.32 Peak displacement of the third storey of building with respect to storey damping under the Kobe earthquake

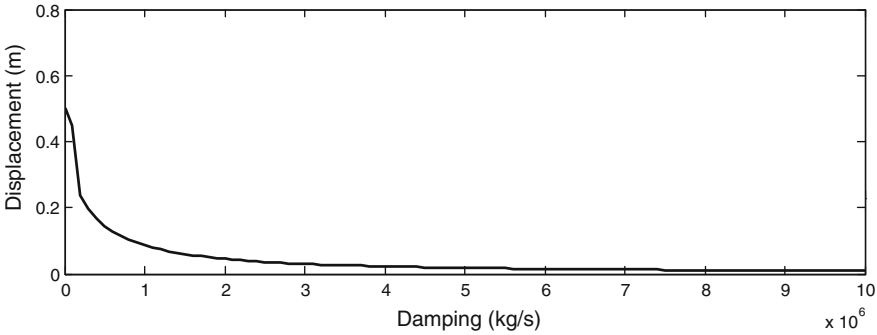

Fig. 5.33 Peak displacement of the third storey of building with respect to storey damping under the Duzce earthquake

by 96, 94, 98 and 99 % has been observed after comparing the above values with the displacements for the large values of storey damping. This fact confirms that enhancing internal damping of the flexible building can be used efficiently to reduce the storey deformations and consequently to prevent from structural pounding, similarly as in the case of increased storey stiffness. It should be underlined, however, that increasing damping to high levels can be in practice very expensive and difficult from the technological point of view.

References

Raheem, A.S.E.: Pounding mitigation and unseating prevention at expansion joint of isolated multi-span bridges. Eng. Struct. **31**, 2345–2356 (2009)

Raheem, A.S.E.: Mitigation measures for earthquake induced pounding effects on seismic performance of adjacent buildings. Bull. Earthq. Eng. **12**, 1705–1724 (2014)

Abdullah, M.M., Hanif, J.H., Richardson, A., Sobanjo, J.: Use of a shared tuned mass damper (STMD) to reduce vibration and pounding in adjacent structures. Earthq. Eng. Struct. Dynam. **30**, 1185–1201 (2001)

Anagnostopoulos, S.A.: Pounding of buildings in series during earthquakes. Earthq Eng. Struct. Dynam. **16**, 443–456 (1988)

Anagnostopoulos, S.A., Spiliopoulos, K.V.: An investigation of earthquake induced pounding between adjacent buildings. Earthq. Eng. Struct. Dynam. **21**, 289–302 (1992)

Anagnostopoulos, S.A.: Building pounding re-examined: how serious a problem is it? Eleventh world conference on earthquake engineering, Acapulco, Mexico, 23–28 June 1996, paper no. 210

Anagnostopoulos, S.A., Karamaneas, C.E.: Use of collision shear walls to minimize seismic separation and to protect adjacent buildings from collapse due to earthquake-induced pounding. Earthq. Eng. Struct. Dyn. **37**, 1371–1388 (2008)

Cimellaro, G.P., Lopez-Garcia, D.: Algorithm for design of controlled motion of adjacent structures. Struct. Control and Health Monit. **18**, 140–148 (2011)

DesRoches, R., Muthukumar, S.: Effect of pounding and restrainers on seismic response of multiple-frame bridges. J. Struct. Eng. **128**, 860–869 (2002)

Divyashree, M., Bhavyashree, B.N., Siddappa, G.: Comparison of bracing and shear walls as seismic strengthening methods to buildings with plan irregularities. Inter. J. Res. Eng. Technol. **3**, 205–210 (2014)

ECS: Eurocode 8: Design Provisions for Earthquake Resistance of Structures. European Committee for Standardization, Brussels (1998)

Falborski, T., Jankowski, R.: Polymeric bearings—a new base isolation system to reduce structural damage during earthquakes. Key Eng. Mater. **569–570**, 143–150 (2013)

Filiatrault, A., Cervantes, M., Folz, B., Prion, H.: Pounding of buildings during earthquakes: a Canadian perspective. Can. J. Civ. Eng. **21**, 251–265 (1994)

Hameed, A., Saleem, M., Qazi, A.U., Saeed, S., Bashir, M.A.: Mitigation of seismic pounding between adjacent buildings. Pak. J. Sci. **64**, 326–333 (2012)

Hao, H., Shen, J.: Estimation of relative displacement of two adjacent asymmetric structures. Earthq. Eng. Struct. Dyn. **30**, 81–96 (2001)

Hrovat, D., Barak, P., Rabins, M.: Semi-active versus passive or active tuned mass damper for structural control. J. Eng. Mech. ASCE **109**, 691–705 (1983)

IBC: International Building Code. International Code Council Inc., USA (2009)

IS: Indian Standard, Criteria for Earthquake Resistant Design of Structures. IS 1893–2002. Bureau of Indian standards, India (2002)

Jankowski, R.: Nonlinear rate dependent model of high damping rubber bearing. Bull. Earthq. Eng. **1**, 397–403 (2003)

Jankowski, R.: Impact force spectrum for damage assessment of earthquake-induced structural pounding. Key Eng. Mater. **293–294**, 711–718 (2005)

Jankowski, R.: Assessment of damage due to earthquake-induced pounding between the main building and the stairway tower. Key Eng. Mater. **347**, 339–344 (2007)

Jankowski, R.: Non-linear FEM analysis of pounding-involved response of buildings under non-uniform earthquake excitation. Eng. Struct. **37**, 99–105 (2012)

Jankowski, R., Wilde, K., Fujino, Y.: Pounding of superstructure segments in isolated elevated bridge during earthquakes. Earthq. Eng. Struct. Dyn. **27**, 487–502 (1998)

Jankowski, R., Wilde, K., Fujino, Y.: Reduction of pounding effects in elevated bridges during earthquakes. Earthq. Eng. Struct. Dyn. **29**, 195–212 (2000)

Jeng, V., Kasai, K., Maison, B.F.: A spectral difference method to estimate building separations to avoid pounding. Earthq. Spectra **8**, 201–223 (1992)

Jeng, V., Tzeng, W.L.: Assessment of seismic pounding hazard for Taipei City. Eng. Struct. **22**, 459–471 (2000)

Kajita, Y., Kitahara, T., Nishimoto, Y., Otsuka, H.: Estimation of maximum impact force on natural rubber during collision of two steel bars. First European conference on earthquake engineering and seismology. Geneva, Switzerland, 3–8 September 2006, paper no. 488

Kajita, Y., Nishimoto, Y., Ishikawa, N., Watanabe, E.: Energy absorption capacity of the laminated fiber reinforced rubber installed at girder ends. International Conference on High Performance Materials in Bridges. Kona, Hawaii, USA, 29 July–3 August 2001, pp 183–192

Kasai, K., Jeng, V., Patel, P.C., Munshi, J.A., Maison, B.F: Seismic pounding effects—survey and analysis. Proceedings of the 10th World Conference on Earthquake Engineering, Vol. VII, pp. 3893–3898. Madrid, Spain, 19–24 July 1992

Kasai, K., Jagiasi, A.R.: Viscoelastic dampers for seismic pounding mitigation. Proceedings of the Structural Congress ASCE, Irvine, CC, pp. 199–204, 1993

Kasai, K., Jagiasi, A.R., Jeng, V.: Inelastic vibration phase theory for seismic pounding mitigation. J. Struct. Eng. **122**, 1136–1146 (1996)

Kawashima, K., Shoji, G., Koshitoge, M., Shimanoe, S.: Design of an Earthquake-Resistant Expansion Joint with Unseating Prevention System. FIB Congress, Osaka, Japan (2002), E-282

Kawashima, K., Unjoh, S.: Seismic response control of bridges by variable dampers. J. Struct. Eng. **120**, 2583–2601 (1994)

Kelly, J.M.: Earthquake-Resistant Design with Rubber. Springer-Verlag, London, UK (1993)

Kobori, T., Yamada, T., Takenaka, Y., Maeda, Y., Nishimura, I.: Effect of dynamic tuned connector on reduction of seismic response—application to adjacent office buildings.

Proceedings of Ninth World Conference on Earthquake Engineering, Vol. V, pp. 773–778. Tokyo–Kyoto, Japan, 2–9 August 1988

Komodromos, P.: Seismic Isolation of Earthquake-Resistant Structures. WIT Press, Southampton, UK (2000)

Komodromos, P.: Simulation of the earthquake-induced pounding of seismically isolated buildings. Comput. Struct. **86**, 618–626 (2008)

Lin, J.-H.: Separation distance to avoid seismic pounding of adjacent buildings. Earthquake Eng. Struct. Dynam. **26**, 395–403 (1997)

Lin, J.-H., Weng, C.-C.: Probability analysis of seismic pounding of adjacent buildings. Earthq. Eng. Struct. Dyn. **30**, 1539–1557 (2001a)

Lin, J.-H., Weng, C.-C.: Spectral analysis on pounding probability of adjacent buildings. Eng. Struct. **23**, 768–778 (2001b)

Lopez-Garcia L.: Separation between adjacent nonlinear structures for prevention of seismic pounding. 13th World Conference on Earthquake Engineering. Vancouver, Canada, 1–6 August 2004, paper no. 478

Loring A., Wyllie J.R.: Strengthening strategies for improved seismic performance. Eleventh World Conference on Earthquake Engineering. Acapulco, Mexico, 23–28 June 1996, paper no. 1424

Luco, J.E., De Barros, F.C.P.: Optimal damping between two adjacent elastic structures. Earthq. Eng. Struct. Dyn. **27**, 649–659 (1998)

Mahmoud, S., Abd-Elhamed, A., Jankowski, R.: Earthquake-induced pounding between equal height multi-storey buildings considering soil-structure interaction. Bull. Earthq. Eng. **11**(4), 1021–1048 (2013)

Mahmoud, S., Austrell, P.-E., Jankowski, R.: Simulation of the response of base-isolated buildings under earthquake excitations considering soil flexibility. Earthq. Eng. Eng. Vibr. **11**, 359–374 (2012)

Mahmoud, S., Gutub, S.: Earthquake induced pounding-involved response of base-isolated buildings incorporating soil flexibility. Adv. Struct. Eng. **16**(12), 71–90 (2013)

Mahmoud, S., Jankowski, R.: Elastic and inelastic multi-storey buildings under earthquake excitation with the effect of pounding. J. Appl. Sci. **9**, 3250–3262 (2009)

Mahmoud, S., Jankowski, R.: Pounding-involved response of isolated and non-isolated buildings under earthquake excitation. Earthq. Struct. **1**, 231–252 (2010)

Mahmoud, S., Jankowski, R.: Modified linear viscoelastic model of earthquake-induced structural pounding. Iran. J. Sci. Technol. **35**(C1), 51–62 (2011)

Maison, B.F., Kasai, K.: Analysis for the type of structural pounding. J. Struct. Eng. ASCE **116**, 957–977 (1990)

Maison, B.F., Ventura, C.E.: Seismic analysis of base-isolated San Bernardino County building. Earthq. Spectra **8**, 605–633 (1992)

Malhotra, A., Carson, D., Gopal, P., Braimah, A., Di Giovanni, G., Pall, R.: Friction dampers for upgrade of St. Vincent hospital, Ottawa. 13th World Conference on Earthquake Engineering, Vancouver, Canada, 1–6 August 2004, paper no. 1952

Malhotra, P.K.: Dynamics of seismic impacts in base-isolated buildings. Earthq. Eng. Struct. Dyn. **26**, 797–813 (1997)

Mitoulis S.A., Tegos I.A., Malekakis A.: Experimental research on the capacity of bridge shear keys. COMPDYN 2013, 4th ECCOMAS Thematic Conference on Computational Methods in Structural Dynamics and Earthquake Engineering. Kos Island, Greece, 12–14 June 2013, pp. 1123–1132

Naeim, F., Kelly, J.M.: Design of Seismic Isolated Structures: From Theory to Practice. Wiley, New York, USA (1999)

Newmark, N.: A method of computation for structural dynamics. J. Eng. Mech. Div. ASCE **85**, 67–94 (1959)

NBC: National Building Code, Technical Standard of Building E.030, Earthquake Resistant Design. Ministry of Housing, Peru (2003)

Ni, Y.Q., Ko, J.M., Ying, Z.G.: Random seismic response analysis of adjacent buildings coupled with non-linear hysteretic dampers. J. Sound Vibr. 246, 403–417 (2001)
Pantelides, C.P., Ma, X.: Linear and nonlinear pounding of structural systems. Comput. Struct. **66**, 79–92 (1998)
Patel, C.C., Jangid, R.S.: Seismic response of dynamically similar adjacent structures connected with viscous dampers. The IES J. Part A: Civ. Struct. Eng. **3**, 1–13 (2010)
Penzien, J.: Evaluation of building separation distance required to prevent pounding during strong earthquakes. Earthq. Eng. Struct. Dyn. **26**, 849–858 (1997)
Polycarpou, P.C., Komodromos, P.: Earthquake-induced poundings of a seismically isolated building with adjacent structures. Eng. Struct. **32**, 1937–1951 (2010a)
Polycarpou, P.C., Komodromos, P.: On poundings of a seismically isolated building with adjacent structures during strong earthquakes. Earthq. Eng. Struct. Dyn. **39**, 933–940 (2010b)
Polycarpou, P.C., Komodromos, P.: Numerical investigation of potential mitigation measures for poundings of seismically isolated buildings. Earthqu. Struct. **2**, 1–24 (2011)
Polycarpou, P.C., Komodromos, P., Polycarpou, A.C.: A nonlinear impact model for simulating the use of rubber shock absorbers for mitigating the effects of structural pounding during earthquakes. Earthqu. Eng. Struct. Dyn. **42**, 81–100 (2013)
Rajaram, C.R., Kumar, P.: Comparison of codal provisions on pounding between adjacent buildings. Int. J. Earth Sci. Eng. **5**, 71–79 (2012)
Ruangrassamee, A., Kawashima, K.: Control of nonlinear bridge response with pounding effect by variable dampers. Eng. Struct. **25**, 593–606 (2003)
Salomón, O., Oller, S., Barbat, A.: Finite element analysis of base isolated buildings subjected to earthquake loads. Int. J. Numer. Meth. Eng. **46**, 1741–1761 (1999)
Shigeki, U.: Repair and retrofit of bridges damaged by the 2010 Chile Maule earthquake. Proceedings of the International Symposium on Engineering Lessons Learned from the 2011 Great East Japan Earthquake. Tokyo, Japan, 1–4 March 2012, Part 2
Shim, V.P.W., Yang, L.M., Lim, C.T., Law, P.H.: A visco-hyperelastic constitutive model to characterize both tensile and compressive behavior of rubber. J. Appl. Polym. Sci. 92, 523–531 (2004)
Sołtysik, B., Jankowski, R.: Non-linear strain rate analysis of earthquake-induced pounding between steel buildings. Int. J. Earth Sci. Eng. **6**, 429–433 (2013)
Soong, T.T., Constantinou, M.C.: Passive and Active Structural Vibration Control in Civil Engineering. Springer, Berlin (1994)
Soong, T.T., Dargush, G.F.: Passive Energy Dissipation Systems in Structural Engineering. Wiley, New York (1997)
Spiliopoulos, K.V., Anagnostopoulos, S.A.: Measures against earthquake pounding between adjacent buildings. Eleventh World Conference on Earthquake Engineering, Acapulco, Mexico, 23–28 June 1996, paper no. 728
Valles, R.E., Reinhorn, A.M.: Evaluation, prevention and mitigation of pounding effects in building structures. Technical Report NCEER–97–0001. National Center for Earthquake Engineering Research, State University of New York at Buffalo, Buffalo, USA (1997)
Wasti, S.T., Ozcebe, G.: Seismic Assessment and Rehabilitation of Existing Buildings. Kluwer Academic Publishers, Dordrecht, Netherlands (2003)
Westermo, B.D.: The dynamics of interstructural connection to prevent pounding. Earthq. Eng. Struct. Dyn. **18**, 687–699 (1989)
Xu, Y.L., He, Q., Ko, J.M.: Dynamic response of damper-connected adjacent buildings under earthquake excitation. Eng. Struct. **21**, 135–148 (1999)
Yang, Z., Xu, Y.L., Lu, X.L.: Experimental seismic study of adjacent buildings with fluid dampers. J. Struct.Eng. ASCE **129**, 197–205 (2003)
Zhang, W.S., Xu, Y.L.: Dynamic characteristics and seismic response of adjacent buildings linked by discrete dampers. Earthqu. Eng. Struct. Dyn. **28**, 1163–1185 (1999)

Zhang, W.S., Xu, Y.L.: Vibration analysis of two buildings linked by Maxwell model-defined fluid dampers. J. Sound Vibr. 233, 775–796 (2000)
Zhu, H., Iemura, H.: A study of response control on the passive coupling element between two parallel structures. Struct. Eng. Mech. 9, 383–396 (2000)
Zhu, H.P., Xu, Y.L.: Optimum parameters of Maxwell model-defined dampers used to link adjacent structures. J. Sound Vibr. 279, 253–274 (2005)

Chapter 6
Design of Structures Prone to Pounding

At the design stage of adjacent buildings or bridge structures, the probability of occurrence of earthquake-induced structural pounding should be carefully analyzed. The minimum separation gap, so as to avoid collisions, is specified in the recent earthquake-resistant design codes (see, for example, ECS 1998, IS 2002; NBC 2003; IBC 2009). On the other hand, in the case when pounding can not be prevented, the assessment of the peak pounding force value expected during the time of the earthquake is important for the design purposes. Such an assessment can be conducted by the use of pounding force response spectrum (Jankowski 2005, 2006). Moreover, the potential structural damage of colliding structures under the design ground motion can be determined with the help of damage indices (Park and Ang 1985; Powell and Allahabadi 1988; Fajfar 1992; Cosenza et al. 1993; Bojórquez et al. 2010; Moustafa 2011).

6.1 Procedures in the Building Codes Related to the Minimum Seismic Gap

A number of building codes for seismic design around the world do not refer to earthquake-induced structural pounding phenomenon and do not include any comments how to prevent adjacent structures from impacts. Only the recent earthquake-resistant design codes, as well as a number of less formal regulatory guides, specify the minimum seismic gap for newly constructed buildings (Rajaram and Kumar 2012). The way to determine the minimum separation distance required to prevent seismic pounding between adjacent structures varies from regulation to regulation. The Canadian code considers the simplest approach in which the absolute sum of the peak displacements of two buildings should be calculated (see Eq. (5.1). The edition of 1997 of the Uniform Building Code (UBC 1997) and the edition of 2003 of the International Building Code (IBC 2003) suggest the formula of the square root of sum of squares (SRSS), as defined in Eq. (5.2). The quadratic combination of the maximum peak displacements has also been employed in

R. Jankowski and S. Mahmoud, *Earthquake-Induced Structural Pounding*,
GeoPlanet: Earth and Planetary Sciences, DOI 10.1007/978-3-319-16324-6_6

Eurocode 8 (ECS 1998). The edition of International Building Code published in 2009 modifies the requirement for determination the seismic gap distance, $d_{\min}$, suggesting that it should be rather calculated based on the following equation (IBC 2009):

$$d_{\min} = \frac{C_D \delta_{\max}}{I} \tag{6.1}$$

where C_D is the deflection amplification factor, which depends on the seismic force-resisting system, $\delta_{\max}$ represents the peak displacement calculated from the elastic analysis and I is the importance factor determined in accordance with the seismic use group. The same formula as given in Eq. (6.1) is also suggested to calculate the minimum separation gap in the guidelines of American Society of Civil Engineers (ASCE 2010).

A number of codes specify the minimum seismic gap using some ways which are independent from the dynamic characteristics of structures. The edition of Taiwan code is a good example of such a situation since the required minimum gap to avoid pounding is suggested to be calculated as a function of the height of the buildings without any computations of the peak displacements (Valles and Reinhorn 1997). Similarly to the Taiwan code, the Federal Emergency Management Agency suggests the determination of the minimum seismic gap as a percentage of the height of buildings in order to prevent their pounding during earthquakes (FEMA 1997).

Some of the regulations suggest to calculate the minimum seismic gap based simultaneously on peak structural displacements and height of structures. The Indian code for seismic design recalls the simple sum of peak displacements of adjacent buildings to be the base for calculating the minimum seismic separation gap together with a response reduction factor (IS 2002). The regulations from the Peru code for seismic design use values of the peak displacements of two adjacent buildings $\left(x^L_{\max}, x^R_{\max}\right)$ as well as the heights of structures as guides. In computing the minimum seismic gap, $d_{\min}$, the following formula is used (NBC 2003):

$$d_{\min} = \frac{2}{3}\left(x^L_{\max} + x^R_{\max}\right) \tag{6.2}$$

However, the calculated value from Eq. (6.2) can not be lower than (NBC 2003):

$$d_{\min} = 3 + 0.004(h - 500) \tag{6.3}$$

where h is the height of the lower building (in cm).

It is worth noting that all the above rules and formulae to calculate the minimum seismic gap in order to avoid earthquake-induced structural pounding can be related to four different forms of expressions (Valles and Reinhorn 1997):

$$d_{\min} \geq factor\left(sum(x^L_{\max},\ x^R_{\max})\right) \tag{6.4}$$

$$d_{\min} \geq factor(h^L,\ h^R) \tag{6.5}$$

$$d_{\min} \geq fixed\ distance \tag{6.6}$$

$$d_{\min} \geq SRSS(x^L_{\max},\ x^R_{\max}) \tag{6.7}$$

6.2 Pounding Force Response Spectrum

In the case when earthquake-induced structural pounding can not be prevented, the design of neighbouring structures should include the appearance of additional forces due to collisions. The assessment of the peak pounding force value expected during the time of ground motion can be conducted with the use of pounding force response spectrum (see also Jankowski 2005, 2006). The spectrum may serve as a very useful tool for the design purposes of closely-spaced structures in seismic areas.

The displacement, velocity and acceleration response spectra are well known practical means of characterising earthquakes and their effects on structures. They allow an engineer to apply the knowledge of structural dynamics to the earthquake-resistant design in order to prevent or reduce structural damage. The response spectrum for a particular quantity is defined as a plot of the peak value of response quantity as a function of the natural vibration period of the system, or a related parameter such as frequency (Chopra 1995). The plot shows the peak response of the structure, modelled as an elastic single-degree-of-freedom (SDOF) system, for a specified value of structural damping. Among response spectra for different quantities, the displacement and acceleration response spectra are the most often used (ECS 1998). In order to predict the maximum relative displacement between two neighbouring structures with different natural periods, the relative displacement response spectrum was considered (Kawashima and Sato 1996). Ruangrassamee and Kawashima (2001) proposed also the concept of relative displacement response spectrum with pounding effect. In this section, the idea of pounding force spectrum for earthquake-induced structural pounding between two closely-spaced structures, modelled as SDOF systems (see Fig. 2.13), is considered.

6.2.1 Response Spectrum for One Existing and One New Structure

Let us first consider the situation when a new building is supposed to be constructed close to the existing one which has different dynamic characteristics. Assuming that the new structure is a right one and the existing building with known properties is a

left one, the pounding force response spectrum can be defined as a plot of the peak pounding force, $F_{\max}$, obtained for different values of T_2 under fixed values of ξ_{S2}, m_2 and d (Jankowski 2005):

$$F_{\max}(T_2, \xi_{S2}, m_2, d) = \max|F(t, T_2, \xi_{S2}, m_2, d)| \tag{6.8}$$

where T_2, ξ_{S2} and m_2 are the natural period, structural damping ratio and mass of the new (right) structure, respectively; d denotes the initial separation gap and t stands for time of the earthquake.

The elastic dynamic equation of motion for pounding-involved response of two structures modelled as SDOF systems (see Fig. 2.13) has been given in Eq. (2.22). The numerical study has been conducted in order to determine the pounding force response spectra for different values of damping ratio, ξ_2, and mass, m_2, of the new (right) structure as well as for various in-between gap sizes. When the effect of one parameter has been investigated, other parameters have remained unchanged. In the analysis, the following basic values describing the properties of the old (left) structure have been used: $m_1 = 10^6$ kg, $T_1 = 0.6$ s, $\xi_{S1} = 5\,\%$. The following values of the non-linear viscoelastic pounding force model's parameters have been applied in numerical simulations: $\bar{\beta} = 2.75 \times 10^9$ N/m$^{3/2}$, $\bar{\xi} = 0.35$ $(e = 0.65)$. The analysis has been conducted for different ground motion records. The examples of pounding force response spectra for the NS components of the El Centro earthquake are shown in Figs. 6.1 and 6.2. In particular, the pounding force response spectra for the gap size of 0.05 m for different values of mass and structural damping of the new structure are presented in Fig. 6.1, whereas Fig. 6.2 shows the pounding force response spectra for mass $m_2 = 10^6$ kg for different values of gap size and structural damping of the new structure.

The results of the study (see Figs. 6.1 and 6.2) show a significant influence of structural damping on peak pounding force obtained during the earthquake. This is obviously due to the fact that increasing damping leads to the reduction in structural vibrations and therefore reduction in the prior-impact velocities, which finally results in the lower values of pounding force. Moreover, it can be seen from Fig. 6.1 that the increase in the mass value of the new building results in substantial increase in the peak pounding force. On the other hand, the results presented in Fig. 6.2 indicate that the increase in the separation gap allows us to prevent collisions for a wider range of the natural vibration periods of the new structure. It is worth noting, however, that for the cases when impacts can not be prevented, the peak pounding forces are not substantially reduced as the gap size value increases.

6.2.2 Response Spectrum for Two New Structures

In this part of the chapter, let us consider the case of two new structures with different dynamic properties to be constructed one close to another (see some examples in Anagnostopoulos 1988; Chau et al. 2003; Karayannis and Favvata 2005;

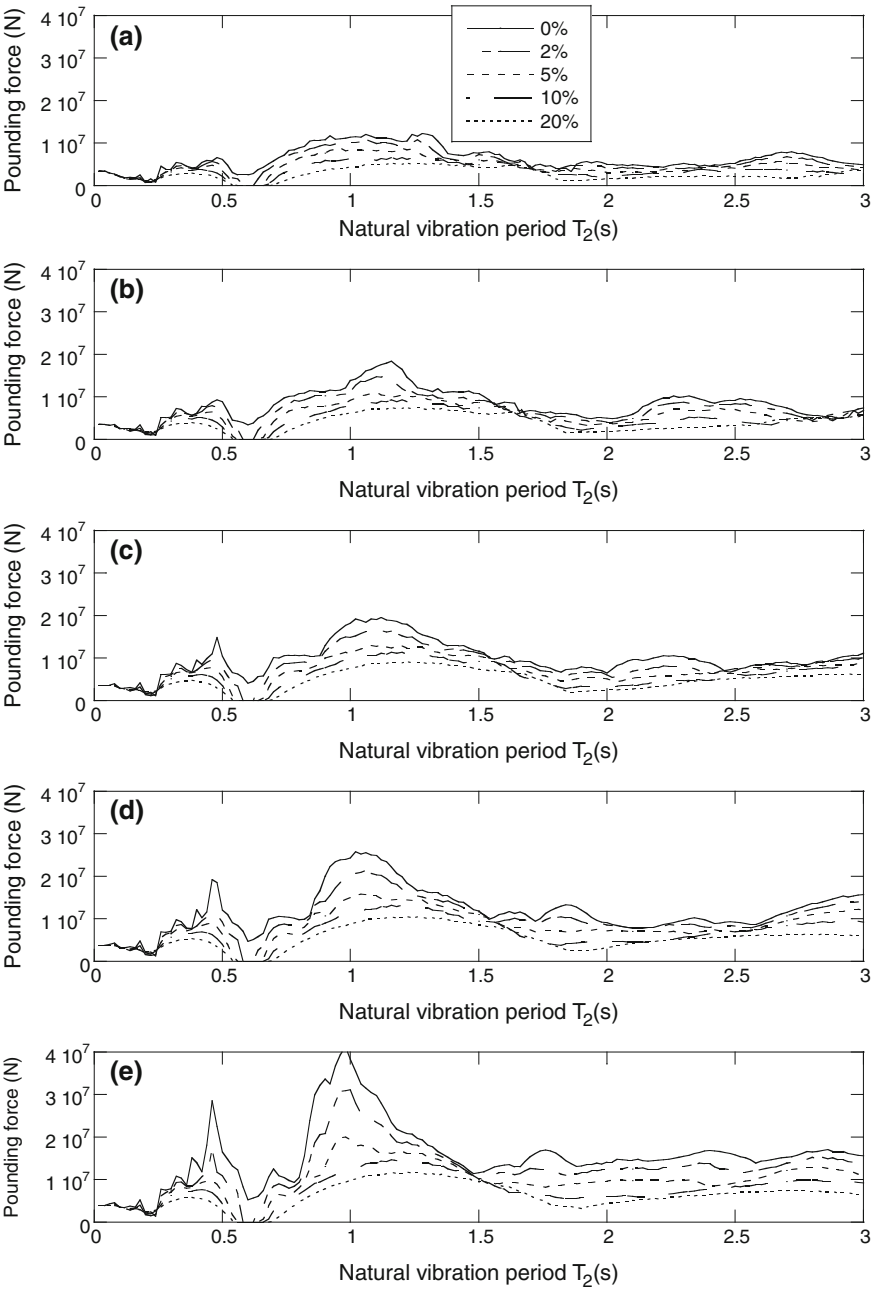

Fig. 6.1 Pounding force response spectra under the El Centro earthquake for different values of mass and structural damping ratio of the new structure (Jankowski 2005). **a** 200,000 kg. **b** 500,000 kg. **c** 1,000,000 kg. **d** 2,000,000 kg. **e** 5,000,000 kg

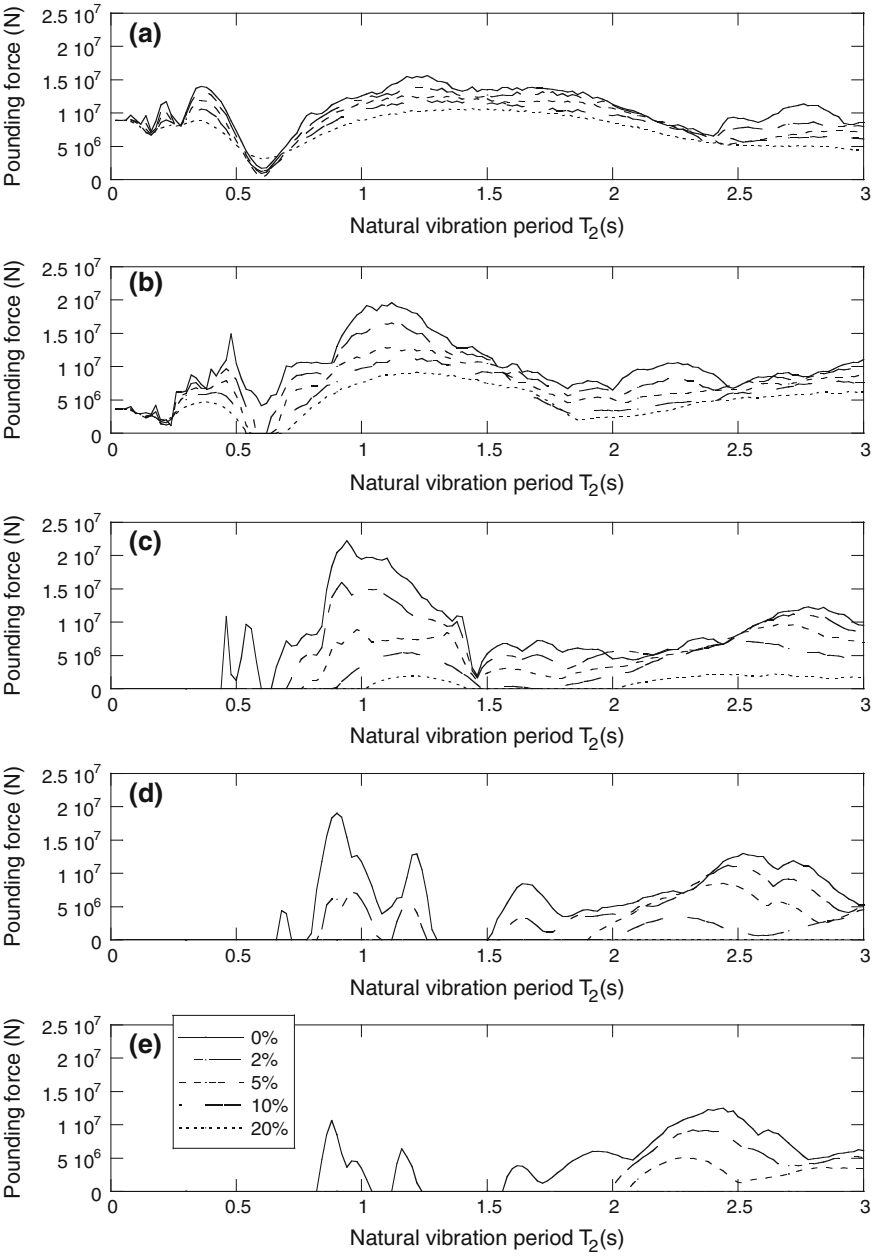

Fig. 6.2 Pounding force response spectra under the El Centro earthquake for different values of gap size and structural damping ratio of the new structure (Jankowski 2005). **a** 0 m. **b** 0.05 m. **c** 0.10 m. **d** 0.15 m. **e** 0.20 m

Jankowski 2007; Mahmoud and Jankowski 2009, 2011; Polycarpou and Komodromos 2010; Sołtysik and Jankowski 2013; Mahmoud et al. 2013). On the contrary to the response spectrum for one existing and one new building (Sect. 6.2.1), the pounding force response spectrum for two new structures will depend on properties of both of them. Moreover, in the case of long structures, such as buildings with spatially extended foundations, bridges or life-line systems, the incorporation of the spatial seismic effects, related to the propagation of seismic wave, might also be important (Der Kiureghian 1996; Zembaty 1997; Jankowski and Walukiewicz 1997; Jankowski and Wilde 2000; Dulińska 2011; Jankowski 2012). In this case, at least the influence of the wave passage effect, resulting in a time lag for the input earthquake records acting on two adjacent structures (or their parts), should be considered (see also Sect. 4.1). Then, the pounding force response spectrum can be defined as a plot of the peak pounding force, $F_{\max}$, obtained for different values of T_1 and T_2 under fixed values of ξ_{S1}, ξ_{S2}, d, m_1, m_2, τ (Jankowski 2006):

$$F_{\max}(T_1, T_2, \xi_{S1}, \xi_{S2}, d, m_1, m_2, \tau) = \max|F(t, T_1, T_2, \xi_{S1}, \xi_{S2}, d, m_1, m_2, \tau)| \quad (6.9)$$

where T_i, ξ_{Si} and m_i are the natural period, structural damping ratio and mass of structure i $(i = 1, 2)$, respectively; d denotes the initial separation gap, τ is a time lag for the input ground motion records and t stands for time of the earthquake. It should be mentioned that, since the pounding force response spectrum defined in Eq. (6.9) is a plot against two natural vibration periods T_1, T_2 simultaneously, the spectrum has to be presented as a 3-dimensional graph (see also Ruangrassamee and Kawashima 2001), as obtained for a pair of two structural damping ratios ξ_{S1}, ξ_{S2}.

The elastic dynamic equation of motion for pounding-involved response of two structures modelled as SDOF systems (see Fig. 2.13) incorporating a time lag for the input ground motion records can be written as [compare Eq. (2.22)]:

$$\begin{bmatrix} m_1 & 0 \\ 0 & m_2 \end{bmatrix} \begin{bmatrix} \ddot{x}_1(t) \\ \ddot{x}_2(t) \end{bmatrix} + \begin{bmatrix} C_1 & 0 \\ 0 & C_2 \end{bmatrix} \begin{bmatrix} \dot{x}_1(t) \\ \dot{x}_2(t) \end{bmatrix} + \begin{bmatrix} K_1 & 0 \\ 0 & K_2 \end{bmatrix} \begin{bmatrix} x_1(t) \\ x_2(t) \end{bmatrix} + \begin{bmatrix} F(t) \\ -F(t) \end{bmatrix} = -\begin{bmatrix} m_1 & 0 \\ 0 & m_2 \end{bmatrix} \begin{bmatrix} \ddot{x}_{g1}(t) \\ \ddot{x}_{g2}(t) \end{bmatrix} \quad (6.10)$$

where $x_i(t)$, $\dot{x}_i(t)$, $\ddot{x}_i(t)$ are the horizontal displacement, velocity and acceleration of structure i $(i = 1, 2)$, respectively, C_i, K_i denote damping and stiffness coefficients, $\ddot{x}_{gi}(t)$ stands for the acceleration of input ground motion for ith structure and $F(t)$ is the pounding force.

The numerical study has been conducted in order to determine the pounding force response spectra for different values of damping ratios, masses, time lag of the input earthquake records as well as for various in-between gap sizes. When the effect of one parameter has been studied, other parameters have remained unchanged. In the analysis, the following basic values of structural model's parameters have been applied: $m_1 = m_2 = 10^6$ kg, $\xi_{S1} = \xi_{S2} = 5\,\%$, $d = 0.05$ m, $\tau = 0$ s. The following values of the non-linear viscoelastic pounding force model's

parameters have been applied in numerical simulations: $\bar{\beta} = 2.75 \times 10^9$ N/m$^{3/2}$, $\bar{\xi} = 0.35$ ($e = 0.65$). The analysis has been conducted for different ground motion records. The examples of pounding force response spectra for the NS component of the El Centro earthquake are shown in Figs. 6.3, 6.4, 6.5 and 6.6.

Figure 6.3 shows the pounding force response spectra for different values of identical structural damping ratios of both structures. As it can be seen from the figure, the influence of structural damping on the peak pounding force is substantial, similarly as in the case of spectra for one existing and one new structure (Sect. 6.2.1). For example, by comparing Fig. 6.3a with Fig. 6.3b, we can see that the increase in damping ratio for both structures from 0 to 2 % results in the decrease in the peak pounding force by 22 % in average (see also Jankowski 2006).

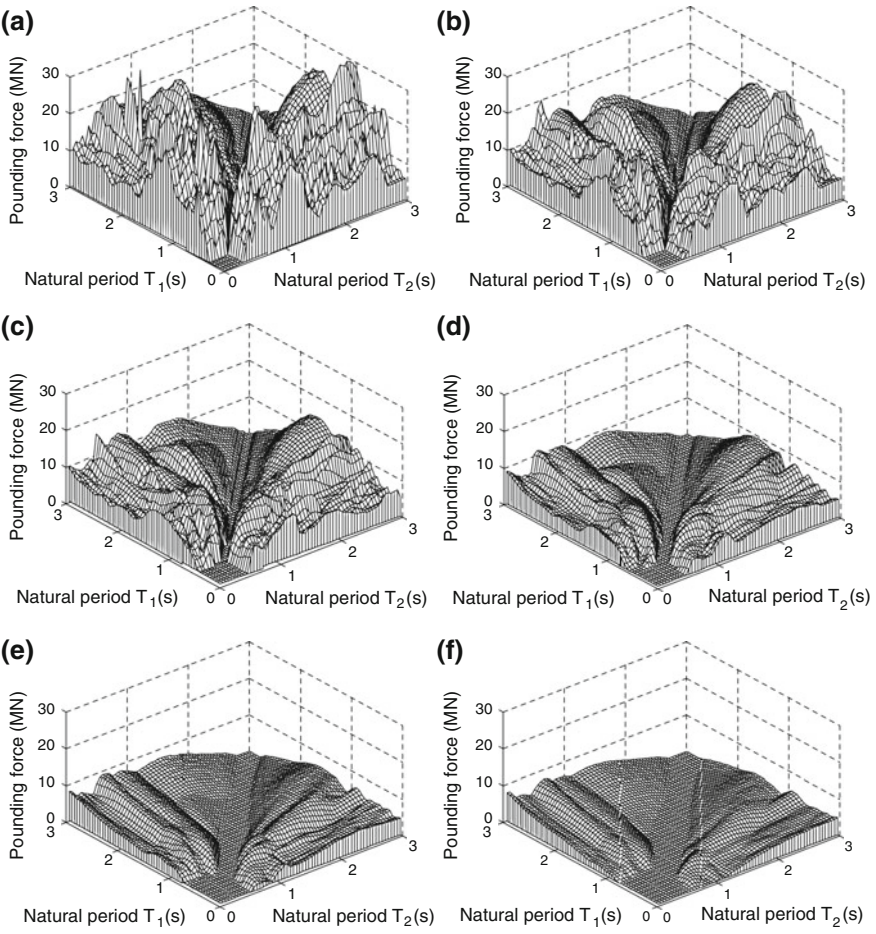

Fig. 6.3 Pounding force response spectra under the El Centro earthquake for different values of structural damping ratios of both structures (Jankowski 2006). **a** 0 %. **b** 2 %. **c** 5 %. **d** 10 %. **e** 15 %. **f** 20 %

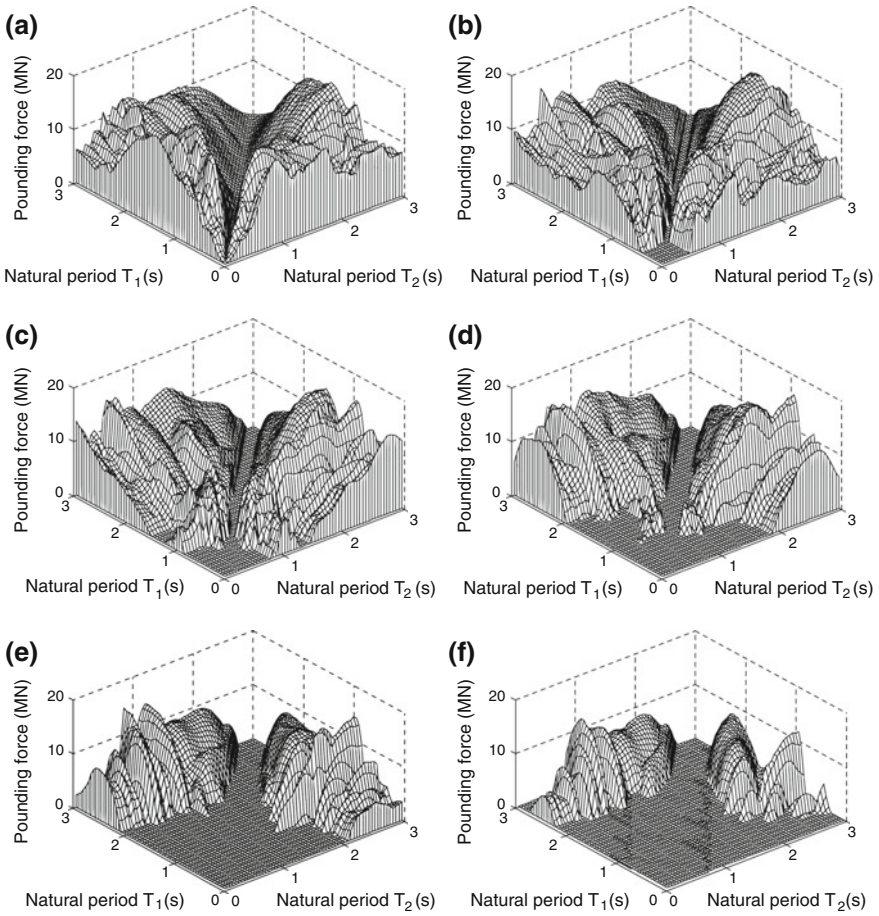

Fig. 6.4 Pounding force response spectra under the El Centro earthquake for different values of gap size between structures (Jankowski 2006). **a** 0 m. **b** 0.05 m. **c** 0.10 m. **d** 0.15 m. **e** 0.20 m. **f** 0.25 m

It can also be seen from Fig. 6.3 that the increase in structural damping results in extension of the region in the spectrum where the peak pounding force is equal to zero. This region is related to the cases when the natural vibration periods are very small for both structures (small displacements which do not lead to collisions) and when the natural periods are equal or nearly equal.

Pounding force response spectra for different values of gap size between structures are presented in Fig. 6.4. The spectra from the figure indicate that the increase in the separation gap allows us to prevent collisions for a wider range of the natural vibration periods of both structures. Actually, in the case of the El Centro earthquake, the gap size of 0.3 m is already sufficiently large to avoid impact for all structural periods analyzed. However, it should be underlined that for the

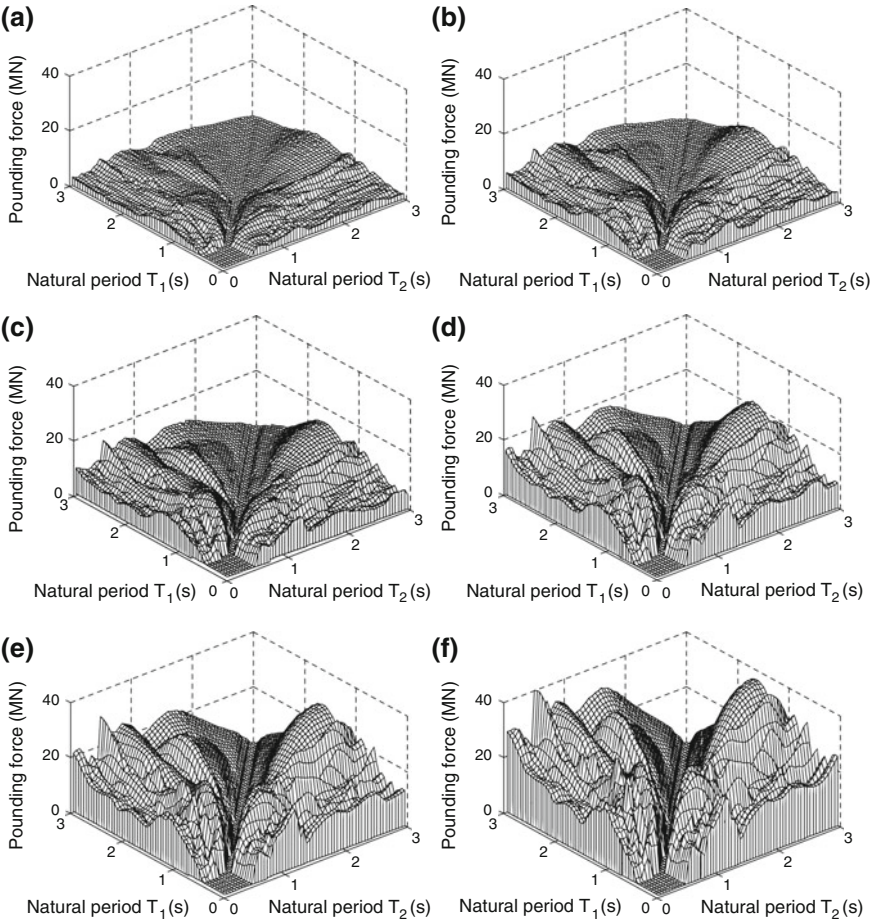

Fig. 6.5 Pounding force response spectra under the El Centro earthquake for different values of masses of both structures (Jankowski 2006). **a** 200,000 kg. **b** 500,000 kg. **c** 1,000,000 kg. **d** 2,000,000 kg. **e** 3,000,000 kg. **f** 5,000,000 kg

cases when pounding can not be prevented, the values of peak pounding force are nearly at the same level for different values of in-between gap size.

Figure 6.5 shows the pounding force response spectra for different values of identical masses of both structures. The figure confirms that the increase in the mass values leads to substantial increase in the peak pounding force. In the case of identical mass values of both structures, the shapes of the pounding force spectra are very similar with nearly linear, quite rapid increase in the peak pounding force values in the range of 200,000–5,000,000 kg (see also Jankowski 2006).

Pounding force response spectra for different values of time lag for the input earthquake records acting on two adjacent structures are shown in Fig. 6.6. The figure indicates that the time lag of at least 0.2 s leads to the disappearance of

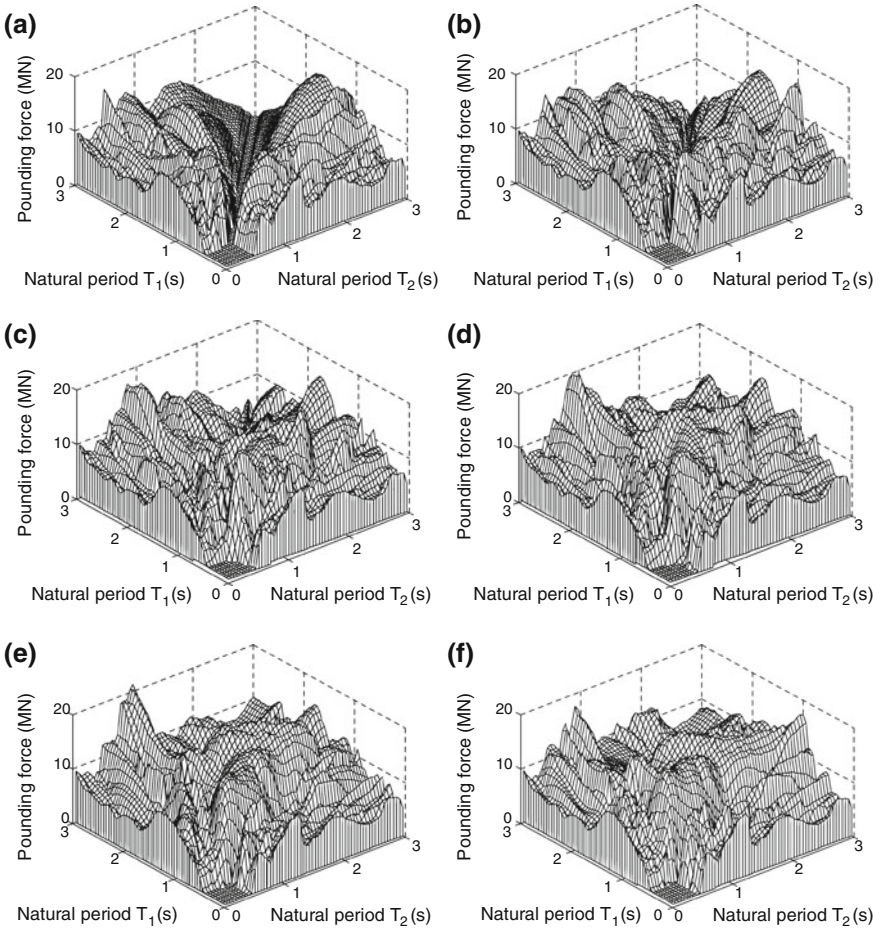

Fig. 6.6 Pounding force response spectra under the El Centro earthquake for different values of time lag for input ground motion records (Jankowski 2006). **a** 0 s. **b** 0.1 s. **c** 0.2 s. **d** 0.3 s. **e** 0.4 s. **f** 0.5 s

the region in the spectrum, in which the pounding force is equal to zero (observed for equal or nearly equal vibration periods of structures, see Figs. 6.3, 6.4 and 6.5). This behaviour results from the fact, that the seismic wave passage effect induces the out-of-phase vibrations even for structures with identical structural vibration periods. It can also be seen from Fig. 6.6 that the shapes of the pounding force response spectra do not change much for the time lag in the range of 0.2–0.5 s. Moreover, the region with zero pounding force observed in the case of very small natural vibration periods is nearly identical for all pounding force spectra apart from the value of time lag. This results from the fact, that the in-between gap size of 0.05 m is large enough to accommodate different, but very small vibrations of two analyzed structures.

6.3 Assessment of Structural Damage

In the design criteria, study against collapse is considered as the main objective. However, performance in terms of functionality and economy still plays important role. Great efforts are made to improve the methods of resistant design against dynamic loads due to earthquakes, not only to avoid failure during strong excitations but also to limit damage under moderate ground motions. The use of damage indices and damage measures for structures under dynamic loads are widely used and they can also be applied for the design purposes of colliding structures under seismic loads. They aim to clarify the different approach methodologies (Powell and Allahabadi 1988; Cosenza et al. 1993; Kappos 1997) and to detail different proposed formulations (McCabe and Hall 1989; Williams and Sexsmith 1995; Fardis 1995).

One of the key parameters used to identify structural damage is the kinematic and cyclic ductility, which can be defined as a function of rotation, curvature or displacement. The amount of kinematic energy dissipated during loading is another important aspect in structural damage.

One of the most often used damage index was proposed by Park and Ang (1985). It defines the structural damage in terms of the peak dynamic response (i.e. peak plastic displacement), as well as the hysteretic dissipated energy, and can be expressed as (see Park and Ang 1985; Park et al. 1985, 1987):

$$DI_{PA} = \frac{x_{\max}}{x_u} + \frac{\beta_{PA}}{F_Y x_u} \int dE \tag{6.11}$$

where $x_{\max}$ is the peak displacement, x_u stands for the ultimate displacement, F_Y is the yield strength, dE denotes the incremental absorbed hysteretic energy and β_{PA} is a nonnegative constant. The level of damage can be defined based on the values of captured damage indices. A building can be considered to have insignificant damage for the assigned damage index $DI_{PA} \leq 0.2$, while for $DI_{PA} \leq 0.4$ damage can be considered as repairable. For $0.4 < DI_{PA} < 1$ damage can not be repairable, although the structure does not collapse and the case when $DI_{PA} \geq 1.0$ denotes total damage of the structure (Park and Ang 1985; Park et al. 1987).

Powell and Allahabadi (1988) proposed a damage index in terms of the peak plastic displacement, independent from the amount of dissipated energy. The formula used to define the damage index, DI_{AP}, can be written as (Powell and Allahabadi 1988):

$$DI_{AP} = \frac{x_{\max} - x_y}{x_u - x_y} \tag{6.12}$$

where x_y is the yield displacement.

Damage indices based on the kinematic or cyclic ductility, as a measure for damage, assume that structural model collapse is mainly due to the induced peak plastic displacement neglecting the effect of a number of plastic cycles and the

energy dissipated under the applied dynamic load. However, it has been shown that these indices can be used for structures with cumulative deterioration, such as in the case of impulse-type or short-duration earthquakes which are characterized by one cycle with a large plastic displacement and other cycles with a small amount of plastic work.

A damage index based on the structure hysteretic energy was proposed by Fajfar (1992) and Cosenza et al. (1993) and can be expressed as:

$$DI_{FC} = \frac{E_H}{F_Y x_y (\mu_u - 1)} \tag{6.13}$$

where E_H and μ_u are the dissipated hysteretic energy and ultimate ductility factor, respectively.

Another measure of structural performance is given as the dissipated hysteretic energy normalized to the input energy of the structure. This index is defined as (Bojórquez et al. 2010; Moustafa 2011):

$$DI_H = \frac{E_H}{E_I} \tag{6.14}$$

where E_I denotes the earthquake input energy, considering the fact that the ground starts shaking until it comes to rest. Note that the damage index of Eq. (6.14) includes the structure's response demanded by the ground motion and the associated structural capacity parameters in an implicit form. Note also that DI_H close to zero implies a linear behaviour, while DI_H larger than zero indicates inelastic behaviour and occurrence of structural damage.

All the aforementioned damage indices are considered in the two successive sections concerning the numerical simulations of earthquake-induced response and damage assessment of two colliding buildings with fixed bases (non-isolated structures) and with isolated bases (base-isolated structures).

6.3.1 Damage Indices in Non-isolated Buildings

For the purposes of the analysis focused on non-isolated buildings, let us use the simplified SDOF structural model shown in Fig. 2.13. The dynamic equation of motion for such a model, considering inelastic (elastic-perfectly plastic) behaviour of both buildings, can be written as [compare Eqs. (2.22) and (3.1)]:

$$\mathbf{M}\,\ddot{\mathbf{x}}(t) + \mathbf{C}\dot{\mathbf{x}}(t) + \mathbf{F}_S(t) + \mathbf{F}(t) = -\mathbf{M}\mathbf{1}\,\ddot{x}_g(t) \tag{6.15a}$$

$$\mathbf{M} = \begin{bmatrix} m_1 & 0 \\ 0 & m_2 \end{bmatrix}; \quad \mathbf{C} = \begin{bmatrix} C_1 & 0 \\ 0 & C_2 \end{bmatrix}; \quad \ddot{\mathbf{x}}(t) = \begin{bmatrix} \ddot{x}_1(t) \\ \ddot{x}_2(t) \end{bmatrix}; \quad \dot{\mathbf{x}}(t) = \begin{bmatrix} \dot{x}_1(t) \\ \dot{x}_2(t) \end{bmatrix} \tag{6.15b}$$

$$\mathbf{F}_S(t) = \begin{bmatrix} F_{S1}(t) \\ F_{S2}(t) \end{bmatrix}; \quad \mathbf{F}(t) = \begin{bmatrix} F(t) \\ -F(t) \end{bmatrix}; \quad \mathbf{1} = \begin{bmatrix} 1 \\ 1 \end{bmatrix} \tag{6.15c}$$

where $x_i(t)$, $\dot{x}_i(t)$, $\ddot{x}_i(t)$ are the horizontal displacement, velocity and acceleration of building i ($i = 1, 2$), respectively, $F_{Si}(t)$ is the inelastic shear force equal to $F_{Si}(t) = K_i x_i(t)$ for the elastic range till the yield strength F_{Yi} is reached and $F_{Si}(t) = \pm F_{Yi}$ for the plastic range, K_i, C_i denote elastic structural stiffness and damping coefficients, $\ddot{x}_g(t)$ stands for the acceleration of input ground motion and $F(t)$ is the pounding force, which is equal to zero when $\delta(t) \leq 0$ and is defined by Eq. (2.16) if $\delta(t) > 0$, where deformation $\delta(t)$ is defined by Eq. (2.23).

As the example, two buildings with the basic dynamic parameters described in Sect. 3.1 have been used in the analysis. Furthermore, the yield strength for the left and the right inelastic buildings have been taken as $F_{Y1} = 1.369 \times 10^5$ N and $F_{Y2} = 1.442 \times 10^7$ N, respectively. The initial separation gap between buildings has been set to $d = 0.05$ m and has been changed later to study its effect on damage of adjacent buildings. The following values of the non-linear viscoelastic pounding force model's parameters have been applied in the analysis: $\bar{\beta} = 2.75 \times 10^9$ N/m$^{3/2}$, $\bar{\xi} = 0.35$ ($e = 0.65$). The time-stepping Newmark method (Newmark 1959) with constant time step $\Delta t = 0.002$ s has been used in order to solve the equation of motion (6.15a–c) numerically. A set of 9 earthquake ground motion records listed in Table 5.1 have been used as input excitations. In the numerical analysis, all acceleration records have been scaled to have the peak ground acceleration of 0.5 g (g stands for the acceleration of gravity) to ensure inelastic response of structures. The parameters of the damage indices have been taken as: $\mu_{u1} = \mu_{u2} = 0.6$ and $\beta_{PA} = 0.15$.

The examples of numerical results, in the form of different damage indices time histories for colliding non-isolated buildings under the El Centro earthquake, are shown in Figs. 6.7, 6.8, 6.9 and 6.10. Additionally, the values of peak damage indices for the left and the right structure under all analyzed ground motion records are summarized in Tables 6.1 and 6.2, respectively (see also Moustafa and Mahmoud 2014). The results of the study indicate that the El Centro, Loma Prieta, Duzce and Kobe earthquakes are among the ground motions which produce the largest damage indices. This could be attributed to the characteristics of these records since they have rich frequency contents, high energy and small source-site distance (near-fault records). In fact, according to the values of Park and Ang damage index for the Loma Prieta and Kobe earthquakes, both buildings are totally collapsed. On the other hand, other earthquake records, especially the Nahanni and San Fernando ground motions, produce much lower damage indices (either repairable damage or damage beyond repair but total collapse does not occur).

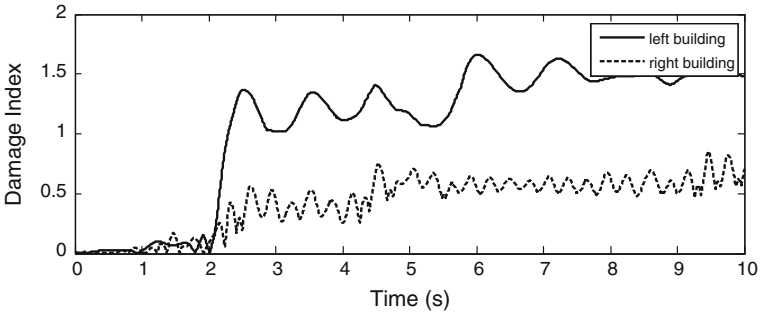

Fig. 6.7 Park and Ang damage index time histories for non-isolated buildings under the El Centro earthquake

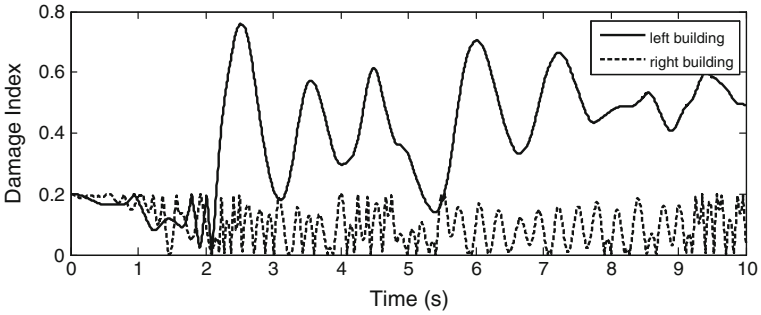

Fig. 6.8 Powell and Allahabadi damage index time histories for non-isolated buildings under the El Centro earthquake

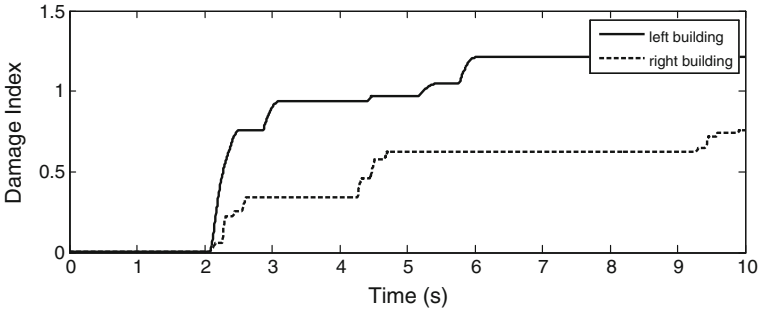

Fig. 6.9 Fajfar and Cosenza damage index time histories for non-isolated buildings under the El Centro earthquake

It can also be seen from Figs. 6.7, 6.8, 6.9 and 6.10 that, in the case of the El Centro earthquake, the values of damage indices for the left building (lighter and more flexible) are substantially larger than for the right structure (heavier and stiffer).

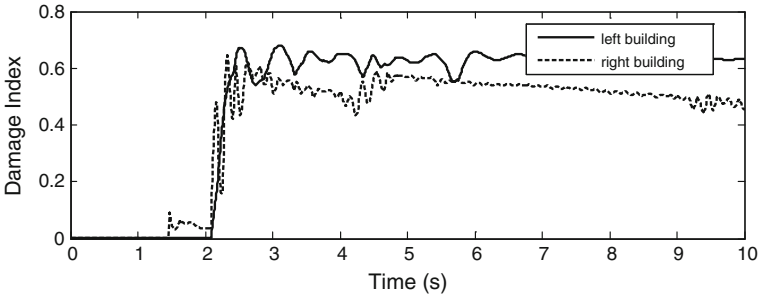

Fig. 6.10 Time histories of damage index based on hysteric energy for non-isolated buildings under the El Centro earthquake

Table 6.1 Peak damage indices for the left non-isolated building under different ground motions

Earthquake	DI_{PA}	DI_{AP}	DI_{FC}	DI_H
El Centro	1.6616	0.7582	1.2100	0.6804
Kocaeli	0.5421	0.2033	0.2743	0.4122
LomaPrieta	1.2138	0.6614	0.6614	0.5441
Duzce	1.4382	0.7898	0.8211	0.7128
Kobe	1.9882	0.8579	1.5627	0.7472
Tabas	0.6043	0.2508	0.3069	0.3354
Nahanni	0.1141	0.2000	0.1226	0.1708
SanFernando	0.4422	0.2000	0.2182	0.7473
Northridge	0.2570	0.2000	0.0571	0.4150

Table 6.2 Peak damage indices for the right non-isolated building under different ground motions

Earthquake	DI_{PA}	DI_{AP}	DI_{FC}	DI_H
El Centro	0.8498	0.2000	0.7568	0.6455
Kocaeli	0.9671	0.2734	0.8863	0.6311
LomaPrieta	1.2390	0.3084	1.1846	0.8545
Duzce	0.8972	0.2000	0.8426	0.5393
Kobe	1.4275	0.2360	1.4685	0.7597
Tabas	0.3170	0.2459	0.1370	0.5240
Nahanni	0.3809	0.2000	0.1508	0.3538
SanFernando	0.4466	0.2000	0.3083	0.3445
Northridge	1.0226	0.2805	1.0889	0.5288

However, this relation is not the same for other ground motions (compare Table 6.1 with Table 6.2) and might be even reversed, as it is in the case of the Kocaeli earthquake for example.

In order to examine the effect of the separation distance on damage indices of colliding non-isolated buildings, the parametric study has been conducted. The value of the gap size between adjacent structures has been varied between 0 and 0.20 m and the responses of both buildings have been determined for each

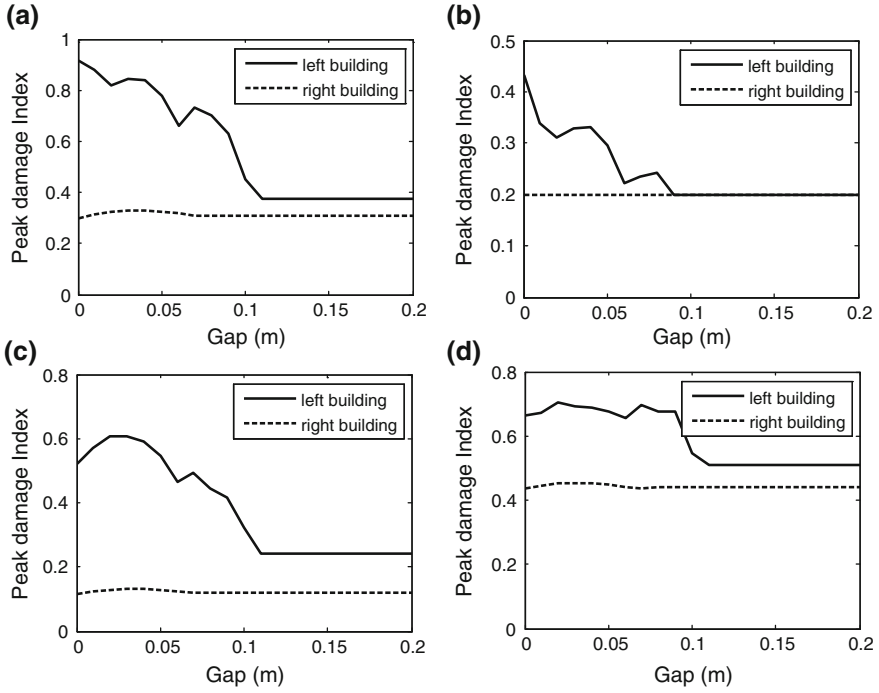

Fig. 6.11 Peak damage indices for non-isolated buildings under the El Centro earthquake with respect to the gap size. **a** Park & Ang. **b** Powell & Allahabadi. **c** Fajfar & Cosenza. **d** Hysteretic

separation distance. Figure 6.11 shows the peak damage indices for both non-isolated buildings under the scaled El Centro earthquake. It should be underlined that, in the case of the ground motion considered, pounding does not occur for a gap size of 0.11 m, which is large enough to prevent collisions. It can be seen from Fig. 6.11 that, starting from this value of the separation distance, damage indices for adjacent buildings are stabilized with constant values. On the other hand, in the range when pounding take place, i.e. between 0 and 0.11 m, structural interactions contribute to the significant increase in damage indices for the left building. It can be seen from the figure that the influence of the gap size on damage indices for this structure is substantial with the general trend of reduction in values of damage indices when the gap size increases.

6.3.2 Damage Indices in Base-Isolated Buildings

For the purposes of the analysis focused on the base-isolated buildings, let us use the simplified structural model shown in Fig. 6.12. The dynamic equation of motion for such a model, considering inelastic (elastic-perfectly plastic) behaviour of both buildings, can be written as [compare Eqs. (6.15a–6.15c) and Eq. (3.6)]:

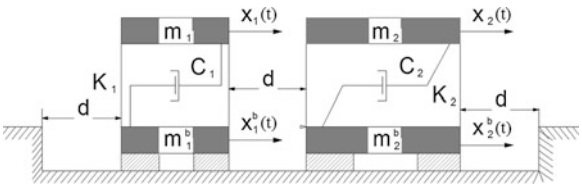

Fig. 6.12 Model of colliding base-isolated buildings

$$\mathbf{M}\,\ddot{\mathbf{x}}(t) + \mathbf{C}(t)\dot{\mathbf{x}}(t) + \mathbf{F}_S(t) + \mathbf{F}(t) = -\mathbf{M}\mathbf{1}\,\ddot{x}_g(t) \tag{6.16a}$$

$$\mathbf{M} = \begin{bmatrix} m_1^b & 0 & 0 & 0 \\ 0 & m_1 & 0 & 0 \\ 0 & 0 & m_2^b & 0 \\ 0 & 0 & 0 & m_2 \end{bmatrix}; \quad \ddot{\mathbf{x}}(t) = \begin{bmatrix} \ddot{x}_1^b(t) \\ \ddot{x}_1(t) \\ \ddot{x}_2^b(t) \\ \ddot{x}_2(t) \end{bmatrix}; \quad \dot{\mathbf{x}}(t) = \begin{bmatrix} \dot{x}_1^b(t) \\ \dot{x}_1(t) \\ \dot{x}_2^b(t) \\ \dot{x}_2(t) \end{bmatrix} \tag{6.16b}$$

$$\mathbf{C}(t) = \begin{bmatrix} C_1^b(t) + C_1 & -C_1 & 0 & 0 \\ -C_1 & C_1 & 0 & 0 \\ 0 & 0 & C_2^b(t) + C_2 & -C_2 \\ 0 & 0 & -C_2 & C_2 \end{bmatrix}; \tag{6.16c}$$

$$\mathbf{F}_S(t) = \begin{bmatrix} K_1^b(t)x_1^b(t) - F_{S1}(t) \\ F_{S1}(t) \\ K_2^b(t)x_2^b(t) - F_{S2}(t) \\ F_{S2}(t) \end{bmatrix}; \quad \mathbf{F}(t) = \begin{bmatrix} F_b(t) \\ F(t) \\ -F_b(t) \\ -F(t) \end{bmatrix}; \quad \mathbf{1} = \begin{bmatrix} 1 \\ 1 \\ 1 \\ 1 \end{bmatrix} \tag{6.16d}$$

where, m_i^b, $\ddot{x}_i^b(t)$, $\dot{x}_i^b(t)$ are the mass, acceleration and velocity of the base of building i $(i = 1, 2)$, respectively; $K_i^b(t)$, $C_i^b(t)$ are stiffness and damping coefficients for isolation devices and $F_b(t)$ is the pounding force at the base level [see Eq. (2.16)].

As the example, two buildings with the basic dynamic parameters described in Sect. 3.1 have been used in the analysis. Furthermore, the yield strength for the left and the right inelastic buildings have been taken as $F_{Y1} = 1.369 \times 10^5$ N and $F_{Y2} = 1.442 \times 10^7$ N, respectively. It has been assumed that the isolation system consists of High Damping Rubber Bearings (HDRBs). In order to simulate the behaviour of the devices, a non-linear strain-rate dependent model has been applied in the analysis [see Eq. (3.4)]. The left building has been equipped with 4 circular HDRBs, with the parameters of the bearing's model described in Sect. 3.3.1 (see also example 3 in Jankowski 2003) and the right building with 4 square HDRBs, with the parameters of the bearing's model described in Sect. 3.3.2 (see also example 1 in Jankowski 2003). The initial separation gap between buildings has been set to $d = 0.05$ m and has been changed later to study its effect on damage of

adjacent buildings. The following values of the non-linear viscoelastic pounding force model's parameters have been applied in the analysis: $\bar{\beta} = 2.75 \times 10^9$ N/m$^{3/2}$, $\bar{\xi} = 0.35$ ($e = 0.65$). The time-stepping Newmark method with constant time step $\Delta t = 0.002$ s has been used in order to solve the equation of motion (6.16a–6.16d) numerically. A set of 9 earthquake ground motion records listed in Table 5.1 have been used as input excitations. Similarly as in Sect. 6.3.1, all acceleration records have been scaled to have the peak ground acceleration of 0.5 g to ensure inelastic response of structures. The parameters of the damage indices have been taken as: $\mu_{u1} = \mu_{u2} = 0.6$ and $\beta_{PA} = 0.15$.

The examples of numerical results, in the form of different damage indices time histories for colliding base-isolated buildings under the El Centro earthquake, are shown in Figs. 6.13, 6.14, 6.15 and 6.16. Additionally, the values of peak damage indices for the left and the right structure under all analyzed ground motion records are summarized in Tables 6.3 and 6.4, respectively (see also Moustafa and Mahmoud 2014). The results of the study reveal that damage indices are considerably

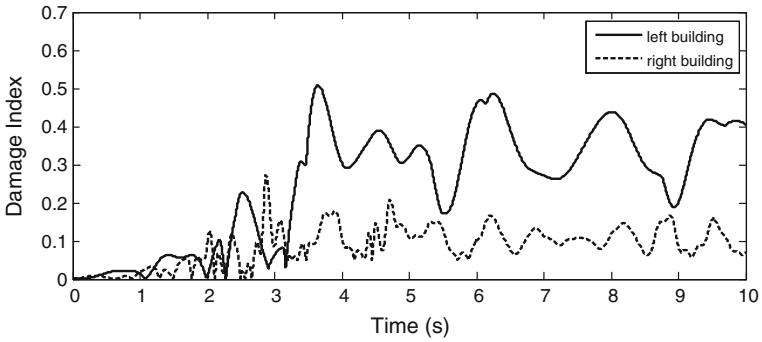

Fig. 6.13 Park and Ang damage index time histories for base-isolated buildings under the El Centro earthquake

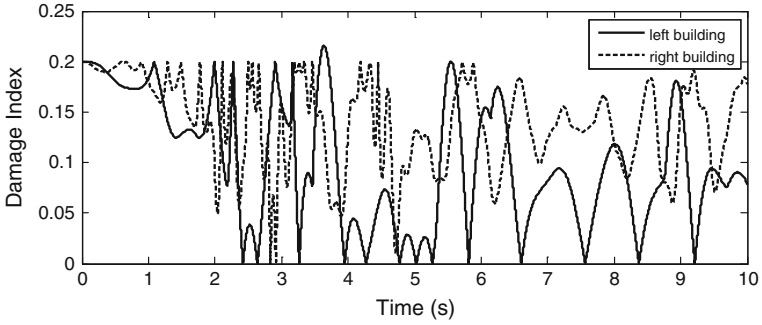

Fig. 6.14 Powell and Allahabadi damage index time histories for base-isolated buildings under the El Centro earthquake

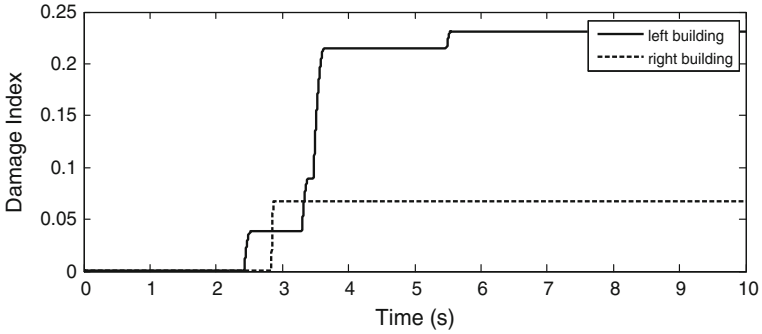

Fig. 6.15 Fajfar and Cosenza damage index time histories for base-isolated buildings under the El Centro earthquake

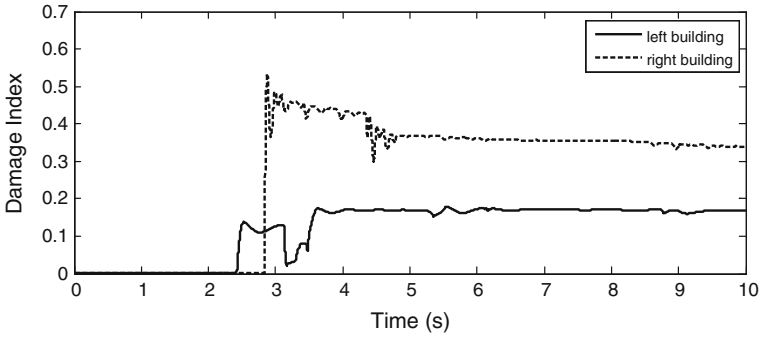

Fig. 6.16 Time histories of damage index based on hysteric energy for base-isolated buildings under the El Centro earthquake

Table 6.3 Peak damage indices for the left base-isolated building under different ground motions

Earthquake	DI_{PA}	DI_{AP}	DI_{FC}	DI_{H}
El Centro	1.9011	0.9670	1.2624	0.5104
Kocaeli	1.0323	0.5467	0.5467	0.6335
LomaPrieta	0.4050	0.2000	0.2306	0.5665
Duzce	1.3632	0.7557	0.7557	0.5205
Kobe	1.3929	0.6570	1.4542	0.6461
Tabas	0.5274	0.2000	0.2941	0.4410
Nahanni	0.0858	0.2000	0.0000	0.0000
SanFernando	0.9885	0.4396	0.6244	0.7903
Northridge	0.3470	0.2000	0.1139	0.4353

different for base-isolated structures as compared to the values obtained for the non-isolated buildings. This is due to the fact that adding isolation devices results in considerable changes of structural natural frequencies. Tables 6.3 and 6.4 indicate

Table 6.4 Peak damage indices for the right base-isolated building under different ground motions

Earthquake	DI_{PA}	DI_{AP}	DI_{FC}	DI_H
El Centro	1.1359	0.3419	1.2559	0.8208
Kocaeli	0.3756	0.2000	0.1690	0.7059
LomaPrieta	0.6049	0.2768	0.3661	0.8333
Duzce	1.2335	0.6738	1.1652	0.8231
Kobe	3.4340	1.4861	3.2333	0.8351
Tabas	0.2942	0.2000	0.0806	0.2761
Nahanni	0.0718	0.2000	0.0000	0.0000
SanFernando	0.6777	0.3227	0.3228	0.8575
Northridge	0.1949	0.2000	0.0178	0.3194

that the El Centro, Kocaeli, Duzce and Kobe earthquakes are among the ground motions which produce the largest damage indices in the case of base-isolated buildings. On the other hand, other earthquake records, especially the Nahanni and Northridge ground motions, produce much lower damage indices. Moreover, similarly as in the case of non-isolated structures, damage indices for the left base-isolated building might be either higher or lower than the values determined for the right structure with the base isolation.

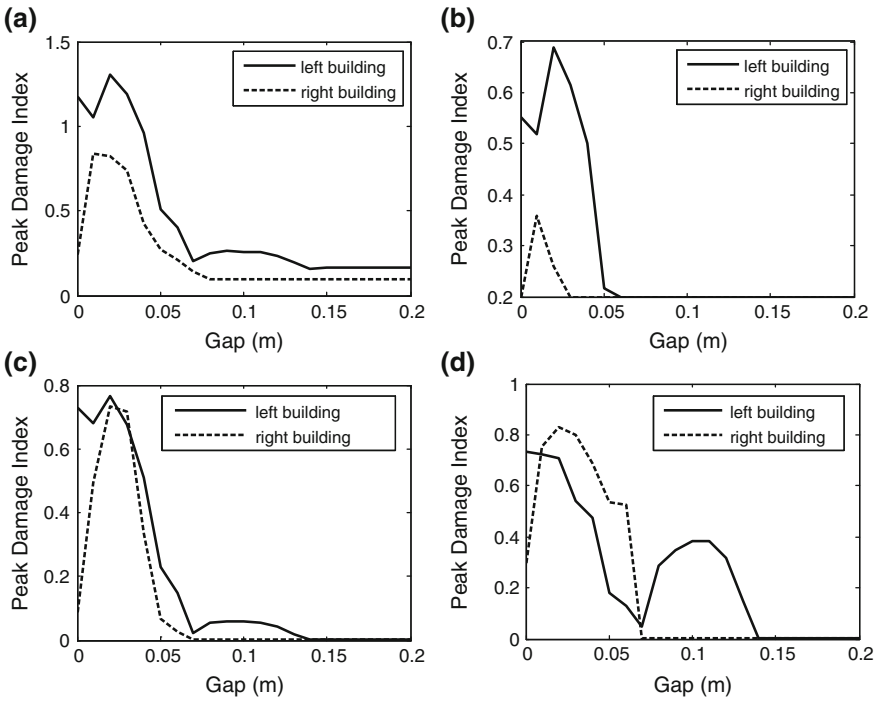

Fig. 6.17 Peak damage indices for base-isolated buildings under the El Centro earthquake with respect to the gap size. **a** Park and Ang. **b** Powell and Allahabadi. **c** Fajfar and Cosenza. **d** Hysteretic

In order to examine the effect of the separation distance on damage indices of colliding base-isolated buildings, the parametric study has also been conducted. Similarly as in Sect. 6.3.1, the value of the gap size between adjacent structures has been varied between 0 and 0.20 m. Figure 6.17 shows the peak damage indices for both base-isolated buildings under the scaled El Centro earthquake. It should be underlined that, this time, pounding does not occur for a gap size of 0.14 m, which is larger than for non-isolated buildings because of the fact that base-isolated structures experience larger response displacements (Kelly 1993; Komodromos 2000; Nagarajaiah and Sun 2001; Agarwal et al. 2007; Komodromos et al. 2007; Mahmoud et al. 2012; Falborski and Jankowski 2013). It can be seen from Fig. 6.17 that, starting from this value of the separation distance, damage indices for adjacent buildings are stabilized with constant values. On the other hand, in the range when pounding take place, i.e. between 0 and 0.14 m, the curves of damage indices for both structures show initially the increase trend and then their values decrease with the increase in the separation gap. Anyway, the results clearly indicate that structural interactions contribute to the significant increase in damage indices of both base-isolated buildings.

References

Agarwal, V.K., Niedzwecki, J.M., van de Lindt, J.W.: Earthquake induced pounding in friction varying base isolated buildings. Eng. Struct. **29**, 2825–2832 (2007)

Anagnostopoulos, S.A.: Pounding of buildings in series during earthquakes. Earthquake Eng. Struct. Dynam. **16**, 443–456 (1988)

ASCE: Minimum Design Loads for Buildings and other Structures SEI/ASCE 7-02. American Society of Civil Engineers, USA (2010)

Bojórquez, E., Reyes-Salazar, A., Terán-Gilmore, A., Ruiz, S.E.: Energy-based damage index for steel structures. Steel Compos. Struct. **10**, 343–360 (2010)

Chau, K.T., Wei, X.X., Guo, X., Shen, C.Y.: Experimental and theoretical simulations of seismic poundings between two adjacent structures. Earthquake Eng. Struct. Dynam. **32**, 537–554 (2003)

Chopra, A.K.: Dynamics of Structures: Theory and Applications to Earthquake Engineering. Prentice-Hall, Englewood Cliffs, USA (1995)

Cosenza, E., Manfredi, G., Ramasco, R.: The use of damage functionals in earthquake engineering: a comparison between different procedures. Earthquake Eng. Struct. Dynam. **22**, 855–868 (1993)

Der Kiureghian, A.: A coherency model for spatially varying ground motions. Earthquake Eng. Struct. Dynam. **25**, 99–111 (1996)

Dulińska, J.M.: Influence of wave velocity in the ground on dynamic response of large dimensional structures. Int. J. Earth Sci. Eng. **4**, 538–541 (2011)

ECS: Eurocode 8: Design Provisions for Earthquake Resistance of Structures. European Committee for Standardization, Brussels, Belgium (1998)

Fajfar, P.: Equivalent ductility factors, taking into account low-cycle fatigue. Earthquake Eng. Struct. Dynam. **21**, 837–848 (1992)

Falborski, T., Jankowski, R.: Polymeric bearings—a new base isolation system to reduce structural damage during earthquakes. Key Eng. Mater. **569–570**, 143–150 (2013)

Fardis M.: Damage measures and failure criteria for reinforced concrete members. In: Proceedings of 10th European Conference on Earthquake Engineering. Vienna, Austria, 28 August–2 September 1994, Rotterdam, Netherlands: Balkema, pp. 1377–1382 (1995)

FEMA: NEHRP Guidelines for the Seismic Rehabilitation of Buildings. Federal Emergency Management Agency, FEMA Publication 273, USA (1997)

IBC: International Building Code. International Code Council Inc., USA (2003)

IBC: International Building Code. International Code Council Inc., USA (2009)

IS: Indian Standard. Criteria for Earthquake Resistant Design of Structures. IS 1893–2002. Bureau of Indian standards, India (2002)

Jankowski, R.: Nonlinear rate dependent model of high damping rubber bearing. Bull. Earthq. Eng. **1**, 397–403 (2003)

Jankowski, R.: Impact force spectrum for damage assessment of earthquake-induced structural pounding. Key Eng. Mater. **293–294**, 711–718 (2005)

Jankowski, R.: Pounding force response spectrum under earthquake excitation. Eng. Struct. **28**, 1149–1161 (2006)

Jankowski, R.: Assessment of damage due to earthquake-induced pounding between the main building and the stairway tower. Key Eng. Mater. **347**, 339–344 (2007)

Jankowski, R.: Non-linear FEM analysis of pounding-involved response of buildings under non-uniform earthquake excitation. Eng. Struct. **37**, 99–105 (2012)

Jankowski, R., Walukiewicz, H.: Modeling of two-dimensional random fields. Probab. Eng. Mech. **12**, 115–121 (1997)

Jankowski, R., Wilde, K.: A simple method of conditional random field simulation of ground motions for long structures. Eng. Struct. **22**, 552–561 (2000)

Kappos, A.J.: Seismic damage indices for RC buildings: evaluation of concepts and procedures. Prog. Struct. Mat. Eng. **1**, 78–87 (1997)

Karayannis, C.G., Favvata, M.J.: Earthquake-induced interaction between adjacent reinforced concrete structures with non-equal heights. Earthquake Eng. Struct. Dynam. **34**, 1–20 (2005)

Kawashima, K., Sato, T.: Relative displacement response spectrum and its application. In: Eleventh World Conference on Earthquake Engineering, paper no. 1103. Acapulco, Mexico, 23–28 June 1996

Kelly, J.M.: Earthquake-Resistant Design with Rubber. Springer, London, UK (1993)

Komodromos, P.: Seismic isolation of earthquake-resistant structures. WIT Press, Southanpton, UK (2000)

Komodromos, P., Polycarpou, P.C., Papaloizou, L., Phocas, M.C.: Response of seismically isolated buildings considering poundings. Earthquake Eng. Struct. Dynam. **36**, 1605–1622 (2007)

Mahmoud, S., Abd-Elhamed, A., Jankowski, R.: Earthquake-induced pounding between equal height multi-storey buildings considering soil-structure interaction. Bull. Earthq. Eng. **11**(4), 1021–1048 (2013)

Mahmoud, S., Austrell, P.-E., Jankowski, R.: Simulation of the response of base-isolated buildings under earthquake excitations considering soil flexibility. Earthquake Eng. Eng. Vibr **11**, 359–374 (2012)

Mahmoud, S., Jankowski, R.: Elastic and inelastic multi-storey buildings under earthquake excitation with the effect of pounding. J. Appl. Sci. **9**(18), 3250–3262 (2009)

Mahmoud, S., Jankowski, R.: Modified linear viscoelastic model of earthquake-induced structural pounding. Iran J. Sci. Technol. **35**(C1), 51–62 (2011)

McCabe, S., Hall, W.: Assessment of seismic structural damage. J. Struct. Eng. **115**, 2166–2183 (1989)

Moustafa, A.: Damage-based design earthquake loads for single-degree-of-freedom inelastic structures. J. Struct. Eng. **137**, 456–467 (2011)

Moustafa, A., Mahmoud, S.: Damage assessment of adjacent buildings under earthquake loads. Eng. Struct. **61**, 153–165 (2014)

Nagarajaiah, S., Sun, X.: Base-isolated FCC building: impact response in Northridge earthquake. J. Struct. Eng. **127**, 1063–1075 (2001)

Newmark, N.: A method of computation for structural dynamics. J. Eng. Mech. Div ASCE **85**, 67–94 (1959)
NBC: National Building Code, Technical Standard of Building E.030. Earthquake Resistant Design. Ministry of Housing, Peru (2003)
Park, Y.J., Ang, A.H.S.: Mechanistic seismic damage model for reinforced concrete. J. Struct. Eng. **111**, 722–739 (1985)
Park, Y.J., Ang, A.H.S., Wen, Y.K.: Seismic damage analysis of reinforced concrete buildings. J. Struct. Eng. **111**, 740–757 (1985)
Park, Y.J., Ang, A.H.S., Wen, Y.K.: Damage-limiting aseismic design of buildings. Earthquake Spectra **3**, 1–26 (1987)
Polycarpou, P.C., Komodromos, P.: Earthquake-induced poundings of a seismically isolated building with adjacent structures. Eng. Struct. **32**, 1937–1951 (2010)
Powell, G.H., Allahabadi, R.: Seismic damage prediction by deterministic methods: concepts and procedures. Earthquake Eng. Struct. Dynam. **16**, 719–734 (1988)
Rajaram, C.R., Kumar, R.P.: Comparison of codal provisions on pounding between adjacent buildings. Int. J. Earth Sci. Eng. **5**, 72–82 (2012)
Ruangrassamee, A., Kawashima, K.: Relative displacement response spectra with pounding effect. Earthquake Eng. Struct. Dynam. **30**, 1511–1538 (2001)
Sołtysik, B., Jankowski, R.: Non-linear strain rate analysis of earthquake-induced pounding between steel buildings. Int. J. Earth Sci. Eng. **6**, 429–433 (2013)
UBC: Uniform Building Code. International Conference of Building Officials, USA (1997)
Valles R.E., Reinhorn A.M.: Evaluation, prevention and mitigation of pounding effects in building structures. Technical Report NCEER–97–0001: National Center for Earthquake Engineering Research. State University of New York at Buffalo, Buffalo, USA (1997)
Williams, M.S., Sexsmith, R.G.: Seismic damage indices for concrete structures: a state-of-the-art review. Earthquake Spectra **11**, 319–349 (1995)
Zembaty, Z.: Vibrations of bridge structure under kinematic wave excitations. J. Struct. Eng. **123**, 479–488 (1997)